Experimental Mechanical and Fluid Mechanical Investigations of the Brass Instrument Lip-reed and the Human Vocal Folds

Michael James Newton

A thesis submitted in fulfilment of the requirements
for the degree of Doctor of Philosophy
to the
University of Edinburgh
2009

Abstract

The mechanical properties of the lips are of crucial importance to the function of a brass instrument. The natural resonance modes must be able to usefully interact with the instrument air column in order to sustain oscillations. Mechanical frequency responses of human and artificial lips used to play a brass instrument were measured using a high-speed digital video technique in an attempt to classify the true nature of the lip-reed. The results revealed the presence of at least two lip modes that exhibited the characteristic outward-inward striking behaviour seen in many *in vitro* replica lip-reed measurements. The Q-values of the human lip resonances were considerably lower than those seen for the replica lips. Transverse mechanical response measurements were also performed on an *in vitro* lip-reed to investigate the coupling between the outward and inward striking modes. The two dimensional motion of the lips during full oscillations was investigated. It is shown that a computational four degree-of-freedom model would be required to fully simulate the observed mechanical motion.

The fluid behaviour downstream from an *in vitro* vocal fold model was investigated using particle image velocimetry (PIV). A 'free jet' configuration with no downstream acoustical coupling was first investigated. The measurements revealed an unsteady glottal jet flow, consisting of a high velocity jet core, a transitional region of high jet deceleration and a turbulent mixing region. The jet was consistently skewed at angles to the glottal centreline, and appeared to oscillate back and forth across the centreline during the glottal cycle. The behaviour of the jet core was investigated in detail. A temporal asymmetry was observed in the mean velocity across the jet core such that the highest jet velocities were encountered during the closing phase of the vocal folds. The overall jet behaviour also showed a strong turbulent asymmetry between the opening and closing phases. High levels of vorticity and turbulent motion encountered during the closing phase were associated with the deceleration of the jet.

Three vocal fold configurations that included static replicas of the ventricular bands were finally investigated with the aim of characterising the aerodynamic interaction between the ventricular bands and the vocal folds. A marked effect on the glottal jet was observed for all configurations. The most physically realistic configuration appeared to stabilise the glottal jet, leading to a reattachment of the jet to the ventricular bands and a subsequent secondary flow separation from the downstream end. The implications of the aerodynamic interaction is discussed, with particular note to its possible relevance to the lip-reed and mouthpiece interaction in brass playing.

Declaration

I do hereby declare that this thesis was composed by myself and that the work described within is my own, except where explicitly stated otherwise.

Michael James Newton
April 2009

Acknowledgements

"*The solution to any problem - work, love, money, whatever - is to go fishing, and the worse the problem, the longer the trip should be.*" - John Gierach

Doing a PhD is made immeasurably more enjoyable by sharing the experience with similarly suffering and occasionally exuberant individuals. Throughout my PhD I have made some great friends, and remarkably few enemies (cardboard boxes and polystyrene cups don't count). The A-team of 4201, in no particular order: Ali 'The Braid' Braden, Alan Woolman, Daz, Dave Skulman, LaShonda, Linus, Robbie Earl, Sammy Hagar and Sandra. Or by their pseudo-names: Alistair, Alan, Darren, Dave, Seona, Lin, Rob, Samuel L. Jackson and Sandra. Through all the (somewhat frequent) guitar-based interludes, YouTube obsession, uncontrollable model helicopters and rotten bananas a thesis was born.

Particular thanks to Seona for showing me the door to artificial lips heaven, to Dave and Rob for introducing me to the PIV setup, to Sam for lending me your lips and for providing a phenomenal supply of (occasionally suspect) jokes, to Lin for introducing 4201 to an... alternative selection of music, to Darren for being Darren (not easy), to Alistair for providing such a great example of a hard-working and organised PhD student (only 3 years!) and introducing me to such an interesting selection of mobile phone ring tones, to all the visiting students from France who brought a taste of continental class to our common British office, to Les for your practical help in the labs, and most of all to Rob for being the best brother-in-arms I could have hoped for throughout all my PhD, with the endless shared hours in the PIV lab, shared hours of write-up, help with the lips experiments and all the other general foolery which would take up too much space to list. Pancake day, say no more.

Special thanks to Lucie Bailly for being such a superb collaborator, for explaining the Bernoulli equation more times than should have been necessary and for making the trip to sunny Edinburgh for such a mad-hat experiment.

Special thanks to Murray Campbell, my supervisor, for his unfailingly positive outlook on all matters thesis related, despite underperforming lasers and insufficiently wobbly lips. Your encouragement was always sincerely appreciated. While I'm going

through seniority figures, special thanks are also due to Joel Gilbert. My sincerest thanks for encouraging me through my experimental purgatory, for laying the gauntlet down for the JASA paper, and for providing a bit of Gallic cheer to JCMB every February. Would you like to drink a coffee? Special thanks also to Jean-Christophe (JCV) for your extremely useful help in the early days of my PIV analysis meanderings, and for bringing yet more Gallic cheer to the group.

The support of my parents has been a very important reason for my arrival at submission day. Be it satay chicken, (un)successful fishing trips and obsessive football talk, or just a wee natter, having a pair of encouraging parents who were always interested to know how I was getting on was a real gift, and one for which I am very grateful. Just as important were the (slightly more) successful fishing trips, curry-based excursions and pints of Trade Winds shared with brother and true pal Steve dog.

Special thanks to Ju, my favourite horse-riding French ladybird, for putting up with the past 8 months of pure write-up heaven. For trips to Mull and Christmas fois gras, for introducing me to the tummy-joy of mussels and the beauty of Paris, thank you.

There are probably only two people without whom I can truly say made my thesis would not have been possible, Andrew Downie and Derek Lowe. Without them and the other skilled folks who live in the JCMB mechanical workshop, we'd all be a lot worse off. Thanks to Derek for your great work on the double-shanked mouthpiece, and to Andrew for your helpful suggestions and expert construction of the new artificial lips. May they long vibrate in your honour. Thanks also to the JCMB postal delivery folks, who made seemingly endless trips to 4201 with all our mail order junk.

Thanks to AJ and TJ for your lips, and for doing such a great job with the impossibly awkward trombone setup.

Thanks very much to Lawrence for your help with LaTeX and general computer tooling around.

Culinary matters matter, particularly to those of us endowed with a true love for curry. The finest culinary establishment in Edinburgh, The Kebab Mahal, was a true palace of stomach-burning curry sauce and nutritional merriment. The fine culinary efforts of Julie and Tam, of the Julie's cafe, discovered too late on in our quest for edible foodstuffs around the Kings Buildings, are also gratefully acknowledged.

The financial support of the ESPRC is gratefully acknowledged.

Contents

List of Figures

List of Tables

Part I

Introductory Notes and Background Theory

Chapter 1

Introduction and motivation

"*They say you forget your troubles on a trout stream, but that's not quite it. What happens is that you begin to see where your troubles fit into the grand scheme of things, and suddenly they're just not such a big deal anymore.*" - John Gierach

1.1 Introduction

The human vocal folds and lips have been used to produce sound for millennia. The oscillating vocal folds form the primary source of sound during voiced speech, or phonation, and in singing. The vibrating lips of a musician, known as the lip-reed, form the primary source of sound in brass playing. In either situation, it is the periodic vibration of a deformable mechanical structure - the vocal folds or the lips - acting as a flow control valve that leads to the production of sound.

Sound production by the vocal folds features in the lives of almost every inhabitant of the planet on a daily basis. The production of speech is central to human communication, and as such presents itself as a subject ripe for research. Similarly, the sound produced by a brass instrument is well known to many people. Whether it is the smooth, calming tones of Chet Baker's trumpet, or the ragged, staccato jitterings of a free jazz trombonist, the sound of a brass instrument is instantly recognisable.

The field of vocal fold research is considerably larger than that of the lip-reed. This is perhaps unsurprising, given that the gamut of vocal fold research draws from both the physical and medical sciences. This is not to say that little effort has been focussed on the lip-reed. On the contrary, the physics of brass playing, and the wider field of musical acoustics, have been studied by some of the most eminent scientists of the last 200 years. It was none other than Hermann Helmholtz[Helmholtz, 1877], writing in 1877, who provided the first serious attempt to describe the physics of wind and brass instruments.

In the modern era much of the literature on vocal fold research has been concerned with the development of computational models to simulate their behaviour. The most

crucial development in this regard was the computational two-mass model of Ishizaka and Flanagan[Ishizaka and Flanagan, 1972]. This model demonstrated the ability of the vocal folds to undergo self-sustained oscillations resulting from an aerodynamic interaction with the airflow through the larynx. In contrast, the vast majority of lip-reed research has concentrated on the interaction between the lips of the player and the strong acoustic field within the bore of the brass instrument. Elliot and Bowser[Elliot and Bowsher, 1982] provided a comprehensive treatment of this problem.

The fascinating reality is that the operation of both the vocal folds and the lip-reed can be described with essentially the same set of equations. Each system functions as the result of an aerodynamic interaction between a set of deformable biological tissues and an airflow. The physical description of the mechanical motion may be approximated by some combination of masses and damped springs, as in the ubiquitous lumped element models[Kob, 2004b]. A comprehensive fluid mechanical description should take account of the considerable jet flow component of the airflow, as well as the influence of any acoustical waves it generates.

In much of the published literature, the key differences between the treatment of the vocal folds and the lip-reed lie in the details of how the fluid behaviour is described. In particular, the relatively strong acoustical field created in the bore of the brass instrument has led to the wide use of a highly simplified flow description that neglects almost all subtleties of the flow behaviour. The general assumption has been that it is the acoustical field that is the most important source for an alternating driving force on the lips, regardless of exactly how the necessary volume flow is generated.

In contrast, most descriptions of the vocal folds have adopted the so-called "source-filter" theory. In this description the vocal folds are assumed to operate in total independence of any surrounding acoustic field, be it in the trachea or the vocal tract. The source of an alternating driving force has to be explained by considering in more details the flow behaviour around the vocal folds.

However, regardless of the conventional treatments of the vocal folds and the lip-reed, it is clear that both the systems include a strong pulsatile jet flow through the oscillating valve, as well as some degree of an acoustical field. This fundamental similarity suggests that for a truly comprehensive treatment of either system, it is necessary to consider both the detailed flow mechanics, as well as the acoustic fields. Several studies have demonstrated that it is not possible to understand the full range of vocal fold behaviour in complete absence of the acoustical effects of the vocal tract[Guerin, 1981; Rothenberg, 1981; Titze and Story, 1997]. It is similarly impossible to explain the oscillations of the lips during brass playing without some recourse to the fluid mechanics of flow separation and the boundary layer approximation[Elliot and Bowsher, 1982; Cullen *et al.*, 2000].

At the most fundamental level the governing principles of any fluid motion are described by the fully viscous and unsteady Navier-Stokes equations[Tritton, 1988].

These equations are almost impossible to analytically solve for anything beyond a highly idealised situation[Schlichting and Gersten, 2000]. However, by considering the relevant non-dimensional parameters of the flow through the vocal folds and the lip-reed it is possible to neglect many of the terms in the equations, leading to a greatly simplified description of the flow that may be computationally simulated with relative ease. The most common flow assumption is that the bulk of the flow is incompressible and inviscid, so that the Bernoulli equation may be applied. For most situations, with the exception of extremely loud brass playing[Hirschberg *et al.*, 1996a], it is possible to used a linear treatment of the acoustic propagation. Most contemporary treatments, of both the vocal folds[Lous *et al.*, 1998; Adachi and Yu, 2005] and the lip-reed[Adachi and Sato, 1995; Adachi and Sato, 1996], routinely use these two assumptions. A more detailed explanation of the fluid mechanics relevant for both the vocal folds and the lip-reed is presented in section 2.5.

1.2 The present work

The bulk of the work described in this thesis originates from experimental work. Much of the work has been concerned with the development of novel experimental techniques to investigate both the vocal folds and the lip-reed under a variety of conditions. This work falls into two main categories. The first category includes investigations into the mechanical properties of the lip-reed, under both *in vitro* and *in vivo* conditions. The second category includes investigations into the fluid mechanical phenomena encountered during self-sustained oscillations of the vocal folds under *in vitro* conditions, with particular attention paid to the aerodynamic influence of the ventricular bands. The implications of this work to the case of the lip-reed is examined in detail.

The thesis is structured into four key sections. Introductory comments and an overview of the physics relevant to vocal fold and lip-reed operation form part I of the thesis. This work may be found in chapters 1 and 2. A particular attempt is made to underline the fundamental overlap of the basic physics that has already been mentioned above in section 1.1, and to thus justify the way in which they have been studied together within the thesis.

The main bulk of the thesis, including parts II and III and comprising chapters 3 to 8, is then concerned with describing the experimental setups, results and analysis of the experimental mechanical and fluid mechanical investigations.

Part II presents investigations into the mechanical properties of the lip-reed. This work concentrates on the details of the mechanical configuration of the lips during brass playing, in an attempt to verify the true nature of their behaviour. The use of both *in vivo* and *in vitro* experimental setups was a vital part of the work. It allowed for the first comprehensive comparison to be made between the well documented behaviour of

the *in vitro* lip-reed replicas, which have featured extensively in research over the past decade, with novel measurements performed directly on human subjects.

Part III describes an investigation into the fluid behaviour of the air jet produced by an *in vitro* vocal fold replica during full self-sustained oscillation. The objective was to investigate the possible influence on the vocal folds of a number of downstream configurations. This work, while clearly concentrated on the specific case of the vocal folds, is strongly tied to the first half of the thesis. The downstream conditions investigated were very similar to those encountered in the case of the lips and the mouthpiece in brass playing.

Part IV of the thesis, comprising chapter 9, presents a summary of the important conclusions arising from the work.

1.3 Thesis aims

The principal work of this thesis involved the development and application of experimental techniques to study the physics of the brass instrument lip-reed and human vocal fold oscillation mechanisms. The overall story was wide ranging in its approach, involving two separate experimental setups to study first the mechanical, and then the fluid mechanical features of these self-oscillating mechanical valves.

Five primary objectives were formed to govern the overall path of the work. The objectives are described throughout parts II and III (chapters 3 to 8) as outlined above. The first objective involved the development of a new *in vitro* brass instrument lip-reed. The second and third objectives focussed on a study of the lip-reed mechanism, using the new *in vitro* lip-reed model, together with *in vivo* human lips. A new experimental technique for measuring the mechanical response of the lip-reed was developed for this purpose. Objectives four and five were focussed on a study of the airflow produced by self-sustained oscillations of an *in vitro* model of the human vocal folds. The five primary objectives of the thesis will now be outlined in more detail.

1.3.1 Objective One - Develop a new *in vitro* replica of the brass instrument lip-reed

The first objective of the thesis was to develop a novel *in vitro* replica of the brass instrument lip-reed. Similar replicas, also referred to as 'artificial lips', have in recent years featured extensively in research into the physics of brass instrument playing[Cullen, 2000; Neal, 2002; Richards, 2003]. They provide a stable, repeatable testing bed for investigations into the destabilisation of the lips during brass playing, and the nature of the valve - instrument interaction.

In the first half of chapter 3 a new artificial lips replica is presented. The new replica was designed in collaboration with the mechanical workshop of the School of Physics,

drawing inspiration from the artificial lips developed by Richards[Richards, 2003], and from a similar replica of the human vocal folds originally developed at the Technische Universiteit Eindhoven in the Netherlands, and latterly used at the Institute de la Communication Parlée in Grenoble, France.

There were two key design aims for the new replica over previous models: improved stability and repeatability, and improved optical access to the all regions of the replica lips. Both of these criteria were met with the new replica. It was used extensively as part of the investigations into the lip-reed mechanism, presented in chapter 4.

1.3.2 Objective Two - Investigate the mechanical response properties of *in vivo* human lips formed into playable embouchures

The second objective of the thesis was to develop and implement a new experimental method, capable of performing mechanical response measurements on the brass instrument lip-reed under *in vivo* conditions. In the second half of chapter 3 the new 'video method' technique for the study of human lips is described in detail. This novel technique used a high-speed digital video camera to record the motion of the lips when formed into a playable embouchure, and acoustically driven over a wide frequency range. This allowed an estimate to be made of their mechanical response properties.

During the experiments on human subjects, the lips were viewed through a specially designed transparent mouthpiece, the details of which are also described in chapter 3. Experimental results and discussion of the results of the *in vivo* lip-reed investigations are presented in the first half of chapter 4.

1.3.3 Objective Three - Investigate the mechanical response properties and two-dimensional motion of the *in vitro* lip-reed replica developed in objective one

The third objective of the thesis was to investigate the mechanical response properties of the newly developed *in vitro* lip-reed, which was constructed to fulfil objective one. The video method, designed as part of objective two, was used as a tool to investigate in detail both the mechanical response properties of the lips, and their two-dimensional motion during full self-sustained oscillation. The target of the investigation was to quantify the nature of the mechanical coupling of the natural lip resonances. It has been hypothesised by Richards[Richards, 2003] that a coupling between two distinct mechanical resonances, each associated with either the 'outward' or 'inward' striking reed regimes first described by Helmholtz[Helmholtz, 1877], may be the mechanism that leads to a destabilisation of the lips during playing. The results of this investigation are presented in the second half of chapter 4.

1.3.4 Objective Four - Development of a new PIV experimental setup

The third objective was to develop and implement a new particle image velocimetry (PIV) experimental setup. PIV is a full-field optical technique used to provide quantitative information about a wide variety of flows. The setup was designed to allow observations to be made of the airflow through an *in vitro* vocal fold model. An outline of the important principles of PIV is presented in chapter 5.

The main challenge of the setup was to allow a full synchronisation to be made between the experimental apparatus and the vocal folds, which were left to execute uncontrolled self-sustained oscillations. The setup was adapted from one used previously to study purely acoustic fields, which was thus designed to synchronise directly with the acoustic signal using a phase lock-in method. A post-synchronisation routine was developed to overcome the inability to phase lock-in the PIV measurements with the free vocal fold oscillations. Full details of the experimental apparatus and techniques are described in chapter 6.

1.3.5 Objective Five - Application of PIV to the flow through a self-oscillating *in vitro* vocal fold replica

The final objective of the thesis was to use the experimental method developed for objective 3 to study the aerodynamic interaction between the human vocal folds and the ventricular bands. Under some conditions the ventricular bands, also known as the false vocal folds, can form a secondary constriction a short distance downstream from the vocal folds. They have traditionally been associated with the production of a number of exotic singing styles, such as Mongolian throat singing. In many of these exotic singing styles they have been shown to undergo a periodic oscillation, apparently driven by some combination of mechanical, acoustic and aerodynamic forcing. Their influence has also been documented in a number of speech pathologies, where they may provide a compensatory mechanism to assist the vibration of the vocal folds. The ventricular band constriction presented a physical scheme with some interesting similarities to that of the lip-reed - mouthpiece system in brass playing. In the case of the lip-reed the mouthpiece throat forms a secondary constriction a short distance downstream from the lips.

Chapters 7 and 8 present a study into the behaviour of the air jet produced downstream of the vocal folds during normal phonation. It was hypothesised that following separation from the vocal folds, the jet traversed the short cavity known as the laryngeal ventricle before impinging on the upstream face of the ventricular bands.

The aim of objective five was to quantify the effect on the air jet caused by the presence of a pair of rigid ventricular bands, located downstream of a pair of self-oscillating *in vitro* vocal folds. A configuration with no vocal tract or ventricular bands was first investigated to quantify the nature of the jet in absence of any downstream

constriction. Two different configurations involving replica ventricular bands were then studied.

Chapter 2

Theory of Lip-Reed and Vocal Fold Oscillation

"*There's a fine line between fishing and standing on the shore like an idiot.*" - S. Wright

2.1 Introduction

The principle sound generation mechanism in brass instruments is the periodic volume flow caused by the oscillation of the lips. In voiced speech it is the periodic jet flow through the vocal folds. From a global perspective the two systems are thus rather similar and it is possible to explain a considerable portion of their behaviours using the same set of physical equations.

In this chapter the mechanical system comprising either the lips or the vocal folds will be collectively known as a *valve*. This general description acknowledges the fact that while there is a considerable portion of overlap between the two systems, it is important that the key subtleties are not forgotten. In particular, the lip-reed forms part of a musical device expected to produce a discrete series of notes (thus the term 'reed'), whereas the vocal folds comprise a more diverse system capable of oscillating over a continuous range of frequencies.

2.1.1 Principles of the experimental process

The destabilisation and resulting self-oscillation of a mechanical valve is a highly non-linear phenomenon and as such it is difficult to draw straightforward intuitive insights about its behaviour. However, significant progress can be made by breaking the valve down and analysing the mechanical and fluid mechanical features separately before assessing the nature of any aeroelastic and acoustical couplings.

This process is a classic example of the scientific principle whereby a system is greatly simplified before being described by the smallest possible set of equations.

Such equations are generally simplified versions of 'reality'. For example, the flow mechanics are generally described by the Bernoulli equation, rather than the fully non-linear Navier-Stokes equations. The complicated geometry of the valve is also generally condensed down into a small number of discrete masses using the so-called 'lumped element' method.

Computational simulation of such a set of mechanical and fluid mechanical equations provides a useful method for controlled analysis of the important behaviours of a valve. This is called a 'physical model'.

Simulation using physical models has traditionally been performed in the time domain[Kob, 2002; Lous *et al.*, 1998]. The model is first set up using a small number of parameters that determine the geometry, the initial mechanical arrangement and the initial pressure/flow conditions. For the first time step the equations of flow are solved to determine the aerodynamic forces around the valve. The resulting motion of the valve is then determined using Newtonian mechanics. The geometrical and mechanical parameters are finally updated, ready for the next time step.

Time domain simulation of lumped-element models is an extremely useful tool. It provides a clear computational interpretation of a simplified real-world system. It is possible to extract useful quantities from the simulation, such as the oscillating acoustic flow, and compare them directly with experimental measurements. However, the task of describing the initial state of the system is not trivial. In particular, the real-world interpretation of model parameters such as 'spring stiffness' is not immediately obvious. It is the job of the experimentalist to provide convincing correlations between experimentaly measurable quantities and the highly simplified mechanics of the physical model.

The experimentalist also has a role to play in determining the validity of the most fundamental principles of physical models. By way of an example, let us consider the assumption that the mechanics of a valve can be usefully described by just two masses oscillating on damped springs. It is not clear, *a priori*, how many degrees of freedom the masses should be allowed. However, experimental observations of the oscillation of the lips in brass instrument playing have clearly shown that the lips can execute both 'shutter' like motion transverse to the mean flow direction, and 'swinging-door' like rotational motion in line with the flow[Yoshikawa, 1995; Copley and Strong, 1996]. Such empirical evidence already provides a strong hint that a truly realistic computational model of the lips should thus allow for motion in at least two dimensions.

2.2 Global context of the lip-reed and vocal fold musical valves

2.2.1 Introduction

The self-sustained oscillations of a musical valve occur because of a dynamic feedback mechanism that couples together the mechanical structures of the valve and the surrounding fluid mechanical fields. A scenario is required whereby the flow of air emanating from the lungs can provide a periodic driving force to the valve surfaces. It is of vital importance that the application of this force is correctly phased in order to help maintain the valve motion despite the presence of mechanical damping.

The case of lip-reed oscillation is a situation that can be usefully compared to the quasi-one dimensional motion of a child on a swing. In order for the child to remain happy, their beleaguered parent must supply a periodic driving force which must be large enough to overcome the internal damping of the swing system. However, as crucial as the mere presence of a periodic driving force may be, the precise timing of the forcing is of equal importance. The parent must push the child with a force that acts in the same direction as the motion of the child. This could be at the peak height, just as the child changes direction. In such a case positive work is done by the parent and the child gains energy. This principle is described by the basic work integral shown in equation 2.1, where W is the work, $\vec{F}$ is the driving force and $d\vec{x}$ is the infinitesimal displacement vector. The equation is a dot product, which means the work is only positive when the force and displacement act in the same direction (for a one dimensional system).

$$W = \int \vec{F} \cdot d\vec{x}. \tag{2.1}$$

The parent is not required to provide huge quantities of energy every cycle. Rather, with intelligent application of the forcing they are only required to impart as much energy as has been dissipated by the internal damping of the swing. Poorly timed application of the forcing, however, means that negative work is performed by the parent. This acts as an extra drain on the mechanical energy of the child, and will quickly result in an end to the swinging

In the case of the brass player, the lips are like the child, and the surrounding aeroacoustic field is like the parent. Sustained oscillation of the lips will only occur if the aeroacoustic field can supply enough energy to overcome the internal damping of the lips. The precise mechanisms by which this supply of energy can occur provide some interesting questions. A number of the mechanisms are described in more detail in section 2.7.1, and throughout chapter 4.

2.2.2 Fundamental destabilisation

We can describe the oscillation of the lip-reed and the vocal folds as the result of the destabilisation of a continuous mechanical structure by the presence of an airflow. The airflow is the result of a pressure difference across the valve caused by an overpressure in the lungs, relative to the ambient outside air pressure. In the case of the lip-reed the pressure difference is established between the mouth of the player and the mouthpiece of the instrument. For the vocal folds the pressure difference is between the trachea and the vocal tract.

A basic description of the brass instrument lip-reed and human vocal folds will first be presented in section 2.2.3. A more detailed outline of the mechanical characterisation will then be presented in section 2.4. The phenomenon of flow separation that leads to the formation of the pressure difference will be described in section 2.5. A brief explanation of acoustic impedance is presented in section 2.6. A more detailed description of the lip-reed will then be presented in section 2.7, and of the vocal folds in section 2.8. Finally, in section 2.9, a brief overview of time domain computational modelling of musical valves will be outlined.

2.2.3 Basic description of the valve

The lip-reed and vocal fold valves are broadly similar in their mechanical construction. They are comprised of a continuous distribution of deformable biological tissues which form obstructions to the flow of air passing through the human airway. Figure 2.1 shows a schematic representation of the important mechanical structures and fluid mechanical parameters of the valves. Details concerning the characterisation of the mechanical description are presented in section 2.4. The basic fluid mechanics of the flow field are then outlined in section 2.5.

While broadly similar in their mechanical construction, the lip-reed and the vocal folds do differ in a number of ways. The lips are rather more massive, and are primarily made of muscle tissue surrounded by skin. The vocal folds, on the other hand, are comprised of a complicated series of tissue layers and ligaments covered in a layer of mucosa[Sundberg, 1987].

Rigorous characterisation of the precise mechanical details of the biological valves such as the lips and vocal folds is a difficult task. A useful approach is to try to capture the essence of the mechanical properties by means of *mechanical response* measurements. This technique is explained in section 2.4.3.

2.2.4 Buzzing lips vs. vocal folds

The vocal folds are smaller in all dimensions than the lips, and are considerably less massive. However, they are both formed from a combination of biological tissues

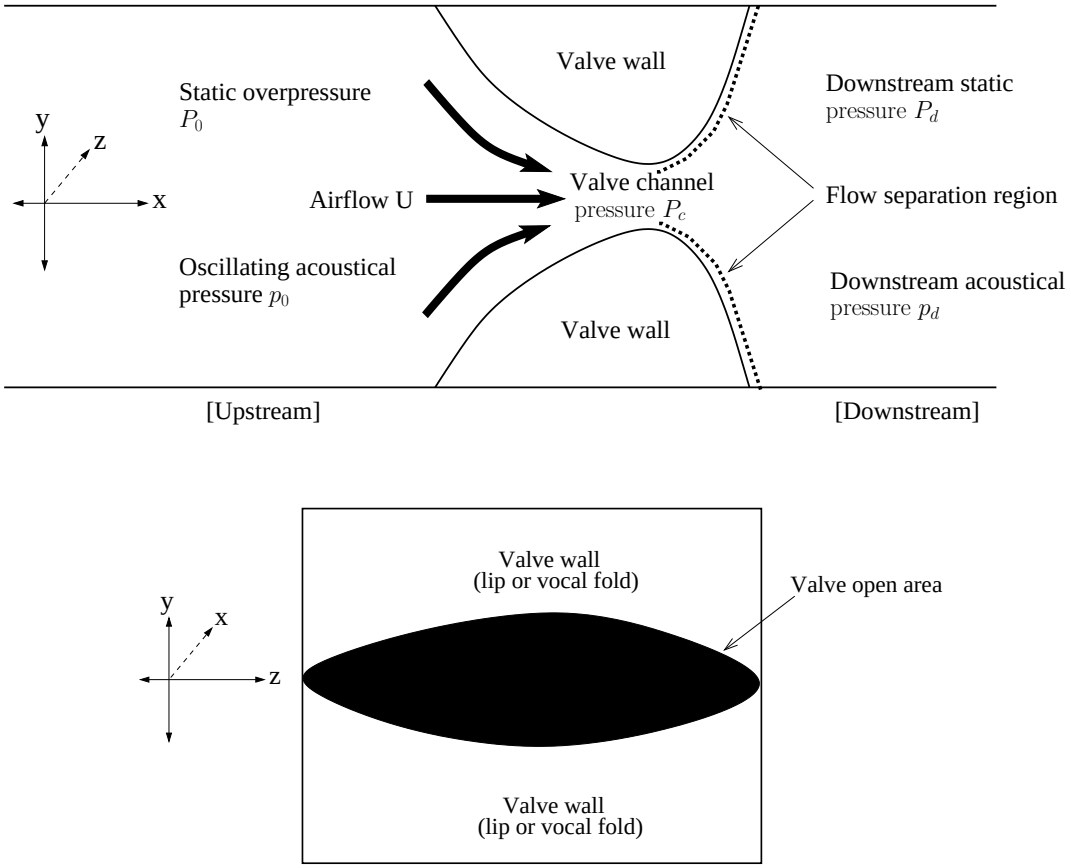

Figure 2.1: A schematic diagram showing the basic mechanical layout and fluid mechanical parameters of the lip-reed and vocal fold valves.

consisting largely of water, and as such share a quite similar overall structure.

Scientific research into the lip-reed and the vocal folds has followed two broadly different paths over the last century. The fundamental reason for this is that during oscillation the lips are subjected to considerable acoustic pressures that are built up in the downstream bore of the instrument, while the vocal folds operate in a much quieter environment. This has led to a strong emphasis on an acoustical description of the lip-reed that largely neglects details of the fluid mechanics, and a more fundamental fluid mechanical description of the vocal folds.

These two approaches are really like two different photographs of the same scene. Each photograph portrays a slightly different slant on a common subject, with different emphases and compositional choices. However, a comprehensive description of either subject really requires attention to both the acoustics and the fluid mechanics. This is why it is useful to consider the lip-reed and the vocal folds together. Each subject, with its corresponding scientific approach, can shed new insight onto the other.

There are three principal theoretical techniques for the study of musical valves.

These are time domain modelling, non-linear dynamics and linear-stability analysis. Time domain lumped element modelling has a long history in the field of vocal fold simulation, and has also been applied to the lip-reed[Elliot and Bowsher, 1982; Adachi and Sato, 1995] and other musical instruments[Dalmont *et al.*, 2003; Silva *et al.*, 2008]. It is described in some detail in section 2.9. A key advantage of this method is that the musical valve system can be broken down into multiple components, with separate formulations for the mechanics, the fluid mechanics, and the coupling between the two. The model is generally run in the time domain, which helps to provide a reasonably intuitive step-by-step break down the the whole process.

One of the most important theoretical tool for the study of the lip-reed is non-linear dynamics[Fletcher, 1999; Campbell, 1999]. This is a mathematical formulation that allows an objective study of non-linear systems. In the case of the lip-reed, non-linear dynamics has been applied to the system of flow control through the lips. This approach is described in section 2.7.1.

2.3 Terminology relevant to the discussion of lip-reed and vocal fold models

The scope of the work in this thesis emcompases a broad range of topics that relate to both the lip-reed and the human vocal folds. As such there are some basic definitions and terminology that must be clearly defined before they are used in the discussion that follow. These terms are:

- Embouchure - this word describes a particular configuration of the lips when used as a lip-reed. It encompasses the global mechanical condition of the lips and the corresponding target note. It may be used to describe the configuration of both real and artificial lips. In general, a specific embouchure will play a specific note, and repeated settings of the same embouchure should reproduce the same note[Bromage, 2006].

- Configuration - this word is used instead of *embouchure* to describe the state of vocal fold models, and as such has a similar meaning[Bailly *et al.*, 2006; Vilain *et al.*, 2004; Ruty *et al.*, 2007].

- *In vitro* -an *in vitro* model is a mechanical replica of a real system. In this work the term '*in vitro* buzzing lips' refers to the mechanical artificial lip system developed to simulate real lips. The term is also used to describe the mechanical vocal fold models relevant to the new artificial lip system described in section 3.2.3.

- *In vivo* - experiments carried out on living subjects take place under *in vivo* conditions. The application of mechanical response measurements to human lips

formed into playable embouchures is an example of an *in vivo* experiment (see section 3.3.4).

2.4 The mechanical properties of the valve

The lips of a brass player are formed from a mixture of biological muscles and tissues. When formed into a brass player's embouchure, they describe a roughly symmetrical pair of deformable shutters within the mouthpiece. The cross-sectional $x-yaxes$ profile (see figures 2.2.3 and 2.2) is highly dependent on the particular player and configuration.

The human vocal folds lie within the greater larynx structure between the lower airway of the trachea and the upper regions of the throat and vocal tract. They are constructed from a complicated mixture of muscles and interconnecting tissues and ligaments. In cross-section they resemble the lips of the brass player. There are some important differences, however, which have already been briefly discussed in section 2.2.4, and which will become increasingly apparent throughout this work.

The inherent complexity in the mechanical structure of biologically based musical valves makes their scientific description particularly challenging. Broadly speaking there are two ways to deal with this complexity, the micro-scale approach and the macro-scale approach.

2.4.1 Micro-scale description

The micro-scale approach seeks to describe the valve using as much detail as possible, and to simulate this description using some of the fastest processing power available. Finite element modelling is a common example of this technique, whereby the mechanical valve structure is discretised into a very large number of small components. There are several examples of this technique in the literature, such as de Vries et al[de Vries *et al.*, 2003], Thomson et al[Thomson *et al.*, 2005] and Tao et al[Tao *et al.*, 2007].

A micro-scale description may simulate an impressive array of behaviours, and certainly embodies a detailed picture of the valve mechanics. However, from a phenomenological viewpoint such models pose a rather tricky problem. It is not a trivial task to extract the fundamental behaviours from a micro-scale model. There are such a huge number of parameters that it may be difficult to understand how they are actually working together to produce the observed behaviour. The issue depends somewhat on the objective of the investigation, be it to simulate the 'best sound', or to simulate a 'good sound' using an efficient model. From a deductive physical standpoint, however, it is highly desirable to formulate the simplest possible description of a musical valve, which still embodies all of the fundamental behaviours. This stripped-down approach seeks to find the 'essence' of the system, and is the basis of the macro-scale description.

Figure 2.2: The macro-scale lumped element approach to musical valve modelling. The entire lip mass is condensed into a single 'lump' of mass m, connected to a rigid bounding wall with a spring of stiffness k and damping B.

2.4.2 Macro-scale description

The macro-scale description of musical valves attempts to describe the valve mechanics using the simplest means possible. The approach reduces the complexity of the multiple layers and constructs of biological tissue to a small number of physical variables. This is the 'lumped element' technique, where the 'elements' are the physical variables and parameters.

The 'elements' of a lumped element model are masses, springs and dampers. It is really just a theoretical implementation of the 'mass on a spring' experiment that is common throughout physics teaching labs the world over. The elements may be described with simple Newtonian equations that calculate the motion of the masses, depending on the stiffness and damping of any connecting springs, due to the applied driving force. In the case of musical valves the force, be it acoustical or aerodynamic in origin, is provided by the surrounding fluid field. Arrangements utilising one or more masses attached to a number of springs and dampers are possible.

The simplest implementation of a lumped element model represents one of the valve walls as a single mass attached to a rigid wall with a damped spring. Such an arrangement is shown in figure 2.2. The fundamental challenge in lumped element musical valve modelling is clear from figure 2.2; how can the small parameter space of the model be related to the complex biological structure of the valve walls? In short, a lumped element model may have just a handful of parameters, but it is not immediately clear how they should be chosen. It is possible to use a trial and error process to estimate the parameter values, but this does not provide a very scientifically satisfying solution.

2.4.3 The mechanical response

The mechanical response provides one means for the characterisation of musical valve mechanics. It is an experimental technique that allows information about global resonances to be extracted from a real world musical valve. This information may

then be related to the simple masses and spring stiffnesses of a lumped element model.

The mechanical response of a musical valve is measured by subjecting the valve to a known driving force and measuring the resulting motion. It is rather like a younger brother periodically prodding his elder sibling until he becomes upset; for certain optimum prodding frequencies the persecuted senior will react particularly strongly. Thus by subjecting a musical valve to a wide range of driving frequencies it is possible to reveal the underlying natural resonances.

The analogy can actually go even further than this simple example. For the younger brother to truly understand the pressure points of the elder he must be able to relate both the prodding frequency and amplitude to the response; he must calibrate his prodding. It may be possible to elicit a large response from the elder with extremely vigorous prodding well away from a natural 'anger' frequency, simply because the large input produces a large output. Similarly, a violent response may be obtained with a relatively gentle prodding action if the younger brother finds precisely the right frequency. For a truly scientific prodding study the younger brother should try thus to irritate the elder with a constant amplitude over the entire prodding frequency range. The practical implications of this calibration requirement are outlined in section 3.3.

Calculation of the mechanical response

A mechanical response measurement is performed by driving the valve surfaces with an acoustic pressure generated by a loudspeaker, and recording the time domain physical motion of the valve as it responds to the driving. The mechanical response is then evaluated in the frequency domain by performing a frequency response function (FRF) between the driving signal and the valve motion signal.

A pressure drop Δp_{mr} is established across the valve by the acoustical signal of the loudspeaker. This forces the valve walls to execute low amplitude vibrations. It is important that the vibrations are low amplitude because the key method used to interpret the results (see section 2.7.1) relies implicitly on the assumption of low amplitude mechanical motion. A small microphone positioned close to the valve, on the loudspeaker side, records the pressure, producing a time domain signal $p_{mr}(t)$. The assumption of a total pressure loss across the valve, due to an assumed turbulent dissipation of the acoustic pressure on its downstream side, means that measured microphone pressure can be directly equated to the total pressure drop

$$\Delta p_{mr}(t) = p_{mr}(t). \tag{2.2}$$

The valve motion may be measured in a number of ways, several of which are described in detail in section 3.3. The important outcome is that a time domain signal $h_{mr}(t)$ is produced which describes how the valve moves in response to the acoustic driving.

A basic mechanical response formulation may be written as the frequency domain ratio of the valve motion to the driving pressure drop

$$\widetilde{M_{mr}}(\omega) = \frac{\widetilde{h_{mr}}(\omega)}{\widetilde{\Delta p_{mr}}(\omega)}. \tag{2.3}$$

where $\widetilde{h_{mr}}(\omega)$ and $\widetilde{\Delta p_{mr}}(\omega)$ are the calculated by taking the Fourier transforms of the acoustic pressure drop Δp_{mr} and the valve motion signal h_{mr}.

In practice mechanical response curves are evaluated using a frequency response function. There are a variety of such formulations available, which are suitable for a wide range of different situations[Mulgrew *et al.*, 1999]. They all rely on a combination of the averaged power spectrum of the lip motion $\widetilde{G_{hh}(\omega)}$, and the averaged cross-spectrum of the lip motion with the microphone pressure $\widetilde{G_{hp}(\omega)}$. The response curves in this work all use the frequency response function

$$\widetilde{H_{mr}}(\omega) = \frac{\overline{G_{hp}(\omega)}}{\overline{G_{hh}(\omega)}}. \tag{2.4}$$

The frequency domain spectral estimates are calculated from the time domain data using the following equations

$$\overline{G_{hh}(\omega)} = \mathcal{F}[h_{mr}(t) * h_{mr}(t)] \tag{2.5}$$

$$\overline{G_{hp}(\omega)} = \mathcal{F}[h_{mr}(t) * p_{mr}(t)] \tag{2.6}$$

where $\mathcal{F}$ represents a Fourier transform, and $*$ signifies a time domain convolution.

A frequency response function based on the power and cross-spectrums of the time domain data is a superior tool to the basic ratio of Fourier transforms used by equation 2.3. This is because it prevents large amplitude spikes resulting from division by zero, and can readily incorporate spectrum averaging to improve the signal to noise ratio of the measurement.

This is a standard function in the PULSE series of digital signal processing tools by the Brüel & Kjær company. A number of these processing tools were used in this work, and they are outlined in more detail in section 3.3.

Equation 2.4 is complex which means that the phase lag between the driving pressure and the valve response may be easily obtained at any frequency, defined as

$$\angle\widetilde{H_{mr}}(\omega) = \angle\widetilde{h_{mr}}(\omega) - \angle\widetilde{\Delta p_{mr}}(\omega). \tag{2.7}$$

A example of a mechanical response measurement is shown in figure 2.3. The top curve shows the magnitude response, the lower curve shows the phase response. There appear to be at least three resonances present in this measurement. They may be

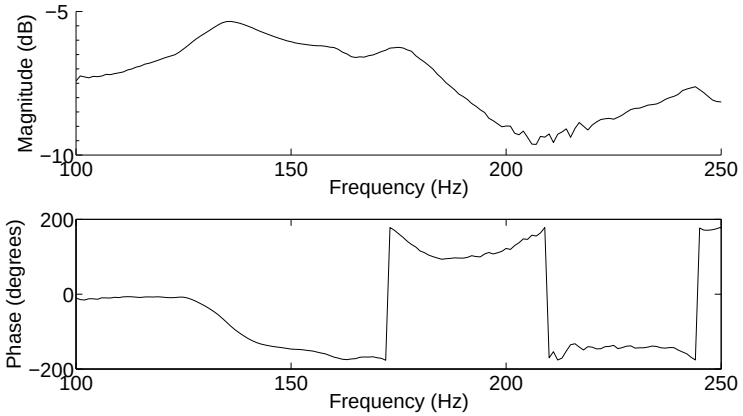

Figure 2.3: An example mechanical response curve. The upper line is the magnitude, the lower is the phase. There appear to be at least three resonances in the frequency range displayed in the plot, located around 140Hz, 180Hz and 245Hz.

identified by the peaks in the magnitude curve, and also by examining the behaviour of the phase response. Where the phase curve crosses -90^o (around 140Hz and 245Hz) or $+90^o$ (around 180Hz) it would be possible for a self-sustained oscillation regime to be established which couples the mechanical resonance to an acoustical one in a suitable resonating air column. The explanation and implications of this important fact are described in section 2.7, on the physics of the lip-reed.

2.4.4 *In vitro* modelling

Mechanical response measurements provide an important means for characterising the mechanical properties of musical valves. Up to now these measurements have had to be carried out on artificial mechanical replicas of the real musical valves, rather than on true biological valves. These *in vitro* models have been developed as scientifically controllable alternatives to human subjects. They provide three distinct advantages over real biological valves:

- They facilitate the use of extensive measurement equipment, such as microphones and flow-meters, which would not be possible with human subjects (for example, it is not an easy exercise to insert a probe microphone into the trachea).
- They allow something close to objective control of the valve parameters, which is crucial for a thorough scientific analysis, and which is rather difficult to achieve with human subjects. This subject is discussed in some detail in chapters 3 and 4.
- They are not pre-disposed to musical ideas and techniques: they are 'stupid', and rely entirely on the careful set-up and adjustment of the experimentalist.

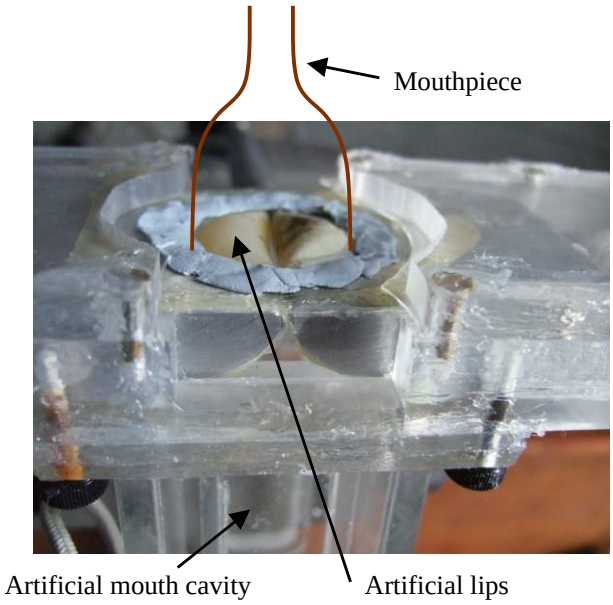

Figure 2.4: Replica B, an example of an *in vitro* artificial brass player that is able to simulate a wide range of playing behaviours (see section 3.2.3). The artificial lips are constructed from water-filled latex. The embouchure is controlled by adjustment of a water column connected to the lips via plastic tubing. A mouthpiece or other downstream bore can easily be coupled to the downstream surface of the artificial lips.

An example of an artificial brass player is shown in figure 2.4. This system is composed of several components:

- Artificial lips - water-filled latex tubing simulates the soft, deformable tissues of the real lips.
- Artificial mouth - this cavity is constructed from perspex, and its volume and shape may be adjusted.
- Mouthpiece and instrument - a normal trombone mouthpiece and instrument may be connected to the downstream side of the artificial player.

Similar systems exist for simulation of an artificial singer. The differences between an artificial brass player and an artificial singer are rather small. The size of the 'lips' must be reduced to match the dimensions of the vocal folds, and the geometry of the connecting ducts must be similarly altered. An artificial singing system known as *replica C* is described in chapter 3. Details of a new version of the artificial brass player, known as *replica B*, which was developed in collaboration with *replica C* are also presented. *Replica C* was used for some of the mechanical investigations in part II of this thesis.

2.4.5 Summary

The apparent crudity of the lumped element approach, while certainly requiring careful application, does allow for something approaching objective control in a computational implementation of the model. It is vitally important, however, that a framework exists to relate such a simple description to real world, measurable quantities. The technique of mechanical response evaluation is of crucial importance in this regard.

Further detail on the computational implementation of lumped element models is provided in section 2.9.

2.5 The dynamics of the flow through the valve

The flow of air through a musical valve is a crucial feature of both the oscillation regime, and the resulting sound production. The dynamics of the valve flow directly determine the driving forces on the valve surfaces, and thus their resulting motion. In a first assumption, the resulting oscillatory volume flow through the valve will then act as a monopole sound source[Zhang *et al.*, 2002]. More complex features of the flow may also lead to secondary source terms, such as noise production from vortices[Kob *et al.*, 2005; Brücker *et al.*, 2004; Neubauer *et al.*, 2007].

One of the main subjects of this thesis is the nature of the aerodynamic flow through musical valves and the resulting aero-elastic interaction between the flow and the valve. This is a complex theoretical subject which may be approached from several angles. The simplest approach involves a severe reduction in the complexity of the flow dynamics to a small number of equations which may be studied with reasonable objectivity in computational models. This has been the approach adopted for much of the preceding century of musical valve research, and will be outlined in this section.

A more rigorous approach is to attempt to describe and solve the flow dynamics using the full Navier-Stokes equations, either in commercial software packages or in bespoke research developments. There are a variety of ways of doing this[Decker and Thomson, 2006; Tao *et al.*, 2007; Thomson *et al.*, 2005; de Vries *et al.*, 2003; de Vries *et al.*, 2002], but the methods will not be dealt with in detail in this thesis. Rather, the objective will be to provide a more simplistic, intuitive description of the flow, which is the essence of the first approach. The emphasis will be on capturing the important physics in the simplest way possible. This will then be used in conjunction with the experimental work to develop a framework for describing the valve airflow.

2.5.1 Dimensionless analysis of the flow aerodynamics

When considering the fluid dynamics of a musical valve, a useful first step is to quantify all the relevant non-dimensional fluid parameters. These allow the system to be categorised in the general scope of fluid behaviours. They provide a quantitative

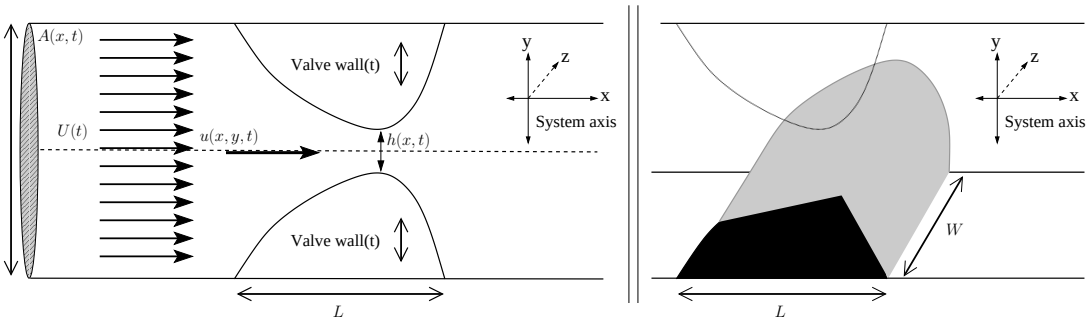

Figure 2.5: At left is a schematic cross-section of a musical valve showing the fluid dynamical quantities that determine the relevant non-dimensional parameters of the system. $A(x,t)$ is the cross-sectional area of the duct as a function of horizontal position x and time, $h(x,t)$ is the valve open height, L is the valve thickness, W is the valve length, $u(x,y)$ is the local fluid velocity and U is the volume flow. At right a three-dimensional projection is shown to illustrate the orientation of the valve width W.

benchmark for the valves under consideration, both in terms of other musical valves and in terms of standard fluid dynamic experimental setups such as laminar and turbulent pipe flow.

Figure 2.5 shows a schematic cross-sectional diagram showing the layout of a general purpose musical valve. It includes the fluid dynamical quantities used to define the dimensionless fluid mechanical parameters in the following subsections of section 2.5. It also shows the overall coordinate scheme adopted throughout this thesis, and the orientations of the various physical dimensions. The vertical arrows within the 'valve wall' regions indicate that the shape of these features can vary over time, resulting in a range of values for the valve height h.

Reynolds number

The flow though a musical valve may be considered as a special case of pipe flow[Fletcher and Rossing, 1991; Hirschberg *et al.*, 1996b]. The Reynolds number provides an important measure of the level of turbulence in fluidic systems[Tritton, 1988], and is thus a relevant quantity for characterising the musical valve flow. It may be defined as the ratio of the inertial to the viscous forces

$$Re = \frac{\rho u_s^2 / D}{\mu u_s / D^2} = \frac{u_s D}{\nu} \tag{2.8}$$

where u_s is the mean fluid velocity, D is a characteristic length of the system, μ is the fluid viscosity and ν is the kinematic viscosity.

The exact choice of D depends on the geometry of the system. In the case of musical valves the minimum height of the flow channel is the most crucial quantity. This is because, in order for a boundary layer assumption to be valid (see section 2.5.2), the

Physical quantity	**Valve type**	**Value**
Thickness L	*Lip-reed*	10-15mm
	Vocal folds	6-9mm
Height h	*Lip-reed*	0-8mm
	Vocal folds	0-3mm
Width W	*Lip-reed*	20 -30mm
	Vocal folds	14-18mm

Table 2.1: Physical quantities relevant for a dimensionless analysis of musical valves (from [Pelorson *et al.*, 1994; Vilain, 2002]).

bulk flow region must be much thicker than the boundary layer regions. This effect is strongly influenced by the total channel width, and is of particular relevance because of the oscillatory nature of musical valves which means that the minimum channel width varies over time. Thus the definition of the Reynolds number for the application of musical valves may be written

$$Re = \frac{u_s h}{\nu} \tag{2.9}$$

where h is the (variable) valve height.

It is immediately evident that the value of the Reynolds number is dependent on the precise height of the valve, and thus on the precise phase of its oscillation. It is maximal at the maximum opening of the valve, which, drawing on the physical and fluid values shown in tables 2.1 and 2.2, corresponds to a value of approximately 10^3. This moderately high value indicates that a non-viscous approximation for the bulk of the flow would be reasonable for much of the oscillation cycle[Pelorson *et al.*, 1994].

The Bernoulli equation describes the physics of such flows, and is ubiquitous in descriptions of musical valve flow. It states that the sum of the static, dynamic and gravitational pressures along a streamline of the flow must be conserved

$$p + \frac{\rho u_s^2}{2} + \rho g = constant \tag{2.10}$$

where p is the static pressure, u_s^2 is the fluid velocity and g is the gravitational constant.

As the valve height becomes small, however, the effects of viscosity become increasingly important. This is because the 'bulk flow' thickness becomes closer to the boundary layer thickness. The assumption of a boundary layer flow regime thus becomes rather more tenuous, and the flow should really be described by the fully viscous Navier-Stokes equations, or a suitable approximation[Hirschberg, 1992].

Fluid quantity	**Value (at 20°C)**
Viscosity μ	1.83×10^{-5} kgm^{-1}s^{-1}
Kinematic viscosity ν	1.51×10^{-5} m^{2}s^{-1}
Density ρ	1.20 kgm^{-3}

Table 2.2: Fluid dynamical quantities relevant for a dimensionless analysis of musical valves operating in air at standard temperature and pressure (S.T.P)

Strouhal number

The oscillation of a musical valve is clearly a periodic phenomenon which results in a periodically fluctuating, unsteady flow field. Thus the Strouhal number is a relevant dimensionless parameter. It provides a measure of flow unsteadiness which may be used to quantify the relevance of a quasi-steady description of the flow (see section 2.5.3). It is defined as the ratio of the acceleration due to the unsteadiness of the flow to the convective acceleration due to non-uniformity of the flow, and may be written

$$St = \frac{f_0 d}{u_s} \tag{2.11}$$

where f_0 is the oscillation frequency and d is a relevant flow distance (usually taken as the streamwise valve length[Hirschberg, 1992; Pelorson *et al.*, 1994]).

Mach number

The Mach number provides a measure of the compressibility of a flow. When it is squared (M^2), it describes the density fluctuations in a flow, relative to the static fluid density. It is defined as

$$M = \frac{u_s}{u_0} \tag{2.12}$$

where u_0 is the speed of sound in the fluid medium.

The full Navier-Stokes equations can be significantly simplified if the flow is assumed to be incompressible. Further simplified descriptions of fluid flow, such as the Euler and Bernoulli equations, inherently rely on this assumption. In the case of musical valve oscillations, the maximum flow speeds are of the order of 10^2ms^{-1}, which means the Mach number is typically of order 10^{-1}, and the flow may be treated as incompressible.

Helmholtz number

The oscillation of a musical valve is a process that produces sound waves. By their very nature sound waves are compressions and rarefactions of their host medium. This seems at odds with the conclusions of the previous section, 2.5.1, where the Mach number was shown to be small enough to permit an incompressible description of the flow. This

apparent discrepancy may be understood if the length scales of the air compressions are considered. These relevance of compressibility effects resulting from the surrounding acoustic field may be estimated by calculation of the Helmholtz number, defined as

$$H_H = \frac{h}{\lambda_0} \tag{2.13}$$

where λ_0 is the acoustical wavelength.

The Helmholtz number is thus typically about 10^{-3}, which is sufficiently small to maintain an incompressible assumption.

Flow dimensionality

The full Navier-Stokes equations describe a three-dimensional flow field. However, for an appropriate pipe profile the dimensionality of the flow may be reduced. In the case of musical valves such as the lip-reed and the vocal folds, the valve length (the z dimension) is typically an order of magnitude larger than the valve height (the y dimension). This relationship may be non-dimensionalised by a characteristic geometrical parameter N_c, such that

$$N_c = \frac{h}{L}. \tag{2.14}$$

The flow may be approximated to a two dimensional description if N_c is much smaller than 1. Drawing from the values in table 2.1, it is typically 10^{-1} at most for the vocal folds, and about 4×10^{-1} at most for the lip-reed. In the case of the vocal folds it is thus reasonable to assume that the flow behaviour is confined to the x and y dimensions, as shown in figure 2.5. In the case of the lips this assumption is more tenuous, but given the fact that small lip widths are rarely seen with large lip widths[Bromage, 2006], the reduction of the flow field to two dimensions is not unreasonable. Under the two-dimensionalisation condition, the flow velocity field may this be written

$$u = u(x, y, 0) = u(x, y). \tag{2.15}$$

2.5.2 A simple theoretical description of the flow aerodynamics

The airflow through musical valves can be described with the physics of pipe flow. The valve, be it the lips or the vocal folds, sits within a pipe system and acts as an obstruction to the smooth flow of the fluid. Four simple caricatures of the possible flow dynamics are shown in figure 2.6. These examples will help to explain the fundamental flow phenomena encountered during the oscillation of musical valves.

In the absence of any valve, and for an appropriate range of the Reynolds number, steady flow in a pipe may be considered as essentially frictionless and laminar. This

means that the inertial forces dominate the viscous forces, and the velocity gradients in the bulk of the flow remain small. It may thus be described by a simple potential flow formulation. The flow is expected to remain attached to the walls of the pipe, regardless of changes in the pipe profile. The required range of the Reynolds number for this fluid behaviour depends on the specific geometrical and fluid conditions, but for configurations such as a simple musical valve it should be around 2000, given the values in table 2.1[Fletcher and Rossing, 1991]. This is high enough that the effects of viscosity are small, but low enough that the flow remains in the laminar regime.

The flow shown in part (a) of figure 2.6 represents such a situation. The total flux of mass must be conserved through all cross-sections. This important fact is described by the mass continuity equation

$$\frac{\partial \rho}{\partial t} + \nabla \cdot (\rho \vec{u}) = 0. \tag{2.16}$$

However, for flow in an incompressible medium, such as can be assumed for musical valves, this reduces to a volume flow continuity equation

$$\nabla \cdot \vec{u}(x, y) = 0. \tag{2.17}$$

This equation is of fundamental importance to the physics of musical valve flow. It states that the total volume flow must be the same through any cross-section of the valve, and its connecting upstream and downstream pipes; flow cannot be 'destroyed'. The volume flow itself can be defined as the product of the velocity field with the cross-sectional area through which the flow passes. In the case of a two dimensional flow field, this may be written

$$\vec{U}(x, y) = \vec{u}(x, y) \cdot A. \tag{2.18}$$

If a one dimensional, quasi-parallel velocity field is assumed, as with the simplest potential flow, the equation reduces to the scalar form of the volume flow

$$U(x) = u(x)A \tag{2.19}$$

This equation is widely used in simple theories of musical valve flow. The valve and its connecting pipes are typically described by a series of tubes with simplified circular cross-sections. This portrays a rather caricatured description of the true pipe flow, but one that may be easily used within computational models.

Part (b) of figure 2.6 shows a laminar flow through a rigid constriction similar in profile to a musical valve. As with case (a) the volume flow is conserved, and the flow remains attached to the pipe walls. Intriguingly, the flow is unaltered by the presence of the valve. The mean flow speed increases through the valve to compensate for the constant volume flow condition of equation 2.19, and then slows on exit from the valve

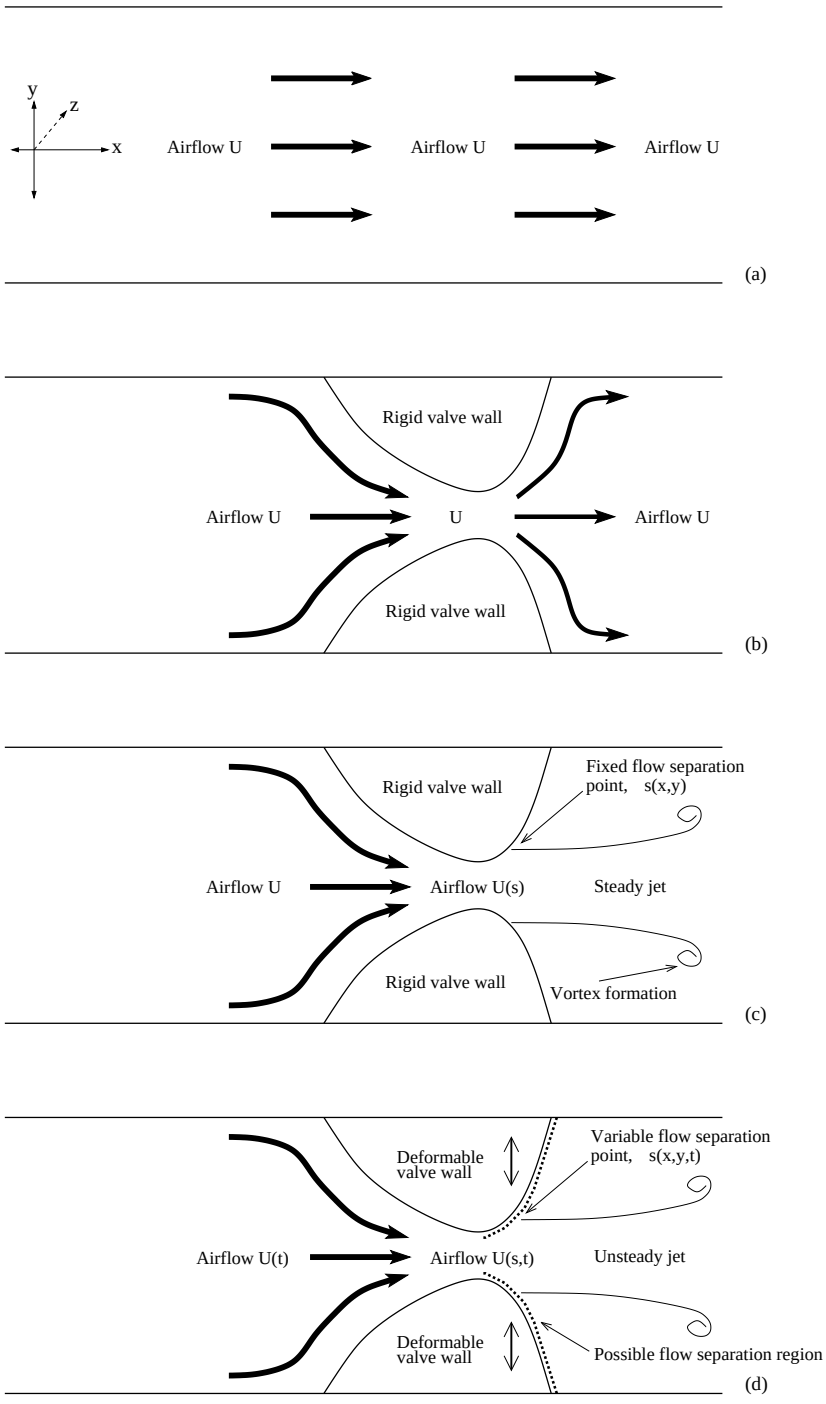

Figure 2.6: A schematic diagram of simple pipe flow regimes: (a) unobstructed laminar flow, (b) obstructed laminar flow, (c) obstructed laminar flow leading to steady jet formation, (d) obstructed laminar flow leading to unsteady jet formation.

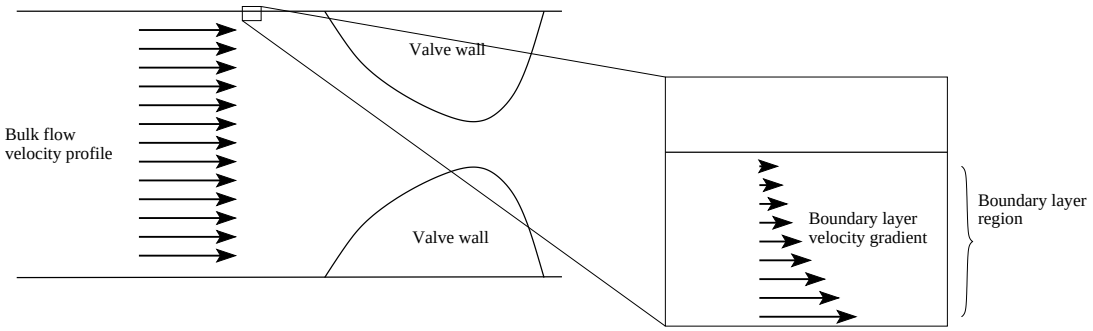

Figure 2.7: A schematic diagram of a simple boundary layer description of pipe flow. The length of the arrows corresponds to the velocity magnitude. The blown-up region shows a possible variation of the velocity profile in the boundary layer region close to the valve wall.

to regain the original speed. The important conclusion from this is that there is no way to explain a modulation of the valve airflow with a simple laminar description of the fluid mechanics.

Part (c) of figure 2.6 shows the same geometry as part (b), but with a more realistic description of the fluid behaviour. The description builds on the assumption of an essentially laminar, inertia-dominated flow corresponding to a moderately high Reynolds number. The key improvement is that, while the effects of viscosity are negligible in the bulk of the flow, they are non-negligable in the regions close to the valve walls. These regions are called *boundary layers*, and the physical description is known as the *boundary layer assumption*[Schlichting and Gersten, 2000]. The behaviour of the fluid in these regions must be described with a separate set of equations to the bulk flow. In particular, the velocity profile must vary from that of the bulk flow at the inner edge of the boundary layers, to the no-slip condition of zero-velocity at the walls, as shown in figure 2.7. Such velocity gradients lead to a significant flow vorticity in the boundary layers, which will be shown to be crucial to the behaviour of the flow as it encounters the varying geometry of the valve walls.

The behaviour of a potential-type flow with viscous boundary layers depends strongly on the geometry of the pipe. For a smooth, continuous geometry, such as in part (a) of figure 2.6, the flow should remain attached to the pipe walls provided that the flow velocity remains constant. However, if the flow encounters sudden changes in geometry, the phenomenon of *flow separation* can be encountered. In such a case the flow may fully detach from one or more of its bounding surfaces surfaces and form a jet.

Flow separations are seen widely in the physical sciences. Jet engine exhaust plumes and tea poured from a pot provide simple examples. In computational models of fluid flows, including those of musical valve flows, the description of the phenomena of flow

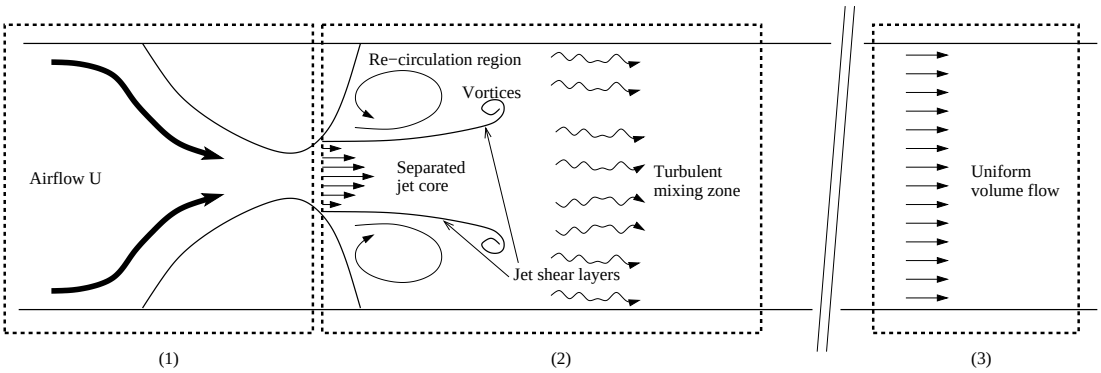

Figure 2.8: Details of the separated jet flow, downstream of a musical valve. There are three primary regions of interest: (1) The inflow region. (2) The separated free jet, including the core, shear layers, vortices and turbulence. (3) The far-field region.

separation is vital. In fact, the location of the flow separation point can be shown to determine the total flux through the valve (see section 2.5.3).

There are several techniques which may be used to describe computationally the flow behaviour and to calculate any flow separations. The 'brute force' approach involves a full numerical simulation of the Navier-Stokes equations, including viscosity. However, we have already seen that for much of the oscillation cycle of a musical valve the flow may be reasonably described with a boundary layer approximation. This leads to the widely-used approach whereby the flow is described using a combination of the Bernoulli equation in the bulk region, and a separate set of equations in the boundary layer. These equations include viscosity terms and must be solved numerically[Pelorson *et al.*, 1994]. It should be noted that the basic Bernoulli formulation may be improved by the addition of inertial terms to the equation.

The physics of flow separation is a topic with an extensive body of theoretical and experimental work[Tritton, 1988; Schlichting and Gersten, 2000], and as such it will not be further explained in this thesis. Rather, the focus will be on the conditions where it might be a relevant phenomenon, and on the implications it might have for the behaviour of a musical valve.

Part (d) of figure 2.6 portrays much the same flow behaviour as part (c), but with deformable valve walls. In this case the aerodynamics around the valve lead to aerodynamic forces that can act on the valve walls and impart mechanical motion. Under appropriate conditions the motion can be periodic, resulting in a periodically oscillating jet flow through the valve. This may act as an acoustical source, allowing for the creation of an acoustical standing wave in the downstream section of the valve. In turn, this acoustical standing wave can provide a further pressure forces on the valve walls.

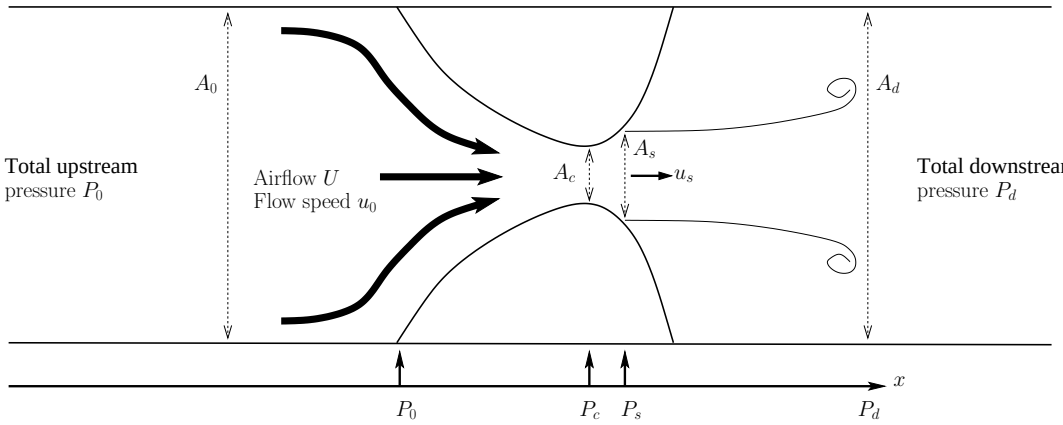

Figure 2.9: Aerodynamic and geometrical parameters applicable in a boundary layer description of the fluid dynamics of a musical valve. The A terms represent cross-sectional areas, the P terms represent total pressures, the v terms represent fluid velocities.

2.5.3 The quasi-steady assumption

The non-dimensional analysis presented in section 2.5.1 has shown that an incompressible boundary layer approximation may be made for much of the oscillation cycle. This greatly simplifies the physics involved, and makes computational simulations considerably more straightforward. However, such simulations also require that the time-dependence of the flow be accounted for with a quasi-stationary approach.

The quasi-steady assumption means that the time-evolution of the flow may be described by a series of discrete 'snapshots' of the flow. Each snapshot is formulated based on the current set of geometrical and aerodynamic parameters. Any resulting motion of the valve is then computed, and the simulation is incremented to the next snapshot. Such an approach neglects unsteadiness in the flow. However, formulations do exist to provide corrective second order terms to improve the description, such as inertial and unsteady corrections to the Bernoulli equation[Ruty *et al.*, 2007; Bailly *et al.*, 2008].

Description of the flow through a musical valve

The situation portrayed in part (d) of figure 2.6 is certainly the most relevant for a study of oscillating musical valves. It is important to understand how such a configuration can lead to the generation of a periodic jet flow through the valve, and in particular, how the nature of the flow separation is a critical controlling factor.

The fluid behaviour is expected to change dramatically, depending on the spatial position within the valve, and the phase of the oscillation cycle. It is thus useful to consider the behaviour in terms of a small number of key regions. It will then

P_0	Total upstream overpressure
P_c	Total pressure at the minimum valve constriction
P_s	Total pressure at the flow separation point
P_d	Total far-field pressure (i.e. atmospheric pressure)
A_0	Cross-sectional area at entrance to valve (i.e. upstream cross-section)
A_c	Cross-sectional area at minimum valve constriction
A_s	Cross-sectional area at the flow separation point
A_d	Cross-sectional area at valve exit (i.e. downstream cross-section)
u_0	Upstream flow velocity
u_s	Flow velocity at separation point

Table 2.3: Aerodynamic and physical quantities labeled in figure 2.9.

be possible to formulate clearly the theoretical description of the flow, based on the applicable fluid and geometrical parameters of the various regions. In reality, any flow may be described by a single formulation, the Navier-Stoke equations, but it has already been emphasised that the approach of this work is to present and investigate the applicability of simplified flow descriptions. Such descriptions inherently rely on a discretisation of the flow regions.

Figure 2.8 presents a simplified schematic of the flow through a musical valve. The figure shows the airflow entering the valve from the left, interacting with the valve walls, separating from a point along the downstream region of the valve, forming a free jet and then degrading through vortex formation and turbulent dissipation into a uniform volume flow field. This diverse selection of flow behaviours may be broken down into three key regions.

- ***Region 1 - Inflow and separation***

  The upstream flow region, from the source up to the point of flow separation, may be described by a boundary layer approximation for much of the glottal cycle. The Bernoulli equation can be used to describe the bulk flow behaviour, while a separate description including viscous effects is required in the boundary layers in order to calculate any flow separations. A full theoretical outline of such an approach will not be presented in this work. The most important conclusion from an application of this theory is that the flow is expected to separate from the valve walls where there is an appropriately rapid change in the geometrical profile, and when the flow has an appropriate value of the Reynolds number (typically 10^3)[Pelorson *et al.*, 1994; Lous *et al.*, 1998].

  The aerodynamic and geometrical parameters relevant for the incompressible, quasi-stationary description of the flow in region 1 are shown schematically in figure 2.9. The parameters are defined in table 2.3.

The pressures in figure 2.9 are described as 'total pressures' because each of them is the sum of a static and an acoustic contribution. It is thus necessary to more precisely define the pressure terms, as shown below

$$P_0 = \bar{p_0} + p_0 \tag{2.20}$$
$$P_c = \bar{p_c} + p_c \tag{2.21}$$
$$P_s = \bar{p_s} + p_s \tag{2.22}$$
$$P_d = \bar{p_d} + p_d. \tag{2.23}$$

The Bernoulli equation may be applied along a streamline from the upstream flow source to the flow separation point

$$P_0 + \frac{\rho v_0^2}{2} = P_s + \frac{\rho v_s^2}{2}. \tag{2.24}$$

Assuming a quasi-one dimensional bulk flow field, the volume flow defined in equation 2.19 must be conserved at all locations along the pipe system. Equation 2.24 may thus be written

$$P_0 + \frac{\rho U^2}{2A_0^2} = P_s + \frac{\rho U^2}{2A_s^2}. \tag{2.25}$$

This equation reveals one of the principle driving forces on the valve surfaces, namely the so-called 'Bernoulli force'. Where the system cross-section becomes narrow, such as between the valve walls, there must be a corresponding local drop in the static pressure to maintain the equality of the equation. This apparent 'suction' is one way for the flow to impart energy to the valve walls.

The fundamental condition for oscillation is that, as with the child and swing analogy in section 2.2.1, over a single cycle the flow must impart more energy to the valves walls than is dissipated through mechanical friction. For the Bernoulli force to impart *any* net energy, however, it must vary with parameters other than the valve opening[Hirschberg, 1992]: there must be a phase shift between the valve motion and the Bernoulli force. If this is not the case, and the valve oscillates in a rigid shutter-like motion, any energy imparted to the valve walls by the Bernoulli force during the closing phase will be returned to the flow during the opening phase in a cycle of endless energy exchange

$$E_{closing} = \int_{h_{max}}^{h_{min}} F_B dh = +W_B \tag{2.26}$$

$$E_{opening} = \int_{h_{min}}^{h_{max}} F_B dh = -W_B \tag{2.27}$$

where dh represents the infinitesimal valve open height.

The Bernoulli force performs positive work during the closing phase when the valve motion and the suction force are in the same direction, and negative work during the opening phase when they are anti-parallel. In this scenario oscillations will soon die out as energy is drawn away from the Bernoulli exchange by mechanical friction within the valve structure. To sustain oscillation, the magnitude of the work performed by equation 2.26 must be greater than that of equation 2.27. This asymmetry in the Bernoulli driving force may be achieved either by an evolution of the valve geometry[Ishizaka and Flanagan, 1972], a movement of the flow separation point[Hirschberg, 1992] or a inertial delay in the pulse of the airflow through the valve[Titze, 1988].

Re-arranging equation 2.25 in terms of the volume flow, and writing the total pressure difference across the valve as ΔP, the following is obtained

$$U = \sqrt{\frac{2\Delta P}{\rho}} A_s \tag{2.28}$$

where the $\frac{1}{A_0^2}$ term has been neglected as, in general, $A_0 \gg A_s$ and so this term is rather small.

This equation describes the simplest possible model for the airflow through a musical valve. It makes no account of inertial, viscous or unsteady effects. However, an unsteady form of the Bernoulli equation does exist, and can be implemented to improve the model[Hofmans *et al.*, 2003; Vilain, 2002; van Hirtum *et al.*, 2007]. It is also possible to add correction terms for viscosity in the bulk flow region[Pelorson *et al.*, 1994]. The use of these equations in computational models is discussed in section 2.9.

Equation 2.28 is written in terms of the total pressure difference across the valve. However, a further common assumption is that the acoustic pressure upstream of the valve is negligibly small. In the case of the vocal folds this can be justified by the fact that the region upstream of the folds is highly damped by the lungs. In the case of the brass player, the assumption is justified by the very large difference in the acoustic impedance between the relatively wide vocal tract, and

the narrow instrument tube. This difference suggests that the acoustic pressure would be much larger in the instrument mouthpiece than in the vocal tract, and so as a first approximation contributions at the vocal tract side are negligible.

The static downstream pressure head is quickly depleted as the flow becomes transitional and turbulent, and it is often assumed to be close to that of the atmosphere beyond the valve system[Hirschberg, 1992; Hirschberg *et al.*, 1996b; Campbell, 1999]. However, under certain conditions it may be possible for the flow to maintain a static pressure head for some distance downstream. This is discussed below in the section on Region 2 physics.

Whatever happens to the static pressure head, if the valve is oscillating and radiating sound the downstream acoustic pressure is clearly not zero. In the case of a brass instrument, in particular, the acoustic pressure in the mouthpiece of the instrument can be of the order of several kPa, and can thus present an appreciable driving force over the downstream surfaces of the valve. In the case of the vocal folds the acoustic pressure is generally much less, but in a comprehensive theoretical model it really cannot be ignored[Campbell, 1999; Titze and Story, 1997; Titze, 2004; Rothenberg, 1981; Guerin, 1981; McGowan, 1988; Hirschberg *et al.*, 1996a]. This issue is discussed further in the section on Region 2 physics.

The oscillation of a musical valve is driven by the pressure forces exerted by the surrounding fluid field. These can be static pressures, such as those associated with the Bernoulli equation, and dynamic pressures, such as those associated with the acoustic fields in and around the valve. It has already been shown at the start of section 2.5.2 that the geometry of the valve can have an effect on the volume flow through the valve, and the resulting pressure field. It is now important to examine the scope of possible valve geometries in more detail, and their likely effects on the flow.

Figure 2.10 shows two possible profiles of a musical valve. Part (a) shows a smooth entry into the valve followed by an abrupt exit (region 1 in figure 2.8). The minimum constriction corresponds to the extreme downstream end of the valve. This geometrical configuration is known as a convergent profile. The flow is forced to separate at the end of the valve, where there is a sudden, rapid expansion of the profile. This causes the flow to rapidly decelerate, and leads to the creation of a large adverse pressure gradient close to the valve walls. If the expansion is sufficiently abrupt, this pressure gradient may be large enough to imply a separation of the flow from the walls[Tritton, 1988].

Part (b) shows a smooth entry into the valve up to the minimum constriction, followed by a smooth divergent profile down to the downstream end of the valve. The minimum constriction occurs well upstream of the valve termination. The

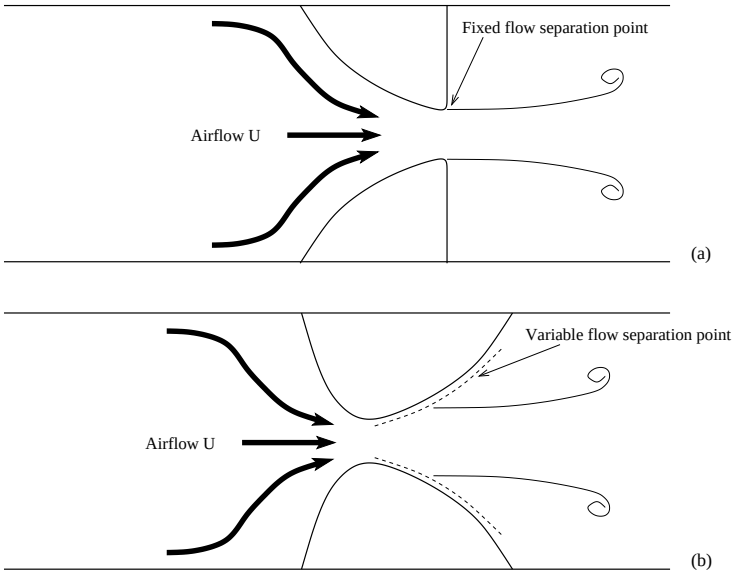

Figure 2.10: Two possible geometrical profiles of a musical valve, and their effects on the flow separation: (a) A convergent profile. (b) A divergent profile.

flow behaviour is much more difficult to predict for this geometry as the gradual divergence causes an instability in the flow separation point. It is impossible to predict this with the basic bulk flow Bernoulli equation. Rather, a boundary layer description is required at the very least, together with an appropriate technique to detect the separation of the boundary layer from the valve wall[Pelorson *et al.*, 1995; Hirschberg *et al.*, 1996c; Vilain *et al.*, 2004]. A flow separation occurs when the fluid velocity adjacent to the wall becomes opposite to that in the bulk flow[Pelorson *et al.*, 1994; Lous *et al.*, 1998]. Recourse to a fully viscous description is also possible, with numerical methods such as finite element and lattice-Boltzmann modelling[Neal, 2002; Alipour and Scherer, 2004; Decker and Thomson, 2006].

- ***Region 2 - Free jet formation and turbulent mixing***

  After the flow has separated from the valve walls a jet is formed. Several of the assumptions that allowed for such a simple description of the flow up to the separation point thus become invalid. In particular, the assumption of a simple potential flow field is no longer applicable, as it is expected that the separated flow will become transitional and possibly turbulent[Neubauer *et al.*, 2007; McGowan, 1988; Shadle *et al.*, 1999; Barney *et al.*, 1999; Triep *et al.*, 2004; Kucinschi *et al.*, 2005; Krane and Wei, 2006; Krane *et al.*, 2007]. This is because the process of flow separation causes the vorticity contained in the boundary layers of the unseparated flow to be injected into the bulk flow of the separated jet[Schlichting and Gersten, 2000]. This process can make the jet become highly rotational, and

under appropriate conditions, it may lead to the total disintegration of a coherent jet structure.

The separated jet is an unstable flow, and a full analytical description of its behaviour is a difficult task. The problem of jet flows is certainly a common one in the field of fluid mechanics[Tritton, 1988; Schlichting and Gersten, 2000], but the inherently unsteady nature of the jet formed through a musical valve is particularly challenging. An experimental investigation of this process, described in chapters 6 and 7, forms one of the key questions of this thesis.

The transitional and turbulent nature of the separated jet leads to a strong mixing of the flow with the surrounding fluid. This causes a significant momentum transfer which leads to a deceleration of the jet. The process is somewhat similar to squirting water through a hose-pipe under a swimming pool. The water separates from exit of the hose-pipe and immediately slows upon mixing with the surrounding water of the pool.

In the case of a musical valve the momentum transfer leads to a significant loss in the static pressure head of the jet flow. It has already been seen in part (b) of figure 2.6 that if a flow remains attached to the valve walls, and the upstream and downstream pipe cross-sections are the same, it is impossible to obtain a pressure difference across the valve. However, with a flow separation and the resulting jet disintegration there is now a mechanism to obtain a pressure difference across the valve. The flow separation also provides a way to control the volume flow through the valve. This is the heart of the 'valve effect' that allows for sustained oscillations of musical valves, and the production of sound.

The geometries presented in figures 2.5 to 2.10 are clearly simplifications of reality. From a conceptual point of view this is not a problem, as it permits a significant simplification of the mechanical and fluid mechanical equations. This allows for a reasonable attempt to model the fundamental oscillation behaviours. However, under certain conditions, it is necessary to investigate the surrounding valve geometry more accurately.

During playing the lips of a brass player are pressed into a mouthpiece. The geometry of this is an important factor in determining some of the playing characteristics of the instrument[Wright and Campbell, 1998; Poirson *et al.*, 2005].

- ***Region 3 - Uniform volume flow field*** After the jet has been formed it expands and disintegrates as turbulence dissipates the flow energy into heat. Well downstream of the jet formation it is generally assumed that a uniform flow field is re-established[Cullen *et al.*, 2000]. This is the uniform volume flow field.

Summary

There are several factors that influence the behaviour of the flow through a musical valve. The valve geometry, the upstream pressure, the downstream couplings and the flow parameters are all crucial elements. For an accurate theoretical understanding of the physics, it is important to consider them all. Similarly, in any useful computational model of a musical valve they should all be considered.

2.6 Acoustic impedance

The downstream bore of a musical valve, be it the narrow tube of a trombone or the wide passage of the vocal tract, may act as an acoustical resonator. For much of the playing range of both brass instruments and vocal folds, the physics of these resonators are well described by linear acoustics. The input impedance is the most useful tool for this analysis. It provides a frequency domain description of the ratio of acoustic pressure to volume velocity at the entrance to the resonator. It may be written as

$$Z(\omega) = \frac{p(\omega)}{U(\omega)} \tag{2.29}$$

where ω indicates that the quantities are considered in the frequency domain.

Under certain conditions the linear acoustical assumption can break down. This remarkable behaviour has been documented in the case of the trombone[Hirschberg *et al.*, 1996a], where shock waves have been shown to occur for very loud playing. Such extreme conditions are not expected in the case of human phonation, though this does not imply a total absence of non-linear acoustical effects. Indeed, the process of vortex formation and turbulent energy dissipation may both provide additional non-linear acoustical sources in both the vocal tract and the brass instrument[McGowan, 1988; Krane and Wei, 2006].

For the simplest phenomenological theories and models of phonation and brass playing, the resonator acoustics are well-described by the linear assumption. The issue of non-linear propagation may be of particular relevance for certain aspects of the sound produced by a musical valve, such as in extremely loud playing of a brass instrument[Hirschberg, 1992], but it seems unlikely to be of consequence to the fundamental function.

2.7 Physics of the lip-reed

The lip-reed is the sound generating mechanism in a brass instrument. It is formed by the lips of the player, pressed into the mouthpiece of the instrument. A schematic diagram of the main components of a brass instrument system is shown in figure 2.11.

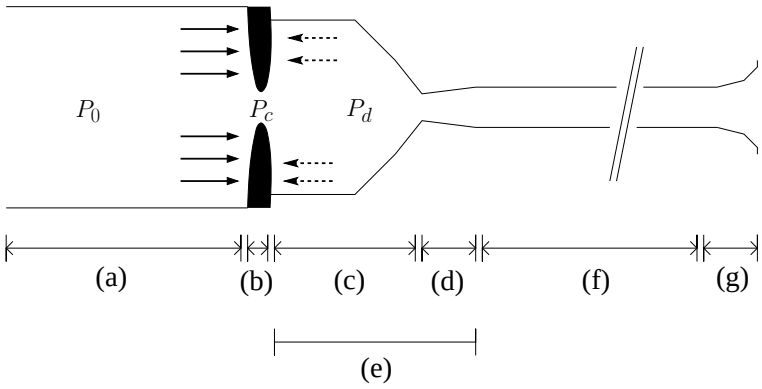

Figure 2.11: A schematic diagram of the layout of a brass instrument (not to scale). The upstream mouth pressure is P_0, the pressure between the lips is P_c and the mouthpiece pressure is P_d. The components are: (a) mouth cavity of the player, (b) player lips (the 'lip-reed'), (c) mouthpiece cup, (d) mouth-pipe, (e) mouthpiece unit, (f) main cylindrical bore of the instrument, (g) flaring bell.

It is possible to explain the oscillation of the lip-reed as a result of an oscillating pressure difference across the lips, from the mouth cavity to the mouthpiece. It has been shown in section 2.5.2 that this pressure difference arises because the airflow through the lips separates from their downstream edge to form a thin jet. The jet then rapidly degrades to form a uniform volume flow field. This process generates an acoustical field which is the source of the oscillating pressure difference.

The lips act as a volume flow valve, permitting a regular series of fluid pulses into the mouthpiece. The periodic volume flow acts as a monopole acoustical sound source[McGowan, 1988; Zhang *et al.*, 2002] which may excite the downstream acoustical resonator. Under appropriate conditions this acoustical energy can accumulate in the resonant modes of the instrument air column and lead to significant acoustic pressures in the mouthpiece. This oscillating acoustical pressure is one of the two key forces involved in the vibration of the lip-reed. Together the with Bernoulli force described in section 2.5.3, a mechanism may be established to transfer energy from these aerodynamic fields to the mechanical structure of the lips. The upstream resonator, the mouth and vocal tract of the player, may also be excited. These resonances are likely to be of significantly less importance than those downstream in most situations. It has been suggested, however, that they may important in providing an acoustical impedance to assist a player in 'buzzing' their lips in the absence of a downstream resonator[Neal, 2002; Richards, 2003].

The dissipation of the jet flow may also provide additional sound sources from processes such as vortex sound generation, though these have been neglected in much of the literature. Indeed, much of the textbook physics on lip-reed function involves severe simplification of the flow dynamics. On the contrary, the companion field of

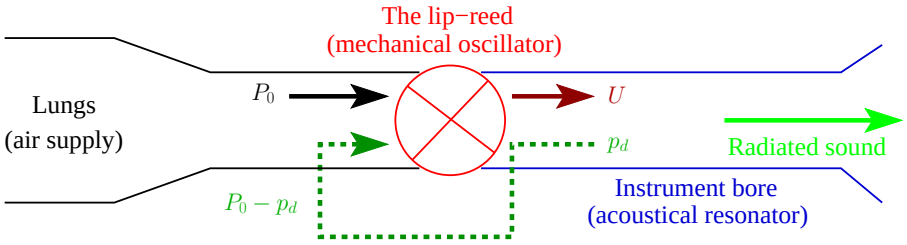

Figure 2.12: A schematic diagram of the flow control feedback loop of the lip-reed. The static upstream pressure is P_0, the oscillating downstream acoustical pressure is p_d, the volume flow through the valve is U.

vocal fold physics has seen considerably more work on the subject[Hirschberg, 1992; McGowan, 1993; Pelorson *et al.*, 1994; Hirschberg *et al.*, 1996c; Thomson *et al.*, 2005; Krane and Wei, 2006], and studies into the lip-reed are increasingly turning to this body of knowledge[Richards, 2003; Vilain *et al.*, 2003; van Hirtum *et al.*, 2007].

2.7.1 Classical reed dynamics

Helmholtz[Helmholtz, 1877] provided the first detailed analysis of musical reed behaviour in the 19^{th} century. His treatment neglected any of the detailed flow dynamics outlined in section 2.5, but provided an important platform upon which much of the proceeding research has been based.

Figure 2.12 shows a schematic diagram of the closed feedback loop traditionally used to model the lip-reed during playing. The lungs supply a nearly constant upstream overpressure P_0, resulting in a flow of air U through the vibrating lips and an acoustical pressure p_d in the mouthpiece. The lip-reed acts as a flow valve, acoustically exciting the downstream resonator with periodic pulses of air. The whole system oscillates close to one of the downstream acoustical resonances.

The musical valve as a second order harmonic oscillator

It is possible to describe the dynamics of the lips using an equation for a second order harmonic oscillator. If the total driving force on the lips is F, and they are driven close to a natural lip resonance ω_v, the equation may be written

$$\frac{d^2h}{dt^2} + \frac{\omega_v}{Q_v}\frac{dh}{dt} + \omega_v^2 h = \frac{F}{m_i} \tag{2.30}$$

where h is the valve opening height, Q_v is the quality factor of the valve resonance and m_i is the effective mass of the valve. If the driving force is provided by a pressure difference across the valve driven from upstream, as in section 2.7.1, equation 2.30 may be written as

$$\frac{d^2h}{dt^2} + \frac{\omega_v}{Q_v}\frac{dh}{dt} + \omega_v^2 h = p_0(\frac{1}{\mu_B} - \frac{1}{\mu_D}) \tag{2.31}$$

where the lip factor μ_D is the lip mass m_i divided by the area over which the upstream pressure acts, in this case the internal face of the lips, and the lip factor μ_B is the lip mass divided by the area of the lip channel. μ_B is related the the Bernoulli effect between the lips (see section 2.5.3). The lip factors may be condensed into a single factor μ_v such that

$$\frac{d^2h}{dt^2} + \frac{\omega_v}{Q_v}\frac{dh}{dt} + \omega_v^2 h = \frac{p_0}{\mu_v} \tag{2.32}$$

which is the main equation used to describe the time domain mechanics of the lips.

Equation 2.32 may be written in the frequency domain as a complex mechanical response function[Cullen, 2000]

$$H(\omega) = \frac{h(\omega)}{p_0(\omega)} = \frac{-j\frac{Q_v}{\omega\omega_v}\frac{1}{\mu_v}}{1 + \frac{j2Q_v(\omega^2-\omega_v^2)}{\omega\omega_v}} \tag{2.33}$$

where $h(\omega)$ and $p_0(\omega)$ are the frequency domain lip opening and upstream pressure respectively. This equation provides a theoretical description of the valve response which may be directly compared to the experimental mechanical response measurements presented in chapter 4. The magnitude of the theoretical mechanical response may approximated around the valve resonance frequency ω_v as

$$|H(\omega)| = \frac{\frac{Q_v}{\omega_v^2}\frac{1}{\mu_v}}{\sqrt{1 + 4Q_v^2(\frac{\omega-\omega_v}{\omega_v})^2}} \tag{2.34}$$

where the substitutions $\omega\omega_v \approx \omega_v^2$ and $\omega^2 - \omega_v^2 \approx 2\omega(\omega - \omega_v)$ are assumed to be valid. This equation may be used to fit the experimental data in order to estimate the values ω_v, Q_v and μ_v. These quantities may then be used in computational models of the second order oscillator described in equation 2.32.

Self sustained oscillations of the valve

The oscillatory behaviour of the system in figure 2.12 may be described as *self-sustained* if a regimes exists whereby the valve and the air column act together to transfer energy from the flow into the acoustical resonances and the mechanical motion of the valve. This means that the valve must behave such that an increase in the downstream pressure p_d causes an increase in the flow U, which further increases p_d[Campbell, 1999]. This has the effect of re-inforcing the standing wave in the resonator, and will occur if the magnitude of the phase difference between U and p_d is less than $\frac{\pi}{2}$[Fletcher, 1993].

At least two discrete scenarios exist which allow for this positive feedback, depending

on the phase relationship between the aerodynamic driving force and the valve motion: the 'inward' and 'outward' striking valve regimes. The function of these regimes may be understood by considering how energy is delivered to the standing wave in the resonator.

The instantaneous energy transfer into the air column W may be written as the product of the total flow U and total pressure P_d, measured at the entrance to the resonator

$$W = UP_d. \tag{2.35}$$

The flow and pressure terms may be written as a product of stationary (average) and oscillatory terms, such that

$$U = \bar{U} + u \tag{2.36}$$

$$P_d = \bar{P}_d + p_d. \tag{2.37}$$

This means equation 2.35 may be rewritten

$$\begin{aligned} W &= (\bar{U} + u)(\bar{P}_d + p_d) \\ &= \bar{U}\bar{P}_d + u\bar{P}_d + \bar{U}p_d + up_d. \end{aligned} \tag{2.38}$$

The first term of equation 2.38 describes the energy dissipation in the stationary flow field, which does not affect the energy transfer into the oscillatory system. The second and third terms sum to zero over a complete oscillation cycle. The total energy transfer into the oscillatory system is given by the last term, up_d. This must be positive for the standing wave to be re-inforced over a single cycle, a condition met when the phase difference ϕ_{up} between u and p_d is less than $\frac{\pi}{2}$ in magnitude. Under this circumstance, more energy is provided to the air column during the positive half of the cycle than is drawn away during the dissipative half of the cycle.

The total pressure difference across the valve may be written as

$$\Delta P = P_0 - P_d. \tag{2.39}$$

Under the assumption of a purely static upstream pressure P_0, and a purely oscillatory downstream pressure p_d, the oscillatory pressure difference across the valve may then be written as

$$\Delta p = p_0 - p_d$$

$$= \quad -p_d. \tag{2.40}$$

A maximum in the pressure difference Δp occurs when there is a minimum in the downstream pressure p_d. There is thus a phase difference of π between the phase described by the pressure difference Δp and p_d, which is the pressure typically measured in experiments. This phase shift must be taken into account when performing the mechanical response measurements briefly described in section 2.4.3, and outlined in more detail in chapter 3.

Neglecting air inertia and assuming a quasi-stationary, frictionless and incompressible flow the mechanical opening h_{valve} of the valve may be assumed to directly control the oscillatory flow u. The phase difference between the downstream oscillatory pressure and flow thus becomes the same as that between the pressure and valve opening

$$\begin{aligned} \phi_{up} &= \angle u - \angle \Delta p_d \\ &= \angle h_{valve} - \angle \Delta p_d. \end{aligned} \tag{2.41}$$

This assumption may break down if, for example, the flow separation is a function of more than just the valve opening (see section 2.5).

Inward and outward striking reeds

The classical approach to reed dynamics considers the effects of variations in the upstream and downstream pressures on the valve opening. The work of Helmholtz defined two kinds of reeds (valves), according on their reaction to a slow increase in the upstream supply pressure:

- Inward striking: the valve opening decreases, and may only vibrate below both its natural resonance frequency, and the acoustical resonance frequency of the air column.

- Outward striking: the valve opening increases, and may only vibrate above both its natural resonance frequency, and the acoustical resonance frequency of the air column.

The aerodynamics of the lip-reed may be brutally simplified such that two discrete forces are assumed to act on the lips: the pressure difference $P_0 - p_d$ across the lips, and the Bernoulli force between the lips due to the flow of air U (see section 2.5). The pressure difference may be related to the outward striking regime, and the Bernoulli force to the inward striking regime.

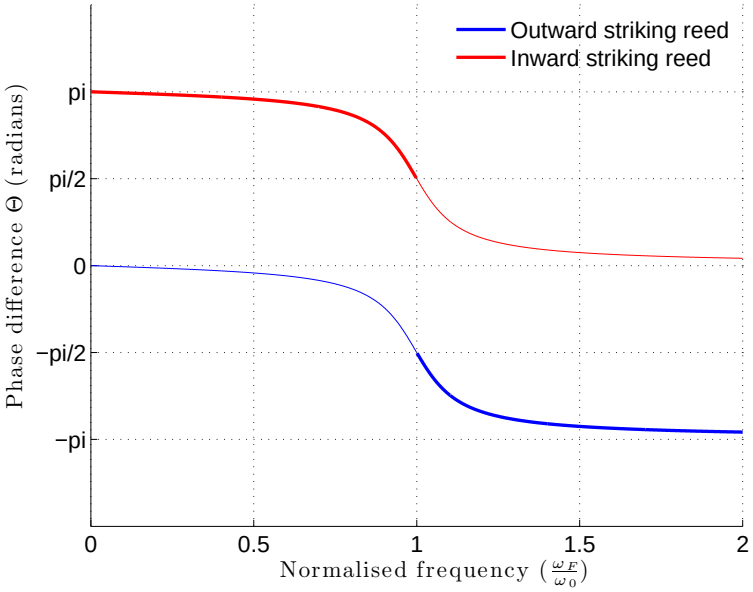

Figure 2.13: The phase difference Θ between the driving pressure and valve opening, under a simple driven harmonic assumption. The thick lines indicate where the valve may co-operate with the air column to sustain oscillations.

The musical valve as a driven harmonic oscillator

The driving force on the lips is due to the surrounding aerodynamical field. If the driving force is defined to be positive when it causes the valve to open, it becomes clear that the force must be in phase with the pressure difference for an outward striking reed, and exactly out of phase (π radians) for an inward striking reed.

If the lips are assumed to oscillate like a simple harmonic oscillator, the phase angle between the complex driving force $\tilde{F}$ and the complex displacement $\tilde{x}$ may be written as[Richards, 2003; Fletcher, 1993]

$$\phi_x - \phi_F = \angle[(\omega_0^2 - \omega_F^2) - 2j\alpha\omega_F] \tag{2.42}$$

where ω_0 is the forcing frequency, ω_0 is the natural resonance frequency of the oscillator and α is a damping coefficient.

The 'inward striking' reed

The inward striking reed may now be rigorously defined as one for which the phase difference between the driving pressure and the reed motion is between π and 0

$$\Theta_{inward} \quad = \quad \phi_{valve} - \phi_F$$

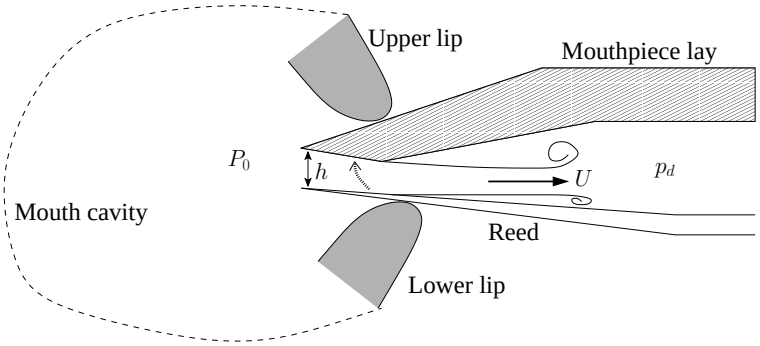

Figure 2.14: A schematic diagram of a clarinet mouthpiece. The upstream static pressure is P_0, the reed opening is h, the volume flow through the reed is U and the downstream acoustic pressure is p_d. The dotted arrow shows the motion of the reed as the supply pressure is slowly increased, according to the 'inward striking' classification. At a critical valve of P_0 the reed shuts tight and the fluid flow stops.

$$= \quad \phi_{valve} - (\phi_{\Delta p} - \pi). \tag{2.43}$$

Together with the condition for the phase difference between the flow and pressure (following equation 2.38) at the entrance to the resonator it can be seen that an inward striking reed may only function for a phase difference Θ_{inward} of between π and $\frac{\pi}{2}$.

Figure 2.13 provides a plot of equation 2.43, showing how the phase difference Θ varies as a function of the driving frequency. The phase condition immediately reveals that the system may only maintain oscillations *below* the natural resonance frequency of the valve.

Figure 2.14 shows a schematic diagram of a clarinet reed, which is the classic example of an inward striking valve. As the supply pressure is increased, the reed is forced towards the mouthpiece lay. The Bernoulli force resulting from the flow of air through the valve acts to re-inforce this motion.

The natural resonance frequency of a clarinet reed is typically in the kilohertz range, and it is played in the musical range of a few hundred hertz. This means it is operating in a stiffness-dominate regime where the reed quickly changes its opening to reflect the oscillating pressure. The clarinet reed is truly 'led' by the instrument air column, with embouchure adjustments by the player acting only to slightly modify the playing frequency[Campbell and Greated, 1987]. The physical description of the clarinet reed is well understood, and most of its playing behaviours can be simulated with an inward striking one mass model (see section 2.9).

The lip-reed has sometimes been described as inward striking[Saneyoshi *et al.*, 1987a]. However, there is significant evidence in the literature to challenge this conclusion, and to suggest that a single classification does not fully explain the observed behaviour[Helmholtz, 1877; Yoshikawa, 1995; Chen and Weinreich, 1996; Cullen, 2000;

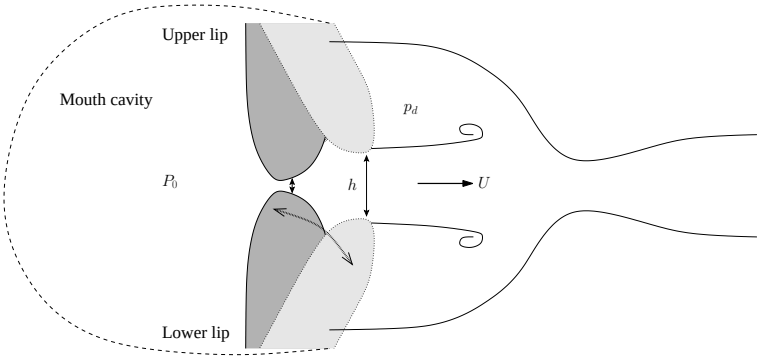

Figure 2.15: A schematic diagram of the lip-reed. The upstream static pressure is P_0, the acoustical downstream pressure is p_d, the reed opening is h, the volume flow through the reed is U. The dotted arrow shows the motion of the reed as the supply pressure is slowly increased, according to the 'outward striking', or 'swinging door', classification. The reed motion itself is also suggested with the overlaid lip motion.

Neal, 2002; Richards, 2003].

The 'outward striking' reed

It is similarly possible to rigorously define the outward striking reed as one for which the phase difference between the driving pressure and the reed motion is between 0 and $-\pi$

$$\begin{aligned} \Theta_{inward} &= \phi_{valve} - \phi_F \\ &= \phi_{valve} - \phi_{\Delta p}. \end{aligned} \tag{2.44}$$

Together with the flow and pressure phase condition at the entrance to the resonator, the outward striking reed can be seen to function for a phase difference $\Theta_{outward}$ of between $-\frac{\pi}{2}$ and π.

Figure 2.13 also provides a plot of equation 2.44, showing how the phase difference Θ varies as a function of the driving frequency. The phase condition immediately reveals that the system may only maintain oscillations *above* the natural resonance frequency of the valve.

Helmholtz originally classified the lip-reed as outward striking. Under this classification the lips are assumed to undergo a kind of outward swinging motion as the supply pressure is increased. This 'swinging door' model is shown schematically in figure 2.15.

The lips are considerably more complicated than the clarinet reed. The lips themselves form the reed, together with an associated, and highly variable, mechanical description. The player has much greater freedom to vary the playing frequency of the

system with embouchure adjustments, and so a full description is more challenging.

2.7.2 The two degree-of-freedom lip model: an 'outward-inward' reed

One of the key problems with both the outward and inward striking models of the lips is that they cannot account for one of the most interesting aspect of brass playing: a good player is able to 'lip' a note either side of the fundamental impedance peak of the note. The player does not appear to be limited to specific playing frequencies as would be expected of these models. Richards[Richards, 2003] investigated this in some detail, and found that a more complicated model, able to act as both an inward and outward striking reed, was necessary to simulate this behaviour. Adachi[Adachi and Sato, 1996] performed similar work using a one-mass model of the lips with two degrees of mechanical freedom. An experimental investigation of this issue forms one of the key aims of this thesis, and is described in chapter 4.

Upon consideration of section 2.5 on the flow dynamics of musical valves, it becomes apparent that the behaviour of the lip-reed might be expected to be more complex. In particular, it has been shown that the constriction between the lips gives rise to a local 'Bernoulli force'. This force tends to pull the lips together, in direct opposition to the swinging motion driven by the pressure difference across the lips. This is in contrast to the case of the clarinet, where the Bernoulli force acts alongside the pressure difference to close the reed. It is a non-trivial task to directly formulate a theory to describe the interplay of these two forces. Rather, a thorough computational simulation provides the most useful analysis[Richards, 2003; Adachi and Sato, 1996].

2.8 The human vocal folds

The broad similarities between the lip-reed and the human vocal folds have already been discussed in section 2.2.4. The second half of this thesis concentrates on an investigation into the flow behaviour downstream of a self-oscillating *in vitro* replica of the vocal folds. The objective of the investigation was to study the aerodynamic interaction between the vocal folds and a constriction located a short distance downstream. In the human larynx the region immediately downstream from the vocal folds consists of a short gap around 16mm in length known as the laryngeal ventricle. At the downstream end of this ventricle lie the ventricular bands. They are formed from a pair of large, deformable masses of tissue, located on either side of the airway.

2.8.1 The ventricular bands compared to the brass mouthpiece

The overall system comprising the vocal folds and the ventricular bands shares, in a structural sense, a remarkable similarity to the situation encountered with the lip-reed. Figure 2.16 shows a schematic layout of the the lip-reed - mouthpiece system,

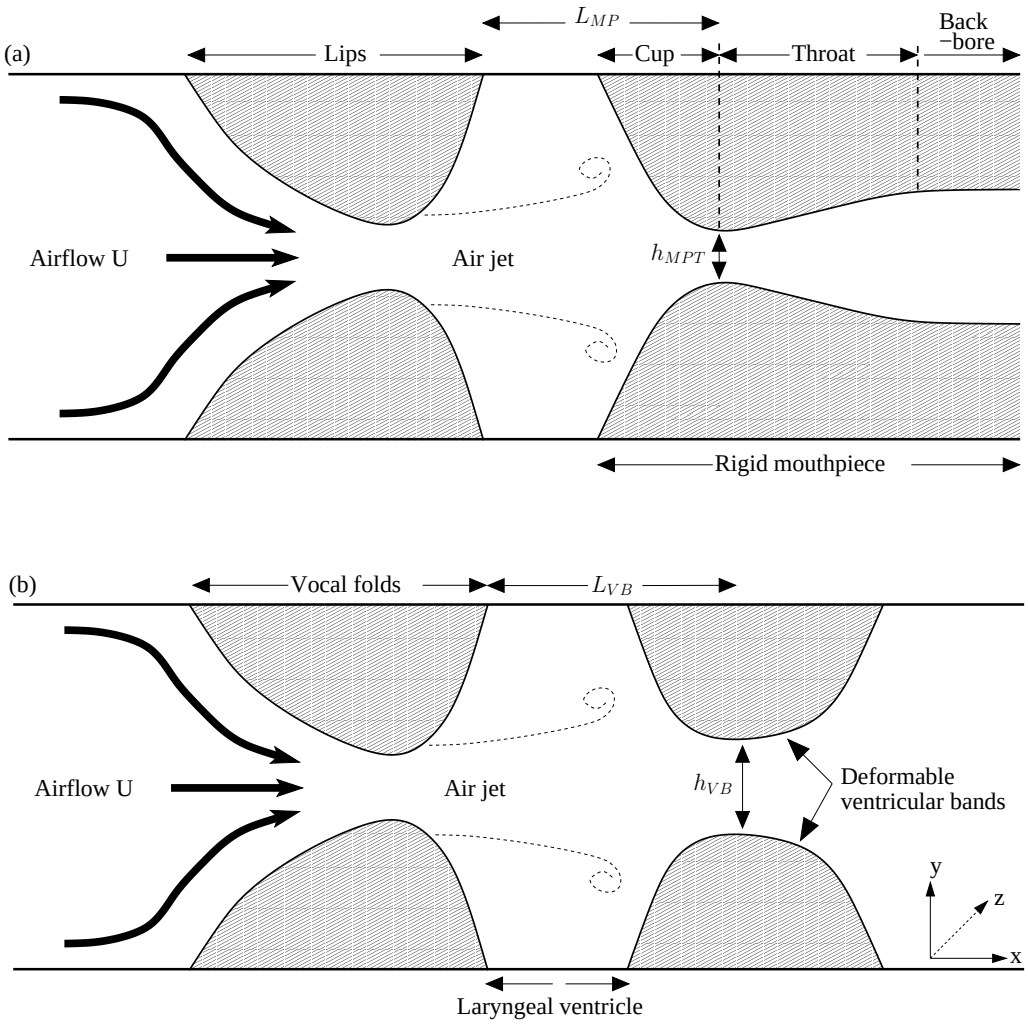

Figure 2.16: A schematic comparison between the lip-reed - mouthpiece system shown in (a), and the vocal folds - ventricular folds system shown in (b). L_{MP} is the distance from the downstream end of the lips to the minimum mouthpiece constriction, h_{MPT} is the minimum height within the mouthpiece (typically the mouthpiece throat, which is fixed for a particular mouthpiece), L_{VB} is the distance from the downstream end of the vocal folds to the minimum separation between the ventricular bands, h_{VB} is the minimum separation between the ventricular bands (a variable quantity).

together with a similar schematic outline of the vocal folds - ventricular bands system. It highlights the global similarities between the two layouts, whereby a secondary constriction to the airflow occurs a short distance downstream of the oscillating valve.

The interest in the ventricular bands arises from clinical studies which demonstrate their apparent involvement in some voice disorders. In particular, it has been postulated that their presence may function as a compensatory mechanism when there has been damage to the vocal folds[Nasri *et al.*, 1996]. Their importance for some obscure singing styles has also been demonstrated. These include the throat-singing of Tibetan monks[Fuks *et al.*, 1998], known as *Dzo-ke*, and the Mongolian *Kargyraa*[Kob, 2004a] vocal style. High-speed photography of the larynx has revealed that during such singing styles the ventricular bands appear to exhibit a period-doubling phenomenon, whereby they undergo an oscillation at half the fundamental frequency of the vocal fold oscillation[Fuks *et al.*, 1998; Bailly *et al.*, 2007; Bailly *et al.*, 2008]. This phenomenon strongly suggests an interaction between the vocal folds and the ventricular bands. An investigation into whether the interaction has an aerodynamic component, in addition to any mechanical and acoustical components, formed the objective of this study.

In brass playing the lips of the player are pressed into the mouthpiece of the instrument. The mouthpiece generally has a profile similar to that shown in part (a) of figure 2.16. Immediately downstream of the lips lies the mouthpiece cup, a tapered section that leads to start of mouthpiece throat, which is the minimum constriction. The the throat is generally tapered to gently expand into the backbore. This is the final section of the mouthpiece, and it approximately matches the cross-sectional area of the instrument leadpipe.

There are two key differences between the two systems. The first is that the mouthpiece presents a rigid constriction, while the ventricular bands are deformable. The adduction of the ventricular bands is also variable to some extent, through the contraction of the surrounding neck muscles. Under certain conditions the ventricular bands can form a secondary oscillator, but their influence may not be limited to a full oscillation regime. There appears to be a range of adduction distances that may have a feedback effect on the full oscillations regime of the vocal folds[Fuks *et al.*, 1998]. Similarly, it is the experience of many brass players that the presence of the mouthpiece facilitates the 'buzzing' of the lips in the absence of a full instrument, as compared to lip buzzing in the absence of any downstream constriction. Most studies have explained this effect in acoustical terms, whereby the large impedance peak of the mouthpiece, typically around 500Hz, provides enough acoustical compliance at the lip oscillation frequency, around 100-200Hz, to aid their destabilisation. However, it is possible that a similar aerodynamic effect may also exist in the case of the lips and mouthpiece.

The second key difference is that in the case of the vocal folds, the downstream bore presents a rather small overall impedance, due to the relatively large cross-section of the vocal tract. There is some strong evidence that the acoustical effects of the vocal

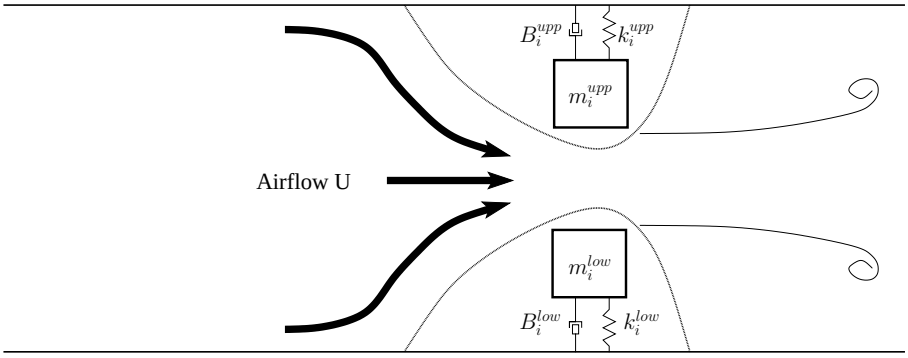

Figure 2.17: A simple lumped element, one-mass model of a musical valve. The element mass is m, k_i is the spring stiffness, B is the spring damping.

tract may be significant when the fundamental vocal fold frequency lies close to the first vocal tract resonance[Rothenberg, 1981; Titze and Story, 1997; Adachi and Yu, 2005; Joliveau *et al.*, 2004], but its influence for the lower range of phonation remains an issue of some contention [Titze, 2004]. Below the first resonance it provides a degree of acoustical compliance which may aid the vocal fold oscillations. However, the strength of this assistance may be quite small due to the soft walls of the vocal tract which result in rather damped acoustical resonances. In contrast, the firm-walled, narrow-bored brass instrument that lies beyond the mouthpiece presents an approximately harmonic series of large impedance peaks to the lips. The interaction between the lips and the acoustic resonances of the instrument bore is well documented[Elliot and Bowsher, 1982; Campbell, 1999; Cullen *et al.*, 2000], and has been outlined in section 2.7.

2.9 Musical valve modelling

In a computational implementation of the quasi-stationary theory of valve oscillation, it is necessary to calculate the total aerodynamic driving force on the valve surfaces. Thus it is necessary to formulate equation 2.25 in terms of the pressure profile along the valve walls:

$$P(x) = P_0(1 - \frac{A_s^2}{A(x)^2}) \tag{2.45}$$

where $P(x)$ is the pressure at a point x along the valve wall.

This equation must be integrated along the valve walls to calculate the total aerodynamic driving force. However, the lips and the vocal folds are both continuous, flexible mechanical structures. It is thus rather difficult to accurately model such an interaction. The most common work-around for this problem is to employ a caricature of the mechanical structure known as a *lumped element model*. The complex muscular

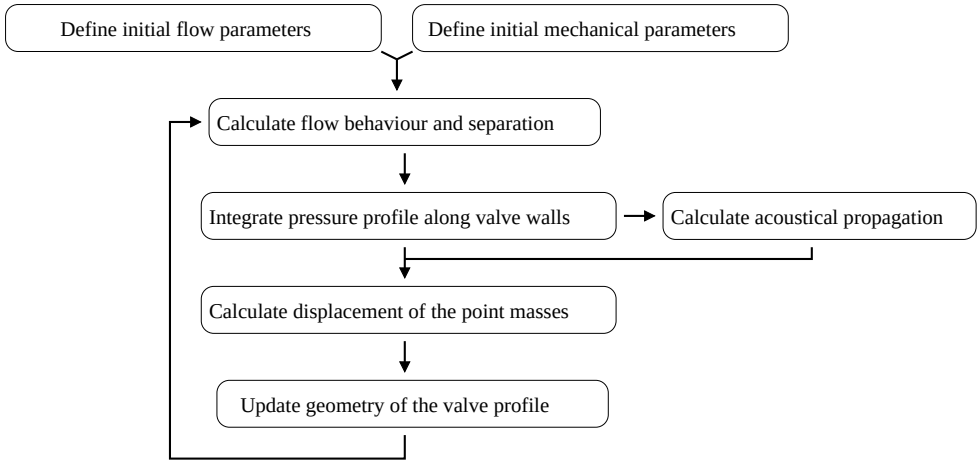

Figure 2.18: Signal flowchart of a time domain musical valve model.

structure of the valve, and the various interconnecting tissues, are brutally simplified into a number of masses, springs and dampers. This system can be easily modelled using Newtonian mechanics, and significantly reduces the complexity of a musical valve model.

The simplest lumped element model is the symmetrical one-mass model, shown in figure 2.17. In this model each valve wall is represented by a single point mass, and is connected to a ridge surface with a spring-damper system. The two valve walls are symmetrical, which further simplifies the mathematical formulation.

This model is implemented in the time domain. Figure 2.18 shows a simplified flowchart of a time domain model, such as in [Pelorson *et al.*, 1994; Deverge *et al.*, 2003; Richards, 2003; Kob, 2002].

The one-mass model has been widely used to model musical valves such as the clarinet[Fletcher and Rossing, 1991; Dalmont *et al.*, 2003; Silva *et al.*, 2008] and the lip-reed[Elliot and Bowsher, 1982; Cullen *et al.*, 2000; Richards, 2003]. It has proven to be remarkably successful at reproducing experimentally observed behaviours. These include predictions of threshold oscillation pressures and frequencies[Cullen *et al.*, 2000], and some 'lipping' behaviour[Campbell, 1999]. Lipping is a playing technique whereby the played note can be pulled up or down in frequency, away from the fundamental resonance of the instrument bore.

There are two principle drawbacks with the model:

- It cannot function in the absence of acoustical feedback.
- It can only 'lip' away from the acoustical frequency in one direction: either higher in pitch, or lower, but not both.

These issues are addressed in section 2.7 on the physics of the lip-reed.

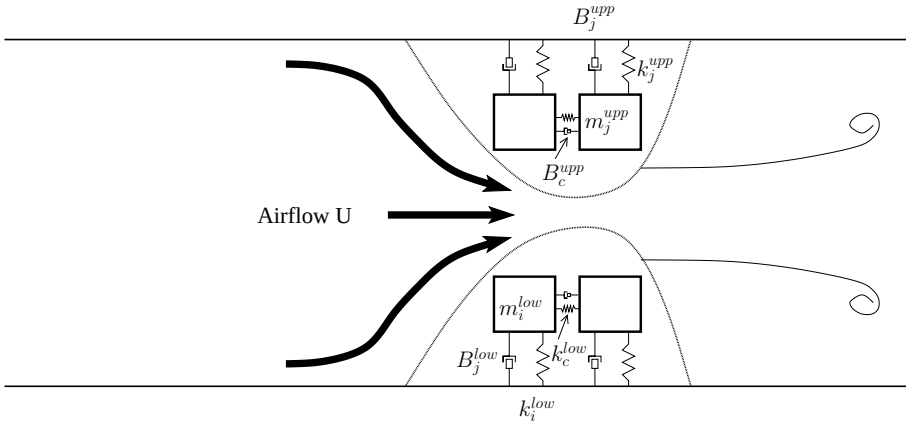

Figure 2.19: A lumped element, two-mass model of a musical valve. The left element mass is m_i, k_i is the left element spring stiffness, B_i is the left element spring damping, the right element mass is m_j, k_j is the right element spring stiffness, B_j is the right element spring damping, k_c is the coupling spring stiffness, B_c is the coupling spring damping.

The two-mass model has been used widely in vocal fold research[Ishizaka and Flanagan, 1972; Lucero, 1993; Lous *et al.*, 1998], and more recently in lip-reed research[Adachi and Sato, 1996; Richards, 2003]. A simple version is shown in figure 2.19. This model has proven to be remarkably useful for investigations into the physics of musical valves. It seems to be capable of simulating enough of the physics to be useful, while remaining simple enough that simulations can be performed quickly with some objectivity.

2.10 Summary

The work in this chapter has outlined the most important mechanical and fluid mechanical principles concerned with the function of the brass instrument lip-reed and the human vocal folds, collectively lumped together under the description of 'musical valves'. The similarities between these two systems, both in their structure and surrounding aerodynamic fields, has been particularly highlighted. An overview has finally been presented of the basic principles of lumped element musical valve modelling, which form a crucial component of the research field. This has been included to inform the following chapters, throughout which much reference is made to such models.

Part II

Experimental Investigations into the Mechanical Properties of the *in vitro* and *in vivo* Brass Playing Lip-reed

Chapter 3

Experimental methods for investigations into the mechanical properties of real and artificial lips

"*The best fishermen I know try not to make the same mistakes over and over again; instead they strive to make new and interesting mistakes and to remember what they learned from them.*" - John Gierach

3.1 Introduction

The mechanical structure of a musical valve forms a crucial element of the overall valve-aerodynamic system. Its natural resonance frequencies affect the oscillation frequency of the system[Campbell and Greated, 1987; Fletcher and Rossing, 1991; Cullen *et al.*, 2000]. The internal damping of the mechanical valve also affects the overall energy loss mechanisms in the valve system, which in turn influences the amount of aerodynamic forcing required to maintain oscillations.

The complex structure of a biological musical valve means that *ad hoc* assumptions about its detailed characteristics are rather dangerous. In physical descriptions of the global behaviour the mechanical structure has thus traditionally been condensed into a small number of degrees of freedom, in a desire to uncover the fundamental behaviour. Simplified models, such as the one and two-mass lumped element versions described in section 2.9, provide a computational workshop for such simplifications.

The parameter space for the computational workshop includes quantities such as *spring stiffness*, *damping* and *effective mass*. Such parameters cannot be immediately derived from human players, and it is rather difficult to provide a clear interpretation of

them from the gamut of human experience. The parameters may, however, be estimated from experimental measurements performed on *in vivo* and *in vitro* valve systems.

To provide useful parameters the theoretical framework of the computational model of concern must be used to interpret the experimental results. In the simplest case this means the lips may be assumed to behave like the second order harmonic oscillator described in section 2.7.1 and equation 2.30. Under this assumption, curve fitting of the experimental data may be performed based on the theoretical formulations of the model's mechanical structure[Cullen, 2000; Ruty *et al.*, 2007]. It is then a straightforward task to extract parameters such as the resonance frequency and quality factor from the fitted curve.

It has been shown in section 2.4 that the mechanical response provides a useful tool for characterisation of the mechanical properties of a musical valve. It allows data about the global mechanical resonances to be easily extracted, as required by the parameter space of computational models.

This chapter first outlines the mechanical models used to replicate the *in vivo* lip-reed in the laboratory in section 3.2. The development of a novel *in vitro* replica is included in the discussion, described in section 3.2.3. An outline of the standard experimental techniques used to evaluate the mechanical response of such *in vitro* models is presented in section 3.3.2. A novel technique to measure the mechanical response of *in vivo* human lips is described in section 3.3.4. The motivation is to obtain direct measurements of the mechanical properties of real lips, in order to verify the validity of the lumped element models proposed in sections 2.7 and 2.9. A verification of the new experimental method against traditional methods for evaluation of the mechanical response is included in section 3.3.3.

3.2 *In vitro* models of the brass player's buzzing lips

3.2.1 The artificial brass player

Replica models of the brass player have been used in musical acoustics research for more than a decade, and there are several examples in the literature[Gilbert *et al.*, 1998; Vergez and Rodet, 1998; Cullen, 2000]. Such models provide a number of distinctive advantages over real human players:

- An embouchure may be established and maintained over a long period of time, allowing greater scope for controlled scientific investigation.
- It is possible to repeatedly form an embouchure based on a small number of control parameters.
- Measurement apparatus such as microphones and flowmeters may be placed in and around the artificial player in ways far too obtrusive for real players.

- An artificial player is musically untrained, and as such holds no pre-conceived musical tendencies or opinions.

Two artificial brass playing systems were used in this work. The first was the system developed by Richards[Richards, 2003], which itself was a development of the systems of Cullen[Cullen, 2000] and Gilbert[Gilbert *et al.*, 1998]. No alterations were made to the construction mechanics, a photograph of which is shown in figure 3.1. In the work presented here the model of Richards is referred to as *replica A*. Detailed specifications may be found in [Richards, 2003; Bromage, 2006].

The second system was a new development, drawing inspiration from the model of Richards[Richards, 2003], and from a similar replica developed for the human vocal folds at the *Institute de la Communication Parlee* in Grenoble, France[Vilain *et al.*, 2003; Bailly *et al.*, 2006]. This new model is referred to as *replica B*, and details of it may be found in section 3.2.3.

Two models were used because they each provided particular benefits and drawbacks, depending on the nature and objective of the experiment. The original model of Richards[Richards, 2003], replica A, was very quick to set up and adjust, and allowed for extensive 'tweaking' of the mechanical parameters in order to play a wide range of notes. This benefit also provided the main drawback: it was very difficult to be objective about the precise nature of the adjustments. The diligent experimentalist could quickly learn how to manipulate the replica lips into useful embouchures, but such apparent artistry was nearly impossible to rigorously record and quantify.

The new model, replica B, significantly reduced the number of control parameters in an effort to increase the stability and repeatability of the embouchure settings. Multiple configurations were often required over a period of weeks, and each configuration needed to function consistently over several days. Replica B successfully responded to these challenging demands. Detailed experiments to investigate the behaviour of replica B are described in section 4.5.2.

3.2.2 Replica A: an *in vitro* lip-reed model designed for adjustability

The artificial mouth developed by Richards and shown in figure 3.1 has proven to be very useful for scientific investigations into the lip-reed[Richards, 2003]. It allows a great deal of control over the position of the lips and their mechanical configuration. It can easily be coupled to a wide range of brass instruments as it does not require a fixed mouthpiece like the artificial mouth of Cullen[Cullen, 2000].

The model is quite simple in its design. There is a large *mouth cavity* connected to a pressure source, which is typically an air compressor (Air Control Industries Ltd. 8MS11 0.25kW air pump), but may also be sourced from a large industrial pressure reservoir. This cavity is visible in figure 3.1 as a large black box with a glass window in one of the side walls. Attached to the front of the mouth cavity is the *face plate*.

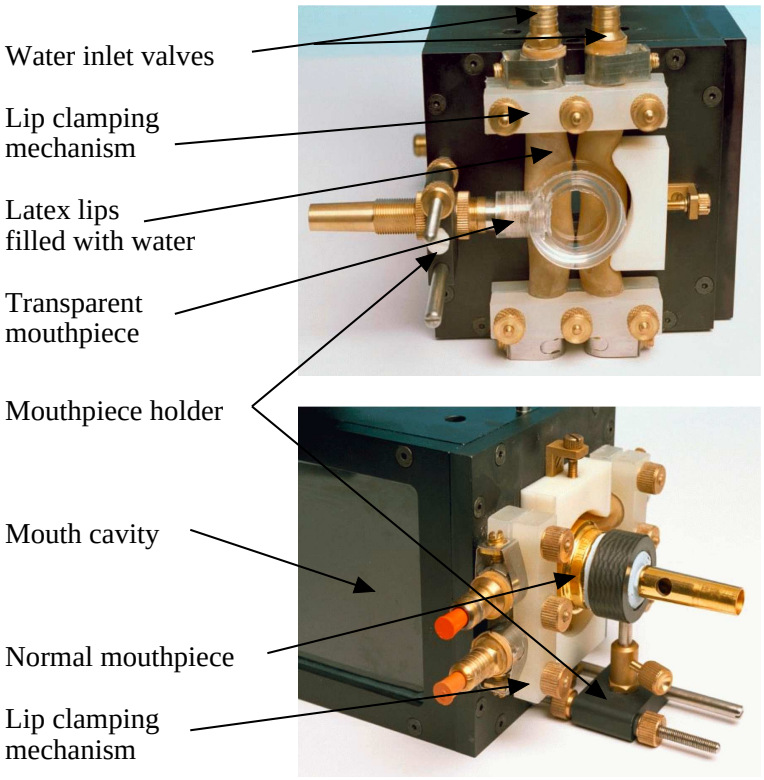

Figure 3.1: A photograph of the artificial brass player developed by Richards[Richards, 2003], and referred to as *replica A* in this thesis (it is sometimes also referred to as an 'artificial mouth' in the text). In the top photograph it has been coupled to a transparent mouthpiece to facilitate improved optical access to the lip opening[Richards, 2003; Bromage, 2006]. In the lower photograph it has been coupled to a standard trombone mouthpiece (the hole in the shank is for a pressure transducer).

This provides the platform onto which the artificial lips, the artificial lip clamping and support mechanism, the mouthpiece support and mouthpiece are attached.

In the centre of the face plate is a circular hole of 20mm diameter, representative of the gap between the teeth of a player when the lips are opened to form an embouchure. The two artificial lips lie directly across this hole on the outside of the face plate, positioned to interfere with the airflow that emanates when the pressure source is switched on. They are held in place with a clamping and support mechanism, which can be seen in figure 3.1. These clamps are not adjustable. At rest the lips are held approximately 3mm apart, which is an empirically-determined setting which seems to allow the maximum adjustability. The shape of the lips when coupled to the mouthpiece is determined by hand. In the top photograph of figure 3.1 this effect can clearly be seen; at the white clamps the lips lie several millimetres apart, but in the central region they are deformed to form a tight seal around the mouthpiece.

The artificial lips are composed of latex tubes of 15mm diameter, filled with water

and connected to a water column. The height of water in the water column is one of the principal control parameters of the model, as it determines the volume of water in the lips and thus the tension and stiffness of the latex. This parameter is measured as a pressure, in units of Pascals, and may be calculated by measuring the height of top of the water column above the centreline of the artificial lips. Consideration of the Bernoulli equation along a streamline in the water column shows that the overpressure acting on the lips is due to the weight of water above the lips, such that

$$P_{internal} = \rho g h \tag{3.1}$$

where ρ is the water density, g is the gravitational acceleration 9.81ms^{-2} and h is the height of the water column.

The lips are coupled to a mouthpiece by means of a mouthpiece clamping mechanism, which can be seen in figure 3.1. This provides a rigid support to prevent excessive movement of the mouthpiece when an instrument is coupled. In practice this design can sometimes fail to provide enough support, as even minor movements of the instrument provide a high torque on the mouthpiece and lips, disturbing the embouchure. To minimise this effect any instrument must be securely held in place with a series of stiff metal clamps.

The main control parameter for the artificial lips of replica A is the internal water pressure $P_{internal}$. This is affected by the height of the water column and the pressure exerted on the lips by the mouthpiece. Raising the height of the water column increases $P_{internal}$ because of the increased weight of water.

The water column may be treated as imposing either a constant pressure or constant volume condition. If the system is hermetically sealed after adjusting the height of the water column a constant volume condition is imposed. If the system is left open to the atmosphere a constant pressure condition is imposed. These two conditions lead to noticeably different behaviours. For example, under a constant pressure condition the lip oscillation can be modulated by oscillation of the water column itself. This results in a continuous initiation and termination of the lip vibration. In general, a constant volume condition was thus imposed. More detailed analysis of this issue may be found in [Vilain *et al.*, 2003].

In the case of a constant volume mechanical boundary condition, pushing the mouthpiece harder into the front of the lips increases $P_{internal}$ as it squeezes the water in the lips. On the contrary, if a constant pressure condition is imposed then applying a force from the mouthpiece has little effect on the internal lip pressure. In the case of a constant pressure boundary condition, the precise force applied by the mouthpiece to the lips thus affects both the mechanical position of the lips, and the internal water pressure. It hence provides an important control mechanism for the whole embouchure setup.

An embouchure can be varied and adjusted by changing the value of $P_{internal}$. Increasing its value tends to raise the pitch of the played note, and decreasing its value tends to lower the pitch[Cullen *et al.*, 2000]. The internal water pressure may be used along with the static upstream overpressure P_0 to define the basic characteristics of an embouchure. Careful re-settings of the artificial mouth, using a particular set of the parameters $P_{internal}$ and P_0, usually allowed reproduction of the same note.

The artificial mouth of figure 3.1 is able to replicate a wide range of the behaviours seen in real players. These features include:

- The ability to initiate and sustain a musical note when coupled to a brass instrument mouthpiece on its own.
- The ability to initiate and sustain a musical note when coupled to a full brass instrument.
- The ability to play a brass instrument both above and below the principal bore impedance frequency of a particular note regime.
- A substantial range of playing frequencies (though not as wide a range as human players).
- The production of multi-phonic and chaotic sounds.

Such an impressive range of playing features is certainly of significant scientific and musical interest. However, it rather belies the inherent difficulty of forming objective procedures with which to control the replica. Put another way, replica A can be made to play in the manners outlined above, but it is not easy to define clear adjustment sequences and techniques for doing so. Adjustments are very empirical, often requiring extensive 'prodding' and 'nudging' of the artificial lips until a particular note is attained.

For many musical and experimental procedures this difficulty is little more than a time-consuming annoyance. However, for the flow experiments detailed in chapters 7 and 8 it was crucial that specific mechanical configurations could be reliably created and maintained over several days. One solution to this problem was to dramatically reduce the number of control mechanisms. This objective lead to the development of replica B.

3.2.3 Replica B - an *in vitro* lip-reed model designed for stability

A new artificial mouth was developed as part of the work presented in this chapter. It was designed to improve upon several of the issues encountered with the previous systems, and to provide an alternative mechanical model to test against the real lips.

The principal design target for replica B was a model which had the fewest possible adjustment options, whilst maintaining a reasonable level of control. The

objective was to create a model which could couple to a brass instrument with stable and easily repeatable embouchure settings. The main problem with the model of Richards[Richards, 2003] in this respect was that it allowed for such extensive uncalibrated manipulation of the artificial lips.

These issues were addressed by the model shown in figures 3.2, 3.3 and 3.4. The principal change with the new model, as compared to replica A, was a complete re-design of the faceplate and artificial lips. This was achieved by way of five key features:

- The artificial lips were formed from water-filled latex. The latex was glued directly to supporting *lip blocks* which provided the lips with their default shape and profile, as opposed to the latex tubes used by Richards.

- The only dynamic mechanical control parameter was the internal water pressure of the artificial lips, determined by the height of the water column.

- Changes to the lip block profile provided the only other mechanical control parameter. Such changes required a rebuilding of the model and as such may be described as non-dynamic control. Several pairs of lip blocks were constructed, each with a slightly different shape being more suited to a particular range of notes (see figure 3.5).

- The artificial lips were mounted within the faceplate, rather than on the outside. Their rest position was fixed and could not be adjusted, other than through alterations to the internal water pressure, or through choice of an alternate lip block profile. A glass viewing window in the faceplate permitted optical access to the region directly between the lips (see figure 3.2).

- The artificial lips were decoupled from direct contact with the instrument mouthpiece by means of a thin but rigid faceplate cover.

Replica B shared the same basic idea of replica A, which was to replicate the lips of a brass player by using water-filled latex. However, the practical implementation presented here was novel. The new replica should not be thought of as a 'better' artificial brass player, but rather as an alternative implementation of the same idea, with a slightly different set of experimental objectives (namely stability vs. adjustability).

Replica B also drew inspiration from an *in vitro* human vocal fold model developed at the *Institute de la Communication Parlee* (ICP) in Grenoble, France[Bailly *et al.*, 2006]. This model is called replica C, and was used for the flow-based experiments of chapters 6, 7 and 8. These experiments were part of an official collaboration between the Acoustics and Fluid Dynamics Group of the University of Edinburgh and the GIPSA-lab in Grenoble (see section 7.1).

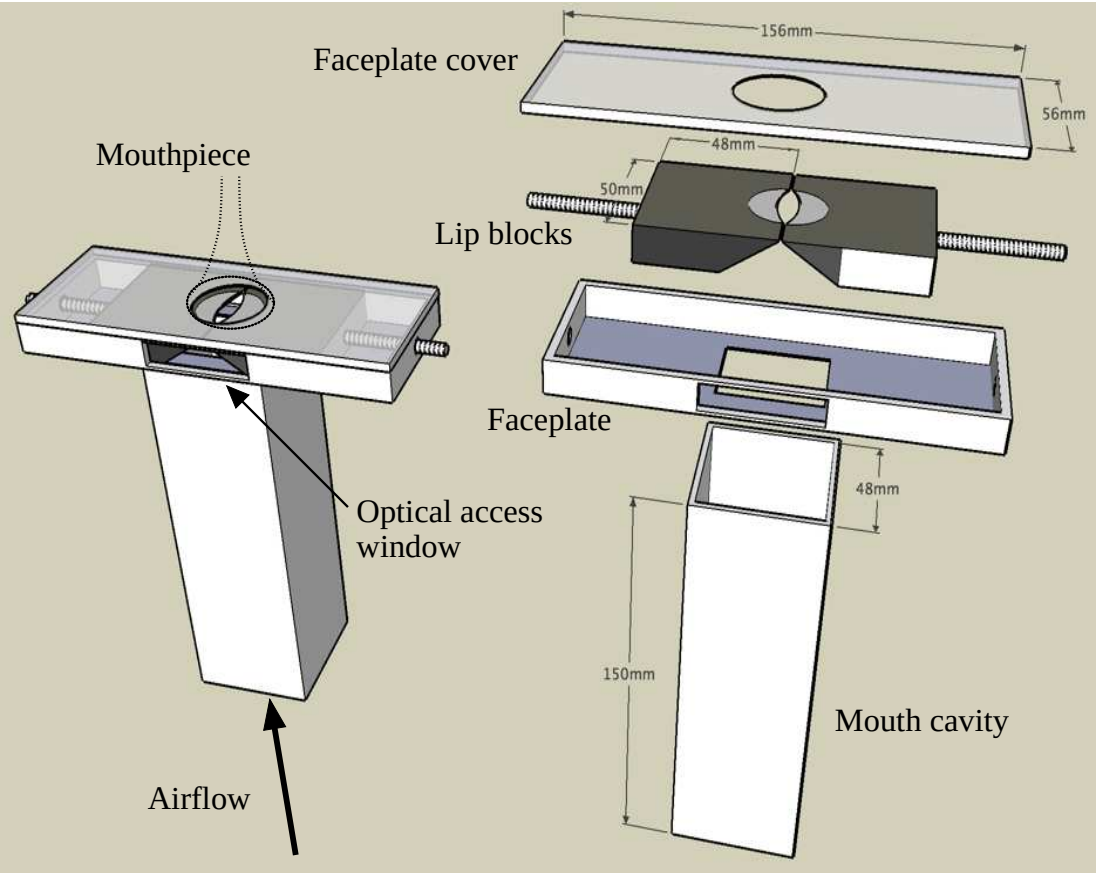

Figure 3.2: A schematic diagram showing replica B. The left hand side shows the assembled replica together with a mouthpiece, and the right hand side shows the constituent elements. The downstream bore may be a mouthpiece (with or without an instrument), as shown, or another acoustical resonator such as an open tube. The optical access window permits a view directly between the artificial lips in cross-section, which is useful for performing both fluid flow and mechanical behaviour experiments.

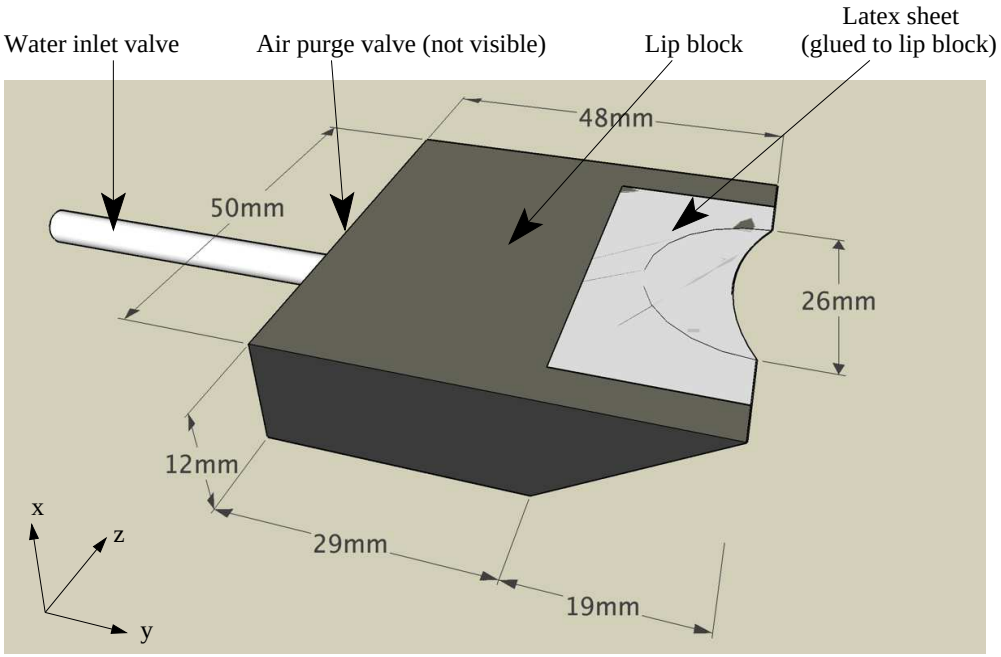

Figure 3.3: A schematic diagram showing the layout of an artificial lip (lip block) from replica B. The latex sheeting is glued directly to the lip block with super-glue. A small air purge valve is not visible on the rear of the block, which is used to remove air bubbles from the system.

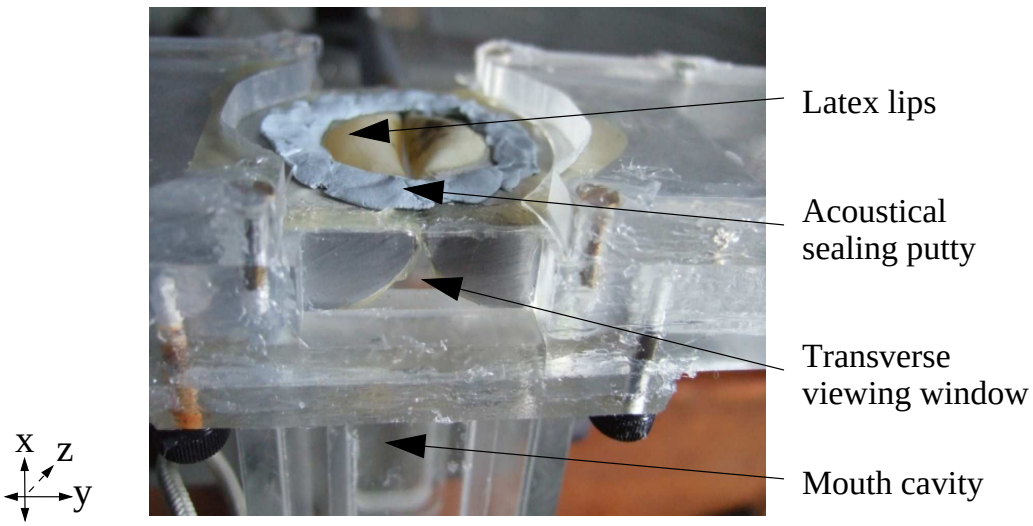

Figure 3.4: A photograph showing replica B. The angle of view approximately corresponds to the view shown in figures 3.2 and 3.3. The transverse viewing window is visible in the centre of the image.

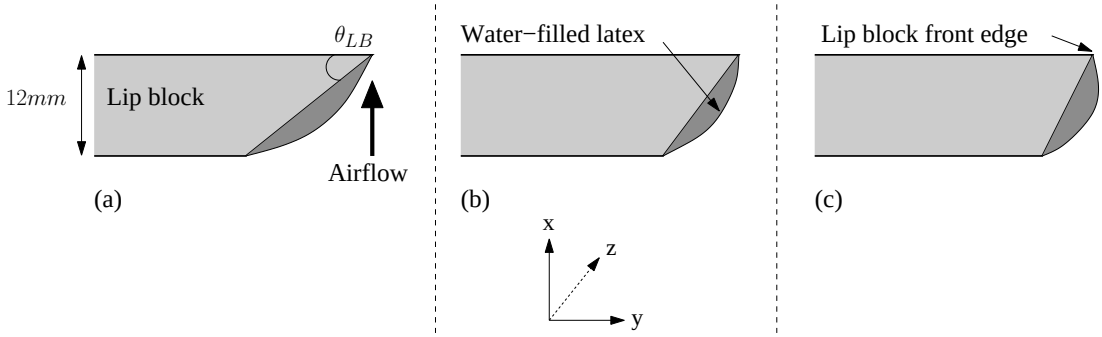

Figure 3.5: Schematic diagrams showing how alterations to the lip block profile affect the static shape of the water-filled latex artificial lips. The lip block is shown in cross-section (see figure 3.3), with the airflow direction during playing as shown. θ_{LB} is the critical lip block angle: alterations to this angle, for a given thickness of lip block (12mm for a human lip replica), directly control the static shape of the water-filled latex. θ_{LB} is smallest for profile *a*, and largest for profile *c*.

Practical usage of replica B

Replica B required a careful setup procedure, which may be summarised as follows:

1. Select an appropriate pair of lip blocks (see figure 3.5 and the text below).
2. Glue a piece of latex sheeting to either lip block using super-glue, and leave to dry for at least 15 minutes.
3. Connect the water column to the lip blocks and fill with water, taking care to purge any air bubbles with the purge valve.
4. Position the lip blocks in the faceplate, and lay the faceplate cover on top (see the right hand side of figure 3.2).
5. Seal the whole area with silicone sealant. Wait for 2 hours to allow the sealant to set.
6. Connect the air supply to the upstream end of the artificial mouth cavity, and if required connect a downstream bore to the faceplate (take care to seal the connection with acoustic putty).
7. Set the internal water pressure with the water column.
8. Apply the upstream static overpressure with the air supply, and note the pressure. The artificial lips should play a note, or buzz freely.

Replica B proved to be a useful alternative to the artificial brass player of replica A. The initial setup time of an embouchure was relatively long, as it required careful gluing

of latex sheeting to the lip blocks. However, once this initial procedure was completed the model could be used for long periods of time with no further adjustments, and with pleasing stability. When a rebuild was required, it was possible to follow the same setup procedure, and in most cases the resulting playing behaviour was directly comparable to the previous configuration.

In addition to the dynamic control parameter of the internal water pressure of the artificial lips, the system could be controlled by changes to the profile of the lip blocks. Such changes are described as a non-dynamic control parameter. Figure 3.5 shows three alternative lip block profiles in cross-section.

The shape of the lip block profile determined the static rest position of the water-filled latex. It affected the latex profile of a single lip, and in turn this affected the rest separation of the two lips when assembled into the faceplate. For a given thickness of lip block (12mm for a human lip replica), a critical lip block angle θ_{LB} was the key control parameter.

For moderate values of θ_{LB} (between approximately 35-45°) the water in the latex was pulled by gravity to be relatively far away from the front edge of the lip block, and towards the upstream side of the block (figure 3.5 (b)). The net effect of this profile was that the static lip separation was relatively large for a given internal pressure. In order to reduce the lip separation to a point where destabilisation could occur it was necessary to increase the internal lip pressure. This had the effect of increasing the tension and stiffness of the latex, thus raising the frequency of the natural mechanical resonances. Such a profile was well suited to playing the middle register of a brass instrument.

For large values of θ_{LB} (between approximately 45-55°) the static shape of the latex was more rounded, with less water held towards the upstream end of the lip block (figure 3.5 (c)). This had the net effect that the static lip separation was relatively small for a given internal pressure. This allowed the lips to be destabilise quite easily with only small internal water pressures, and consequently rather low natural mechanical resonances. Such a block was well suited to playing the lower register of a brass instrument.

The parameters of the various lip block profiles were empirically determined to function reliably with a wide range of brass instrument notes. The design of the replica B could therefore not be directly compared to the control mechanisms of a real lip-reed. However, the simple implementation and reduced parameter space did allow for an relatively clear understanding of how the model behaved as the *in vitro* system was adjusted. This was a useful improvement over the design of replica A, and provides a further evolution of the *in vitro* models towards a more fully controllable replica.

3.2.4 Summary of the *in vitro* lip-reed and vocal fold models

Over the past decade a number of *in vitro* models have been built as laboratory tools to investigate the physics of brass playing. These have included Cullen's[Cullen, 2000] original artificial mouth, the improved artificial mouth of Richards[Richards, 2003] and the recent development of replica B as part of this thesis.

A number of *in vitro* vocal fold replicas have also been built. These models are functionally similar to the lip-reed models, and as such it is useful to consider the overall development of the two types of model together.

Table 3.1 provides a summary of the *in vitro* lip-reed and vocal fold replicas that are relevant to the work in this thesis. The table provides details of their overall development timeline, together with brief notes about the various features incorporated into each version.

3.3 Mechanical response measurement techniques

The mechanical response of a musical valve provides a measurement of its mechanical properties. An evaluation of the mechanical response can be used to determine the global resonances of the valve. The measurement can also yield useful information about the dynamics of the valve system and its ability to destabilise and play a particular note or range of notes.

The interpretation of the mechanical response in the current work is based on the theory of classical valve physics outlined in section 2.7.1. The key outcome of this theory is that there are two classes of musical valves: inward striking and outward striking (a third class, the 'sideways' striking valve has also been proposed, but it is equivalent to the inward striking valve in this discussion[Campbell, 1999]). Each of these valves is expected to interact with an air column standing wave in a different way, producing differing behaviours (see section 2.7.1). It is possible to use a mechanical response measurement to determine the 'striking' classification of a musical valve.

3.3.1 Brief history of mechanical response evaluation methods

A mechanical response measurement of a musical valve requires a signal to represent the motion of the valve in response to a calibrated driving force. In some early work using an *in vitro* brass player this signal was acquired by shining a laser vibrometer down the shank of a regular trombone mouthpiece and onto the frontal surface of a single artificial lip[Gilbert *et al.*, 1998]. When the lips were driven by a loudspeaker their small amplitude oscillations included some front-to-back motion which was detected by the vibrometer.

The key problem with the use of a vibrometer in this way is that the detectable lip motion is limited to a single degree of freedom. It might be possible to orient the

Model	Location	Date	Key features	Designer
Original artificial mouth	Edinburgh, UK	2000	First model to use latex tubes to represent the lips. Lips contained inside a sealed mouth box. Embouchure controlled by a water column and by controllable 'teeth' plate. Mouthpiece screwed into mouth box, so no direct coupling to lips.	Cullen [Cullen, 2000]
Replica A	Edinburgh, UK	2003	Inspired by Cullen's[Cullen, 2000] model. Moved the latex lips to the outside of the mouth box, so they could be more easily manipulated. Direct coupling between lips and mouthpiece. See section 3.2.2.	Richards [Richards, 2003]
Original vocal fold replica	Technische Universiteit Eindhoven, Holland	2005	Designed as a scaled model of the human vocal folds. Used latex wrapped around shaped metal blocks to represent the vocal folds. Vocal folds contained within larger 'face plate' which had to be clamped tight to keep water inside the latex vocal folds. Connections upstream to a trachea, and downstream to a vocal tract.	Hirschberg *et al*[Hirschberg, 2006; Pelorson, 2007; Bailly, 2008]
Replica C	GIPSA, Grenoble, France	2006	Inspired by the Eindhoven model, Bailly's[Bailly, 2009] version provided improved clamping of the latex to the metal blocks. This version also incorporated a number of different and variable downstream conditions, such as ventricular bands.	Bailly *et al*[Bailly *et al.*, 2008; Bailly, 2009]
Replica B	Edinburgh, UK	2007	Designed as a lip-reed model. Used the basic idea from the Eindhoven and GIPSA model of metal blocks wrapped with latex to form the lips (known as 'lip blocks' in case of replica B). Improved on their design by using glue to provide a reliable seal between latex and metal, which eliminated the need for the extensive clamping systems of prior versions. Also provided improved optical access to the lip cross-section See section 3.2.3.	Present author

Table 3.1: A table summarising the various versions of the *in vitro* lip-reed and vocal fold models relevant to this thesis.

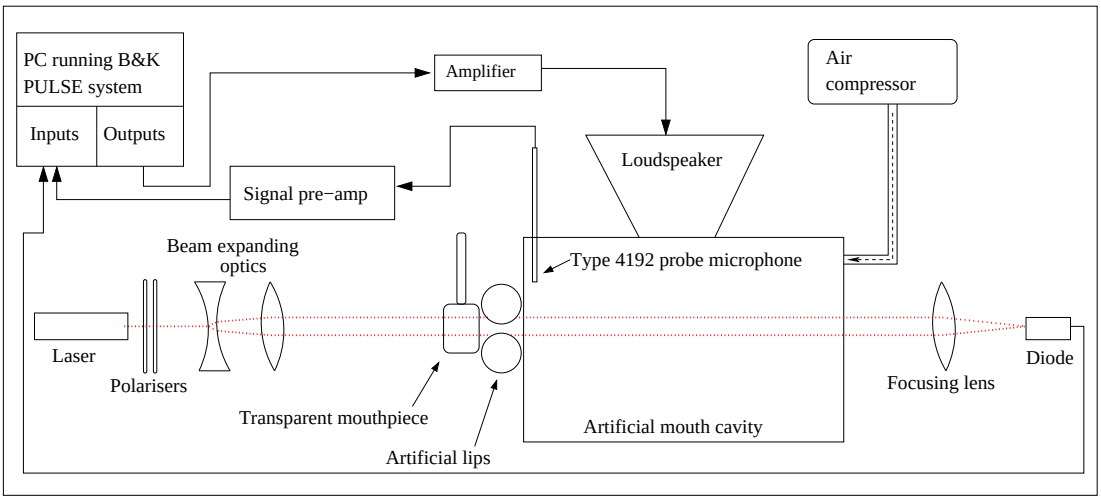

Figure 3.6: A schematic diagram showing the layout of the transmission method experiment for use on *in vitro* lip-reed models. The apparatus was mounted on an optical rail. In this example the subject of the experiment is replica A[Richards, 2003] (see section 3.2.2).

vibrometer in a number of directions, but each one can only yield information about lip motion in line with the laser beam.

The classical theory of musical valve physics presented in section 2.7.1 is based on the assumption that the fluid system is incompressible, quasi-stationary and frictionless in the bulk of the flow. The phenomenon of flow separation from the valve surface is assumed to occur at a fixed point along the valve, typically the minimum cross-section. Under this assumption, the flow of fluid through the valve is a unique function of the upstream and downstream pressures, and the valve cross-section at flow separation. This is the reason that great significance has been attached to the evolution of the valve opening during playing[Bromage *et al.*, 2005; Gilbert *et al.*, 2005; Bromage, 2006].

3.3.2 The *transmission* method for measurement of the mechanical response of *in vitro* artificial lips

The importance of the valve opening has meant that a mechanism to determine the mechanical response using the total (or partial) lip opening is preferable to the single dimensional approach of the laser vibrometer. Backus[Backus, 1961] first used a photoelectric method to study the open area evolution of an artificial clarinet reed during playing. His approach involved illumination of the reed opening with a light source, and collection, with a photomultiplier, of the light on the other side. The light intensity was modulated by the oscillations of the reed opening, providing a continuous open reed area signal observable on a cathode ray oscilloscope. This technique became the basis for the laser-diode technique used extensively in the last decade for

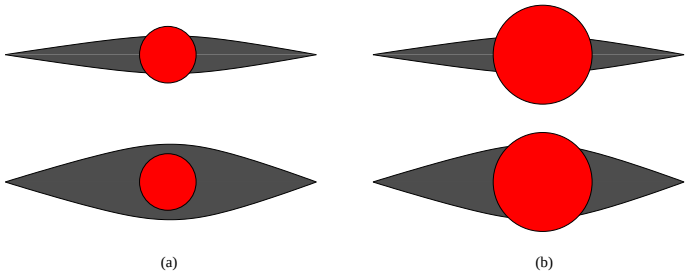

Figure 3.7: A schematic diagram to illustrate the importance of full lip illumination when performing a transmission method mechanical response experiment. (a) The expanded laser beam is sufficiently large at small lip openings, but saturates as the lip opening increases, resulting in a loss of information. (b) The expanded laser beam is large enough to encompass the full dynamic range of lip oscillations. (Note that in this figure only the central opening height region has been illuminated, but the principle of adequate lip coverage remains the same for full lip illumination.)

evaluation of the mechanical response[Cullen *et al.*, 2000; Neal, 2002; Richards, 2003; Bromage, 2006; Vilain *et al.*, 2003; Ruty *et al.*, 2007]. This setup is also known as the *transmission method*.

Figure 3.6 shows a schematic layout of the transmission method experiment used on *in vitro* musical valve models. The lip opening was illuminated with an expanded laser beam from a continuous wave laser (Melles Griot 5mW). The beam was expanded with a pair of diverging lenses. The laser light was directed through a pair of polarisers, the relative alignments of which could be used to vary the beam intensity. The light then passed through the lip opening and through the mouth cavity of the replica, before being focussed down to a small point of light on a photosensitive diode (EG&G HFD-1100), beyond the upstream end of the mouth. It was important that the beam covered a large enough area of the artificial lips, as illustrated by figure 3.7. This was to ensure that the full dynamic range of the lip oscillations was recorded.

Diode calibration

The diode provided an AC voltage output which was related to the lip opening. It was necessary to perform a diode calibration procedure to relate this voltage to the lip opening illuminated by the laser light[Cullen, 2000; Neal, 2002]. The calibration procedure was performed by replacing the artificial lips with an adjustable rectangular slit. The slit was illuminated with the same expanded laser beam and its width varied from fully closed to 3.5mm wide. This had the effect of gradually increasing the light intensity being focussed onto the diode, and thus increasing the diode output voltage.

Figure 3.8 shows the result of a diode calibration. The blue line is a linear fit of the experimental data marked by the black crosses. For an extensive range of light intensities the diode output was almost linear. This meant that the voltage oscillations

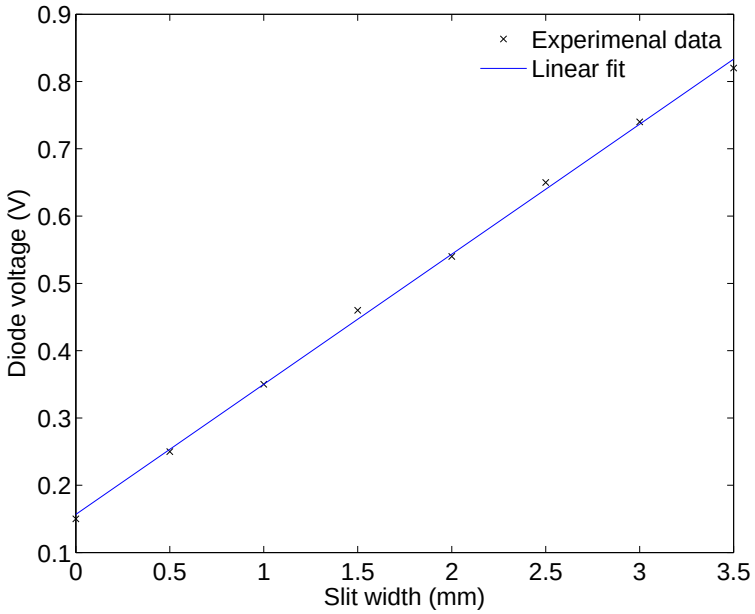

Figure 3.8: A diode calibration plot relating the width of a square slit illuminated with an expanded laser beam to the output voltage of the diode. The blue line represents a simple linear fit of the data.

recorded from the diode were directly representative of the oscillations in the lip opening during a mechanical response experiment.

By calculating the gradient and intercept of the fitted linear curve it was possible to convert the diode voltage obtained from the experiments into an equivalent rectangular slit opening. However, such a calibration calculation was not of significant benefit. The absolute value of the lip openings was not required for a mechanical response calculation: only the time domain oscillation information was needed, obtained directly from the diode AC voltage. The calibration process provided a check that the diode response was suitably linear.

Acoustical driving system

The lips were acoustically driven into small amplitude oscillation by a loudspeaker powered by a studio amplifier. It has been shown by Richards[Richards, 2003] and Neal[Neal, 2002], and explained in section 2.7.1, that the choice of the driving direction does not matter for the relatively low sound pressure levels involved in a mechanical response measurement. It is the dynamic pressure difference Δp across the lips which drives their motion, and this may be established by driving the lips from either side. Thus the loudspeaker may be coupled to the mouthpiece for downstream driving, or to the mouth cavity for upstream driving, and the choice may be dictated by the requirements of the experimental setup. For most of the experiments involving the

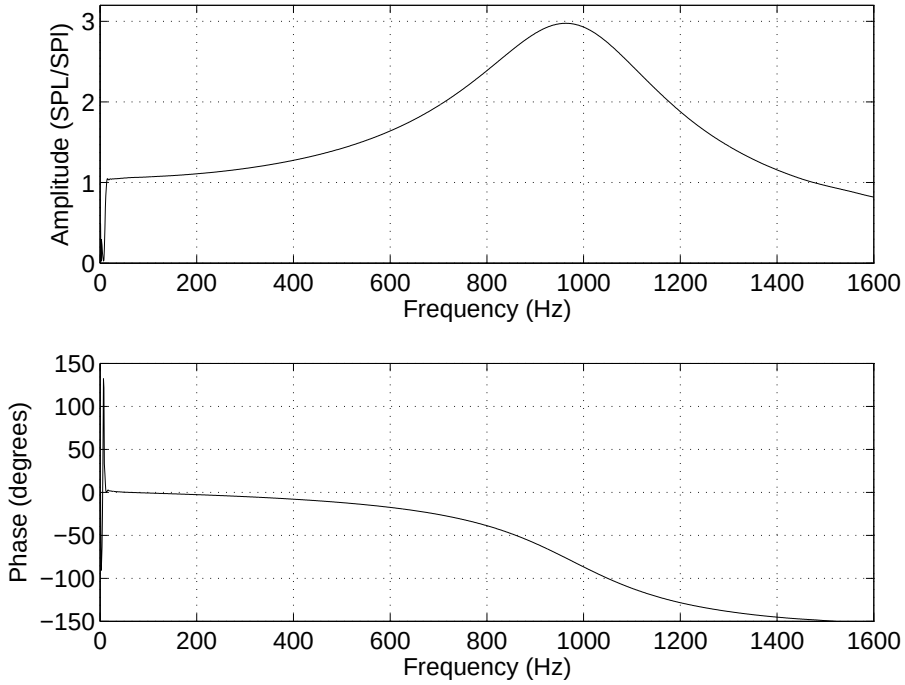

Figure 3.9: A magnitude and phase calibration curve for a Brüel & Kjær Type 4192 microphone with a short probe attachment.

artificial brass players the artificial lips were driven from the mouth cavity.

The acoustical driving signal was a chirped sine wave of approximately 10s duration. A sine wave chirp was used because it could be easily customised to fit the required bandwidth of a particular experiment. The signal could also be calibrated so as to provide the lips with an approximately frequency-flat amplitude spectrum so that the lips received the same amplitude acoustic driving at 70Hz as they did at 350Hz. This step helped to maximise the signal-to-noise ratio of the experiments[Epps *et al.*, 1997; Mulgrew *et al.*, 1999]. This was because the system of the artificial brass player possessed its own natural acoustic resonances which filtered the acoustical driving from the loudspeaker. One of the most important requirements of the experiment was to provide sufficient acoustical driving to impart measurable motion to the lips at frequencies above 150Hz. The calibration procedure ensured that the resonances of the system did not overly degrade the excitation signal for these frequencies.

The calibration was performed by first generating a frequency-flat excitation signal from the loudspeaker apparatus. This signal was then coloured by the resonances of the system and recorded by a microphone in the mouth cavity. The spectrum of the recorded signal was then used to synthesise a new signal that compensated for loud and quiet regions of the recorded sweep and thus providing the lips with a frequency-flat driving spectrum. The Matlab (©The Mathworks Inc.) software platform was used to synthesise the calibrated sine sweep. This platform provided a useful environment for

data manipulation and plotting throughout this thesis.

Microphones

The acoustic pressure in the mouth cavity was measured with a Brüel & Kjær Type 4192 microphone. This microphone used a short probe attachment so that it could be placed close to the lip surfaces and thus accurately monitor the pressure acting on the lips. The probe introduced a magnitude and phase difference which required calibration.

A complex calibration curve $\widetilde{\mathbf{H}_{probe}}$ was obtained using a Brüel & Kjær calibration head and a second Type 4192 microphone as a reference. Both microphones were submitted to a swept sine driving signal in the calibration head, and a frequency response calculation revealed the magnitude and phase deviations introduced by the probe. This data was used to adjust the mechanical response curves obtained using the probe microphone.

An example of a probe microphone calibration curve is shown in figure 3.9. For the frequency range of interest, typically between 50Hz and 350Hz, the addition of the probe caused little alteration of the microphone response in either magnitude or phase. Nevertheless, these small perturbations were accounted for with a calibration program applied in Matlab.

Signal acquisition and processing system

The diode, loudspeaker and microphone signals were coordinated using the Brüel & Kjær PULSE data acquisition and signal processing system. This system allowed for real-time signal input and output. It also provided a rich platform for real-time frequency domain signal processing. Signals could be sampled at a high frequency (typically 60kHz) and quickly analysed.

A calibrate excitation sweep S_{cal} was selected from within the PULSE software environment and outputted to the amplifier through the bespoke hardware interface. The resulting diode voltage and microphone signals were simultaneously sampled from the hardware inputs and passed back to the software. The system was set up to perform a real-time frequency response calculation between the diode signal $h_{mr}(t)$ and the microphone signal $\Delta p_{mr}(t)$, resulting in a complex frequency domain mechanical response measurement $\widetilde{\mathbf{H_{mr}}}(\omega)$. The mathematics of this calculation have been outlined in section 2.4.3.

The mechanical response measurement result is a complex dataset which may be split into two subsets for magnitude and phase:

$$\widetilde{H_{mr}(\omega)} \quad = \quad \mid \mathbf{H}_{mr}(\omega) \mid \tag{3.2}$$

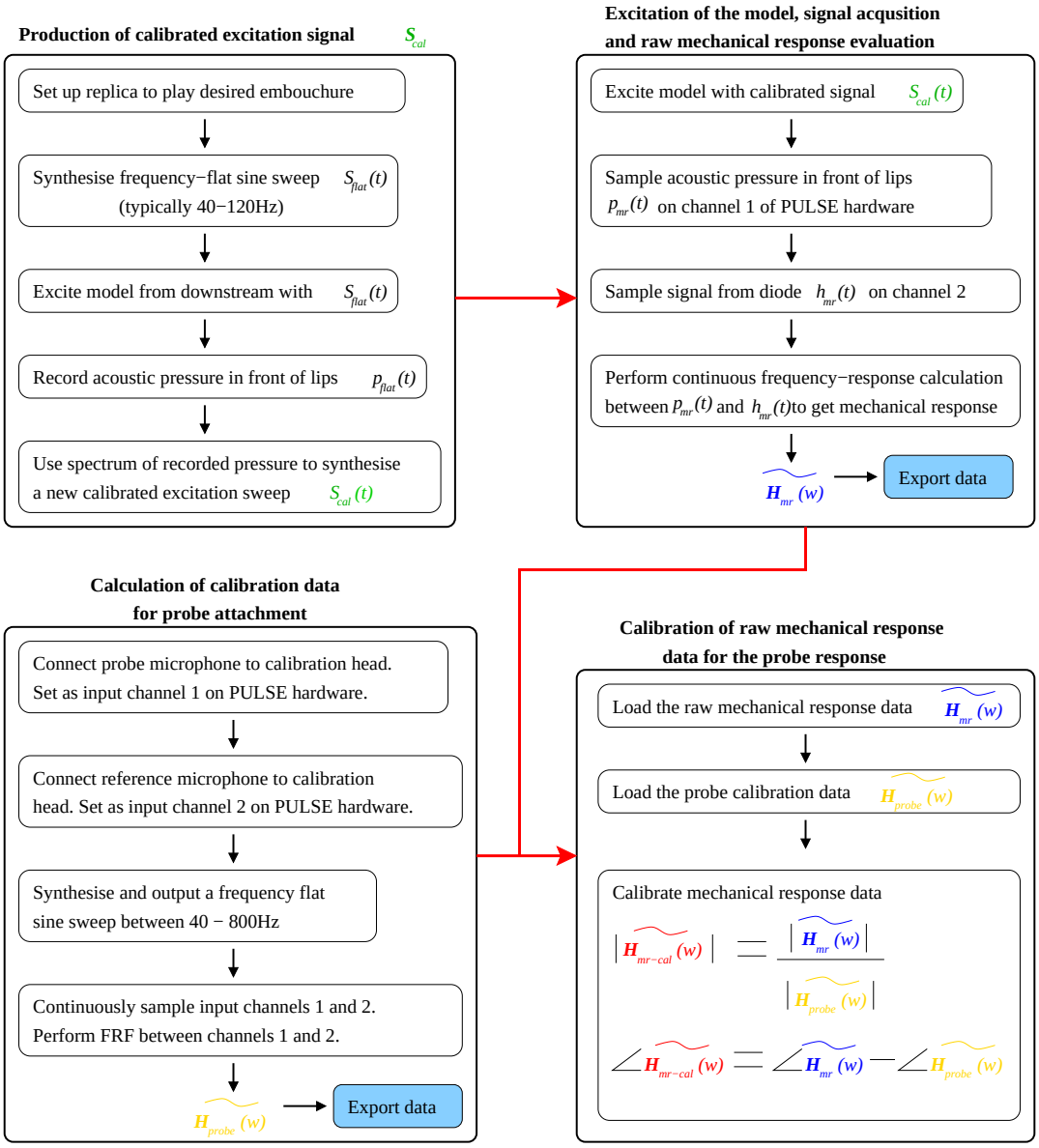

Figure 3.10: A signal flow chart to illustrate the acquisition of a transmission method mechanical response measurement, including calibration of the data for the response of a probe attachment.

$$\angle\widetilde{H_{mr}}(\omega) \quad = \quad \angle\widetilde{\mathbf{H}_{mr}}(\omega) \tag{3.3}$$

A plot of the mechanical response magnitude against frequency may reveal the natural resonances of the mechanical system. The phase plot is also of use because it describes the dynamic relationship between the driving force and the lip motion, and may be used to identify frequencies where self-sustained oscillation of the valve may be possible. This interpretation relies on the classical theory of musical valve oscillation outlined in section 2.7.1. At frequencies where the phase curve crosses the values of $\pm 90^\circ$ ($\frac{\pi}{2}$), the valve may cooperate with an acoustical standing wave to produce self-sustained oscillations.

The mechanical response dataset was exported from the PULSE system as a datafile which could be read by the Matlab software platform. Matlab was then used to re-organise, plot and save the data as required.

The probe calibration measurement was also coordinated using the PULSE system. This allowed a frequency response function for the probe to be instantly calculated as the calibration sine sweep was played back in the calibration head. The data from this measurement was then exported for calibration of the mechanical response datasets. This calibration process was undertaken in the Matlab software platform. The final result was a calibrated complex mechanical response data-set $\widetilde{\mathbf{H}_{mr-cal}}(\omega)$, which could be split into a magnitude curve and a phase curve.

Figure 3.10 provides a signal flow chart illustrating the various processes that were necessary in order to perform a transmission method mechanical response measurement leading to a calibrated data-set $\widetilde{\mathbf{H}_{mr-cal}}(\omega)$. It includes details of the synthesis of the calibrated excitation signal $S_{cal}(t)$, and the acquisition of the probe calibration data $\widetilde{\mathbf{H}_{probe}}(\omega)$.

Traditional and experimentally adapted mouthpieces

A key challenge of the transmission method experiment is that information must be gathered about a large area of the lip-reed. The small diameter of a typical brass instrument mouthpiece makes optical access very difficult, particularly when the mouthpiece is attached to a full instrument.

Copley and Strong[Copley and Strong, 1996] made observations of an oscillating lip-reed by cutting small holes into a normal trombone mouthpiece. Unfortunately the viewing angle allowed by this technique was necessarily limited and the entire lip opening could not be observed during a single measurement. Cullen[Cullen, 2000] and Neal[Neal, 2002] addressed this problem by using straight lengths of copper tubing to represent the brass instrument. It was then possible to illuminate the lip opening with a concentrated light beam. However, the narrowness of the tube diameter restricted the illumination to the central region of the lip opening. This region is known as the

Figure 3.11: At left is the transparent mouthpiece developed by Richards[Richards, 2003]. Also shown is the mouthpiece support mechanism, attached to the mouthpiece from the right hand side of the photo. At right is a Dennis Wick 6BS trombone mouthpiece.

central opening height (see figure 3.7).

The issue of optical access to the lip reed was tackled by Richards[Richards, 2003] with transparent mouthpieces, an example of which is shown in figure 3.11. This dimensions of this mouthpiece were based on those of a Dennis Wick 6BS trombone mouthpiece. The mouthpiece cup and shank of a 6BS were cut in two, and the shank used for the transparent mouthpiece. The cup of the transparent mouthpiece was made from a short tube of perspex with a clear glass viewing window glued into one end. The volume of the cup was designed to match that of the normal 6BS cup. The lips of a player were then pressed into the open end of the perspex cup. The shank was screwed into the cup at right angles, leaving a clear view of the lip opening through the glass window. The player would find the instrument angled at 90° to their face. This uncomfortable orientation meant that the instrument was generally mounted on an optical bench.

The apparent crudity of this mouthpiece belies the fact that many trombone players find it to be very easy to play. Experimental work using the artificial brass playing systems outlined in section 3.2 confirm that it functions in much the same manner as a normal mouthpiece[Bromage *et al.*, 2005; Gilbert *et al.*, 2005; Chick *et al.*, 2005]. However, it provides an extremely useful experimental advantage over traditional mouthpieces because the full lip opening may be clearly observed with no optical distortion.

The remarkable usability of all the transparent mouthpieces begs further investigation. Despite the carefully outlined fluid mechanical considerations presented in section 2.5 that describe the aerodynamic field around the valve, the straightforward functionality of the transparent mouthpieces suggests that, at least in the case of the brass instrument lip-reed, it is the acoustical field that is of most importance. This

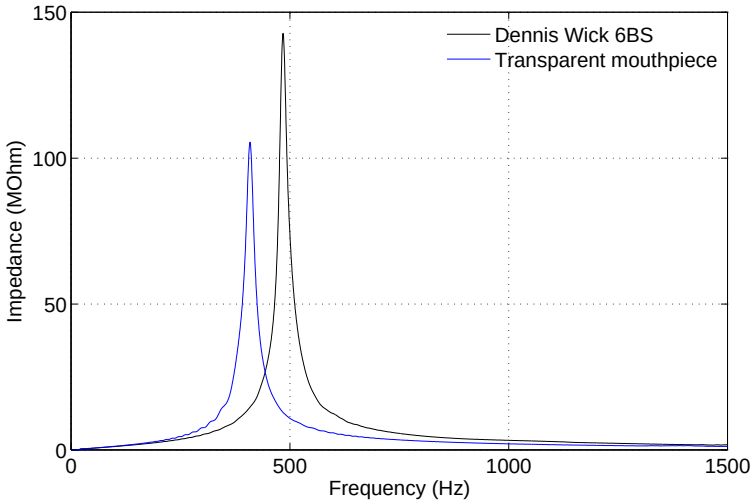

Figure 3.12: Input impedance magnitude curves of a Dennis Wick 6BS trombone mouthpiece and the experimentally adapted transparent trombone mouthpiece.

issue is addressed further in section 8.6, following the results of the flow experiments presented in chapter 7.

Figure 3.12 shows input impedance magnitude curves of the transparent mouthpiece and a Dennis Wick 6BS trombone mouthpiece. They exhibit similar behaviour in overall shape and peak frequency. The transparent mouthpiece has a slightly lower resonance frequency ($\approx$ 460Hz) compared to the 6BS ($\approx$ 500Hz), which is a consequence of the increase in the mouthpiece cup volume (12ml compared to 9ml). The curves were obtained using the BIAS[IWK, 2009] system developed at the Institut für Wiener Klangstil in Vienna. It provides a fast, simple tool for measurement of the input impedance of musical instruments.

Yoshikawa[Yoshikawa and Muto, 2003] also constructed a transparent mouthpiece for experimental investigations into the lip-reed. The mouthpiece was shaped like a traditional horn mouthpiece, but constructed from perspex. It allowed significantly improved optical access to the lip opening over traditional mouthpieces, though the images were unavoidably distorted by the curvature of the perspex.

Choice of the lip illumination region

The use of a transparent mouthpiece for the transmission method experiments meant that the entire lip opening could be illuminated by the laser beam. The full downstream faces of the lips were also available for viewing and measurements. This arrangement permitted a variety of options for measuring the lip motion.

The work of Gilbert *et al*[Gilbert *et al.*, 1998] measured the longitudinal lip motion of a single artificial lip, in line with the airflow, as illustrated in figure 3.13 (this is the

direction of the x-axis in figures 3.3 and 3.5). A laser doppler vibrometer (LDV) was directed onto the outer face of the lip surface as they were excited with a loudspeaker. The resulting mechanical response curves were thus limited to the resonances associated with this single degree of freedom. The artificial lips used in this pioneering work tended to reveal a single dominant resonance with an 'outward striking' phase behaviour. Such a result seems consistent with the longitudinal measurement axis of the experiment.

The transmission method experiments of Cullen[Cullen, 2000] and Neal[Neal, 2002] used the central portion of the lip opening between a pair of artificial lips, as illustrated in figure 3.14. This effectively formed a two-dimensional area, so that the mechanical response curves could exhibit resonances associated with two degrees of mechanical freedom (the directions of the y-axis and z-axis in figures 3.3 and 3.5). Of these degrees of freedom it is motion associated with the open height (the y-axis in figure 3.14) that is of most importance in the mechanical response curves. This is the motion that results in a continuous oscillation of the open area. The degree of freedom associated with the z-direction does not generally contribute significant oscillations during playing.

It is possible, however, that a mechanical system with multiple resonances can exhibit coupling between the resonances. Thus a measurement sensitive to a single degree of freedom is not necessarily limited to the measurement of a single resonance. This can be seen in the mechanical response curves of Cullen *et al*[Cullen, 2000], Neal[Neal, 2002] and Richards[Richards, 2003], where there are normally at least two important resonances present. The lower of these resonances tends to exhibit an outward striking behaviour, with the second resonance displaying an inward striking behaviour. The actual mechanical motion of the valve is expected to be different for these two modes, yet a single mechanical response measurement with effectively one degree of freedom is sensitive to both resonances. This matter is addressed in some detail in section 4.5.2, where mechanical response measurements are performed separately of each component of motion.

Step-by-step summary of a transmission method mechanical response measurement applied to artificial lips

A transmission method mechanical response measurement requires a careful experimental procedure to ensure accurate and repeatable results with artificial lips. The procedure is summarised here.

1. Set up the desired embouchure with the artificial brass player and transparent mouthpiece. Adjust the control parameters to their appropriate values (see sections 3.2.2 and 3.2.3).

2. Note the playing frequency of the embouchure.

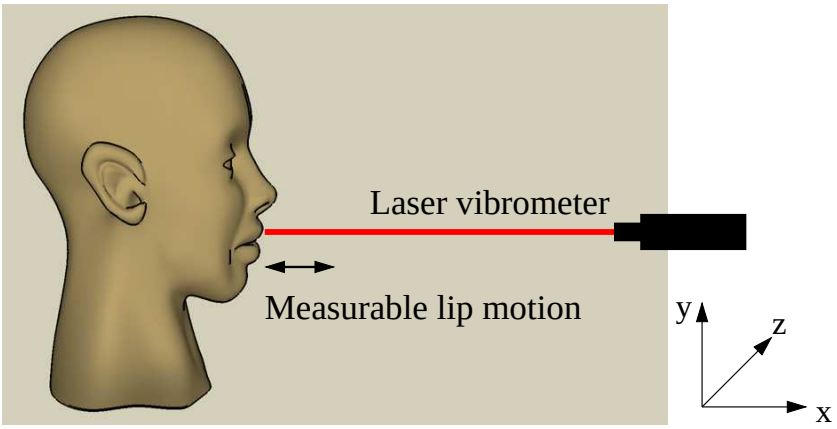

Figure 3.13: An illustration of the longitudinal lip motion measurable with a laser vibrometer, as in Gilbert *et al*[Gilbert *et al.*, 1998].

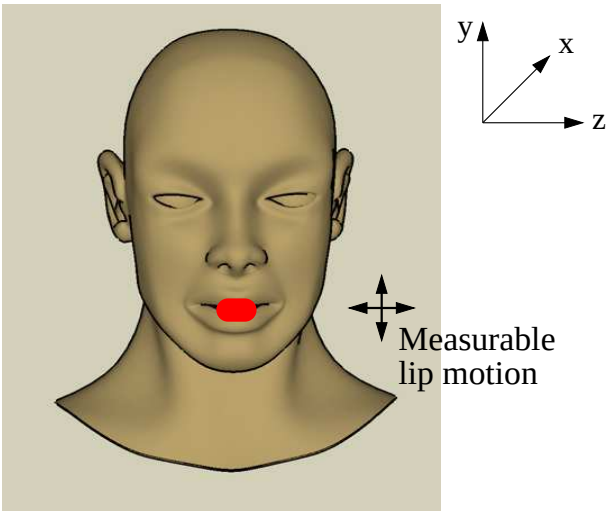

Figure 3.14: An illustration of the transverse lip motion measurable with a transmission method mechanical response experiment, as in Cullen[Cullen, 2000] and Neal[Neal, 2002]. The red circle shows the region of the lips illuminated by the expanded laser beam (shining into the page in this example).

3. Drive the loudspeaker on the mouth cavity with a constant amplitude (in the time domain) swept sine wave, and measure the resulting signal with the probe microphone.

4. Use the spectrum of the probe microphone signal to re-synthesise a new excitation sweep designed to be frequency flat (constant amplitude in the frequency domain) at the probe microphone. This is the lip driving signal.

5. Check the diode and microphone signal levels to ensure that they remain within the dynamic range of the measurement system.

6. Commence the mechanical response measurement with the PULSE system. The excitation signal should be played back three or four times to further increase the signal-to-noise ratio of the measurements (the PULSE system allows for spectrum averaging).

7. Halt the sweep and check the measurement curves. Data may be exported for further manipulation and archiving in Matlab.

For each mechanical response measurement, the frequency domain data from PULSE was exported and placed in an appropriately named folder together with the excitation signal and a copy of the probe calibration data. It was also possible to directly export the raw time domain signals from the PULSE software for manual evaluation of the frequency response function in Matlab. These signals were placed together with the other data in the same folder.

3.3.3 The *video* method for measurement of the mechanical response of *in vitro* artificial lips

The transmission method outlined in section 3.3.2 has successfully been used for several years to investigate the mechanical properties of artificial lips. If performed using the PULSE framework such measurements are quick and reliable to obtain. However, as outlined in section 1.1 the field of musical valve research demands experimental evidence from *in vivo* experiments on human players. The artificial brass players presented in sections 3.2.2 and 3.2.3 appear to provide excellent laboratory simulations of real players, but such comparisons really require evidence to be scientifically satisfying. Such evidence should come from comparisons between measurements on artificial and human players under playing conditions, when the lips are formed into an embouchure.

An attempt has been made to measure the mechanical properties of *in vivo* human vocal folds. Svec *et al*[Švec *et al.*, 2000] used a mechanical shaker to vibrate the relaxed vocal folds and measured their response with a laryngoscope. This setup included a high speed video camera to monitor the vocal fold oscillations. The vocal folds in the study displayed at least three resonances, though the work did not include a commentary on

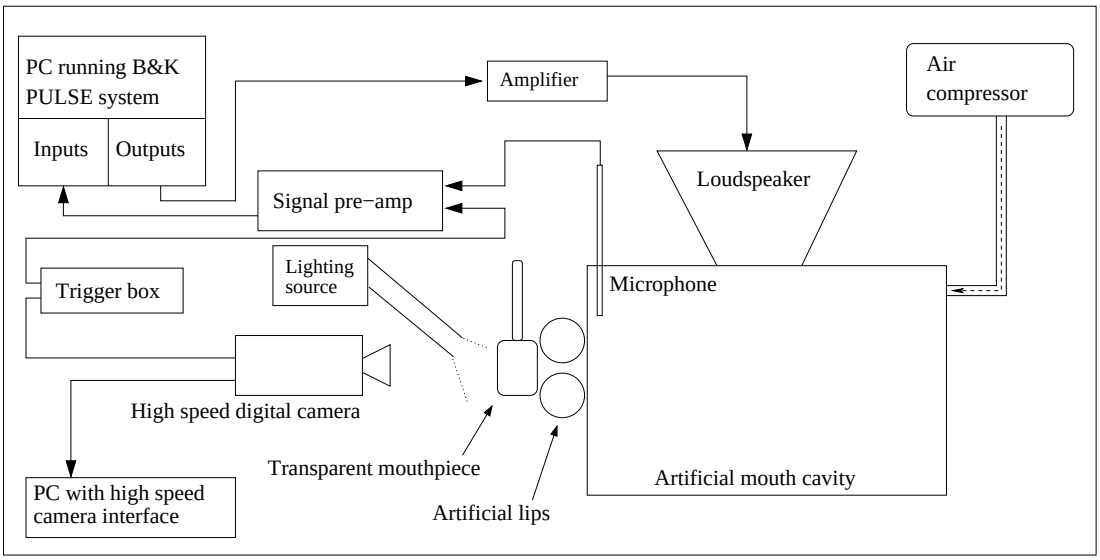

Figure 3.15: A schematic representation of the video method for mechanical response measurements of artificial lips. The artificial lips are driven from the mouth cavity, and the motion is recorded with a high speed digital video camera through a transparent mouthpiece. In this figure the system has been set up to measure replica A (see section 3.2.2).

the implications for acoustical coupling in the system. The method presented here used acoustical driving to excite the lips under playing conditions.

The transmission method was not suitable for application to human players. It required extensive experimental apparatus on either side of the lips in order to accommodate the laser-diode optical system, and this was simply not possible without severe damage to the human subject. Thus a new technique was required that could be directly applied to both artificial and human lips. This new technique is called the *video method* for mechanical response evaluation.

The laser-diode optical system of the transmission method was exchanged for a high speed digital video camera system, as illustrated schematically in figure 3.15. The objective of this change was to enable the open area of the lip-reed to be monitored as with the transmission method, but with a less obtrusive experimental setup.

High speed digital video camera

The high speed digital camera (Vision Research Inc., Phantom v4.1) was set up to observe the lips through the transparent mouthpiece. This viewpoint corresponded to that illustrated in figure 3.14. The camera was capable of recording at frame rates up to several kilohertz, depending on the selected resolution of the CCD. The resolution was variable up to a maximum of 512×512 pixels. At this resolution the camera performed at its slowest frame rate (500 frames per second). A resolution of 128x256 pixels was

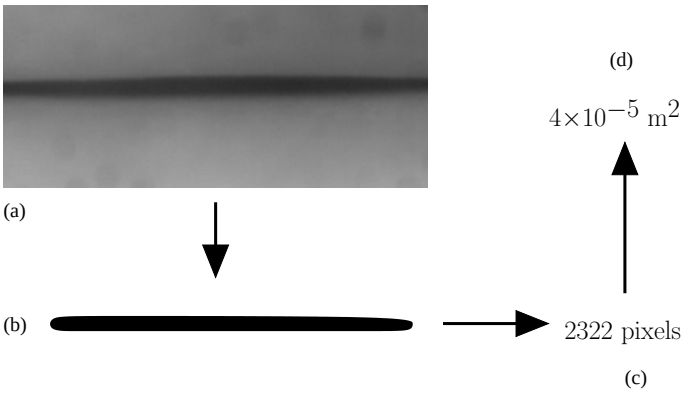

Figure 3.16: The image analysis process for the video method. (a) Raw image extracted from a video of the artificial lips of replica A during a video method mechanical response measurement. (b) The open area region extracted from the raw image based on a threshold pixel intensity. (c) The total number of pixels contributing to the open area. (d) The actual open area in units of m^2 after application of a calibration factor.

the most common choice in this work, which allowed frame rates up to 2000Hz. This meant that the oscillations of the lip opening were discretely sampled as opposed to the continuous analog output of the diode. The analog diode signal was sampled by the PULSE system, but at a much higher frequency than the high speed camera frame rate. This was a key difference between the methods.

The camera had a limited memory buffer which meant that it could only acquire a fixed volume of data. Thus for a given resolution there was an inverse relationship between the frame rate and the total time over which a measurement could run. For example, at a resolution of 128×256 pixels it was possible to record at either 1000Hz or 2000Hz. However, the total number of frames that could be recorded into the memory buffer was fixed (≈ 8100) so that at 1000Hz the camera could run for approximately 8s, and at 2000Hz it could run for approximately 4s. It was important to strike a balance between providing a sufficient frame rate to avoid aliasing of the data, whilst allowing the excitation sweep to drive the lips for a sufficiently long time that a clean response could be measured.

The lips were illuminated with a high intensity light source (Schott KL1500 LCD). It was important to orientate this light source so as to create the maximum possible contrast between the lip surfaces and the open area between them. The lips reflected considerably more light than the open area (essentially the mouth cavity), and so this region was rendered very dark in the video images.

Analysis of the high speed camera video

A mechanical response measurement yielded a video from the high speed camera lasting several seconds. At the typical frame rates of one or two kilohertz this equated to several thousand individual images. In order to deduce the oscillations of the lip opening it was necessary to analyse this sequence of images one by one to determine the instantaneous lip opening for each image. Concatenation of this information lead to a discrete time domain signal showing the oscillation of the lip opening over the course of the measurement.

Analysis of the instantaneous lip opening was performed using a threshold pixel technique in Matlab. A program was written, based on the analysis program of Richards[Richards, 2003] and Bromage[Bromage, 2006], which performed this analysis for an entire set of images. The images were first extracted from the camera video as uncompressed bitmap files using the commercial software package VideoMach[Gromada.com, 2003]. The Matlab program was then set to examine each image and determine the open area based on a threshold pixel intensity. Pixels darker than the specified intensity were considered to be from the open area and thus contributed to the total pixel count for the image. This process is shown in figure 3.16.

Signal synchronisation and mechanical response evaluation

The video method required careful synchronisation between the high speed camera video recording, the acoustical excitation signal and the microphone signal. The camera system was controlled from a dedicated computer and camera interface. The acoustical excitation and microphone sampling were controlled from a second computer running the PULSE platform. The two computer systems were synchronised with a stand-alone external triggering unit (Berkley Nucleonics 500A).

The PULSE computer was first instructed to begin driving the loudspeaker with a calibrated sine sweep (see section 3.3.2). After approximately two complete excitation sweeps to allow the system to settle, the trigger unit was manually triggered to simultaneously send a negative-going voltage edge to the two computers. At this trigger signal the high speed camera began to acquire images into its memory buffer and the PULSE system began to sample the microphone signal and the trigger signal. A pre-delay was set in the PULSE software so that the precise moment of triggering could be determined and temporally synchronised with the microphone signal. The PULSE system was programmed to play back the excitation signal for a time period longer than the camera was able to acquire images. This ensured that the lips were driven for the full duration of the camera acquisition time.

The camera provided a video that was analysed, as described in the previous section, to yield a time domain signal representative of the oscillating lip opening. The PULSE system yielded a recording of the trigger signal and the microphone signal. These data

were exported as data files readable by Matlab and placed in a folder together with the open area data and probe calibration data. A program was written in Matlab to perform the synchronisation of the open area and microphone signals, and to then calculate the mechanical response using the frequency response function described in section 2.4.3. Calibration for the probe microphone was also performed by the program.

The video method required a considerably longer analysis procedure than the transmission method. A single measurement took approximately twenty minutes to analyse and produce a mechanical response curve, as opposed to the near instantaneous results provided by the transmission method run under the PULSE system.

Figure 3.17 shows an overall signal flow chart illustrating the steps necessary to perform a video method mechanical response measurement on an *in vitro* lip-reed or vocal fold model.

Compatibility of the transmission method and video method frequency response function calculations

The video method mechanical response calculation was clearly not performed in the same environment as the transmission method calculation. The former used two discrete time domain signals which were cross-correlated in Matlab. The later used a real-time frequency response calculation which made use of spectrum averaging. It was thus important to ensure that the two methods of calculation were compatible.

The frequency response function used by the PULSE system has been shown in equation 2.4. It makes use of the frequency domain cross-spectrum of the excitation and response signals (the microphone and lip motion), and the power spectrum of the response (the lip motion). The video method mechanical response calculation program was written to take advantage Matlab's implementation of these functions. The program was tested with raw, unprocessed time domain data of a transmission method experiment which was exported from PULSE, along with the usual processed frequency response data. The results of the two measurements were extremely close. The frequencies of all the lip resonances were within the experimental error between consecutive transmission method measurements ($\approx 5\%$).

Step-by-step summary of a video method mechanical response measurement applied to artificial lips

A brief summary of the steps required to perform a video method mechanical response measurement are presented below.

1. Set up the desired embouchure with the artificial brass player and transparent mouthpiece. Adjust the control parameters to their appropriate values (see sections 3.2.2 and 3.2.3).

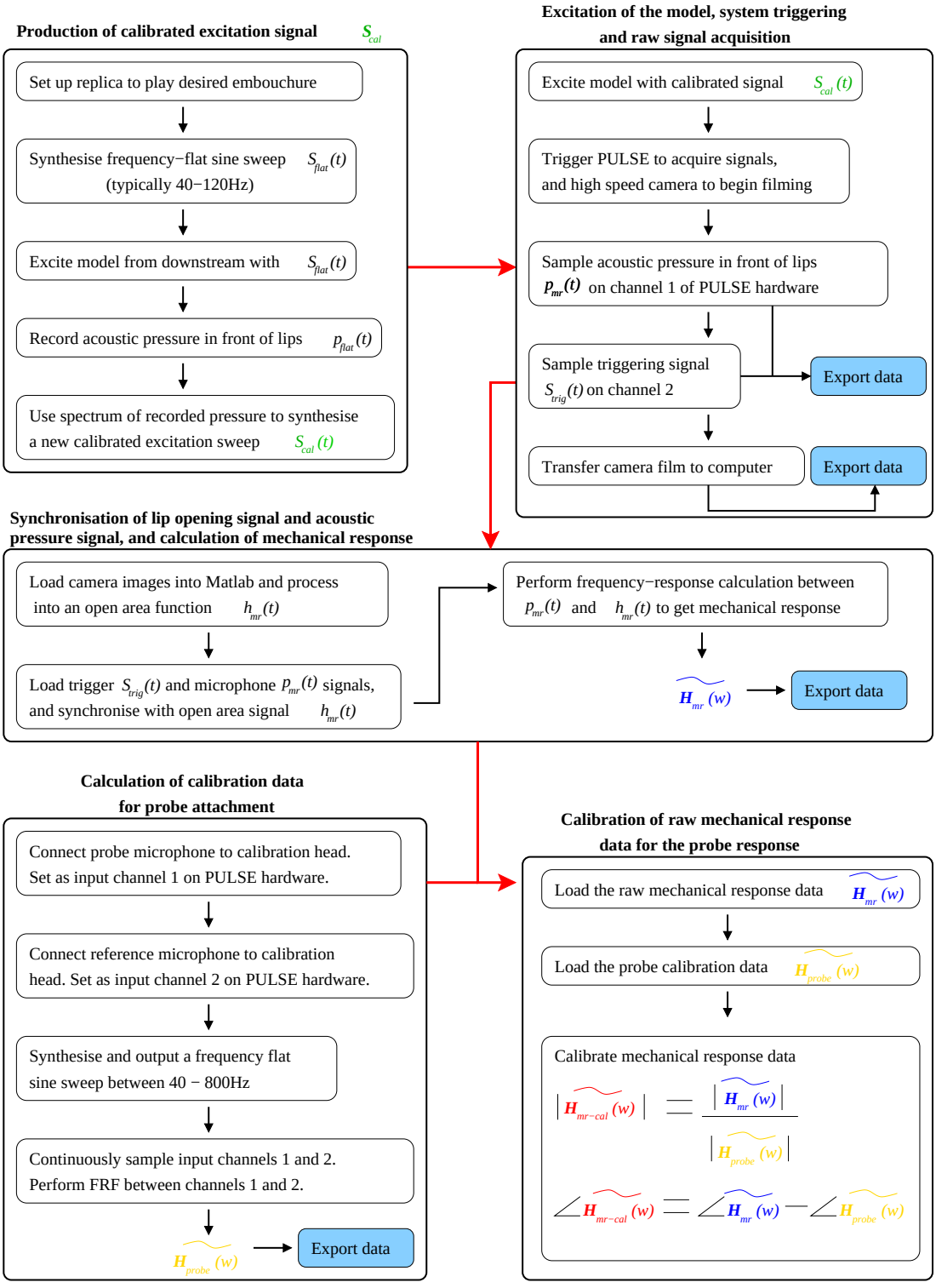

Figure 3.17: A signal flow chart to illustrate the acquisition of a video method mechanical response measurement, including synchronisation of the microphone and high speed camera signals, and calibration of the data for the response of a probe attachment.

2. Note the playing frequency of the embouchure.
3. Synthesize an appropriate driving signal (see section 3.3.2).
4. Setup up the camera and light source to optimally illuminate the lips.
5. Check that the microphone signal level is within the dynamic range of the measurement system.
6. Instruct PULSE to begin driving the loudspeaker.
7. After approximately two complete cycles of the excitation sweep, manually trigger the trigger unit to begin the measurement. One full sweep will then be played back for the actual measurement.
8. When the measurement has completed export the video as a movie file, and the trigger and microphone signals as data files.
9. Analyse the movie file to produce and open area signal.
10. Perform the frequency response function calculation with the Matlab program and save the data into a Matlab data file for archival.

Examples and analysis of video method measurements are presented in sections 4.4 and 4.5.2.

3.3.4 The *video* method for measurement of the mechanical response of *in vivo* human lips

The objective of the video method development was to allow mechanical response measurements to be made on real human lips formed into playable embouchures. The video method setup developed for artificial lips described in section 3.3.3 was not directly suitable for application to human players. The primary reason for this was the issue of the loudspeaker coupling.

The artificial lip setup used a loudspeaker coupled to the mouth cavity to drive the lips, but this was not possible with human players. This meant that the human lips needed to be driven from their downstream side (the instrument side rather than the mouth side). The artificial lips could easily be driven from downstream with a suitable loudspeaker-mouthpiece coupling, as in Richards[Richards, 2003]. With this setup it was possible to first couple a trombone to the mouthpiece in order to establish the required embouchure. The trombone could then be replaced with the loudspeaker coupling for the actual mechanical response measurement[Neal, 2002]. This process was not suitable for human players as it required a considerable amount of time and disturbance to the experimental setup. It was therefore unlikely that a player would be able to maintain a steady embouchure for the course of a measurement.

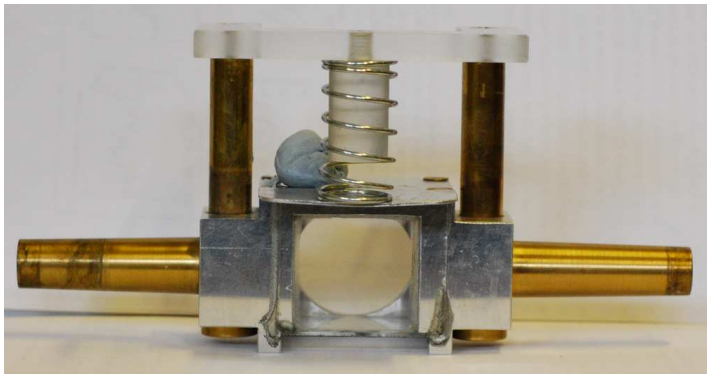

(a)

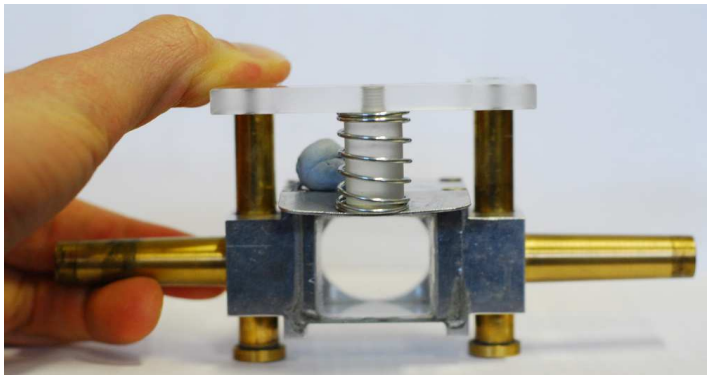

(b)

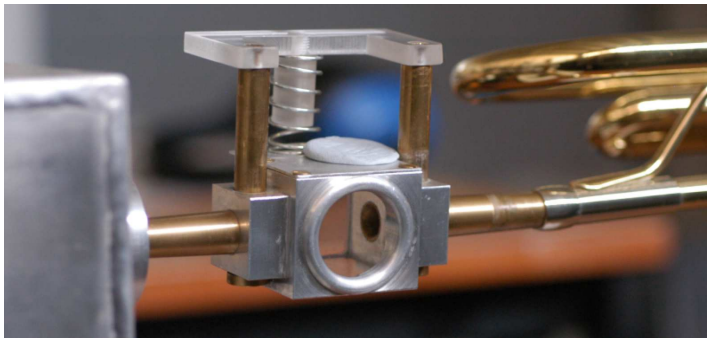

(c)

Figure 3.18: Three photographs of the double-shanked transparent mouthpiece developed for the application of mechanical response measurements to human players. In (a) the mouthpiece is shown from the front, looking towards the mouth of the player. This photograph shows the rest position of the mouthpiece, which permits airflow through only the left-hand shank and into a coupled brass instrument. Photograph (b) illustrates the depression of the spring-loaded control valve, which simultaneously closes off the left-hand shank and opens up the right-hand shank to the loudspeaker coupling apparatus. The blue substance next to the spring is acoustic putty, used to seal a probe microphone into the main cup area. Photograph (c) shows the mouthpiece from the opposite side and simultaneously connected to the loudspeaker driving system at left and a brass instrument at right. The lips of the player couple to the grey metal rim. The valve was un-depressed in the photo, indicating a coupling to the brass instrument.

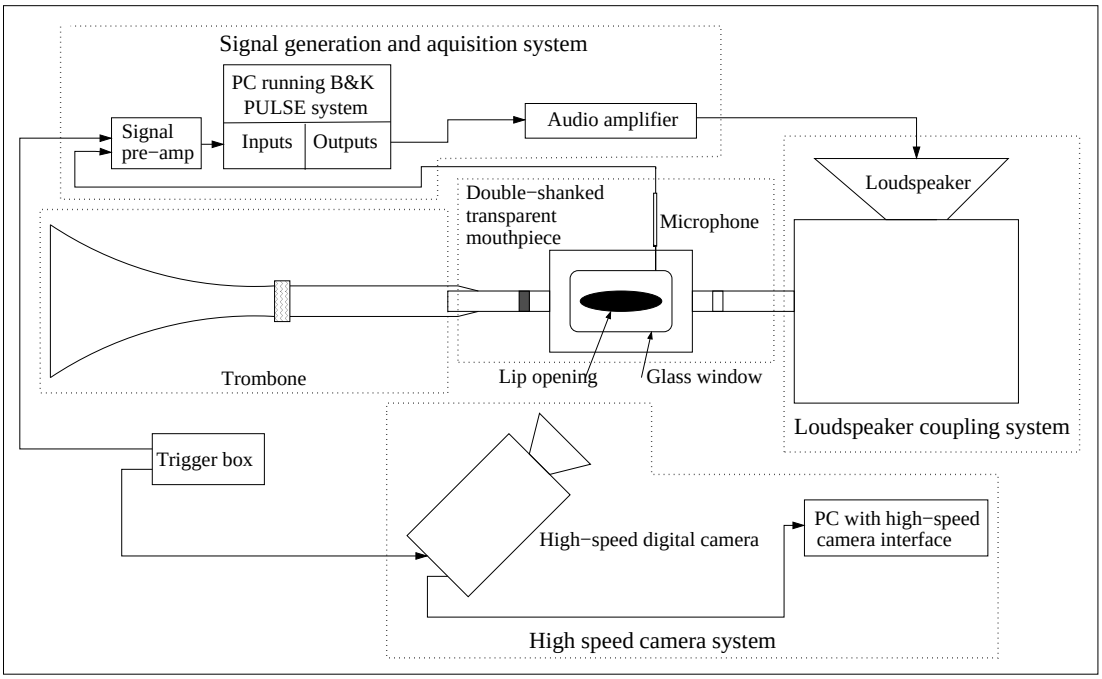

Figure 3.19: A schematic diagram of the setup use to measure the mechanical response of human lips. The signal acquisition system was Brüel & Kjær's PULSE platform. Measurements were triggered externally using a hardware triggering device.

The solution to this problem was the development of a double-shanked version of the transparent mouthpiece. Photographs of this mouthpiece are shown in figure 3.18. The mouthpiece consisted of a single, slightly oversized cup with space for two separate shanks mounted on either side. Both these shanks were direct copies of the shank from a Dennis Wick 6BS trombone mouthpiece. Only one of the shanks was coupled to the cup at any one time. A dual spring-loaded piston controlled the active shank: depression of the valve switched the active shank from one side to the other, as shown in photographs (a) and (b) in figure 3.18. Photograph (c) in the figure shows the mouthpiece simultaneously connected to the loudspeaker coupling system on the left, and a brass instrument on the right.

The double-shanked mouthpiece allowed a player to be alternately connected to a trombone and to the loudspeaker coupling system. The player could then form an embouchure whilst acoustically coupled to the brass instrument, before depressing the control piston and instantly becoming coupled to the loudspeaker apparatus for a mechanical response measurement. A schematic diagram of the video method set up for human lips is shown in figure 3.19.

The total mouthpiece volume, when coupled to a single shank, was slightly larger than that of the original transparent mouthpiece. This meant that the primary acoustical impedance peak of the double-shanked mouthpiece was approximately 150Hz

lower than that of the Dennis Wick 6BS mouthpiece from which it was derived. Input impedance magnitude curves for all three mouthpieces are shown in figure 3.20.

This modification to the mouthpiece impedance had the effect of altering the overall acoustical impedance spectrum of the mouthpiece-trombone system, as shown in figure 3.21. The frequencies of the impedance peaks were not significantly shifted, but the overall envelope of the spectrum was altered, particularly at frequencies above 200Hz. However, the range of notes studied for the lip response measurements corresponded to the lower three impedance peaks, which generally occurred at frequencies below 200Hz. It was therefore concluded that the change in the mouthpiece impedance was not a critical factor in terms of fundamentally modifying the behaviour of the lip-reed.

The acoustical coupling system

The video method for human lip response measurement required downstream acoustical driving. An acoustical coupling system was thus used which connected to one side of the double-shanked transparent mouthpiece. This system consisted of a loudspeaker mounted on a metal box. A hole was made on one side of the box, enabling connection to a mouthpiece shank. A photograph of this system is shown in figure 3.22.

It was important that the acoustical driving system did not posses any strong acoustical resonances that could couple to the lips and interfere with the mechanical response measurements. Neal[Neal, 2002] has already shown that during a mechanical response measurement with the artificial lips coupled to a straight tube it is possible for a mechano-acoustical coupling to take place, the effect of which is to perturb the measured lip response frequency. The main metal coupling box was thus filled with acoustical damping foam. This helped to lower the overall impedance envelope of the loudspeaker system. An impedance plot, measured at the plane of the mouthpiece rim when coupled to the system is shown in figure 3.23. The main impedance peak is slightly lowered in both frequency and magnitude. This suggests that the mouthpiece-acoustical coupling system would be unlikely to perturb the measurement any more than a measurement with just the mouthpiece.

Step-by-step summary of a video method mechanical response measurement applied to human lips

A brief summary of the practical steps required to perform a video method mechanical response measurement with a human subject is now presented.

1. The player should form an embouchure that is capable of playing the desired note on the trombone. This process should be repeated several times to ensure the player is comfortable.

2. Synthesize an appropriate driving signal (see section 3.3.2).

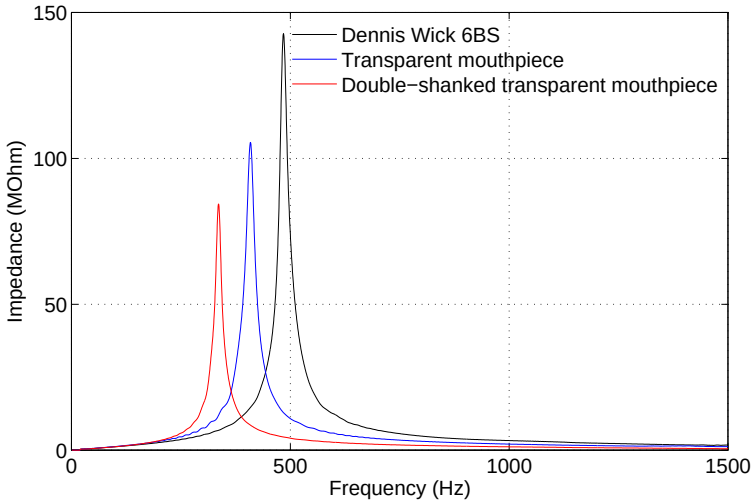

Figure 3.20: Input impedance curves of a Dennis Wick 6BS trombone mouthpiece, the original transparent mouthpiece and the double-shanked transparent mouthpiece developed for the video method mechanical response technique, applied to human lips.

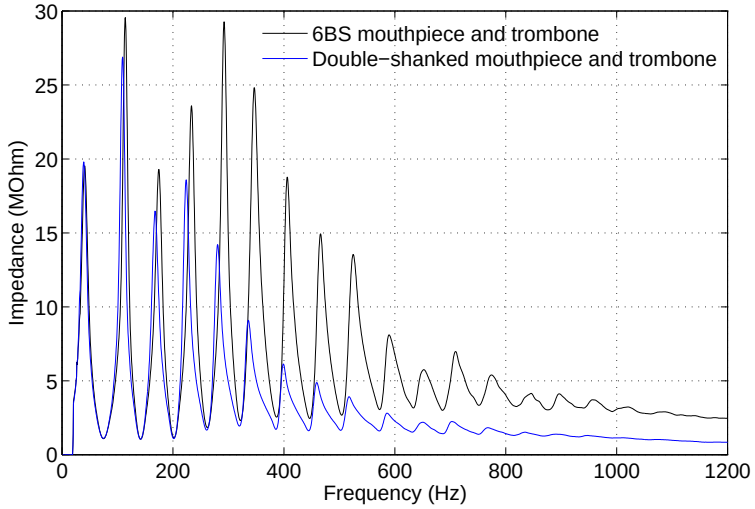

Figure 3.21: Input impedance magnitude curves of a trombone coupled to a Dennis Wick 6BS mouthpiece, and to the double-shanked transparent mouthpiece.

Figure 3.22: A photograph showing the acoustical driving system used for the human lip mechanical response measurements. The loudspeaker is contained in the wooden box and a reverse cone connects it to the main coupling cavity which is filled with acoustical damping foam. On the right hand side of the box is a hole available for connection to a mouthpiece.

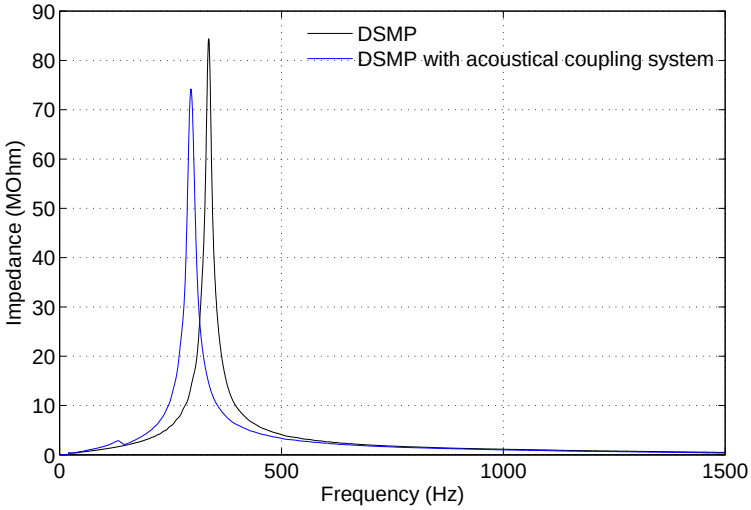

Figure 3.23: An impedance magnitude plot of the loudspeaker coupling system, measured using the BIAS system at the plane of the double-shanked mouthpiece (DSMP) rim. The impedance of the mouthpiece on its own is also shown.

3. Set up up the camera and light source to optimally illuminate the lips.
4. Check that the microphone signal level is within the dynamic range of the measurement system.
5. The player should play the note one final time before depressing the control valve on the transparent mouthpiece so that the acoustical driving system is active.
6. Instruct PULSE to immediately begin driving the loudspeaker (this is controlled by the experimentalist).
7. As soon as the loudspeaker begins to play back the triggering unit should be fired by the experimentalist, instructing the camera and PULSE systems to begin acquisition of the measurement data.
8. After the measurement has completed the data should be exported and processed as with the artificial lip video method.

As with the video method applied to the artificial lips, the process of measurement, processing and calculation of a single experiment required a significant period of time. For this reason a typical investigation would include multiple repetitions of the same embouchure without any actual calculations of the mechanical response. The data were then processed and response curves calculated in bulk.

3.4 Summary of experimental methods

The work in this chapter has presented a detailed overview of many of the experimental apparatus and procedures encountered in the study of the *in vivo* and *in vitro* brass instrument lip-reed. Details regarding the construction of a new *in vitro* lip-reed model, replica B, have been presented in section 3.2.3. The transmission method for obtaining the mechanical response of *in vitro* lip-reed replicas has then been explained in section 3.3.2. In section 3.3.3 a new technique has been described to obtain the mechanical response of a lip-reed without the need for the complex optical setup of the transmission method. This technique is called the video method.

In section 3.3.4 a description of the application of the video method to the *in vivo* lip-reed has been presented. This included the development of a new transparent mouthpiece, which included two mouthpiece shanks. A control valve was incorporated that allowed for a rapid switch to made between the two shanks. The objective of the mouthpiece was to allow connection of one shank to a brass instrument, and the other to an acoustical driving system. This allowed the player's lips first be configured to form a desired target embouchure. Switching of the control valve then allowed the subject to be coupled to the acoustical driving system in order to perform a mechanical response measurement.

Chapter 4

Mechanical Properties and Playing Behaviour of Real and Artificial Lips

"*I used to like fishing because I thought it had some larger significance. Now I like fishing because it's the one thing I can think of that probably doesn't.*" - John Gierach

4.1 Introduction

The mechanical properties of the lips are a crucial component in the total lip-reed system. Unlike the relatively fixed mechanical resonance frequencies of the clarinet reed, the lips form a dynamically adjustable mechanical valve. The resonance properties of the lips appear to be widely variable in frequency, allowing a remarkable range of playing features.

Two methods for determining the mechanical properties of the lip-reed have been outlined in chapter 3. The transmission method has been used widely for investigations into the properties of *in vitro* replica lip-reeds[Gilbert *et al.*, 1998; Cullen *et al.*, 2000; Neal *et al.*, 2002; Neal, 2002; Richards *et al.*, 2002; Richards, 2003] and for experiments with clarinet mouthpieces[Backus, 1961; Dalmont *et al.*, 2003]. This technique was not suitable for use with human subjects. The video method (sections 3.3.3 and 3.3.4) has thus been developed as a tool to investigate the properties of the *in vivo* human lip-reed under playing conditions.

In this chapter the results of experiments with the transmission and video methods are presented, along with a discussion of the implications of these findings. Also included is a comparison between the two methods when applied to the same system, namely the artificial lips in the replica A setup (see section 3.2.2). This important section highlights the general suitability of the video method for performing mechanical

response measurements.

4.2 The transmission method applied to artificial lips

The transmission method has been described in section 3.3.2. It provides a quick and accurate method for measuring the mechanical response of artificial lip-reeds formed into embouchures. Figure 4.1 shows a series of typical transmission method results. Three curves are recorded in this example, each corresponding to a relative measurement of water pressure (low, medium and high pressure). The importance of careful measurement of the lip water pressure has been discussed in section 3.2.2, but in this case the curve is only intended to show the qualitative behaviour.

4.2.1 General features of transmission method mechanical response measurements

Figure 4.1 exhibits many of the same features as the measurements made by Cullen[Cullen *et al.*, 2000], Neal[Neal, 2002] and Richards[Richards, 2003]. Most significant is a pair of resonances, between which lies the natural playing frequency of the embouchure. This behaviour is seen in all three curves in the figure. In the case of the low water pressure curve, the first major resonance appears at approximately 135Hz, as identified in the magnitude curve. The phase angle for this peak is very close to -90^o, which means that it may be classified as an outward striking resonance in the terminology of classical reed physics[Elliot and Bowsher, 1982; Helmholtz, 1877]. A second resonance may be found at approximately 173Hz, again clearly seen in the magnitude curve. The phase angle for this peak is very close to $+90^o$, which means that is may be classified as an inward striking resonance, under the same terminology as for the first peak.

It is also possible to identify resonances by direct examination of the phase curve. It has been shown in section 2.7.1 that any phase crossing which goes smoothly down through either $+90^o$ or -90^o corresponds to a frequency at which the embouchure would be able to couple to a suitable air column, even in the absence of a clear peak in the magnitude curve. In some mechanical response measurements, peaks in the magnitude curves are less well-defined than those in figure 4.1, and must be identified from the phase behaviour. This is particularly true of measurements on human players, described in section 4.4.

Richards[Richards, 2003] showed that a two-mass model can exhibit two predominant resonances, with phase behaviour very similar to that seen in the experimental data presented in figure 4.1. The resonances may couple to each other, and with any strong acoustical impedance peak of the downstream bore, such that the playing frequency lies between the resonance peaks. Such an embouchure can also play either

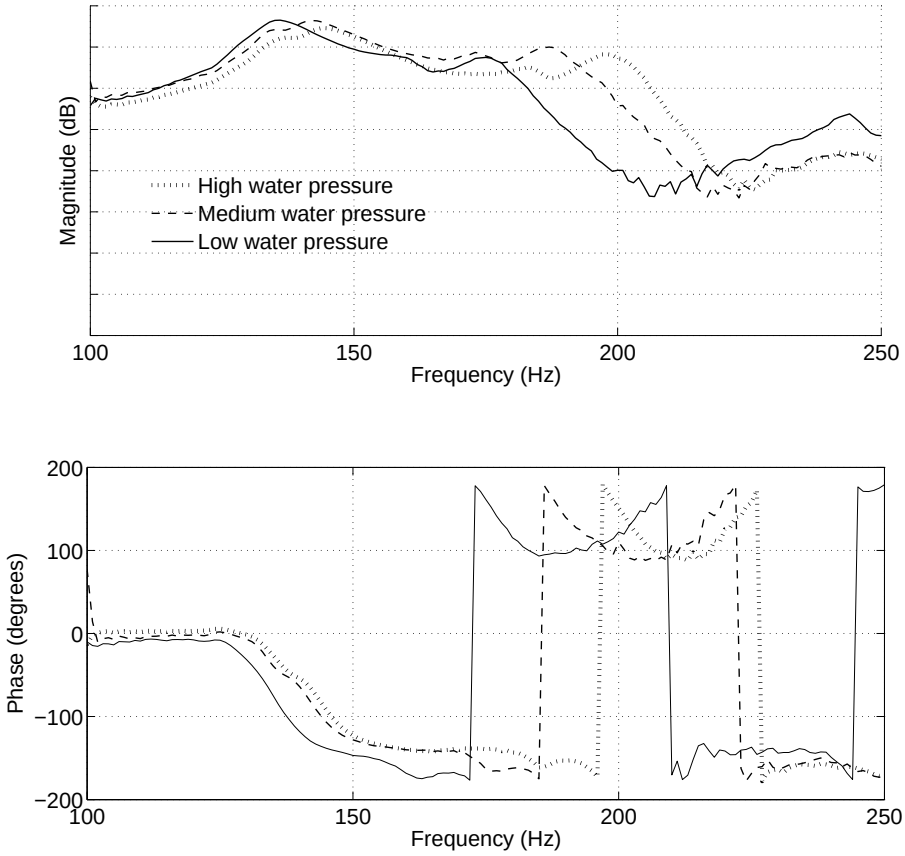

Figure 4.1: A mechanical response measurement of replica A using the transmission method, showing successive increases in the internal lip water pressure $P_{internal}$. The curves have been calibrated for the probe microphone response.

side of the downstream acoustical resonance, as demonstrated by Cullen[Cullen, 2000].

Vocal fold research has also demonstrated that a two-mass model can undergo self-sustained oscillations in the absence of acoustical coupling, as a result of a coupling between the two masses driven by an alternating Bernoulli force between the lips. However, acoustical effects are certainly of great importance for certain phonation frequencies. The clearest example is when the vocal fold oscillation frequency is close to the first resonance frequency of the vocal tract, as frequently occurs during Soprano singing[Rothenberg, 1981; Titze and Story, 1997; Epps *et al.*, 1997; Adachi and Yu, 2005]. The role of acoustics in human phonation is an area of active research and debate, and is addressed in the context of lip-reed physics in chapter 6.

The theory outlined by Richards[Richards, 2003] provides a convincing explanation of the fundamental physics involved in the lip-reed. However, a detailed description relating mechanical response results to specific motions of the lips is not available. It is thus difficult to associate a particular resonance with a particular physical motion of the lips. This means that the design of the optimal computational model for the

lip-reed is not clear. The original two-mass model suggested for the vocal folds by Ishikaza[Ishizaka and Flanagan, 1972], and improved by Lous[Lous *et al.*, 1998], has been shown to exhibit similar magnitude and phase behaviour when analysed with a linear stability method[Richards, 2003; Ruty *et al.*, 2007]. However, there is no reason that such a model should exclusively reproduce this result. Section 4.5.1 provides an investigation of this issue.

4.2.2 Technical performance of the transmission method

The example curves in figure 4.1 all made use of spectrum averaging to increase the signal-to-noise ratio of the measurements. This meant that the replica lips were driven several times with a sweep of 10s duration, and the PULSE signal processing system performed continuous averaging of the frequency response evaluation function. The resulting curves were generally smooth and consistent over multiple repetitions of the measurement.

The video method could not make use of continuous spectrum averaging, and so it was important to consider the effect of removing this processing step from the signal chain. Figure 4.2 shows two mechanical response curves of replica B, made in the absence of downstream acoustical coupling. The black curve shows a typical transmission method measurement, evaluated with a 10s sweep averaged over three full sweep cycles. It shows a very clean response, with little obvious noise in either magnitude or phase. The blue curve used a single shot of the 4.072s sweep used for many of the video method measurements (see section 4.3). The magnitude and phase curves of the single shot measurement clearly exhibit more noise, particularly between 130-160Hz, where the response of the lips to the driving was very small. However, the curves are very close where the lips show resonances, such as the two peaks either side of 100Hz, and the further peaks at 175Hz and 240Hz.

The close agreement of the curves in figure 4.2 suggests that a single, short sweep can yield good quality information about the lip resonances. The resonance frequencies, quality factors and phase angles can be easily obtained from such curves (see section 4.2.3).

Cullen[Cullen, 2000] reported three primary resonances in mechanical response curves of an artificial mouth similar to that of replica A. The lower two resonances consistently exhibited the outward-inward striking behaviour reported in this work. The third resonance showed an inward striking behaviour. Under some mechanical conditions an embouchure could be made to bifurcate from a regime based on the lower two resonances, to one based on the upper resonance.

Richards[Richards, 2003] reported similar behaviour to that seen in Cullen's model, with the exception that under certain conditions two pairs of resonances were measured. A fourth mechanical resonance was found between the lower and upper inward

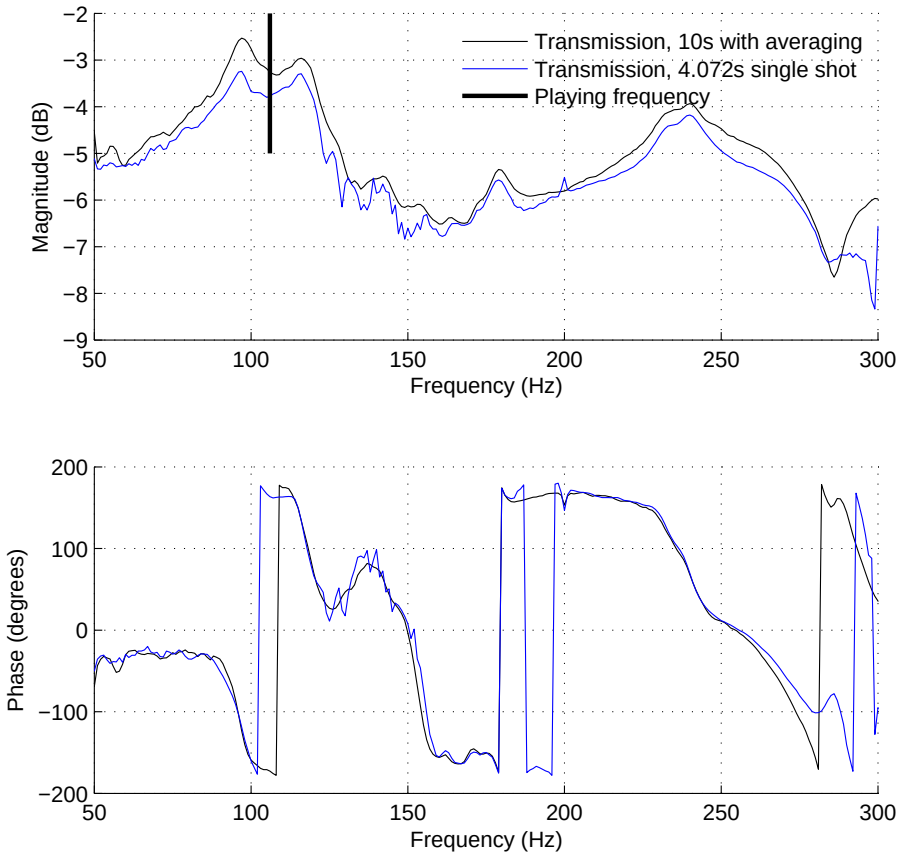

Figure 4.2: Two transmission method mechanical response curves evaluated with an embouchure from replica B (see section 3.2.3). The black curve used a 10s sweep, spectrum averaged over three full sweep cycles. The blue curve used a single 4.072s sweep, as per the video method. The playing frequency was approximately 110Hz and the internal lip water pressure $P_{internal}$ was 440Pa. The magnitude lines have been offset by 0.5dB for display. See table 4.1 for the extracted resonance frequencies.

striking peaks with an outward striking phase response. Thus it appeared that some embouchures clearly showed two separate pairs of outward-inward striking resonances. Such an embouchure could be expected to easily bifurcate between oscillation regimes tied to either of the resonance pairs. The reason for the emergence of the fourth resonance may have been because of the minor technical differences between the two replicas. It was more probably, however, because of the improved frequency resolution and reliability of the transmission method when used with the PULSE system.

Replica B frequently exhibited two pairs of outward-inward striking resonances when measured with the transmission method setup. An example of this behaviour can be seen in figure 4.2. The two primary resonances lies either side of 100Hz, with the phase response providing clear indication of outward and inward striking behaviour. The embouchure naturally destabilised at about 110Hz. The phase response then continues

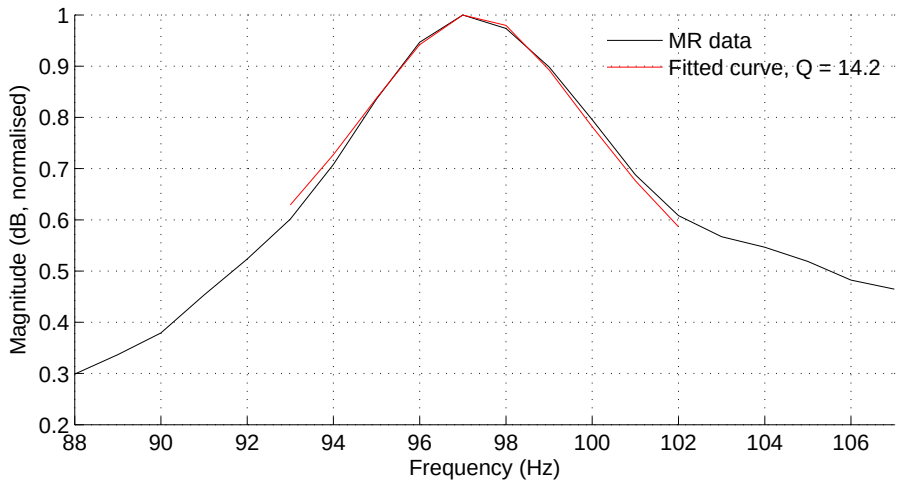

Figure 4.3: Curve fitting of the 95Hz resonance shown in figure 4.2 (spectrum averaged data), using the second order oscillator described by equation 4.1. The response magnitude has been normalised for ease of fitting the equation. A value for Q_v of approximately 14 was found.

smoothly down through -90^0 and $+90^0$ once more. The second -90^0 crossing at approximately 155Hz reveals a small, rather indistinct peak in the magnitude curve, which is clearest in the measurement performed with continuous spectrum averaging. The second $+90^0$ crossing reveals a strong resonance in the magnitude curve, around 240Hz.

4.2.3 Extraction of data from mechanical response curves

A transmission method mechanical response measurement generally yields a magnitude curve containing at least two obvious resonances, and a phase curve describing the phasing of these resonances. This raw experimental data is of great importance in informing the computational models described in section 2.9.

A one-mass model of the lips requires at least three mechanical parameters: the mass, the stiffness of the spring that connects the mass to the rigid wall and the damping of the spring. These are shown in figure 2.17. Such parameters may be estimated from mechanical response data, using curve fitting techniques that fit the data according to the mechanical equations of the computational model, such as the frequency domain mechanical response equation detailed in section 2.7.1, which is repeated here

$$|H(\omega)| = \frac{\frac{Q_v}{\omega_v^2}\frac{1}{\mu_v}}{\sqrt{1+4Q_v^2(\frac{\omega-\omega_v}{\omega_v})^2}}. \tag{4.1}$$

A two-mass model requires further parameters that are not immediately obvious from experimental data, such as the coupling stiffness between the two masses. It is

Quantity	Transmission method (averaged)	Transmission method (single shot)	Video method
f_i	97Hz	96.5Hz	96Hz
Q_i	14.2	16.6	16.4
f_j	116Hz	116.5	115
Q_j	13.3	15	15.4
f_0	105Hz	106Hz	106Hz

Table 4.1: Lip parameters extracted from transmission and video method measurements of replica B (high water pressure embouchure). f_0 is the destabilisation (playing) frequency of the embouchure.

possible, however, to simply fit equation 4.1 around each of the two most significant resonances, and to thus obtain two sets of data for each of the two-masses of the model. Empirical estimates may then be made for the unknown parameters[Vilain *et al.*, 2003], through a trail-and-error process.

It is possible to estimate the total mass of the lips by consideration of the geometrical dimensions of the lip blocks. There are several examples of this in the literature, such as Pelorson *et al*[Pelorson *et al.*, 1994], Cullen *et al*[Cullen *et al.*, 2000], Vilain *et al*[Vilain *et al.*, 2003] and Ruty *et al*[Ruty *et al.*, 2007]. The point mass required by the model, m_i in the case of a lumped element one-mass model, may then be estimated. It is not directly obvious how the total lip mass should be split between the two point masses of a two-mass model, but a 50% split provides the simplest starting point. Again, vocal fold literature contains the most extensive discussion of this, such as Lous *et al*[Lous *et al.*, 1998].

The mass may also be estimated by fitting equation 4.1 around a resonance peak, and extracting the fitted value of μ_v. Together with a measurement of the internal areas of the lip faces and channel, the lip mass may be calculated (see section 2.7.1).

The stiffness of the spring k_i may be estimated using the angular frequency of the resonance peak, ω_i, and the lumped mass m_i, using the equation for a simple harmonic oscillator

$$k_i = \omega_i^2 m_i. \tag{4.2}$$

Note that the angular frequency is related to the frequency by the standard relation

$$f_i = \frac{\omega_i}{2\pi}. \tag{4.3}$$

The principle subject of this study was the lip resonance frequencies and their quality factors, which may be used to estimate the damping of the resonances under the assumption of a damped linear oscillator. The damping can be estimated from the quality factor of the resonance, together with the mass and spring stiffness, using the

standard equation for a damped oscillator

$$B_i = \frac{\sqrt{m_i k_i}}{Q_i}. \tag{4.4}$$

The quality factor may be extracted from the magnitude curve of the mechanical response by fitting the experimental data around the region of the resonance with the theoretical mechanical response described by equation 4.1. An example of this fitting is shown in figure 4.3. A small Matlab program was written for this purpose, which used a least squares method to determine the optimum value of Q_i for an input experimental data set.

The mechanical response curve shown in figure 4.2 contains more than one resonance. The importance of the two resonances close to the playing frequency, located at 95Hz and 120Hz respectively, has already been discussed. It is possible to isolate each of the peaks in turn, and to fit them separately in order to obtain individual resonance frequencies and quality factors. In a standard two-mass model of the lips, for example, each of these peaks may provide the parameters for one of the two masses.

Table 4.1 lists the resonance frequencies extracted from the curves of figure 4.2.

4.3 The video method applied to artificial lips

The optical arrangement required for the transmission method made it unsuitable for application to human players. The *video method* was developed to overcome the limitations of the transmission method in this respect, and to allow mechanical response measurements to be made on human subjects.

The video method was first applied to the *in vitro* lip-reed models described in sections 3.2.2 and 3.2.3, which have already been used for the transmission method experiments described above in section 4.2. This was to enable careful testing and configuration of the new setup against the established setup. An example of the raw time domain response of the lip opening obtained with the video method is shown in figure 4.4. The signal shown in the figures describes the physical motion of the lips with time, as they are driven with the calibrated excitation sweep. A full technical summary of the video method may be found in section 3.3.3.

4.3.1 Comparison between the video method and the transmission method

Figure 4.5 shows two mechanical response measurements of the same embouchure. The dotted line corresponds to a transmission method measurement, and the solid line to a video method measurement. Both measurements used acoustic driving from the upstream cavity, using the replica A artificial lips setup (see section 3.2.2). The internal

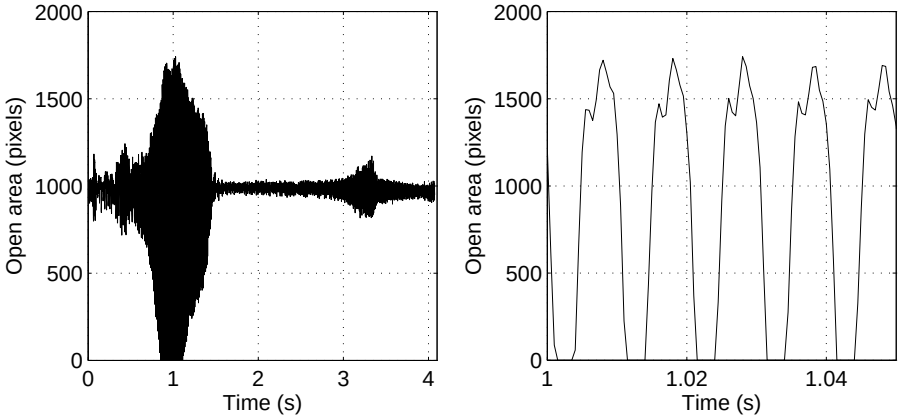

Figure 4.4: An example of the raw open area signal ($h_{mr}(t) \cdot W$, see section 3.3) obtained from analysis of a high speed video recording made with the video method, when driving from 40 - 120Hz. The signal describes the physical motion of the lips. At left the whole response is shown over a period of approximately 4s (two lip resonances can be seen either side of the 1s mark as noticeable 'bumps' in the signal), and at right a small time window of approximately 50ms is shown to highlight just a few cycles of oscillation.

lip water pressure $P_{internal}$ was kept constant between the two measurements, and the same calibrated excitation sweep was used.

The two curves show close agreement in both magnitude and phase. The resonance peaks, identified in the magnitude curve, match each other to within approximately 5%, which is close to the tolerance between consecutive measurements with the transmission method (typically 3%). The video method clearly exhibits more signal noise, particularly at frequencies where the lip response was small, such as between 250Hz and 300Hz.

Figure 4.5 should be consulted alongside figure 4.2, which shows two mechanical response curves evaluated with the transmission method, both with and without spectrum averaging. The video method appears to be comparable to the single sweep transmission method used without spectrum averaging, and as such represents a usable method.

4.3.2 The video method applied to differing regions of the lip opening

One of the advantages of the video method was that it was possible to record the response of the whole lip opening to the driving signal. It was also possible to illuminate the whole lip opening with the expanded laser beam of the transmission method. However, the optical conditions required for this reduced the light intensity reaching the diode, and the resulting signal-to-noise ratio of the mechanical response. Thus, for most transmission method experiments only the central portion of the opening was

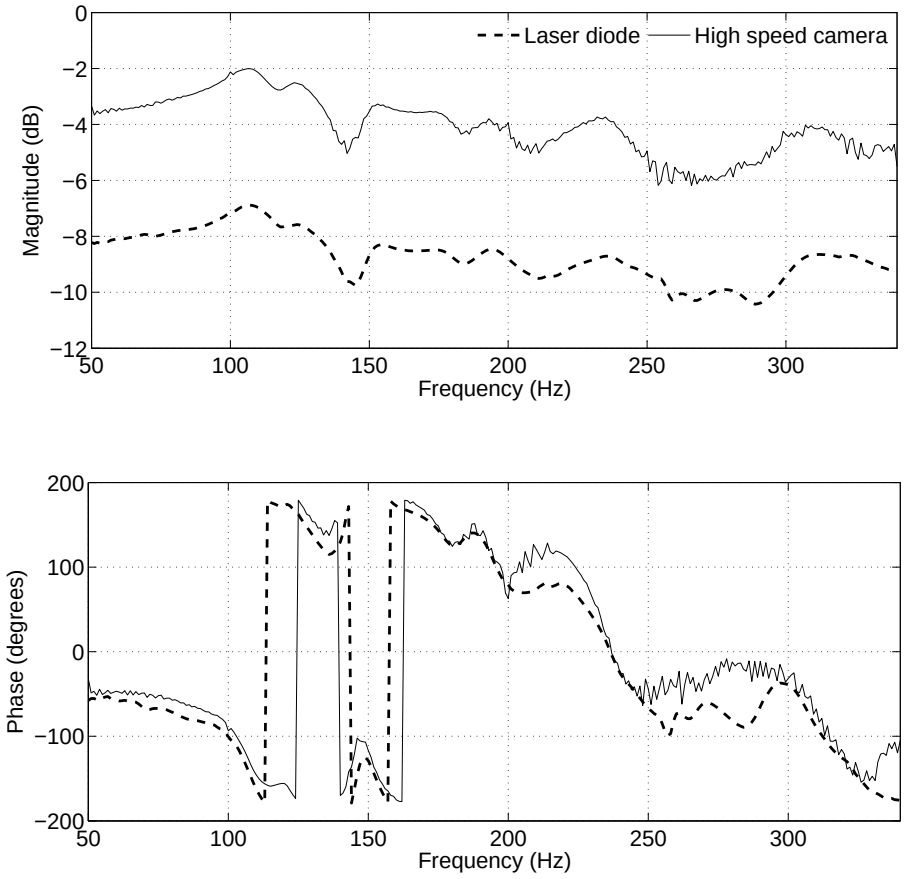

Figure 4.5: A comparison between the transmission and video methods applied to the same replica A embouchure (the magnitude curves have been offset by 5dB for presentation). Both the curves have been calibrated for the probe microphone response.

illuminated by the beam (see section 3.7). The principle limitation of this approach was that it was difficult to clearly align the beam with a specific region of the lip opening.

The video method allowed the entire lip opening to be examined during a measurement. The raw images could then be cropped to show specific parts of the lip opening, before the frequency response analysis was performed. This allowed an investigation into the validity of assumptions commonly made about the homogeneity of the lip length: most computational models rely on the assumption that the lips are homogenous along their length, which is the Z axis direction in figures 3.13 and 3.14. Several different mechanical response curves could thus be calculated from a single video measurement, each corresponding to a different region of the lip opening. An illustration of this is provided in figure 4.6, where the lip opening has been split into three portions.

Figure 4.7 shows four mechanical response curves evaluated on replica B, with an internal water pressure of 440Pa. The black curve shows the mechanical response

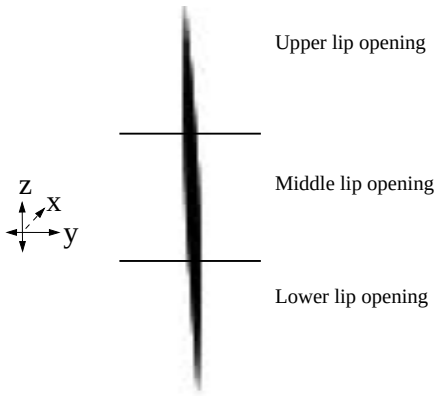

Figure 4.6: An illustration of the frontal lip opening split into three portions, each for a separate evaluation of the mechanical response using the video method. The global system axes are also shown.

evaluated with the whole lip opening. The other three curves were evaluated with the upper, middle and lower portions of the lip opening. A moving average filter was used to slightly smooth the curves.

Examining the main curve evaluated with the whole lip opening, it can be seen that the embouchure displays the common double resonance pair described in section 4.2.2. The first pair of resonances lie either side of 100Hz, with outward and inward striking behaviour. The second pair can be seen at 195Hz and 245Hz, again possessing outward and inward striking behaviour respectively.

The curves evaluated with the partial lip openings all display the key features of the curve of the whole lip opening. Four clear resonances can be seen in the magnitude curves, with frequencies very close to those of the main curve. The two primary resonances either side of 100Hz are very similar for all curves. The actual mechanical response amplitudes are slightly different for each curve, but this is due to differences in the areas of the regions. The middle third of the lip opening, in particular, was of a slightly larger opening area than the upper and lower portions due to the natural curvature of the lip opening (see figure 4.6).

The phase behaviour of all four curves are very similar from 65Hz up to 130Hz. They match to within the accuracy of consecutive measurements of the same embouchure, ranging between $\pm 3^0$ ($\approx$ 5%). This frequency range includes the two primary resonances either side of 100Hz. These are the resonances from which parameters for a two-mass model of the lips may be extracted, so the close alignment of the curves in magnitude and phase suggests that the assumption of homogeneity is likely to be a reasonable one.

Between 125Hz and 180Hz the phase curves do not match each other so closely. The lip response in this frequency range was very small, so the signal-to-noise ratio was

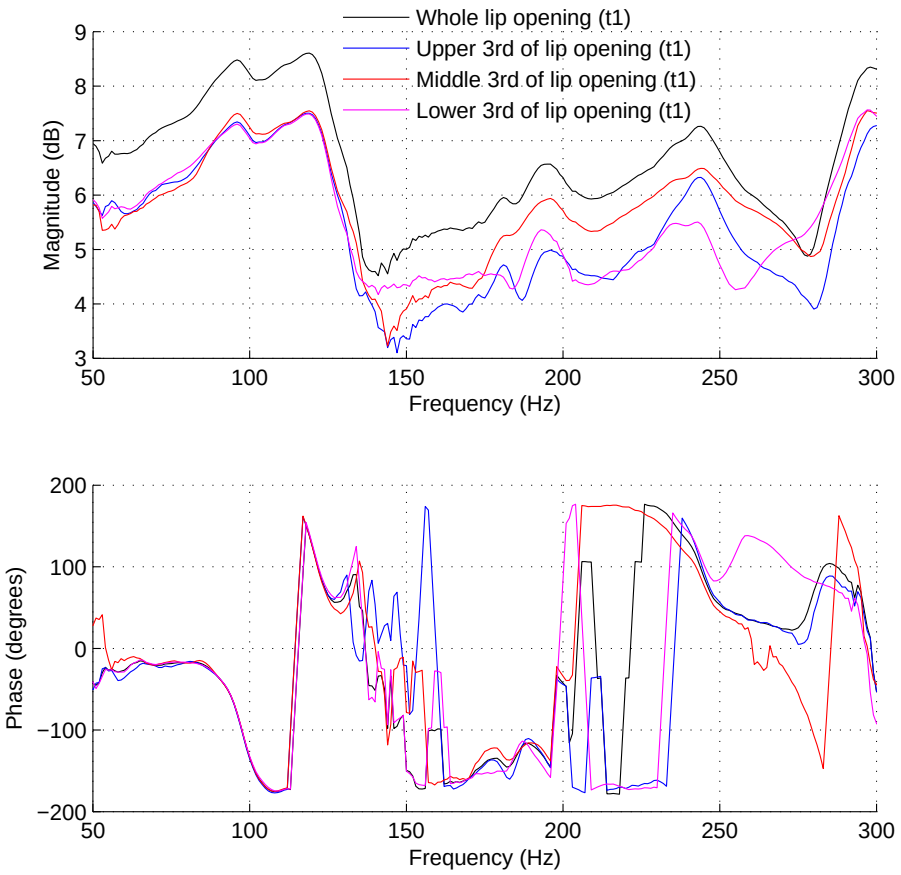

Figure 4.7: Mechanical response curves evaluated with the upper, middle and lower thirds of the lip opening, together with the curve evaluated with the whole opening. The curves have been lightly smoothed using a moving average filter. The internal lip water pressure $P_{internal}$ was 440Pa.

poor, and the curves are clearly noisy. Around the third resonance, at approximately 195Hz, the phase curves become similar once again. However, they do not match each other as closely as for the primary two resonances, ranging between $\pm 10^0$ of each other. This suggests that the phase response at this driving frequency is somewhat asymmetric along the lip length. The lips exhibit a slight wobbling motion, with the upper and lower portions of the opening oscillating slightly ahead and behind the central portion respectively. It is interesting to note that inspection of the raw unprocessed video often reveals this kind of behaviour.

The shape of the amplitude curves between 125Hz and 180Hz match each other quite closely ($Q = 16 \pm 2$). However, the response amplitudes of the three portions are rather different than they are for the two primary resonances. In particular, the middle portion of the lip opening appears to oscillate with a greater amplitude response to the driving signal than either the upper or lower portions. This suggests that there could

be a cut-off frequency, above which the different parts of the lip length do not respond equally to the driving signal. Under such a condition the assumption of homogeneity along the lip length is not longer valid, and a computational model based on this assumption cannot be expected to replicate the experimentally observed behaviour.

The phase curves again fall apart somewhat between the third and fourth resonances, from 200Hz to 235Hz. They then merge quite closely for the $+90^0$ phase crossing at approximately 244Hz. The phase differences between the curves around 244Hz are larger still than around the third resonance, ranging between $\pm 15^0$ of each other.

The magnitude curves for the fourth resonance remain broadly similar in shape and peak frequency, but with a considerably wider range of Q values than those of the lower three resonances ($Q = 17 \pm 10$). It seems that at higher frequencies the lip response is progressively less uniform along the lip length.

The magnitude peaks for the fourth resonance are once again somewhat disparate in amplitude. The lower portion of the lip opening responds the least, while the middle and upper portions appear to respond with a similar amplitude. The lips appear to respond less uniformly still around the fourth resonance than around the lower three. This further supports the suggestion that a low frequency assumption is required for a simple lumped element model to simulate computationally realistic behaviours seen in the mechanical models.

4.3.3 Harmonic relationship between the primary and secondary resonance pairs

It is interesting to note that the two pairs of resonances appear to be related to each other with a simple integer relationship. The first resonance, which is the lower of the primary resonance pair, appears at approximately 95Hz. The third resonance, the lower of the secondary resonance pair, appears at approximately 195Hz. The ratio between these frequencies is very close to two. At the extreme upper frequency limit of the measurement there appears to be a fifth resonance close to 300Hz, which is again in harmonic alignment with the first resonance.

The second resonance, which is the upper of the primary resonance pair, appears at approximately 120Hz. The fourth peak, which is the upper resonance of the secondary pair, appears close to 244Hz. Again the ratio between these peaks is very close to two.

The near linear relationship between the resonance pairs is an interesting result. It suggests that, for this embouchure, the lip behaviour is almost akin to that of a standing wave, which is capable of resonance at both ω_0 and $2*\omega_0$. A physical explanation of this behaviour is quite difficult, however, because it is dangerous, no matter how tempting, to extrapolate the essentially linear idea of a mass-spring-damper system too far when the subject under concern is actually continuous media.

Richards[Richards, 2003] showed that a theoretical mechanical response evaluation of a two-mass model contained more than two resonances. He proposed that that the upper resonances, those beyond the primary pair, resulted from the non-linearity of the model. His theoretical results differed somewhat from the experimental data presented here. The individual mechanical response curves of each of the two masses showed two peaks related with an approximately harmonic relationship. The overall mechanical response of the embouchure, analogous to the black line in figure 4.7, then showed four main peaks. The upper two peaks did not appear to be harmonically related to the lower two, which were in fact harmonically related to each other. The results presented here appear to be subtly different to those of Richards[Richards, 2003]. Whilst both sets of results show multiple lip resonances, most of which exhibit either outward or inward striking behaviour, the relationships between the resonances appear to be different.

The experimental mechanical response work of Richards[Richards, 2003] was based on replica A (see section 3.2.2). The lips of replica A are composed of latex tubes mounted into a faceplate. They are held in place by the pressure of a mouthpiece mounted downstream. However, this setup means that the length of the lips lying outside the mouthpiece is relatively free to move. Observation during playing and during mechanical response measurements confirms that the whole lip length clearly undergoes a degree of oscillation under such conditions. The regions of the lips outside the mouthpiece rim are clearly coupled to those inside, as the lips are continuous media. This suggests that the lips might possess more oscillation modes than the relatively confined lips of replica B, which are contained within metal lip blocks (see section 3.2.3). Mechanical response measurements appear to confirm this, as curves evaluated with replica A tend to show more peaks than replica B. Several of these extra peaks do not appear to show clear outward or inward striking behaviour, and may be the result of excess longitudinal oscillations along the lip length.

The frontal mechanical response measurements of replica B suggest that it has mechanical behaviour closer to a two degree-of-freedom model than replica A. It exhibits fewer resonances, and those it does possess are almost always identifiable as outward or inward striking, a behaviour shown to exists by Richards[Richards, 2003] in a traditional two-mass model. Further analysis of this issue is presented in section 4.5, where the transverse two-dimensional motion of replica B is investigated.

4.4 The video method applied to human lips

The frontal video method was further developed from the setup described used for artificial lips, described in section 4.3, in order to allow application of the technique to human players. Technical details of this development have been outlined in section 3.3.4. In this section results obtain with this method are presented together with analysis and discussion of their implications. A significant portion of the work contained

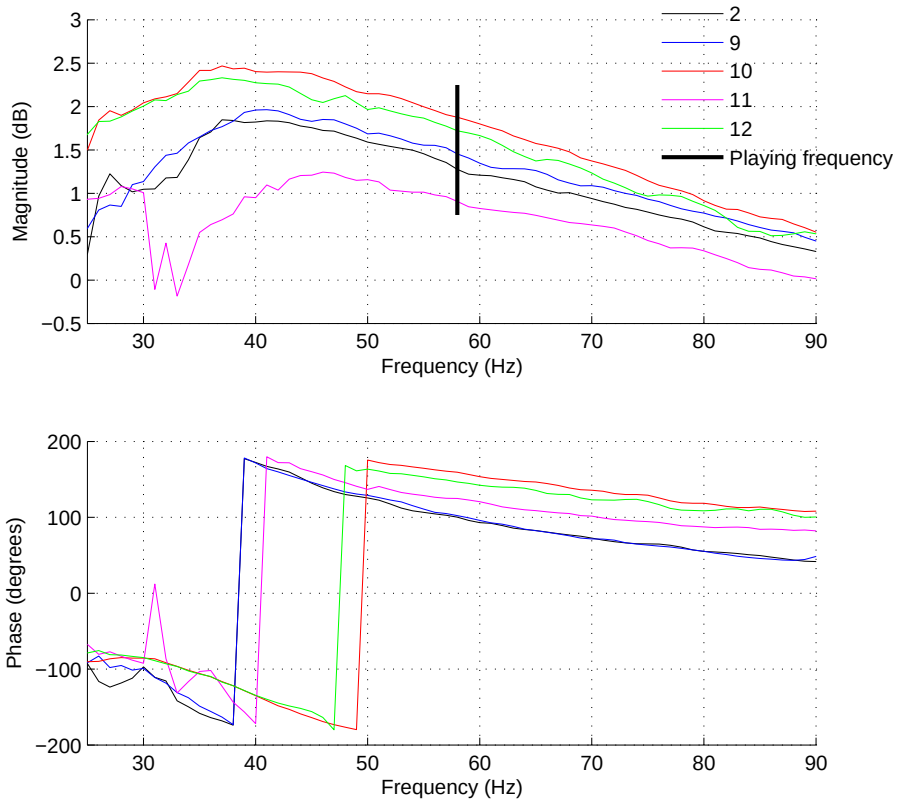

Figure 4.8: Five mechanical response curves obtained for player AJ when asked to form an embouchure for $B_1^{\flat}$, the pedal note. The curves have not been filtered, but have been adjusted for the response of the probe microphone. The numbers refer to the individual take references.

in the section has been published in [Newton *et al.*, 2008].

There were two principal challenges with mechanical response measurements performed on human lips. Firstly, the human element of the experiment decreased the repeatability of the measurements. The method required that a measurement subject maintain a constant embouchure for at least four seconds. This was a difficult task, particularly with inexperienced players. However, it was within the realms of reason with the more experienced players, who were better able to cope with the somewhat uncomfortable measurement conditions.

The human factor also made setting up a measurement considerably more time consuming than with the artificial lips. This was because it was difficult to maintain good quality lighting and camera focus on human subjects that were susceptible to the needs and distractions of any living organism.

Two experienced trombone players were used for the measurements presented in this section. Players AJ and TJ had several years of experience playing in semi-professional orchestras.

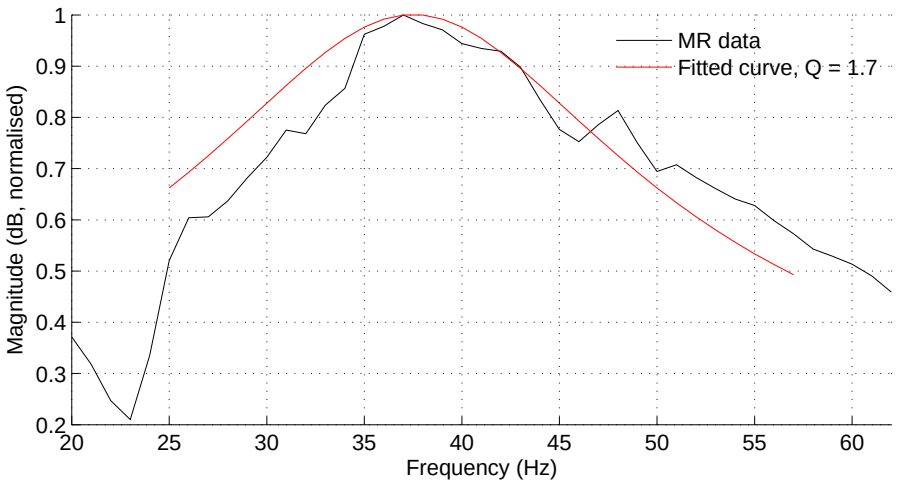

Figure 4.9: An example of fitting the theoretical mechanical response described by equation 4.1 around a human lip resonance. The measurement was performed on player AJ (take 9 in figure 4.8), with an embouchure that destabilised at approximately 58Hz (B_1^b). The asymmetry of the human lip resonances decreased the accuracy of the fit compared to the artificial lip resonances.

4.4.1 Results obtained with player AJ

Figure 4.8 shows five mechanical response curves obtained from player AJ, when asked to form an embouchure to play a B_1^b pedal note, the frequency of which is also marked at 58Hz. The subject's lips were driven with a calibrated sine sweep between 25Hz and 100Hz, over approximately 4s. The camera frame rate was 2000Hz.

All the curves in figure 4.8 show a single dominant resonance which peaks at approximately 38Hz ($\pm 3Hz$). The curves were fitted with the same theoretical mechanical response function (equation 4.1) as the artificial lips, described in section 4.2.3, to extract quality factors for the resonance. An example of this fitting is shown in figure 4.9. This process suggested Q values in the region of 1.5 - 2.4, with a mean of about 1.8. It was not possible from these data to clearly isolate further resonances in the magnitude curves.

Examination of the phase curve suggests that the dominant resonance has an outward striking behaviour (-90^0). For curves 10 and 12 the phase crossing at -90^0 occurs almost precisely at the peak in the magnitude curve. For the other three curves, the phase crossing occurs slightly lower in frequency than the apparent magnitude peak, but close enough that they may be associated with each other. A similar phenomenon has frequently been observed with measurements on artificial lips[Neal, 2002; Richards, 2003].

The lip-reed was originally classified by Helmholtz as outward striking[Helmholtz, 1877], and the curves presented for B_1^b in figure 4.8 support this proposition. However,

two of the curves reveal a phase crossing at the inward striking angle, $+90^0$, and the other three all come to within 10^0 of this angle in the higher frequency range of the measurement. The presence of this phase crossing is a strong indication that, despite the apparent absence of a clear resonance in the magnitude curve, the lips would be capable of acting like an inward striking reed.

Cullen[Cullen, 2000] noted that some mechanical response measurements performed on artificial lips revealed a $+90^0$ phase crossing above the one at -90^0, despite any obvious peak in the magnitude spectrum. It was demonstrated that application of a slight static overpressure during the measurement often sufficiently destabilised the embouchure that a peak in the magnitude curve would appear where previously, during a normal measurement, there was none. This technique was attempted multiple times during the measurements on human players, but it was found to be extremely difficult to consistently and smoothly apply a suitable overpressure from the players' lungs. The overpressure was either so excessive that the lips actually destabilised into self-sustained oscillations during the measurement sweep, or the overpressure was inconsistent over the measurement, resulting in a noisy lip response. Controlled application of an overpressure using a high pressure supply similar to that used with the artificial lips could provide a solution to this problem.

It is interesting to note that while the general shape of the curves remains similar for repeated takes of the same target embouchure, there are slight differences in the absolute values of the peak resonance frequencies. The clearest example is the difference between takes 2 and 9 which are very similar to each other, and takes 10 and 12 which are also very similar to each other. There is a difference of 15Hz between the two pairs of -90^0 phase crossings, and the peak amplitudes are similarly around 5Hz apart. Such differences may be due to unavoidable experimental error, in which case minimum error in repeatability is approximately 10%, which is twice that seen with artificial lip measurements. It is also possible that the human factor has a contributing effect to this increased spread of results. It may actually be quite a difficult task for a player to repeatedly form exactly the same embouchure. It is possible that the skill of a player may allow them to play a particular note with more than one specific embouchure. It is also possible that the player may have slightly relaxed or tightened their embouchure during the measurement, only to later make a small adjustment necessary to facilitate production of the note.

Figure 4.10 shows another mechanical response measurement performed on player AJ. The player was again asked to form an embouchure targeted at the pedal note, B^b_1. This measurement provided direct evidence of a second resonance in the magnitude curve. The second peak corresponded to a $+90^0$ phase crossing, indicating that it had inward striking character. The small amplitude of this second peak meant that it was relatively difficult to fit the theoretical mechanical response function around it and obtain a Q value. However, an estimate of between 2 and 2.5 was made, which was

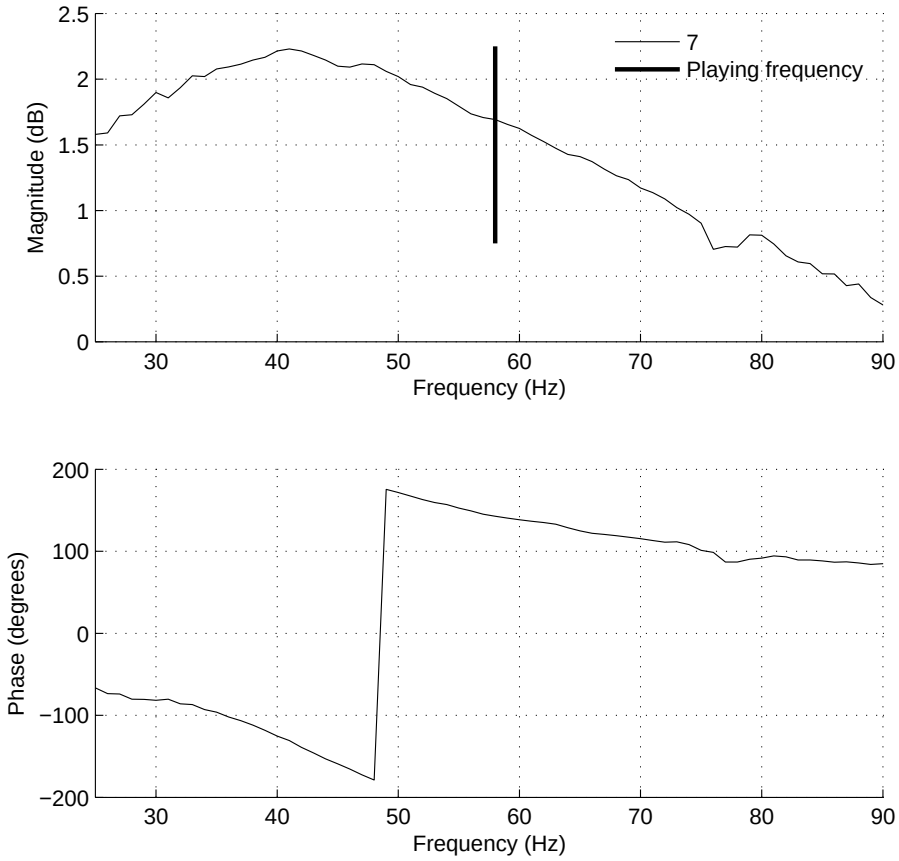

Figure 4.10: .
A mechanical response curve of human lips clearly showing two resonances forming an outward-inward striking pair, identified in both magnitude and phase. The player was AJ, asked to target B_1^b.

quite similar to the estimates made for the lower resonance.

Figure 4.11 shows two mechanical response curves obtained from player AJ. The player was asked to form an embouchure targeted at B_2^b, which is an octave higher than the note targeted in figures 4.8 and 4.10. Both examples in the figure reveal at least two resonances. The lower, dominant resonance again shows an outward striking character, with a quality factor of around 1.7. Take 18 reveals a surprisingly strong upper inward striking resonance, with a Q value of approximately 5. Take 20 reveals a smooth $+90^0$ phase crossing, accompanied by a gentle peak in the magnitude curve at 140Hz. The playing frequency fell between the two resonances.

It appears that the lip-reed of player AJ was capable to acting as both an outward and an inward striking reed, as has been proposed by Richards[Richards, 2003]. Crucially, these two modes of operation appear in a single measurement, rather than as a part of a continuous transition between modes, as has been suggested by Adachi and Sato[Adachi and Sato, 1996]. This issue is discussed further in section 4.4.3 below.

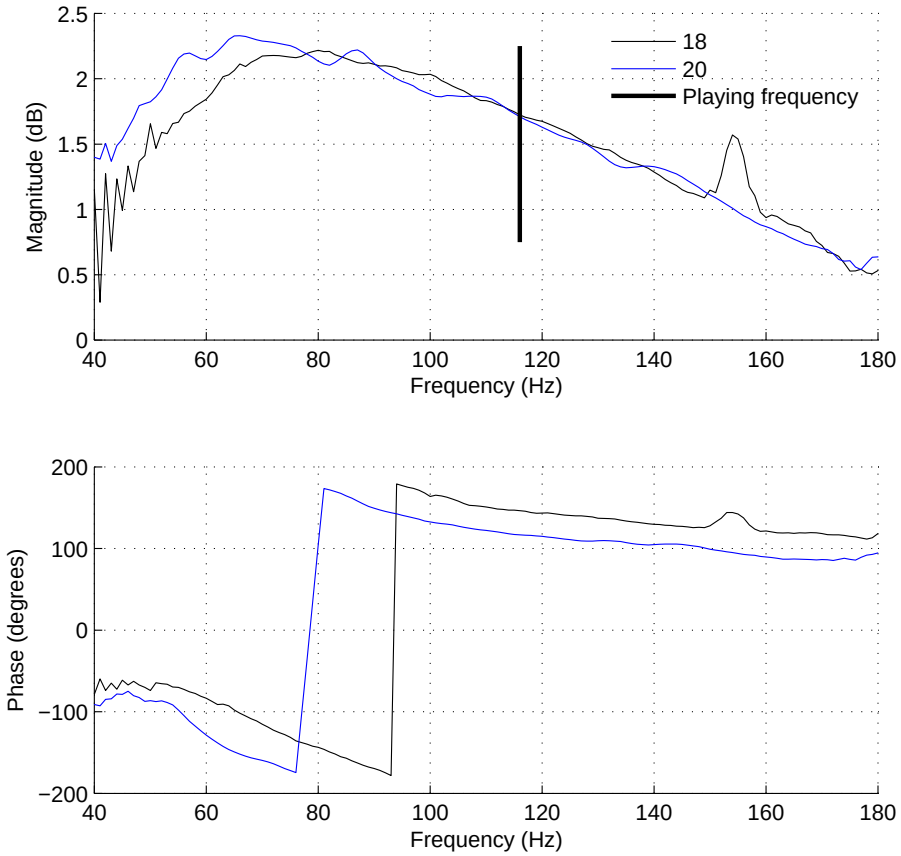

Figure 4.11: Two human lip mechanical response curves evaluated from player AJ. The player was asked to form an embouchure targeted at $B_2^{\flat}$, which is normally at approximately 116Hz.

4.4.2 Results obtained with player TJ

Figure 4.12 shows two mechanical response curves evaluated from player TJ when asked to form an embouchure targeted at $B_2^{\flat}$. The curves show a similar response to the measurements performed on player AJ, with a single dominant resonance exhibiting outward striking behaviour. For this embouchure the dominant resonance occurred between 55Hz and 58Hz in the magnitude curves, which was a good result in terms of repeatability ($\approx 5\%$ error). The phase curves were slightly further apart, but still within the 10% margin noted for player AJ in section 4.4.1. The fitted Q values of this resonance lay within the range already seen for player AJ, between 1.6 and 2.4.

Both curves in figure 4.12 show a clear second resonance, which occurs between 165Hz and 173Hz. In the case of take 3, the phase curve goes very close to the inward striking angle at $+90^0$, which seems to be directly correlated with the magnitude peak. The phase curve of take 8 does not directly cross the $+90^0$ phase angle, but the general downward trend of the curve around 180Hz, which was the limit of the excitation

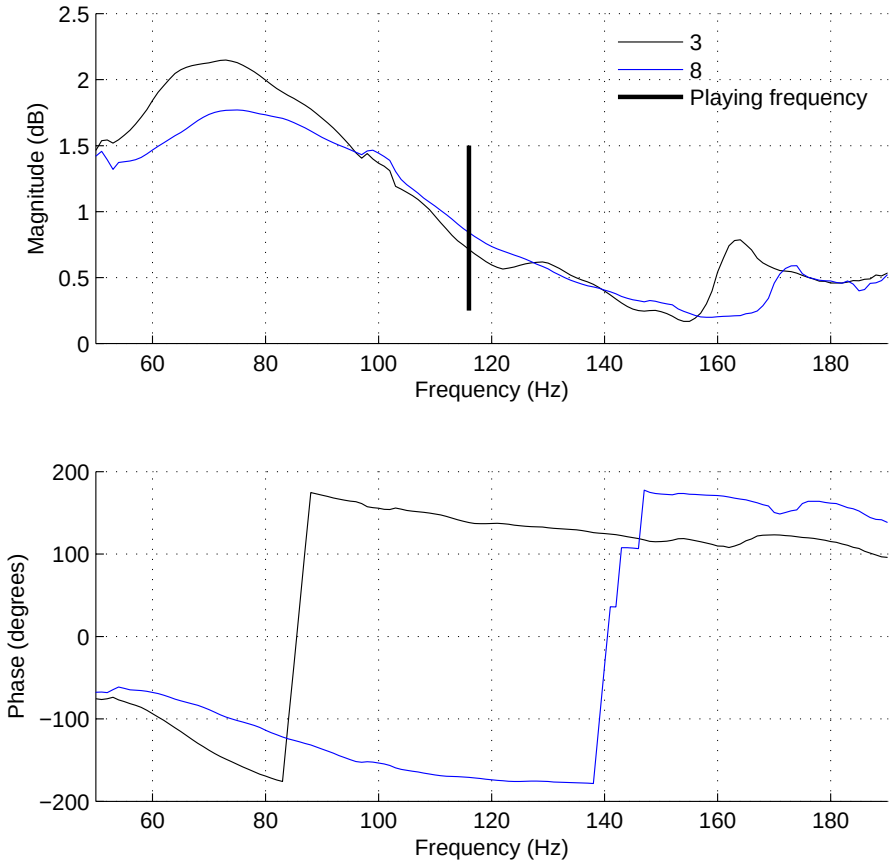

Figure 4.12: Two human lip mechanical response curves evaluated from player TJ. The player was asked to form an embouchure targeted at B_2^b (116Hz), which is marked on the figure.

sweep, suggests that it would have done so just outside the measurement range. Where a second resonance was measurable, as in figure 4.12, it was interesting to note that its fitted Q value once again gave a higher value than the lower resonance, of between 2.8 and 5. The playing frequency once again fell between the outward and inward striking resonances.

Player TJ adapted to the setup extremely well, and was therefore asked to attempt a wider range of notes than AJ. Figure 4.13 shows the result of a measurement on an embouchure targeted at F_3. This note is normally expected to play at approximately 174Hz, but in this measurement the player played the note at 170Hz. This was due to the larger mouthpiece cup required by the double-shanked mouthpiece (see section 3.3.4).

Figure 4.13 shows three distinct peaks. Once again a clear outward striking resonance can be seen at approximately 100Hz, with a Q factor of about 1.7. A second peak appears at about 175Hz, which is very close to the playing frequency of

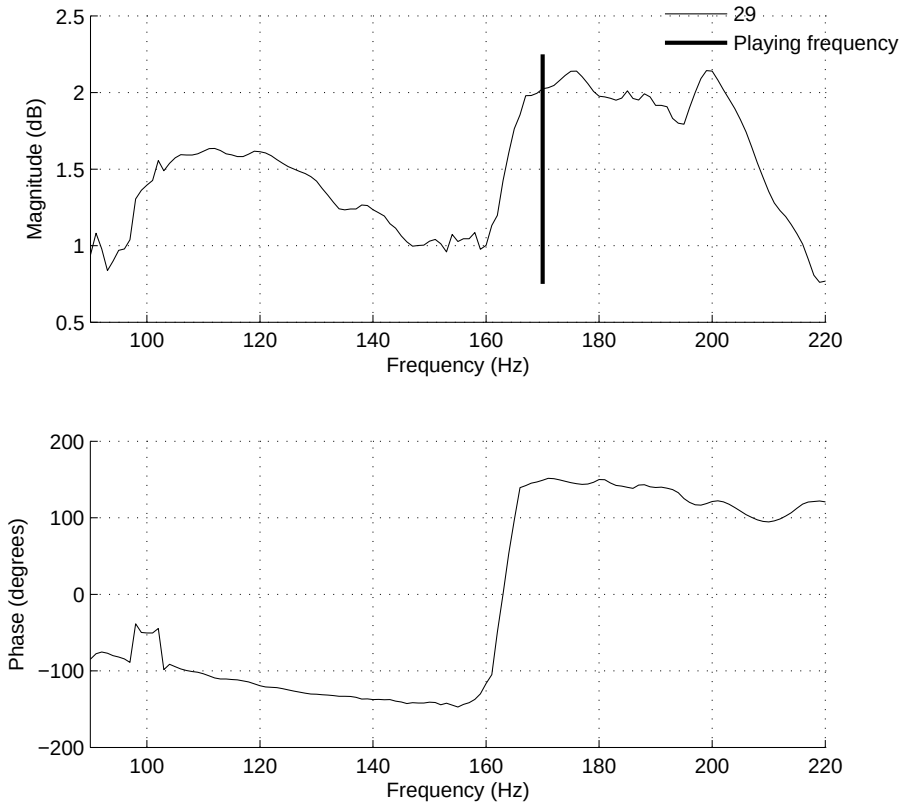

Figure 4.13: A human lip mechanical response curve evaluated from player TJ. The player was asked to form an embouchure targeted at F_3 (174Hz).

the embouchure. A further resonance is also seen around 200Hz, which shows inward striking character. This resonance has a higher Q value than the lower one, between 4 and 5, which is in line with the results of player AJ in section 4.4.1.

The curve thus appears to show the same kind of outward-inward striking resonance pair seen in the other measurements. The presence of the third peak between the two main resonances, however, provides an interesting difference. The player mentioned that during the measurement their lips may have slightly destabilised into self-sustained oscillations at one point during the sweep. It is likely that this third peak is the result of the lips being destabilised to a point very close to, or just over, this point of self-sustained oscillation.

The peak lies very close to the measured playing frequency of the embouchure, and any slight deviation could have been caused by small changes in the embouchure between the playing test and the measurement. The player also noted that during the measurement he had expelled a small, steady stream of air through the embouchure. This slight overpressure may have been just enough to push the lips into self-sustained oscillations at the appropriate frequency during the sweep. It is also interesting to note

that the inward striking resonance appears much more strongly in this measurement than in most of the other measurements presented in this work. This is a behaviour well documented for artificial lips[Cullen, 2000; Neal, 2002; Richards, 2003], whereby phase crossings at $+90^0$ are not always accompanied by obvious peaks in the magnitude curve. Application of a small overpressure sufficiently destabilises the lips that this second resonance may then suddenly appear in the magnitude curve.

The emergence of the inward striking resonance, in both human and artificial lip measurements, is a strong indication that it plays an important role in the destabilisation of the lip-reed. It suggests that a coupling between the two resonances, as well as between the resonances and the air column, is a common feature of the lip-reed mechanism. This is an effect rather similar to the well documented vocal fold two-mass, two degree-of-freedom models which are required in the absence of acoustical feedback. The apparent presence of such a mechanism in the lip-reed gives further clues to the shared physics of both of these biological oscillators.

4.4.3 Overall features of human lip resonances

Helmholtz[Helmholtz, 1877] originally classified the lip-reed as being outward striking in character. An outward striking single-mass model of the lips should exhibit a phase behaviour of -90^0 at resonance, in the convention presented in this work (see section 2.7.1). Saneyoshi[Saneyoshi *et al.*, 1987b] suggested that the lip-reed should be classified as inward striking, at least in the high registers. An inward striking single-mass model of the lips should exhibit a phase behaviour of $+90^0$ at resonance. Both Yoshikawa[Yoshikawa, 1995] and Chen and Weinreich[Chen and Weinreich, 1996] have visualised the lip-reed from the side, and demonstrated that it undergoes two-dimensional swinging and stretching motion during oscillation. Such behaviour is impossible to replicate with a model that is singly outward or inward striking.

Adachi and Sato[Adachi and Sato, 1996] demonstrated that a computational simulation of a lip-reed can have inward striking behaviour for higher register notes. Their model also showed predominantly outward striking behaviour in the lower registers. However, no computational model that forces the lips to be uniquely outward or inward striking is capable of replicating the commonly witnessed ability of brass players to 'lip' a single note either side of the relevant impedance peak of the instrument bore.

Cullen[Cullen *et al.*, 2000], and later Richards[Richards, 2003], demonstrated that a model incorporating at least two degrees of freedom is required to simulate such behaviour. Their measurements of the mechanical response of artificial lips showed that the lip-reed clearly possess more than a single resonance, which immediately breaks open the argument for a single-mass, single degree-of-freedom lip model. Richards[Richards, 2003] showed that a two degree-of-freedom model, with both

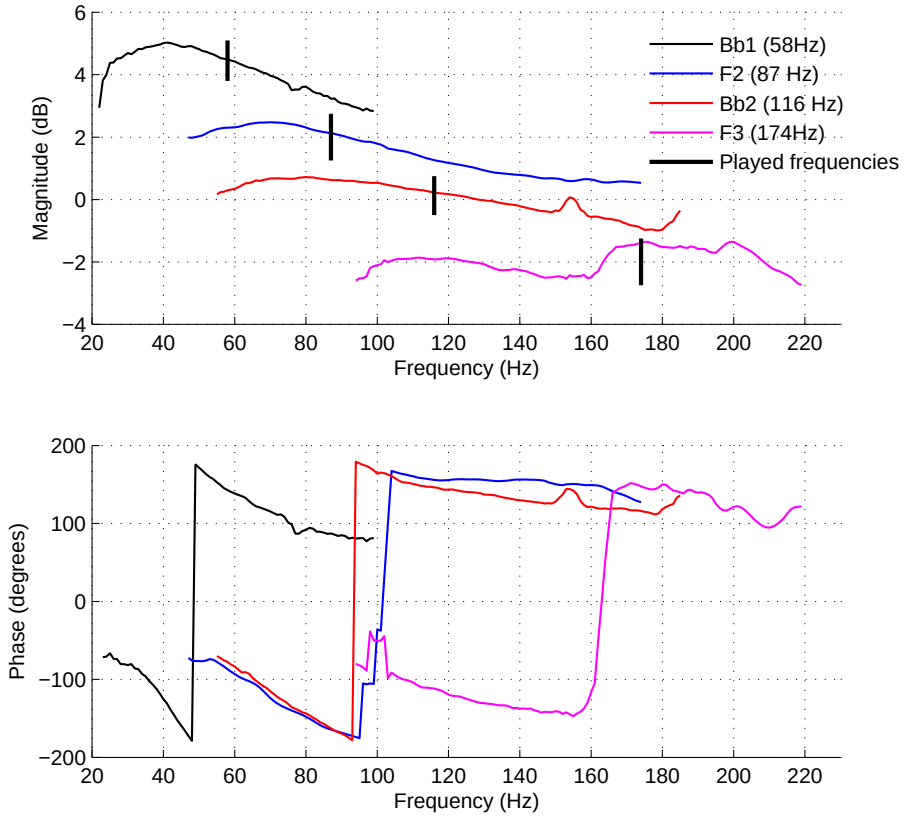

Figure 4.14: Four mechanical response curves evaluated with human lips, covering the lower to mid register of the tenor trombone. The magnitude curves have been vertically offset by a few dB from each other to facilitate easier viewing.

outward and inward striking behaviour, was capable of replicating some of the behaviour seen in the experimental measurements, such as note 'lipping'. Such a model also exhibited at least two clear mechanical response resonances, with further resonances at higher frequency emerging from the non-linearity of the coupling between the resonances.

Figure 4.14 shows four mechanical response curves evaluated with human lips formed into playable embouchures, across the lower to mid register of a tenor trombone. The work presented here suggests that the fundamental properties and behaviour of the human lip-reed and the artificial lip-reed are similar. Throughout the range of embouchures studied there were consistently two clear resonances in the human lip-reeds, either identified by magnitude peaks or by $\pm 90^0$ phase crossings. The two key differences between the human and artificial lip measurements were the number of resonances measured, and the quality factors of the peaks when fitted with a simple theoretical mechanical response curve.

Resonance quality factors

Table 4.2 lists lip parameters obtained from this work and from the available literature. Where studies have identified two resonances, such as the artificial lip measurements of Cullen[Cullen, 2000] and the present work, note has been made of both peaks. Note has also been made of the Q value of the resonances.

The table shows that studies over the past twenty-five years have measured and proposed a wide range of lip resonance frequencies and quality factors. Whilst it is reasonable to assume that the resonance frequencies may be highly variable in order to facilitate the production of a wide range of notes, the large variation in quality factors is more questionable.

A recent study by Gazengel *et al*[Gazengel *et al.*, 2007] made an estimate of the primary resonance frequency and damping of a human lip derived from a mechanical impedance measurement. The study also investigated the properties of an artificial lip alternately filled with water and glycerine. The study found that the real lip possessed a single dominant resonance, with a much lower Q value that the resonances measured with the artificial lip. The real lip resonance had Q values between of 1.4 and 1.6, the glycerine-filled lip resonance had Q values between of 4 and 6, whilst the water-filled lip resonance had Q values similar to those seen in the present work (8-16). It appeared that filling the artificial lip with a more viscous liquid, and thus lowering the overall Q value of the system, better approximated the behaviour of the human lip.

The lip in the study by Gazengel *et al*[Gazengel *et al.*, 2007] was not formed into an embouchure designed to play a trombone, but was used as part of a setup to play a clarinet. While the study was thus not directly comparable with the present work, the general similarity in the results confirms that the value of Q is an important difference between real and artificial lips. It also provides a useful hint as to a relatively simple way of improving *in virtro* lip-reed models such as those described in this work.

The low Q values measured with human lips suggest that the coupling between the mechanical oscillator of the lips and the acoustical oscillator of the instrument air column would be dominated by the high Q factors of the air column resonances (see figure 3.21, for example). This in turn implies that a human player might find it easier to 'lip' a note above and below the air column resonance than the artificial lips.

Number of resonances measured

All measurements on human lip-reeds show that the lowest, outward striking resonance was predominant in the magnitude curves. For static measurement, those with no overpressure applied by the player, the peak of this dominant resonance was at least an order of magnitude above any other resonances. This provides a clue as to the difficulty of obtaining clean measurements of a second resonance. Any second resonance must be higher in frequency than the dominant lower peak, which implies a smaller amplitude

Study	Quantity				
	f_i	Q_i	f_j	Q_j	f_0
Replica A[Richards, 2003] (s.s. 3.2.2, present study, transmission method)	120 - 215 Hz	8 - 20	210 - 265 Hz	8 - 20	135 - 200 Hz
Replica B (s.s. 3.2.3, present study, transmission method)	80 - 140 Hz	10 - 16	100 - 180 Hz	11 - 15	90 - 150 Hz
Cullen's artificial mouth[Cullen, 2000]	182 - 237 Hz	6 - 12	225 - 278 Hz	8 - 16	$\sim$ 190 - 250 Hz
Elliot & Bowsher [Elliot and Bowsher, 1982]	N/A	0.5	N/A	0.5	N/A
Saneyoshi *et al* [Saneyoshi *et al.*, 1987b]	N/A	N/A	N/A	5	N/A
Gazengel *et al* [Gazengel *et al.*, 2007] (glycerine-filled artificial lip)	$\sim$ 100 Hz	4 - 6	N/A	N/A	N/A
Gazengel *et al* [Gazengel *et al.*, 2007] (natural lip)	$\sim$ 100 Hz	1.4 - 1.6	N/A	N/A	N/A
Human lips (s.s. 4.4, present study, video method)	32 - 60 Hz	1.5 - 2.4	70 - 100 Hz	1.2 - 5	$\sim$ 50 - 80 Hz

Table 4.2: Lip parameter value ranges, as extracted from artificial and human lip mechanical response measurements. Quantities not recorded in the other studies[Richards, 2003; Cullen, 2000; Elliot and Bowsher, 1982; Saneyoshi *et al.*, 1987b; Gazengel *et al.*, 2007] are noted as not applicable (N/A), except for the lip resonance frequencies of Elliot & Bowsher[Elliot and Bowsher, 1982] and Saneyoshi[Saneyoshi *et al.*, 1987b] which included a much larger bandwidth than was possible with the human lip video method. f_0 is the destabilisation (playing) frequency of the embouchure, if noted.

response to the same driving level. Together with the generally low Q values of the lip resonances compared to the artificial lips, the cumulative effect was to push higher frequency resonances close to the noise floor of the measurement procedure. Application of a small overpressure by the player was demonstrated to aid the emergence of a second, inward striking peak, in a manner similar to that demonstrated with artificial lips. However, this technique was often difficult and unreliable, and resulted in many poor quality measurements.

Repeated measurements of the same target embouchure were required in order to clearly show the presence of two resonances. The absence of a resonance in some measurement does not signify that the lip-reed is incapable of both outward and inward striking behaviour. Rather, the difficulty of the experimental procedure warranted

careful repetition of the measurements, and with this repetition it became clear that a second resonance was present in many embouchures. It is certainly possible that some embouchures possessed only one main resonance, and could be well described by a single degree-of-freedom computational model. However, the many examples of embouchures exhibiting two resonances is strong evidence that a model incorporating at least two degrees-of-freedom would be a much more suitable model for general purpose lip-reed simulations.

The mechanical nature of the lip-reed

All of the video method measurements presented thus far, for both artificial and human lips, have used the technique applied to the front of the embouchure to measure the modulation of the opening area. What has been measured is thus the cumulative effect of any lip resonances on the open area function. Measurements have revealed both outward and inward striking resonances, which suggests that the two-mass, two degree-of-freedom computational model proposed by Cullen[Cullen, 2000] and Richards[Richards, 2003] may be suitable. However, the precise way in which outward and inward striking modes arise from the mechanics of the human lip-reed is unclear. Both the traditional 'piston'-like two-mass model postulated for the vocal folds[Ishizaka and Flanagan, 1972; Lous *et al.*, 1998], and the simple one-mass model capable of executing swinging and stretching motion[Adachi and Sato, 1996] possess two degrees-of-freedom, and both seem able to provide an adequate summary of the physics involved in the lip-reed. Both are certainly capable of exhibiting outward and inward striking properties, as has been demonstrated with both human and artificial lips. It thus remains difficult to identify the most suitable configuration for an optimal computational lip-reed model. Section 4.5 attempts to investigate this issue.

4.5 Transverse two-dimensional application of the mechanical response video method to artificial lips

4.5.1 Motivation for further application

Early measurements[Gilbert *et al.*, 1998] of the mechanical response of artificial lips relied on a laser vibrometer to provide information about the lip motion, as described in sections 3.3.1 and 3.3.2. Measured resonances were therefore associated with the degree of freedom along which this one-dimensional measurement took place, as illustrated in part (a) of figure 4.15. In the case of a laser vibrometry measurement this degree of freedom was the 'outward' swinging motion measurable in the x direction.

Measurements performed by Gilbert *et al*[Gilbert *et al.*, 1998] were based on an artificial brass player similar to that of Cullen[Cullen, 2000]. They revealed two strong

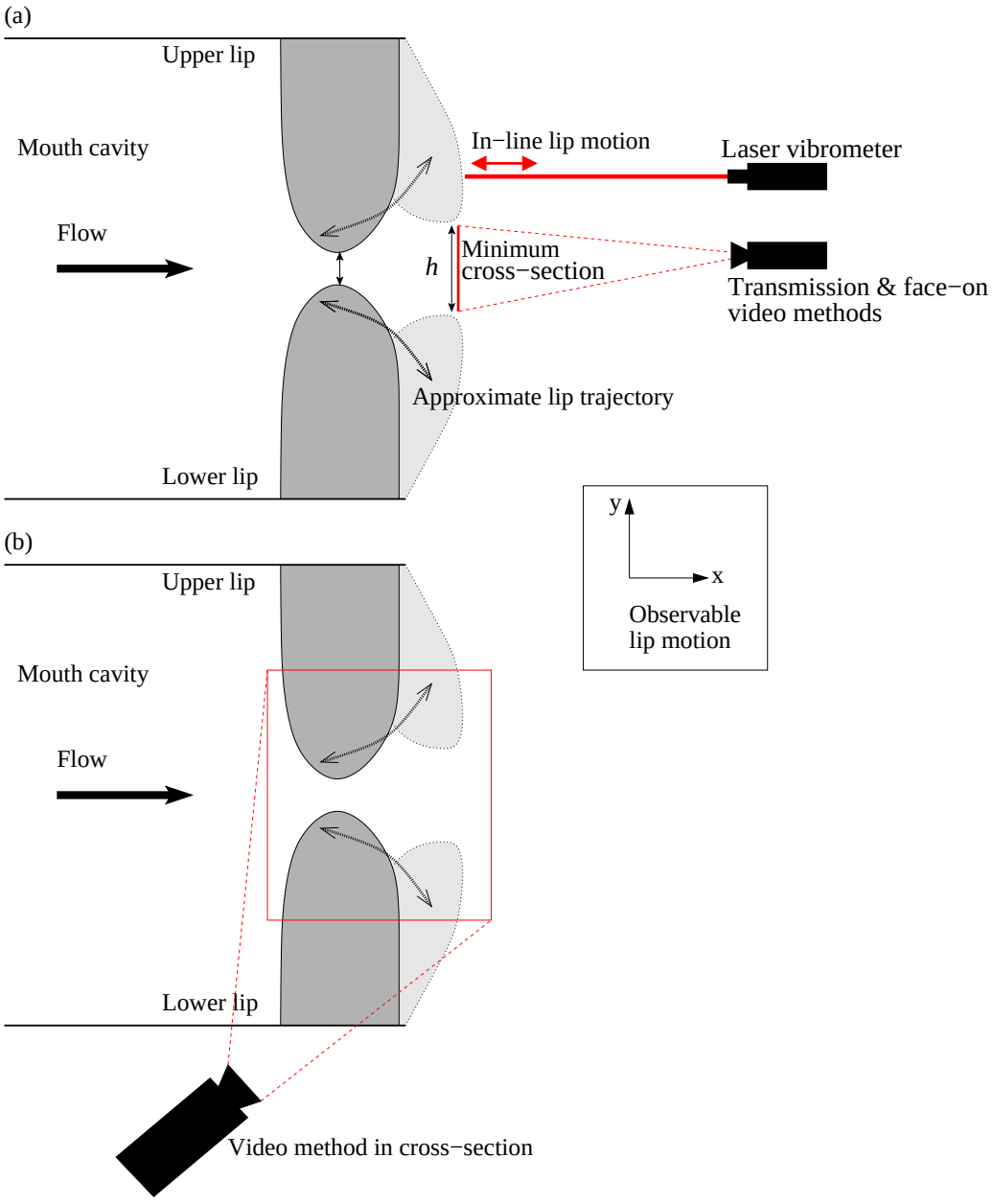

Figure 4.15: (a) A diagram showing the viewing axes of the vibrometer, transmission and face-on video methods. The vibrometer method measures motion in the x direction, whilst the transmission and face-on video methods measure the transverse y motion. (b) A diagram showing the video method set up in cross-section. Both the horizontal and vertical (x and y) axes of lip motion are directly observable with the camera set up in this way.

resonances, each with outward striking behaviour. Such a result was not surprising, given that it was heavily biased in sensitivity towards motion in an outward swinging direction.

The development of the transmission method used a different measurement axis. Instead of the longitudinal motion in line with a targeted laser beam, the total or partial lip opening was used to record the motion of the lips. This method has been described in section 3.3.2, with results presented in section 4.2. Under the assumption of minimal oscillations along the length of the lips (see section 4.3.2), this was effectively a one dimensional measurement recording the net effect of the various lip motions, both 'inward' moving and 'outward' swinging, on the lip opening. Such a measurement was thus sensitive to resonances in some way coupled to the y axis. This is also highlighted in part (a) of figure 4.15.

The video method presented one major advantage over the transmission method when applied to artificial lips, namely the ability to record the lip motion in multiple dimensions without immediate reduction of the data to a single degree-of-freedom. This allowed the simultaneous calculation of a mechanical response of the lips based on, for example, both the total lip opening, and only the central open height (again see section 4.3.2). Such an approach could rely on a single measurement data set, improving the comparability of the two calculations.

The video method was a particularly useful tool when applied to the study of replica B (see section 3.2.3). This was because this new *in vitro* model of the lip-reed allowed for extensive optical access to the lip cross-section, including the region directly between the lips. In previous versions of the artificial lips the area directly between the lips has been difficult to view, so most studies have relied on the frontal open area motion, visible through the glass window of the transparent mouthpiece[Cullen, 2000; Neal, 2002].

The main drawback of the laser vibrometry approach to multi-dimensional measurements of the lip motion was that the laser illuminated a fixed point in space, rather than a fixed point on the lips. This made it difficult to be precise about which lip motions were being recorded: any part of the lip that passed through the fixed point of illumination could contribute to the lip motion signal. The video method presented an improvement in this regard because real-life images were available that could be studied in order to understand the motion of a specific point on the lips.

Part (b) in figure 4.15 shows a schematic diagram of the video method set up to view replica B in cross-section. In this orientation a video recording of the lips was able to record the motion along two distinct axes of motion. Such a measurement was sensitive to resonances associated with both the outward (x) and inward motions (y) of the lips, without any reduction of the data to a single degree-of-freedom.

It was possible to use the sideways video technique to study the lip motion during a mechanical response measurement, and during full self-sustained oscillations.

Mechanical response measurements have clear relevance to the scope of work in this chapter, but measurements of the lip motion during self-sustained oscillation also presented a useful avenue of investigation.

Several studies[Martin, 1942; Copley and Strong, 1996; Yoshikawa and Muto, 2003] on real lips have highlighted the two-dimensional motion of the lips during self-sustained oscillation. Martin[Martin, 1942] used stroboscopy to observe the lip motion from the front and the side, though there was little analysis of any transverse motion. Copley and Strong[Copley and Strong, 1996] also used stroboscopy to observe the frontal and transverse lip motion. They tracked the motion of a point close to the centre of the upper lip, along the x and y axes described by figure 4.15. A strongly two-dimensional elliptical motion was reported, with the y component amplitude approximately twice that of the x component. Yoshikawa and Muto[Yoshikawa and Muto, 2003] tracked the tip of the upper lip through a conical transparent mouthpiece. Again, significant oscillations were found in both the x and y directions.

Richards[Richards, 2003] measured the transverse motion of replica A using a high speed digital camera, and reported two-dimensional motion. The vertical motion along the y axis was again dominant over the outward swinging x motion, by a factor of approximately 2:1.

The transverse viewing window in replica B allowed for controlled measurements of the transverse motion of the artificial lips. An investigation into this motion is presented in section 4.6.

4.5.2 The transverse mechanical response video method applied to replica B

The sideways video method was used to measure the mechanical responses of two embouchures formed with the artificial lips of replica B. The embouchures were characterised by the internal water pressure $P_{internal}$ of the lips, as detailed in section 3.2.3. The first embouchure had an internal pressure of 350Pa, and was referred to as the *low water pressure* embouchure. The second embouchure used a slightly higher water pressure of 390Pa, and was referred to as the *high water pressure* embouchure. The use of two different embouchures was required in order to test the robustness of the technique. It was also desirable as a method to investigate the behaviour of the artificial lip properties as the key control parameter, the internal water pressure, was altered.

The artificial lips were viewed from the side through the small glass viewing window that provided transverse optical access to the lip opening, as shown in figure 3.4. Details of replica B can be found in section 3.2.3. The camera was oriented so that the upper and lower boundaries of the video image were aligned along the vertical y axis, according to the convention in figure 4.15. The left and right sides of the image thus corresponded

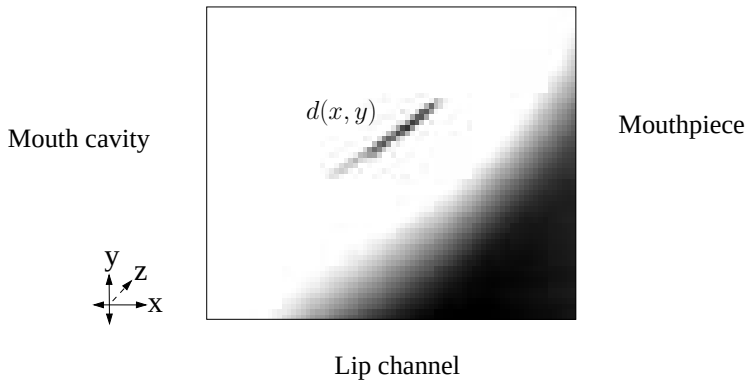

Figure 4.16: A single frame extracted from a transverse video method mechanical response measurement of replica B.

to the horizontal x axis. No mouthpiece was used for the measurements so as to limit the effect of any downstream acoustical interaction with the lips, and to facilitate easier setup of the various technical apparatus around the replica.

As with the transmission and frontal video methods (see section 3.3.2) the lips were driven into forced oscillation using a four second calibrated excitation sweep from a loudspeaker. A single dot was marked on the lips, approximately half way around the lip profile. A single dot was used because the wide range of lip motions during a four second excitation sweep made it very difficult to accurately track multiple dots. It was, however, possible to track more than one dot during steady self-sustained oscillations. This is described in section 4.6.

Figure 4.16 shows a single frame extracted from a transverse high speed video of replica B, during a mechanical response measurement. The coordinates of the central dot in the image were denoted $d(x, y)$. The background was visible as a dark region towards the lower right of the image.

An analysis procedure was required in order to measure the centroid of the dot within the image frames. This was performed in Matlab. The entire four second video, comprised of 16288 individual frames, was first extracted to a folder as individual bitmap images. The analysis program then imported the raw images into the Matlab workspace one by one in a loop. The program allowed the user to set a binarisation threshold that converted all pixels in an image to either black or white. Pixels above the threshold were converted to pure black, and pixels below the threshold to pure white. Careful adjustment of the threshold allowed the individual dots to be separated from the background. A routine was then called that detected any isolated regions of connected pixels in the binary image. A single group of connected pixels were grouped together as a single point, the centroid of which could be immediately calculated within the image frame.

The dot centroid location $d(x, y)$ was calculated for each video frame, and the data concatenated to provide a dot position signal over the entire excitation sweep. The horizontal (x) and vertical (y) components of the dot motion were then used to calculate mechanical response curves for the lip in both directions.

The mechanical response in two dimensions

The theoretical definition of the mechanical response outlined in section 2.7.1, and defined in equation 2.33, is based on the assumption that a periodic pressure difference across the lips causes a periodic modulation of the opening height between the lips.

The mechanical response may be obtained experimentally by a frequency response function between the driving pressure, measured with a microphone, and the opening area, measured face-on with the transmission or video method. The opening height measured this way is thus comparable with the vertical motion in the y direction shown in figure 4.15, measurable with the transverse video method, but with one important difference. While the frontal transmission and video methods measured the minimum open area resulting from the three-dimensional motion of the lips, the transverse vertical y component measured the absolute motion of a specific point on the lips.

The discrepancy between a minimum open area measurement and an absolute open height measurement arose because of the possibility of non-uniform vertical motion along the lip width (the x axis in figure 4.15). The face-on methods have already been shown to produce an essentially one-dimensional interpretation of the lip motion, condensing the open height and open length dimensions into a single signal (see section 4.3.2). This approach also limited the detail obtainable from lip motion along the x axis. It was not possible to observe the effects that different parts of the lip along the x direction had on the minimum open area. Rather, it was simply possible to measure the combined effect of them all in producing a single minimum open area signal. Richards[Richards, 2003] postulated that if different regions along the lip width moved out of phase with each other during an excitation sweep, such motion might be the source of the higher resonance peaks observed in mechanical response measurements.

On the contrary, the transverse y signal that arose from tracking a dot marked on a lip provided an almost pure representation of the vertical motion of the underlying lip region. It could not be considered a completely 'pure' measurement because it was necessary to observe the lip motion from a slight angle in order to gain optical access to the dot. However, this angle was generally very small, less than 5^o, as shown in figure 4.17. It has thus been neglected in this analysis. This small camera rotation was more relevant for the motion of the dot along the x direction, but was also neglected for this analysis.

The outward and inward striking regimes outlined in section 2.7.1 have be defined in terms of the relative phasing between a driving pressure and the resulting open height

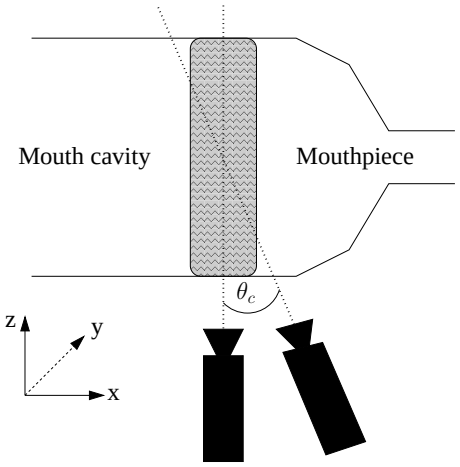

Figure 4.17: A schematic view showing the slight camera offset angle required to view the dot on the lip during a transverse mechanical response measurement. θ_c, the offset angle, was typically less than 5^o.

modulation of the lips. Such an analysis may therefore be quite readily transfered to a discussion of the mechanical response based on the vertical y motion extracted from a transverse video measurement.

The horizontal lip motion must be considered carefully in respect to the established methods of mechanical response evaluation, which are based on the lip opening. The many examples of mechanical response curves provided by Cullen[Cullen *et al.*, 2000], Neal[Neal, 2002], Richards[Richards, 2003] and in the present work demonstrate that the essentially one-dimensional measurement of the mechanical response based on the open area is capable of observing resonances with either outward or inward striking behaviour. This is due to the inherent coupling between the horizontal and vertical motion of the lips. For example, excitation of a predominantly horizontal mode, which causes the lips to move outwards into the mouthpiece, also results in a modification of the open area. This motion is clearly measurable with the frontal transmission and video methods.

The horizontal-vertical coupling arises because the lips are continuous media, with relatively fixed contact points at the valve walls. Deformation of a lip caused by horizontal motion forces all of the lip surfaces to distort, including components parallel to the vertical y axis. This stretching along both axes results in a vertical restoring force in the latex (or lip tissue), which may be modeled computationally by damped springs. Thus a horizontal distortion of the lips inevitably results in a corresponding upwards vertical motion, as illustrated in figure 4.18. The figure shows a single lip at rest (solid line), and after horizontal distortion resulting from the stretching motion imparted by acoustic driving (dashed line). The stretching motion along the x axis causes the leading lip surface, marked in red, to stretch from its fixing at point B. The resulting

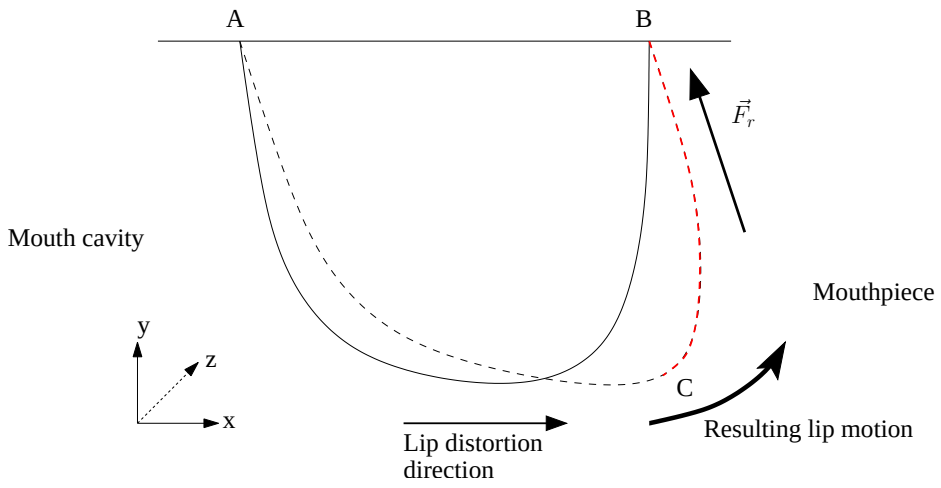

Figure 4.18: A schematic diagram showing how horizontal distortion of a lip leads to a vertical restoring force. F_r is the approximate restoring force, acting along the latex surface in the case of an artificial lip, which results from a stretching of the lip along the x axis. The lip anchor points at A and B mean that any distortion of the lip results in a vertical component of the elastic restoring force.

elastic restorative force, $\vec{F_r}$, has components along both the x and y axes. In the dynamic situation during a mechanical response measurement, the vertical component of $\vec{F_r}$ causes the lip to move upward as well as outwards as the lip is forced by the acoustic signal. This allows a predominantly horizontal 'outward striking' mode to be recorded by the transmission and frontal video methods.

The horizontal component of the lip motion may be compared to the vibrometer signal used by Gilbert *et al*[Gilbert *et al.*, 1998] (see part (a) of figure 4.15). The main difference between the signals was that the vibrometer method focussed a laser beam onto a fixed point in space, through which any part of the lips could pass, while the horizontal motion from tracking a dot recorded the unique motion of the underlying lip region. Classification of any resonances by their phase behaviour was defined, as normal, by the phase angle between the driving acoustic pressure and the lip oscillations. The lip opening used for transmission and video method measurements was simply replaced by the horizontal motion signal. Motion of the lip towards the vibrometer, or along the positive x axis for the transverse video method, was regarded as an increase in the lip position.

The results of Gilbert *et al*[Gilbert *et al.*, 1998] revealed two strong lip resonances, typically at 100Hz and 200Hz, each with outward striking behaviour. Such a result appears logical based on the preceding commentary. While it is clear that motion along the x axis may be recorded with a transmission method measurement, it is not clear how a mode strongly linked to the vertical direction would be measurable by the laser vibrometer. This issue will be addressed in the context of results obtained with

the transverse video method.

It is worth noting that throughout this discussion an implicit assumption has been made regarding the association of lip resonances with the x and y axes. While these two degrees-of-freedom form the primary detection axes for vibrometer, transmission and video method measurements, care should be taken to avoid pigeonholing lip resonances classified as outward or inward striking with motions purely along these axes. The lips may well, for example, possess purely rotational modes which 'leak' into measurements evaluated along the Cartesian axes of the experimental setup. The complex, continuous nature of the lips, both real and artificial, mean that without more sophisticated measurement methods it has been difficult to describe lip resonances beyond the rudimentary level thus far described.

The low water pressure embouchure

Figure 4.19 shows three mechanical response measurements of the low water pressure embouchure. The black curve represents a typical spectrum averaged transmission method measurement, while the blue and red curves have been evaluated using the horizontal and vertical components of the dot motion during a transverse video method measurement.

Consider first the low frequency region between 50Hz and 150Hz. The transmission method revealed two resonances at approximately 96Hz and 111Hz, with outward and inward striking behaviour respectively. The transverse video measurement evaluated along the horizontal x component of motion revealed a strong resonance at 96Hz, appearing to match the outward striking peak seen in the transmission method curve. The phase behaviour around this peak matched that of the transmission method extremely closely, to within the typical error margin for consecutive transmission method measurements, confirming its classification as outward striking. The quality factor of the transverse method peak, about 13.6, was slightly lower than that of the corresponding transmission method peak, about 14.5.

The transverse video measurement evaluated along the y component of motion was noisier than the measurement evaluated along the x component. This was because the typical amplitude of the vertical motion was approximately an order of magnitude less than that of the horizontal direction.

Between 50Hz and 150Hz the y component magnitude curve suggested the presence of three resonances, at 88Hz, 96Hz and 110Hz. The first of these was difficult to account for, as it did not appear in either the transmission method or the horizontal x component measurements. The second resonance, at 96Hz, matched the frequency of the outward striking peak found in both the transmission method and horizontal x axis measurements. However, the phase behaviour of this peak was not very close to the outward striking phase angle of $-90°$. This may have been due to the fairly low

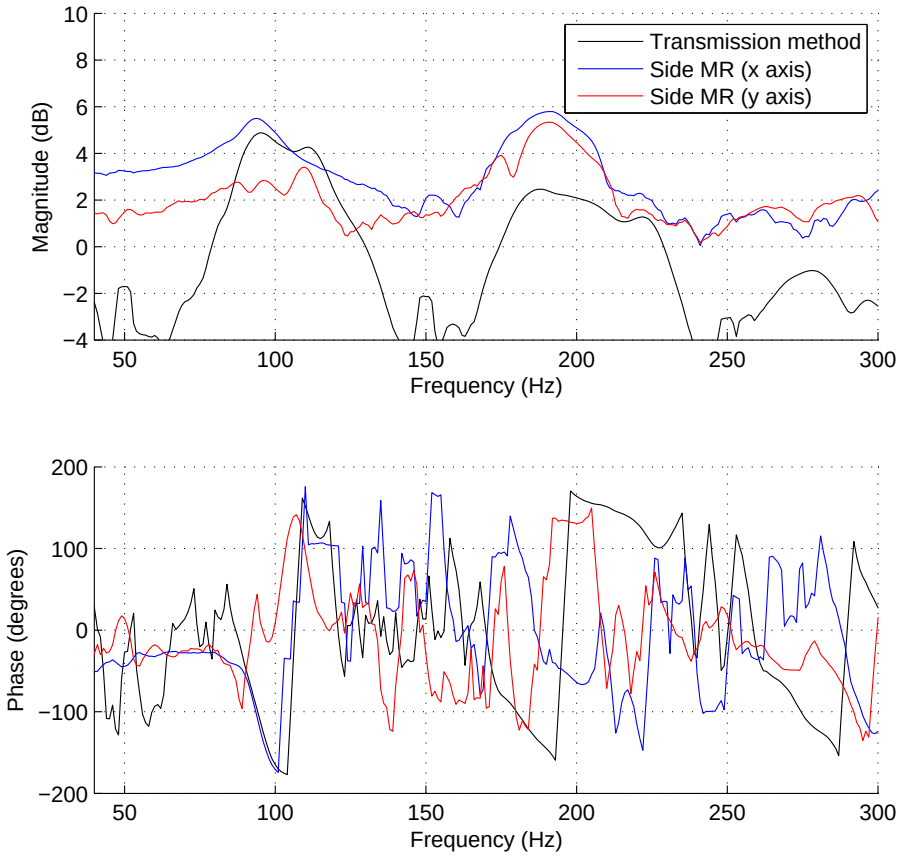

Figure 4.19: Three mechanical response curves evaluated with the low water pressure embouchure.

signal-to-noise ratio that resulted from the relatively low amplitude of the lip motion. It is also possible that it suggested a degree of coupling between the measurements obtained with the x and y components of the motion, which could have resulting in a 'mixing' of the phases.

The third resonance, at 110Hz, exactly matched the frequency of the inward striking peak observed in the transmission method measurements. The phase behaviour of this peak passed smoothly through the inward striking angle at $+90^o$, confirming this as an inward striking resonance. Interestingly, the phase curve for the vertical y component of the motion appeared to pass more cleanly through the inward striking angle than the curve of the transmission method.

The phase behaviour of the vertical transverse video method goes straight through 90, as opposed to the transmission method, where it doesn't actually go right through.

Now consider the region of figure 4.19 between 150Hz and 300Hz. The transmission method measurement recorded outward and inward striking resonances at 188Hz and 222Hz respectively. The horizontal x axis transverse measurement captured both of

these peaks in the magnitude curve. The phase response was rather noisy, however, and could only be really trusted around the 188Hz resonance. In this region the curve went through the outward striking angle at -90^o, but at a frequency slightly higher than the transmission method curve. The phase behaviour around the 222Hz resonance appeared to pass down through the inward striking angle, but the signal-to-noise ratio here was quite poor.

The vertical y axis measurement between 150Hz and 300Hz also recorded the two resonances at 188Hz and 222Hz in the magnitude curve. However, the signal quality of the phase curve was too poor for further analysis.

The high water pressure embouchure

Figure 4.20 shows three mechanical response measurements of the high water pressure embouchure. The black curve represents a typical spectrum averaged transmission method measurement, while the blue and red curves have been evaluated using the horizontal and vertical components of the dot motion during a transverse video method measurement.

The basic features of the curves in figure 4.20 were quite comparable with those obtained from the low water pressure embouchure, shown in figure 4.19. The horizontal x axis measurement revealed a prominent resonance in the magnitude curve at approximately 97Hz, which matched the corresponding transmission method curve. This resonance did not appear to be significantly shifted in frequency compared to the low water pressure embouchure, despite an increase of 40Pa in the water pressure. The phase curve matched the transmission method measurement extremely closely right across the resonance, from 60Hz up to 110Hz.

The vertical y axis measurement revealed the same three magnitude peaks around 100Hz as were reported in the low water pressure embouchure. However, while the first of these at 88Hz remained small in amplitude, the other two were significantly larger. This suggested that the small peak may have been an Fourier transform artifact due to the low lip signal level around that region.

The second of the magnitude peaks, at approximately 97Hz, matched the outward striking peak found in the horizontal and transmission method measurements. The phase behaviour around the resonance was somewhat different to that seen in figure 4.19. It passed down through $+90^o$, in contradiction to the phase behaviour of the other measurement methods.

The third resonance was at 117Hz, noticeably higher in frequency than the corresponding resonance in the low water pressure embouchure. This resonance once again matched the inward striking peak found in the transmission method curves in both frequency and phase behaviour, confirming it as an inward striking resonance.

The magnitude curves from the transverse video methods revealed several other

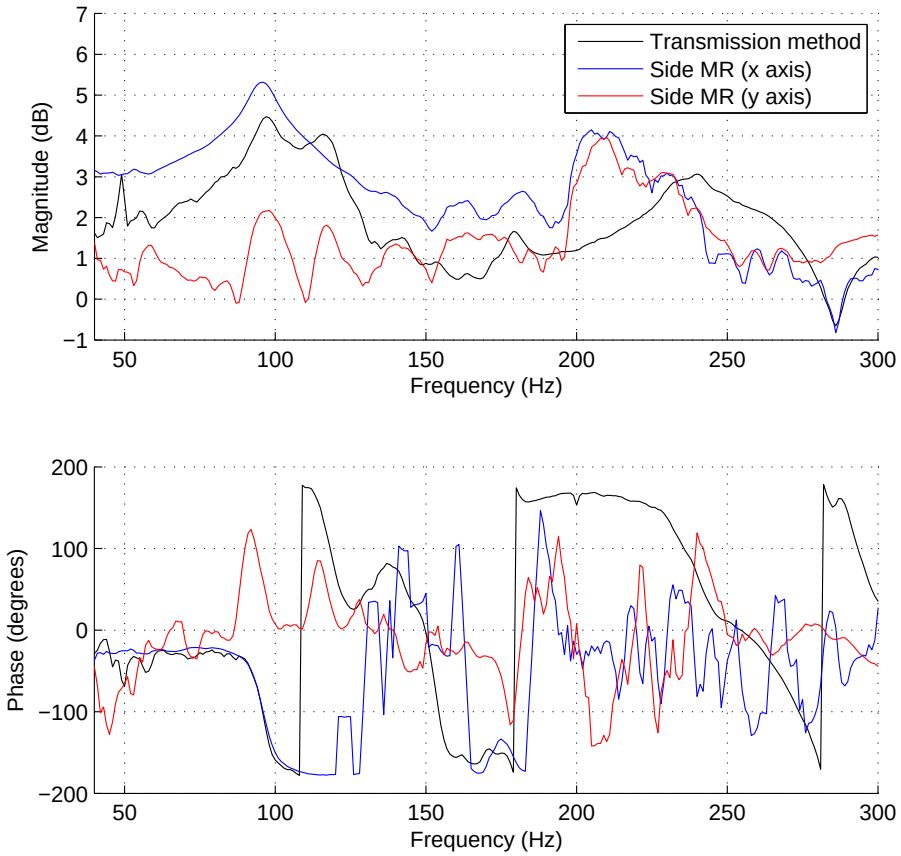

Figure 4.20: Three mechanical response curves evaluated with the high water pressure embouchure.

resonances in both the horizontal and vertical. Some of these peaks, such as the one close to 140Hz, appeared along both axes, and in the transmission method curve. The peak around 180Hz also appeared quite strongly in all three magnitude measurements, with all three phase curves also passing close to-90^o around this frequency. This peak appeared to thus be the lower, outward striking resonance of the secondary resonance pair, as described in section 4.3.3.

The transverse data signal quality was quite poor between 190Hz and 230Hz, so it was difficult to usefully interpret the curves over this frequency region. Both the horizontal and vertical axes revealed resonances around 210Hz, but these were rather noisy, and the phase response was very noisy. Small peaks were recorded at 244Hz which matched the prominent peak that occurred at this frequency in the transmission method curve. The horizontal x axis phase response was very poor here, but the vertical y axis response appeared to be considerably cleaner as it passed through $+90^o$, very similarly to the transmission method phase response. This indicated that it was the upper, inward striking resonance of the secondary resonance pair.

Analysis of the two dimensional motion of the lip-reed

The preceding two sections have outlined the main features present in mechanical response curves obtained with the transverse video method. These features have been described alongside similar commentary on curves obtained with the standard transmission method. The objective of the discussion was to try to provide a more complete mechanical description of the lips by taking into account their two-dimensional motion. The method used for this analysis was to calculate mechanical response curves based on the horizontal x and vertical y components of motion. This parametric approach was chosen because these degrees-of-freedom have long been associated with the outward and inward striking resonance modes, respectively, defined in many classical descriptions of musical valves[Helmholtz, 1877; Elliot and Bowsher, 1982; Fletcher, 1993; Campbell, 1999]. The analysis presented here thus attempts to investigate the similarity between theoretical valve descriptions, and valve motions observed experimentally. It is an attempt to analyse in more detail the underlying valve motion that gives rise to the experimentally observed outward and inward striking resonances.

The transverse video method measurements measured the lip motion as it occurred parallel and at right angles to the streamwise flow direction, along the x and y axes defined in figure 4.15. This so-called 'lip motion' was in fact the motion of a single, isolated part of the lip (point d), chosen to be approximately halfway around the lip surface (see figure 3.5 for a graphical representation of the lip shape).

The transmission method measurement relied on the minimum area of the lip opening when viewed from downstream, which has been shown to be directly related to the vertical component of the lip motion. At rest, this minimum open area was determined by a region of the lips that lay further upstream (along the negative x direction) than point d. This can be seen from the example image frame shown in figure 4.16, which shows the position of the dot in relation to the rest of the lip surface. A substantial part of the lip lay upstream of the dot, and it can be seen from the vertical y profile that this upstream region created a smaller cross-sectional lip opening than the region in line with the dot. Thus it can be seen that the transverse video method and transmission methods recorded the lip motion using different parts of the lip surface. As will be shown in the following section (c.f. section 4.6), substantial phase shifts occur along the lip width (i.e. different points along the x axis) during full self-sustained oscillations. This lays the foundation for a deeper analysis of the lip behaviour seen in figure 4.21, and its relation to the transverse video, and standard transmission method measurements.

Figure 4.21 shows the raw two-dimensional motion of the point $d(x, y)$ as a function of the driving frequency for the high water pressure embouchure (figure 4.22 shows the spatial orientation of figure 4.21). This parametric plot shows the actual motion of the

dot as the lips were subjected to an approximately frequency flat excitation sweep. This amplitude of the dot motions in the figure were thus strongly related to the transverse mechanical response magnitude curves in figure 4.20. The dot motion that occurred for the first two resonance frequencies, at 97Hz and 117Hz in the transmission method curve, have been highlighted in yellow and red.

One of the most striking overall features of the plot was the clear two-dimensional motion of the dot. The descriptions of the two-dimensional valve responses presented in the preceding two sections clearly indicated that the motion of the dot was not simple. However, a raw display of the actual dot motion acted to strongly reinforce the fact that, even under the low amplitude acoustical excitation conditions of a mechanical response measurement, the lips followed a remarkably complex trajectory. It is also important to note that this motion was only that of a single point on the lips. As will be shown in section 4.6, under a full self-sustained regime, different portions of the lip width oscillate with quite different amplitude and phase.

In the low frequency region, from 40Hz up to 110Hz, the horizontal x component of the motion produced an almost perfect outward striking resonance for both the low and high water pressure embouchures. This resonance appeared to correlate exactly with the outward striking resonance found in the transmission method measurements in frequency and phase behaviour. The measurement evaluation along the horizontal component of the motion relied solely on the motion of the lip parallel to the flow, in a direction that would be directly into and out of the mouthpiece. It is clear from the parametric plot of figure 4.21, however, that the actual lip motion around the 97Hz 'outward striking' resonance had both horizontal and vertical components. This can be clearly seen in the two-dimensional projection of figure 4.21, shown in figure 4.23. In this figure the dot motion during the entire sweep has been plotted in just the spatial dimensions, with the motion around the 97Hz resonance highlighted in yellow.

The 97Hz resonance evident in the x component mechanical response curve in figure 4.20 resulted from a frequency response function between the motion directed along the x component (shown in figure 4.23), and the microphone signal. The horizontal x motion around the resonance was approximately an order of magnitude larger than the vertical y component of the motion. Nevertheless, evaluation of the mechanical response based on the vertical y component of the motion at this driving frequency did provide an amplitude peak in the y component mechanical response magnitude curve shown in figure 4.20.

The dot motion displayed a hysteretic trajectory which traced out something like a figure-of-eight shape. This meant that there must have been a phase difference between the horizontal and vertical components of the dot motion around this resonance. This may explain why the phase crossing of this outward striking resonance, when evaluated with the y component of the dot motion, did not pass smoothly through the $-90°$ phase angle, as seen in figure 4.20. It is also possible that there was a phase difference between

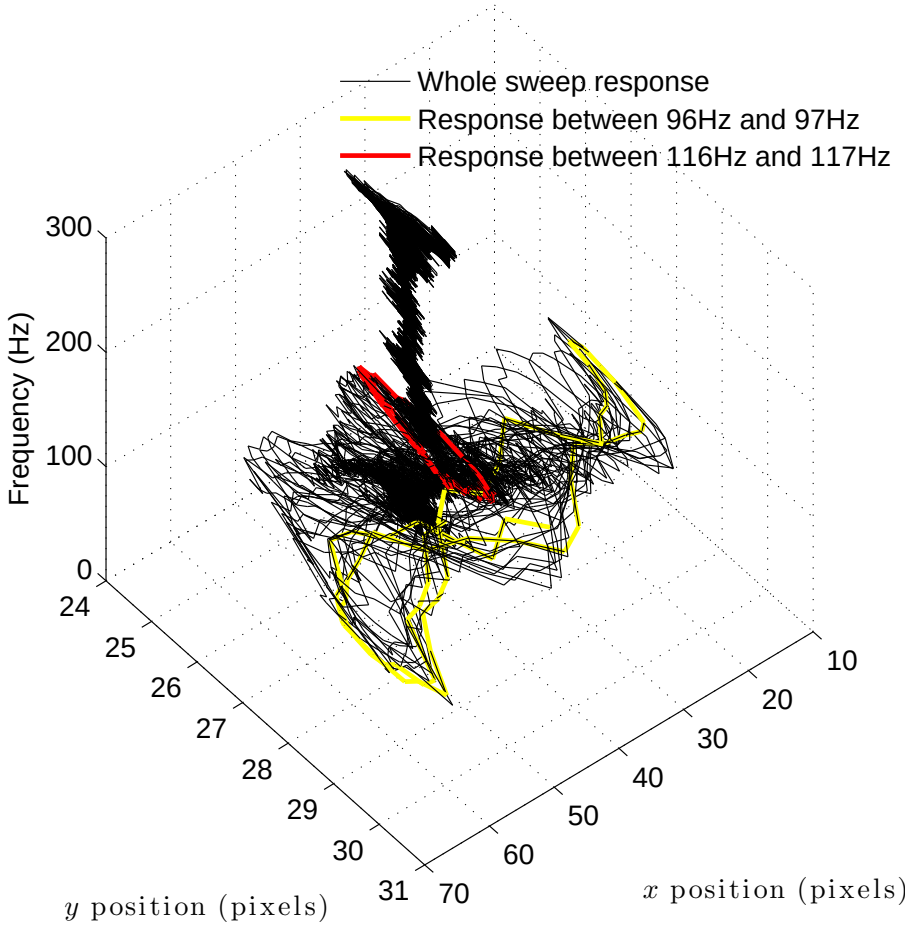

Figure 4.21: The two-dimensional motion of the single point $d(x, y)$ during a mechanical response measurement, as a function of the excitation frequency. The lips were excited from 40Hz - 300Hz. The lip motion at the frequencies of the first two resonances observed in the transmission method measurement (see figure 4.20) are highlighted.

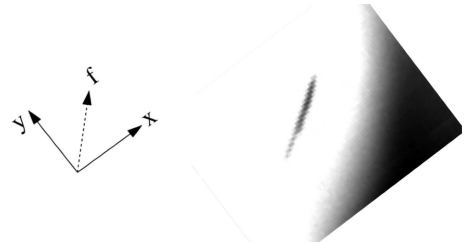

Figure 4.22: An example image frame from a transverse video method measurement, oriented to aid interpretation of figure 4.21.

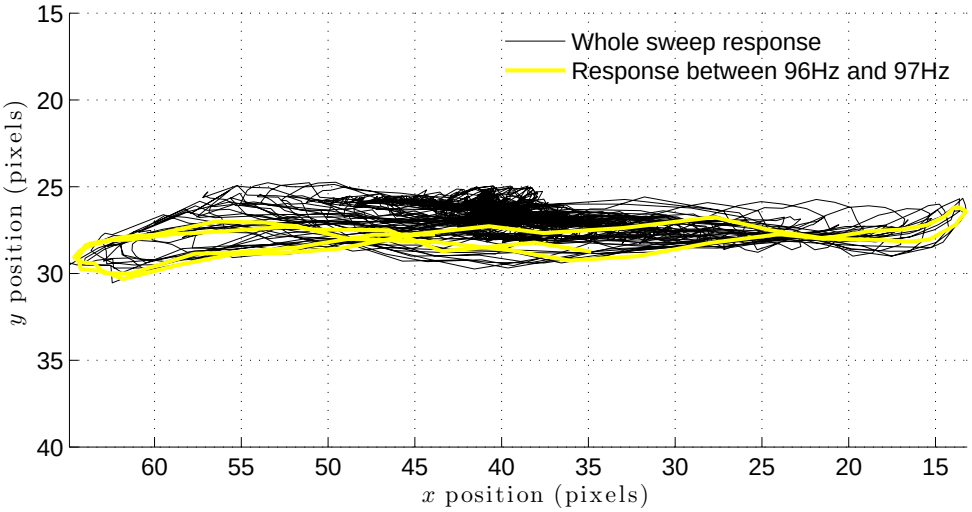

Figure 4.23: The two-dimensional motion of the point $d(x, y)$ whilst being acoustically driven by a calibrated sine sweep, for the high water pressure embouchure. The motion around the 97Hz outward striking resonance is shown in blue. The figure has the same spatial orientation as the image frame shown in figure 4.16, and the schematic diagram shown in figure 4.18.

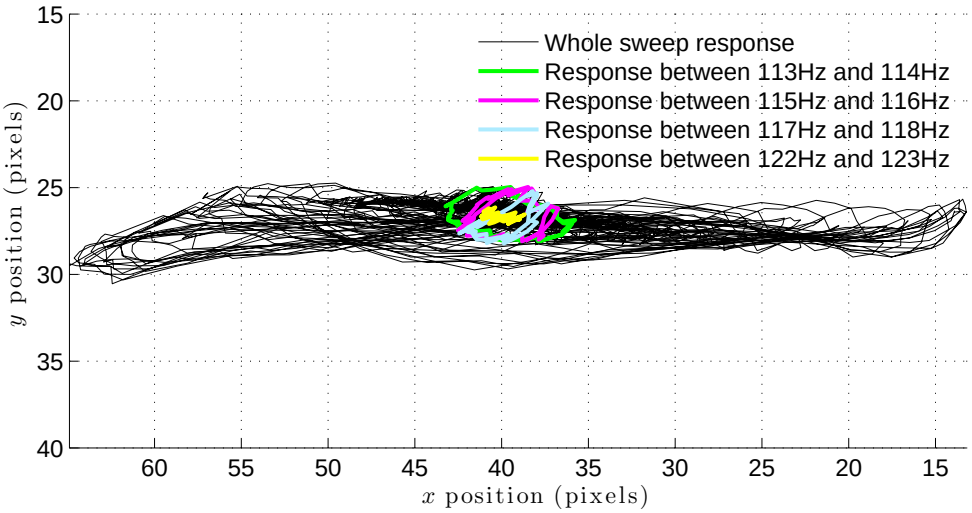

Figure 4.24: The two-dimensional motion of the point $d(x, y)$ whilst being acoustically driven by a calibrated sine sweep, for the high water pressure embouchure. The motions around the 117Hz inward striking resonance have been highlighted. The figure has the same spatial orientation as the image frame shown in figure 4.16, and the schematic diagram shown in figure 4.18.

the part of the lip where the dot was placed, and the part of the lip that accounted for the minimum open area which provided the benchmark transmission method curves. To fully answer this issue would require more extensive tracking of multiple dots along the lip surface during a mechanical response measurement. What can be concluded is that the x component of the motion is unquestionably coupled to the y axis at the frequency of the lower outward striking resonance.

The inward striking peak, seen in the transmission method curves at 117Hz, was also seen in the vertical y axis measurement. The peak frequency and phase of the resonance was very similar for the two measurements. This peak was not strongly present in the horizontal x axis measurement, despite the clear horizontal motion visible in figure 4.21, and in the two-dimensional projection of the dot motion shown in figure 4.24. There was also little indication in the phase plot to indicate its presence.

Four narrow frequency bandwidths around 117Hz have been highlighted in figure 4.24. These cover the frequency range from 4Hz below the resonance peak, to 6Hz above it. They demonstrate why the 117Hz inward striking resonance did not appear in the horizontal x component measurement: as the resonance was approached from below, the amplitude of motion along the x component decreased, while the amplitude of the y component of motion slightly increased.

The figure shows that below the resonance the dot oscillated elliptically, with a greater x axis amplitude than y axis amplitude. As the resonance was approached the motion became more confined to the vertical y direction, as the x component of the motion decreased in amplitude. Above the resonance the horizontal component again became larger than the vertical. This result strongly implies that the inward striking behaviour of the lip-reed is associated with the motion at right angles to the flow, in the vertical y direction. This result reflects the theoretical description of an inward striking reed.

Coupling between the outward and inward modes of the lip-reed

One of the essential findings of the two-dimensional mechanical response measurements was that at the outward striking frequency, the lip motion was predominantly confined to the streamwise x direction. Motion in this direction, however, was inherently coupled to the vertical y axis. This was because the deformation of the lip along the y axis, caused in this case by the acoustical excitation of a mechanical resonance aligned with the y axis, resulted in a restoring force with both horizontal and vertical components. The restoring force arose because the artificial lips were formed from latex, a material with elastic properties. Figure 4.18 has illustrated this effect, by demonstrating that any deformation of the lip results in some degree of vertical restoring force, as the lips are attached to bounding walls that lie at the upper and lower edges of the mouth cavity.

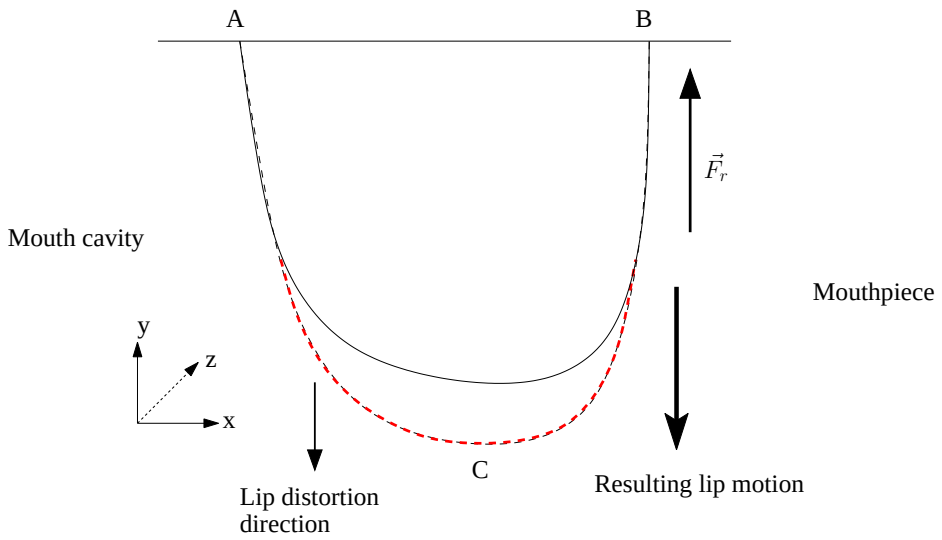

Figure 4.25: A schematic diagram showing how vertical distortion of a lip leads to only a vertical restoring force. F_r is the approximate restoring force, acting along the latex surface in the case of an artificial lip.

The inherent coupling between the horizontal and vertical components of the lip motion at the lower outward striking frequency meant that the outward striking resonance could be recorded by the vertical y component of the lip motion using the transverse video method, as well as by the frontal transmission and video methods, which were sensitive to this degree-of-freedom.

At the frequency of the inward striking resonance the lip motion was predominantly confined to the vertical y direction. A resonance peak was detected by both the frontal transmission and video methods, and by the vertical component of the transverse video method. However, no response was measured by the horizontal component of the transverse video method. The magnitude curve of the transverse y axis measurement showed a completely smooth progression past the inward striking frequency. This suggested that at this frequency the resonance was the result of a primarily vertical motion, which could not be detected by the transverse x axis measurement.

The behaviour of the inward striking resonance can be explained by once again considering the mechanical restoring forces that acts within the lips when they are deformed. Deformation of the lip along the streamwise x axis inherently leads to a vertical as well as horizontal motion. However, deformation of the lip along the vertical y axis is not expected to produce any restoring force aligned with the x axis. Figure 4.25 illustrates graphically why a vertical lip resonance is not expected to produce any significant horizontal motion. The lips are anchored at points A and B and any deformation force, such as that which results from an acoustical excitation at the vertical resonance frequency, must *a priori* have a vertical component. However, in

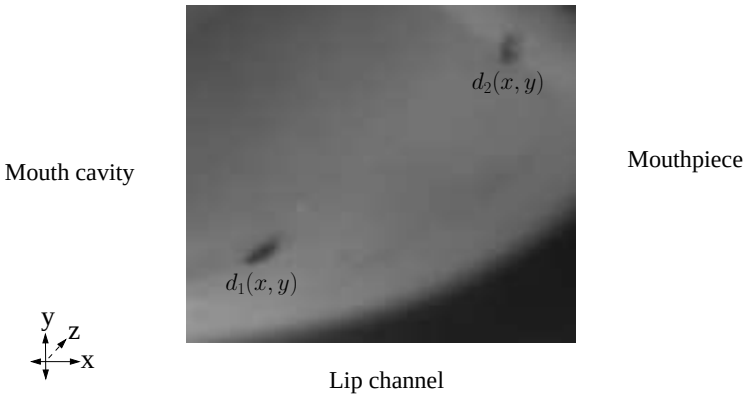

Figure 4.26: An image extracted from a video of replica B during self-sustained oscillations. The two black points were marked on the lip to allow the transverse motion to be tracked. The position of the mouth cavity, mouthpiece and lip channel are shown.

the absence of a horizontal driving force, there is no reason for the lips to experience a horizontal driving force.

The behaviour of the lips around the inward striking resonance suggests that at this frequency there should be little or no coupling between the horizontal and vertical motion. However, this hypothesis can only be valid where a purely vertically aligned resonance has been excited. It appears that at the inward striking resonance frequency the observed resonance was in fact caused by a vertical motion of the lips, and so the hypothesis may be made.

The preceding discussion has outlined an explanation for the mechanical response behaviour of the artificial lips around the lowest two resonances. It would be possible to extend this discussion to include the resonances seen at higher frequencies, but this task is left as an avenue of future work.

4.6 Two dimensional motion of replica B during self-sustained oscillations

The two dimensional motion of replica B was investigated during full self-sustained oscillations using the high speed digital camera setup outlined for mechanical response measurements in section 3.3.3. The camera was directed through the small glass viewing window in the side of the replica, as shown in figure 3.2. In order to track the motion of specific points on the lip, two small dots of black ink were drawn onto the latex. An example of the dots marked onto an artificial lip is shown in figure 4.26. The dots were placed at points approximately one third and two thirds of the way around the lip profile (see figure 3.5 for an explanation of the lip profile). As the lips oscillated,

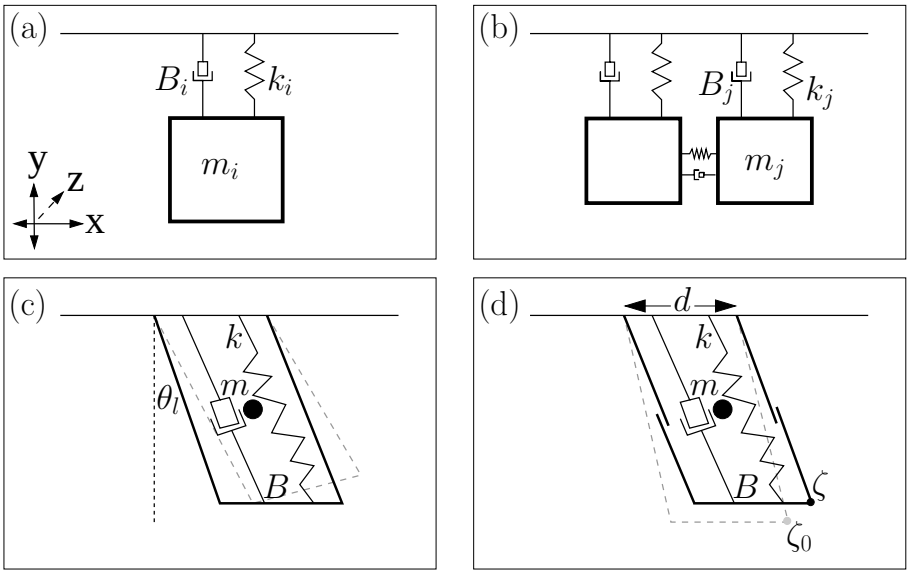

Figure 4.27: A comparison between four lumped element models of the lip-reed. (a) The traditional one degree of freedom one-mass model. (b) The two degree of freedom two mass 'piston' model[Richards, 2003] (c.f. vocal fold models[Ishizaka and Flanagan, 1972; Titze, 1988; Lous *et al.*, 1998]). (c) The one degree of rotational freedom one-mass model[Elliot and Bowsher, 1982]. (d) The two degree-of-freedom one-mass model proposed by Adachi[Adachi and Sato, 1996] (as (c), but extensible along the y-axis).

the dots of ink moved according to the underlying lip trajectory.

The objective was to find evidence which indicated the most suitable computational model to describe the lip-reed. A range of lumped element models have been proposed for the lips, including one-mass and two-mass models. Four examples of such lumped-element musical valve models are shown in figure 4.27. Parts (a), (c) and (d) are variations on a one-mass model. The traditional two-mass model adapted from vocal fold models is shown in part (b). This model is capable of executing a piston-like motion whereby the two masses oscillate, along the y axis, in anti-phase. Such motion has been shown to be important for controlling the Bernoulli effect along model surface, as described in section 2.5. The target of the investigation was to determine the extent of any two-dimensional motion of the artificial lips, and to observe the uniformity of the motion along the lip width (the x axis), in order to suggest whether a one-mass, two-mass or other configuration was most suitable.

Two separate points were marked onto one of the artificial lips. The point furthest upstream was denoted dot one, $d_1(x, y)$. The point furthest downstream was denoted dot two, $d_2(x, y)$. High speed video footage was taken of the lips during self-sustained oscillations. Individual video frames from a short sequence of the video were then extracted as bitmap images. The individual dots were isolated from the background of the image using the thresholding procedure described in section 4.5.2. The process

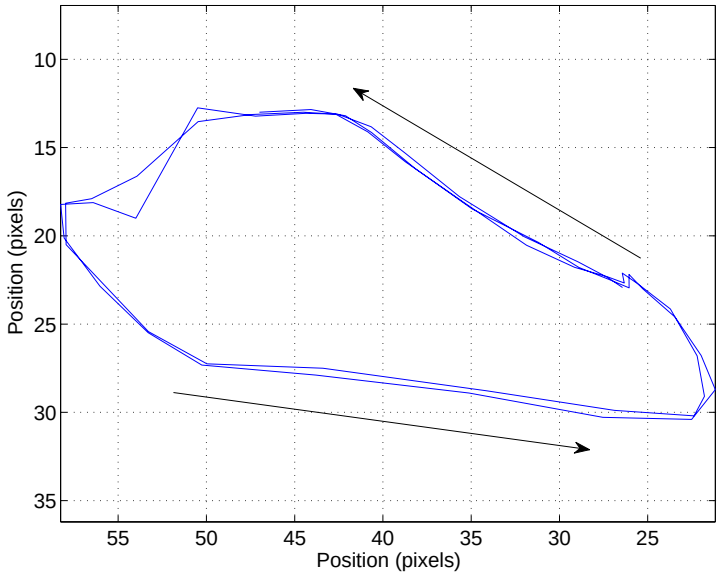

Figure 4.28: The motion of the point d_2 during self-sustained oscillations, as extracted from a video sequence of 68 images. The axes are inverted so the data can be directly compared with the example image in figure 4.26.

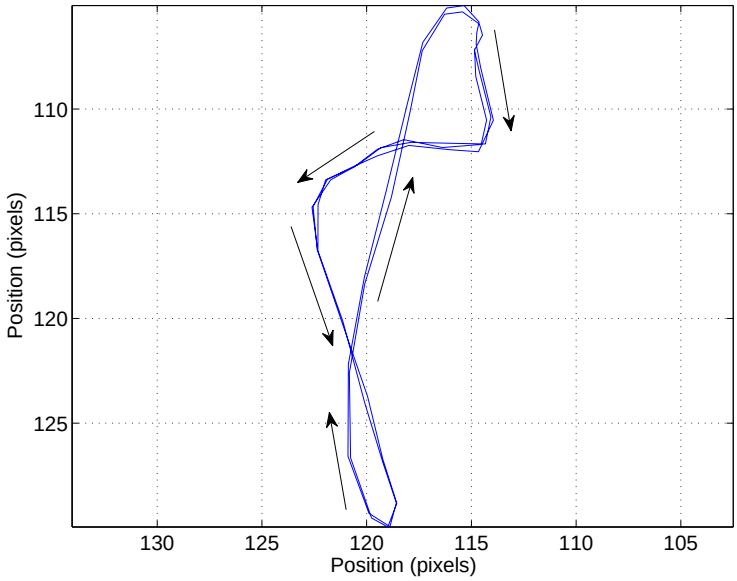

Figure 4.29: The motion of the point d_1 during self-sustained oscillations. The axes are inverted so the data can be directly compared with the example image in figure 4.26.

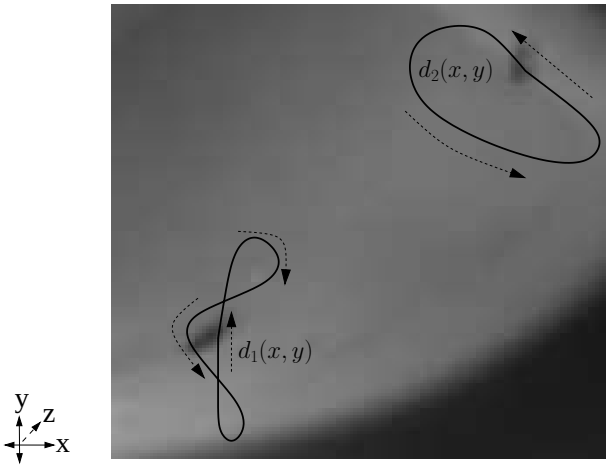

Figure 4.30: The measured motion of the two dots overlaid onto a single image frame (not strictly to scale).

was performed for both dots and for all images in the sequence, leading to two data sets describing the x and y positions of each of the dot centroids, throughout the measurement period.

4.6.1 Motion of point d_2

Figure 4.28 shows the two-dimensional motion of the point d_2 over approximately three full cycles of oscillation. The motion is also presented overlaid onto a single image frame from the high speed video recording in figure 4.30. This point was close to the downstream edge of the artificial lip, and clearly exhibited two-dimensional motion. In contrast to many transverse measurements on human lips, the horizontal swinging motion appeared to dominate the vertical motion by a factor of approximately 2:1. The motion thus followed an elliptical path. At the extreme downstream limit of the horizontal motion d_2 actually moved slightly downwards, acting to reduce the open area. This type of motion has been suggested for the human vocal folds[Story and Titze, 1995; Kob, 2002], and differs from the behaviour observed in human lips by Yoshikawa[Yoshikawa and Muto, 2003]. His measurements showed that the lip tip tended to have a maximal upward velocity as it reached the limit of its horizontal motion.

Simulations of the lip-reed performed by Adachi and Sato[Adachi and Sato, 1996] included two-dimensional plots of the transverse motion of the upper lip. Their model is shown in part (d) of figure 4.27. A strong elliptical motion was observed, with a lip trajectory remarkably similar to that of point d_2. In particular, at the extreme downstream limit of the lip trajectory, the vertical component of the motion was downwards (the negative y direction), acting to close the lip opening.

4.6.2 Motion of point d_1

Figure 4.29 shows the two-dimensional motion of the point d_1 over approximately three full cycles of oscillation. Again, the motion is also shown overlaid onto a single image frame in figure 4.30. This point was at the upstream end of the lip, closest to the mouth. It exhibited motion in the direction of both axes, though the trajectory was more complicated that that of point d_2. In contrast to point d_2, the vertical amplitude of motion was significantly larger than the horizontal amplitude, by a factor of approximately 2.5:1. The point appeared to move back and forth twice in the x direction during a single cycle of oscillation. The vertical motion was smoother, with no such doubling back.

4.6.3 Overall two-dimensional $x - y$ motion of the lip

Figures 4.28, 4.29 and 4.30 clearly show that the motion of the artificial lip was not uniform along its length during self-sustained oscillations. The downstream end of the lip followed a elliptical path, while the upstream end traced out a something close to a figure of eight motion. Direct examination of the video recording confirmed these results. It was possible to observe the water in the lip switch back and forth in the x direction during a single cycle, dragging the rear point along a similar path and creating an apparent 'wobble'.

4.6.4 Phasing of the lip motion

Figure 4.31 shows the oscillation of the individual x and y components of the dot motions over time. The amplitude of point d_2 in the x direction was almost five times that of point d_1. In contrast, the amplitude of point d_2 in the y direction was just two thirds that of point d_1.

The figure clearly demonstrates that the two points did not move in phase with each other. The relative phase difference between the two points was calculated at the fundamental lip oscillation frequency of approximately 110Hz, which was shared by all components of motion. For the horizontal oscillation, point d_2 lagged about 96^o, just over a quarter of a cycle, behind point d_1. For the vertical oscillation, point d_2 lagged about 115^o behind point d_1.

The curved surface of the artificial lips made precise measurement of the dot locations difficult. This was particularly the case when a number of different internal lip pressures were studied in succession, resulting in a variety of different rest positions for the dots. Thus the results presented here may only be taken as an opening clue to the true behaviour of the lips. If the points had been placed further apart, it is quite possible that even larger phase differences would have been observed.

Observation of the video recordings by eye certainly confirm the phase difference

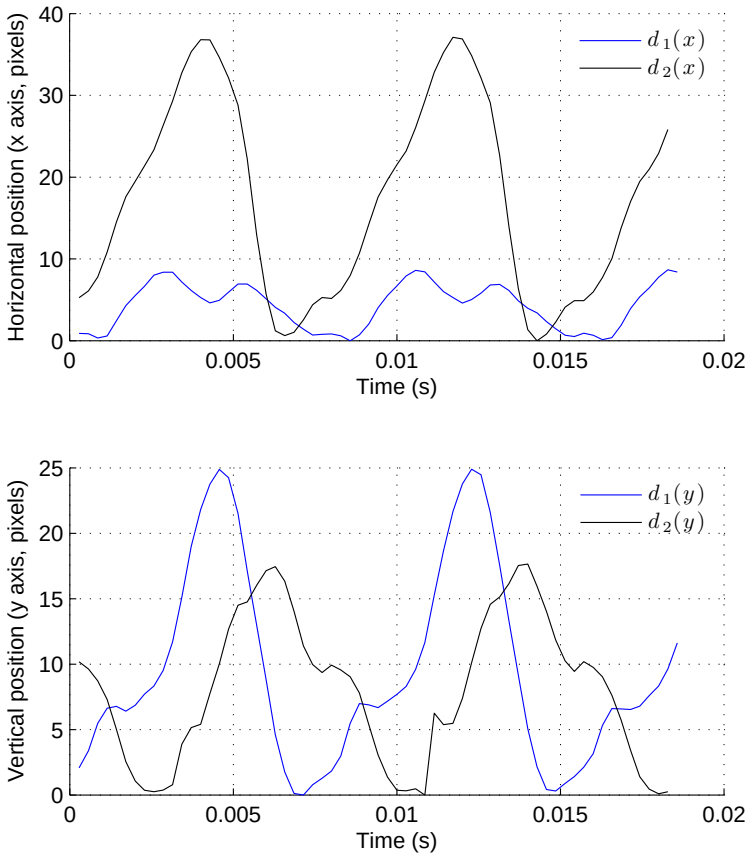

Figure 4.31: The horizontal (x axis in figure 4.30) and vertical components (y axis) of motion of points d_1 and d_2, plotted against time.

along the width of the lip. They further suggest that the region of the lip at the extreme downstream end would have a phase lag of considerably greater than the 115^o measured for point d_2. Further controlled experiments would be useful to investigate the extent of this phenomenon.

The vertical phase difference between the two points indicates that the artificial lips undergo something similar to the piston-like behaviour of the two-mass vocal fold models[Lous *et al.*, 1998]. This is in addition to the large amplitude motion along the horizontal x axis, particularly of the point d_2. This suggests that the lips do indeed follow both outward and inward striking trajectories during the same oscillation cycle.

4.6.5 An optimal lumped element model of the lip-reed

The strongly two dimensional motion of the two points suggests that a one-mass model of the lip-reed is insufficient. The simplest possible model that may allow an accurate simulation of this behaviour would be a two-mass model, with each mass free to move in both the x and y dimension. Such a model would thus have four degrees-of-freedom.

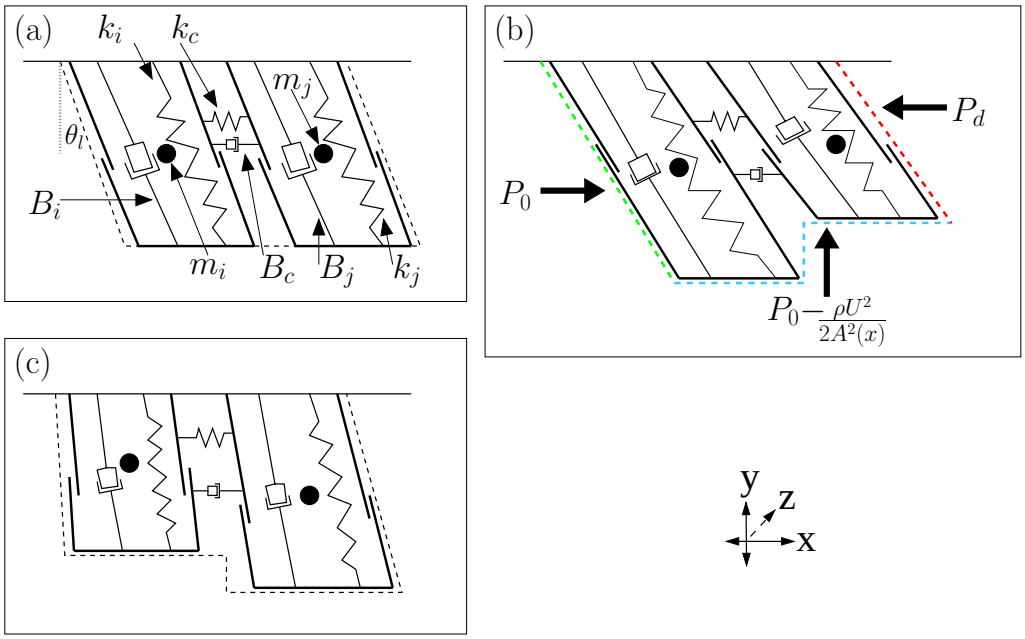

Figure 4.32: A modified two-mass model to represent the lip-reed, with three different phases of an oscillation period shown. (a) k_c and B_c are the coupling stiffness and damping, m_i is the upstream mass, connected to the valve walls with a spring of stiffness k_i and damping B_i, m_j is the downstream mass, with spring stiffness and damping k_j and B_j. (b) P_0 is the total upstream pressure, P_d is the total downstream pressure, $P_0 - \frac{\rho U^2}{2A^2(x)}$ is the lip channel 'Bernoulli' pressure. (c) Another possible orientation of the model at a later phase point.

Figure 4.32 presents one possible incarnation of a four degree-of-freedom lip-reed model. The model is based on a traditional two-mass vocal fold model[Lous *et al.*, 1998], modified to allow the masses to move in the x direction as well as the y direction. This would allow the masses to execute the swinging-type motion demonstrated by Adachi's one-mass, two degree-of-freedom model[Adachi and Sato, 1996], and by the experimental measurements presented in this work.

Part (a) shows the masses, springs and dampers required by the model. The two masses are coupled to each other with a spring of stiffness k_c and damping B_c. The masses drive a lip surface geometry (black dotted line) that is variable according to the their positions. The other quantities are as in the two-mass model shown in figure 2.19, with the exception of θ_l, the lip deflection angle which has not been included in the present model.

Each mass is able to execute motion in both the x and y directions. In the x direction the masses are coupled by a spring-damper, but are otherwise free to move independently of each other. In common with the two-mass vocal fold models, the masses are both free to execute independent motion in the vertical y direction, subject

to the vertical component of the coupling stiffness.

Also in common with the two-mass models, a total upstream pressure P_0 acts on the upstream face of the valve, shown as a green dotted line in part (b). A 'Bernoulli force' acts on the lip faces within the lip channel (blue line). Calculation of this pressure may include account of instationary terms. The total downstream pressure in the mouthpiece acts on the downstream lip face (red line).

It is important to raise the question of whether a four degree-of-freedom model such as that presented in figure 4.32 is truly required to capture the 'essence' of the lip-reed operation. It certainly seems necessary in order to replicate the physical motions observed with both real and artificial lips. However, the remarkable ability of the two degree-of-freedom model to simulate complex features of the lip-reed, such as the ability to 'lip' notes above and below the air column resonance, suggests that the most fundamental behaviour may be relatively simple. Adachi's model seems to be particularly neat, comprised of a single mass free to move in the x and y directions, and able to act as both an outward and inward striking reed.

Lumped element models are, by their nature, great simplifications of reality. It is possible that the more complex motions encountered in this report represent second order effects that are not key to the fundamental behaviour of the lips, and their interaction with the acoustical resonator. The extensive two dimensional motion of all points along the lip surface may appear crucial at face value, but it is possible that this motion is of relatively little importance for the basic function of the lip-reed. In particular, Elliot and Bowsher[Elliot and Bowsher, 1982] pointed out that the resistance of the lips to the flow becomes small once they are sufficiently open. Any mechanical motion, however complex and two-dimensional, would then have little or no effect on the basic function of the valve-resonator system.

Hirschberg[Hirschberg, 1992] has pointed out that in the case of phonation, the effect of the vocal folds as a volume source should be considered at most a second order effect for most of the oscillation cycle. This would imply that in the case of the lip-reed the complex motion observed during large parts of the cycle may produce little fluid dynamical effect. However, as the valve separation becomes small, and the Reynolds number rises, Deverge *et al*[Deverge *et al.*, 2003] have demonstrated that the subtleties of the valve wall motion may become much more important in determining the fluid mechanical behaviour. This suggets that truly realistic musical valve simulations should actually include more complex models of the mechanical structure, such as the four degree-of-freedom model.

The field of vocal fold modeling has recently seen a number of more complicated mechanical models, such as the sixteen mass model of Kob[Kob, 2002], or the finite element model of de Vries *et al*[de Vries *et al.*, 2003]. However, these models pose a difficult issue in terms of the increased parameter space. Simulations may provide fascinating results, but the many more parameters required seem to reduce the

objectivity of the whole process. All the while the simple two-mass, two degree-of-freedom models are capable of simulating a huge spectrum of behaviours, and seem to capture something close to the essence of the reality.

The outstanding issue from the results presented here is thus the level of simplification required to reliably simulate the reality of musical valve operation. To answer this question, a full implementation of the four degree-of-freedom model would be required in conjunction with further measurements of the artificial and human lip motion. This would allow an investigation into whether the features reported here are of fundamental importance, or whether they represent the interesting details. The main difficulty with this approach would be in assigning parameters to the various mechanical quantities. It would also be important to include a more sophisticated fluid mechanical description than the grossly simplified, fixed point flow separation model used for the one-mass models.

In the longer term, it does seems inevitable that truly realistic mechanical models will require a distributed system of many masses and non-linear restoring springs, such as suggested by Elliot and Bowsher[Elliot and Bowsher, 1982]. The finite element method is one way of dealing with such an approach. However, the question of whether such an approach can prove to be a greater aid in understanding the fundamental physics remains to be answered.

4.7 Conclusions

4.7.1 Mechanical response properties of human lips

Mechanical response measurements were performed on a small number of experienced trombone players. At least two important mechanical resonances were observed in several different embouchures. The lower of resonance consistently displayed an outward striking character, while the upper resonance showed an inward striking character. The played frequency of the note consistently lay between the two resonances. This behaviour was precisely the same as that seen in *in vitro* replicas of the lip-reed[Cullen *et al.*, 2000; Richards, 2003].

It was found that the quality factors of the human lip resonances were considerably lower than those seen in artificial lips. Typical artificial lip resonances were measured between 10 and 16, whereas values of between 1 and 2.5 were encountered in most of the human lip measurements. A small number of peaks showed slightly higher Q-values of around 5. These results seem to tie in well with a recent paper by Gazengel *et al*[Gazengel *et al.*, 2007], where the mechanical impedance of a human lip was found to lie between 1.2 and 1.5.

The Q-values obtained directly from human lip resonances may help to inform the parameter choice in computational models of the lip-reed. Up to now, computational

models have relied on parameters derived from *in vitro* replicas. The large discrepancy between the human and artificial lip Q-values suggests that current models of the lip-reed should really be modified to reflect the highly damped lip resonances encountered in the study.

4.7.2 Transverse mechanical response measurements of artificial lips

The mechanical response properties of the newly developed *in vitro* lip-reed replica were investigated using the transmission method, the frontal video method and the transverse video method. The objective was to examine the nature of the coupling between the two primary mechanical resonances observed in experimental measurement of the lip-reed. It has been suggested by Richards[Richards, 2003] that two mechanical degrees-of-freedom may provide the best explanation for the ability of a brass player to play a note on either side of its fundamental acoustic resonance.

Mechanical response measurements were performed on two embouchures. A traditional frontal transmission method measurement was first made, in order to provide a reference benchmark with which to characterise the embouchure. The transverse video method was then used to provide two further mechanical response measurements, one derived from the horizontal x motion, and the other from the vertical y motion.

It was found that the lower, outward striking resonance recorded in the transmission method measurement was also recorded very cleanly by the transverse horizontal x measurement. It appeared that the vertical y axis transverse measurement was also sensitive to the resonance. An explanation for this behaviour was provided, which showed how the excitation of a horizontally aligned mechanical resonance always gives rise to a quantity of vertical motion. This was the mechanism by which the outward striking resonance, which was strongly associated with motion along the x axis, could be measured by the both the transmission method and the vertical y component of the transverse video method. It was thus suggested that the lower, outward striking resonance is mechanically coupled to the upper, inward striking resonance.

It is possible that this lower resonance was in fact due to a rotational motion, and not a purely horizontal motion, forcibly coupled to the vertical axis. However, the raw time domain plots of the lip trajectory during the course of the excitation sweep showed a strongly horizontal motion, the amplitude of which was order of magnitude larger than the vertical motion.

The upper resonance showed an inward striking character. This resonance was detected strongly by the transmission method and the vertical y component of the transverse video method. It did not appear at all, however, in the horizontal x measurement of the method. This behaviour was accounted for by considering the effect of a purely vertical distortion of the lip, caused by the excitation of a vertical mechanical resonance. The anchor point of the lip meant that in the absence of a horizontal forcing,

there was no mechanism by which horizontal motion could be imparted. This meant that a purely vertical lip motion could not be recorded by the horizontal component of the video method. The result also suggested that the inward striking resonance was a strongly vertical one, associated with an oscillation along the y axis.

4.7.3 Transverse oscillations of the artificial lips

Investigation of the two-dimensional motion of an artificial lip during full self-sustained oscillations revealed that different parts of the lip followed quite different trajectories over the course of an oscillation cycle. Two points along the lip were studied, both positioned on the centreline of the lip opening, and at a separation of approximately 6mm in the streamwise x direction. Both points executed significant motion in both the x and y directions.

It was perhaps unsurprising to note that a four degree of freedom model would be required in order to simulate the behaviour of two points on the lip that were free to move in two dimensions. Indeed, an obvious question could be raised about the possibility of studying four points, or six points or perhaps even a mesh of points. With each new point, given the strongly two-dimensional motion observed in the present work, it could be hypothesised that another two degrees-of-freedom would suddenly be demanded as crucial to capture the full mechanical behaviour. The possibility of including points along the out-of-plane z axis would further complicate matters. The obvious end-point of this line of thought would be that only a full and highly detailed finite element type measurement, whereby the whole lip surface was mapped throughout an oscillation cycle, would be sufficient to fully describe the lip motion.

Clearly, such an approach would be a long way from the noble efforts of lumped element modelling, which have sought to simplify the lips as much as possible in order to extract just the most *essential* mechanical behaviour. The remarkable versatility of the two-mass model, both for simulating the lip-reed and the human vocal folds, is testament to the success of this approach. So the question remains, just how complicated a model is required in order to realistically replicate, to a suitable degree of accuracy, the overall mechanical behaviour of the lips during brass playing?

To answer the question posed, it would be necessary to track a larger number of points along the lip surface, in order to determine just how localised are the two-dimensional motions of the two points tracked in this work. By studying a much larger number of points, it is possible that some kind of convergence regime could be determined, such that the overall lip motion could be split up into a small number regions that are suitably 'alike' so as to be lumped together. There could be, for example, four key regions, or even fewer. This is, of course, the essential idea behind the lumped element approach. However, by performing such a measurement it would be possible to determine to a much deeper level the most suitable model.

The important point missing from the preceding discussion is that of a *functional* comparison of the computational models with the *in vivo* lip-reed. Despite the obviously complex motion of both the *in vivo* and *in vitro* lip-reeds, it has been demonstrated time and time again that remarkably simple models seem capable of fulfilling a wide gamut of the known *playing* behaviours. Richards[Richards, 2003] provided an example of this. Using just a two-mass, two degree-of-freedom model it was possible to replicate one of the most dynamic and creative aspects of brass playing, that of being able to 'bend' a note both above and below the fundamental acoustical resonance of the bore.

It is possible that the formulation of more complex models, such as the four degree-of-freeom model of figure 4.32 could provide an important advantage over the simpler models under extreme playing conditions, such as the so-called 'brassy' regime. The subtle behaviour of the lips when the open area is very small is likely to be important in determining the shape of the resulting flow pulse, as the effects of a secondary source of volume flow due to the lip motion become important. An investigation into this issue would form an interesting avenue of future work.

The most important conclusion from the study of the two-dimensional motion is that at least one extra degree of freedom should be introduced to the two-mass lip-reed models in order to allow simulation of the outward-swinging behaviour. This would lead to a model that incorporates the ideas of Adachi and Sato's[Adachi and Sato, 1996] one-mass, two degree-of-freedom model, and the traditional two-mass vocal fold models. Such a model would allow for both the outward swinging motion, and the piston-like two-mass motion that have been experimentally observed.

Part III

Experimental Fluid Mechanical Investigations into the Influence of the Ventricular Bands on Phonation

Chapter 5

Particle Image Velocimetry (PIV)

"*If people don't occasionally walk away from you shaking their heads, you're doing something wrong.*" - John Gierach

5.1 Introduction

Particle image velocimetry (PIV) is an optical tool for the quantitative measurement of fluid flows[Raffel *et al.*, 1998; Sveen and Cowen, 2004; Grant, 1997; Various, 2004]. It presents a quantitative, non-obtrusive method, based on the imaging of small, neutrally buoyant tracer particles distributed throughout the flow. It differs from the more qualitative techniques, such as schlieren flow visualisation[Davis, 1971], in that a full representation of the instantaneous velocity field of the flow is obtained. This allows the quantified study of fine-structures within the fluid flow field, such as vortices, as well as larger scale features such as the volume flow. Some quantitative details can be obtained from schlieren-based images with suitable image processing[Vergez *et al.*, 2005], though the technique's strength really lies in its flow visualisation capabilities.

PIV has several advantages over other techniques for quantified fluid velocity measurement. Hot-wire anemometry[Brun, 1995] allows for precise instantaneous velocity measurement, but only at a single point in a flow field. This technique also requires insertion of a measurement probe into the flow, which can disturb the fluid. Laser doppler vibrometry[Adrian, 1993; Cullen *et al.*, 1999] (also known as laser doppler anemometry, or LDA) also allows for continuous, localised measurement of the fluid velocity. Being an optical technique, it also has minimal impact on the flow under study. However, in order to obtain enough data to represent an entire field, multiple measurements must be made in order to build up a full-field representation of the flow.

Particle tracking techniques related to PIV, such as particle tracking velocimetry[Agüí and Jiménez, 1987] and laser speckle velocimetry[Simpkins and Dudderar, 1978;

Meynart *et al.*, 1987], represent interesting alternatives. However, they do not directly provide the instantaneous, full-field velocity maps obtained as standard from PIV analysis.

5.2 Basic principles of PIV

The basic premise of PIV is rather simple, for it is quite similar to the everyday use of a photographic flash designed to freeze the motion of a sprinting olympic athlete. The fluid flow field under study is first seeded with small, neutrally buoyant tracer particles. Common examples include smoke particles and industrial fog, as used in discotheques. The flow is illuminated with a thin sheet of light, and a camera oriented at right angles to the light sheet. The camera is triggered to capture two separate image frames of the illuminated flow field, in sync with two short pulses of the light sheet at times t and $t + \Delta t$.

The light sheet is typically sourced from a pulsed laser. Each image contains a dark background, with the small seeding particles brightly illuminated in the foreground by the light sheet pulses. By correlating the distribution of the seeding particles between the two images, it is possible to determine their mean direction of travel, $\Delta \vec{x_{pix}}$, in the pixel space of the bitmap image. This 'pixel distance' can be converted to a real world distance, $\Delta \vec{x}$, by using a calibration image containing a known physical distance to obtain a pixel-to-metre magnification ratio. Together with the image separation time, Δt, an estimation of the velocity can then be made: $\vec{v} = \frac{\Delta \vec{x}}{\Delta t}$.

The modern PIV technique makes use of a specially designed CCD digital camera, capable of capturing two individual image frames separated by a short time interval. This allows each image to be directly read into a computer as a bitmap file that is easily readable by a wide range of processing applications. The early PIV technique used a traditional negative film developed in wet chemistry, a time consuming process that is no longer used. The most common application of PIV remains the measurement of quasi two-dimensional flow fields. However, extension to three spatial dimensions is also possible using stereoscopic PIV[Various, 2004; Schlicke, 2001].

The correlation process is carried out using sub-regions of the image frame, as shown in figure 5.1. Each sub-region is called an *interrogation window*. A typical image frame is 1024×1280 pixels, and a typical interrogation window is 32×32 pixels. The mean displacement of the imaged tracer particles in each interrogation window is found using a cross-correlation algorithm. This yields a single vector for each interrogation window that describes the average motion of the particles within that window. The process is repeated for each interrogation window in the image frame, resulting in a full, instantaneous velocity map of the imaged flow field.

The cross-correlation algorithm implicitly assumes a homogeneous movement of the particles within an interrogation area. This means that in order to ensure sufficient

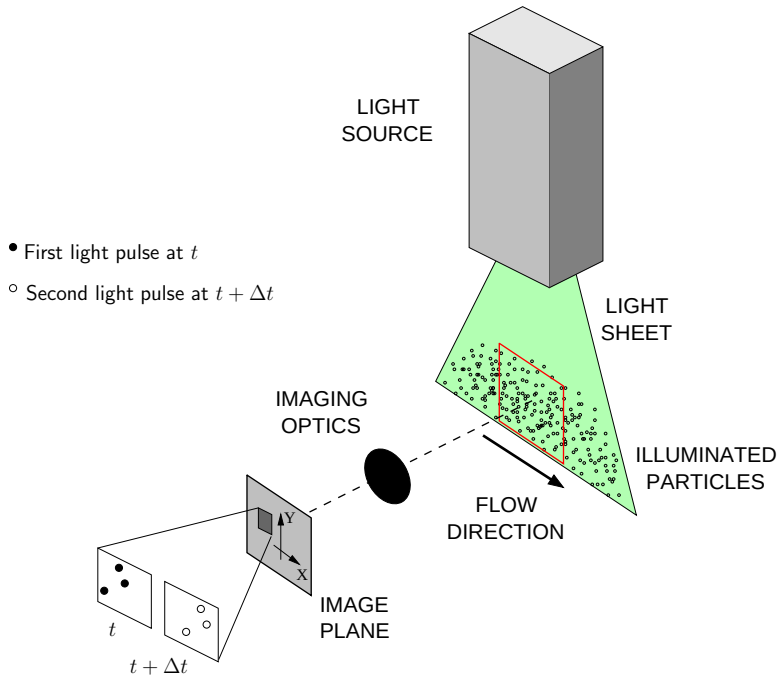

Figure 5.1: A schematic diagram showing the basic experimental process of a PIV measurement. The *image plane* represents the light gathering CCD chip in the digital camera (taken from [Skulina, 2005]).

spatial resolution of small-scale flow features the size of the interrogation areas must be matched to the particular flow situation encountered. It is also important that the bulk of the particles encountered in an interrogation window at time t remain in the same interrogation window at time $t + \Delta t$. Excessive transport of particles from one interrogation window to an adjacent window, typically caused by high flow speeds, reduces the signal-to-noise ratio of the calculation. This places an upper limit on the measurable fluid velocities for a particular size of interrogation window. This effect is also governed by the magnification of the camera optics, and will be further explored in section 5.4.

5.3 Image acquisition

Good quality PIV vector maps can only be obtained from raw images of suitably high quality. Acquisition of quality raw images is thus the central objective of any PIV experimental setup. There are many factors that can influence the image quality. These include the optical alignment of the camera to the light sheet, the thickness of the light sheet, the level of out-of-plane fluid transport (i.e. the two-dimensionality of the flow), the choice of the seeding particles and the ability of the individual light sheet pulses to freeze their motion. For a given fluid flow speed, the inter-image time delay,

Δt, is also of great importance in determining the quality of the cross-correlation.

5.3.1 Illumination of the flow field

PIV relies on freezing and capturing the motion of a fluid field at two instantaneous moments, separated by a short time interval. In the conventional two-dimensional application of PIV presented in this work, the fluid is 'frozen' by the flash of a thin light sheet. The optical source of the light sheet depends on the specific application of the technique. The source must be able to provide a short enough burst of light to prevent blurring of the individual images. It must also provide sufficient light, during each brief flash, that the seeding particles are sufficiently illuminated to enable the camera to detect their presence. Finally, the light source must be able to deliver two pulses of light with a sufficiently small temporal separation that the bulk of the seeding particles in an individual interrogation window during the first pulse, are still there during the second pulse. Thus the light source must provide short, bright pulses of light with small pulse interval times.

The classic light sources for PIV are double-cavity lasers, such as Nd-YAG double-pulsed lasers, and single-cavity pulsed lasers. The latter type was used in this thesis. The model was an Oxford Lasers LS20-50, which is a class IV copper vapour, single cavity pulsed laser. Continuous wave lasers, in combination with mechanical shutters to control the pulse windows, may be used for low fluid velocity measurements. However, for the subsonic jet flows and acoustical fields encountered in this work, the faster class of pulsed lasers was required. The copper vapour laser allowed accurate measurement of flow speeds up to approximately 20ms^{-1}, depending on the optical magnification and the size of the interrogation window. This issue is addressed in more detail in section 5.4.2, and again in section 7.2.3. The laser delivered an average power of 20W, with pulse widths of approximately 25ns, and at a maximum repetition rate of 50kHz. This meant that the shortest possible pulse interval time was 20μs, with approximately 0.4mJ of energy delivered per pulse.

A sheet of light was created from the raw laser pulses by using an Oxford Lasers Fibresheet light sheet generator, as shown in figure 5.2. This optical device took the output of the laser, delivered through a fibre optic cable, and spread out the concentrated beam of light into a thin sheet. The Fibresheet consisted of a pair of parallel mirrors, one of which was partially reflecting, and the other fully reflecting. The light from the fibre optic cable passed into the Fibresheet optics at a 45^o angle and onto the partially reflecting mirror. It then bounced down between the mirrors, creating a sheet of light. The light sheet was controlled with a pair of cylindrical lenses. These could be adjusted so as to place the region of optimum thickness at varying distances from the end of the light sheet. The final usable output from the Fibresheet, where the light sheet was between 1mm and 2mm in thickness, was typically 50mm by 50mm.

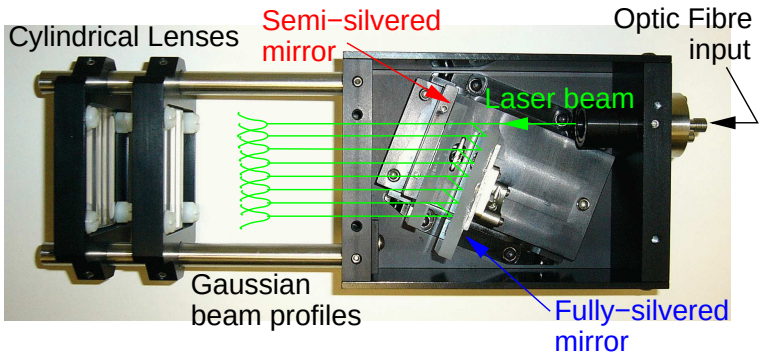

Figure 5.2: The Oxford Lasers Fibresheet used to generate the light sheet. Taken from [Skulina, 2005].

5.3.2 Seeding the flow

To record the fluid motion it was necessary to introduce light-scattering seeding particles to the flow. These particles reflected some of the light from the laser pulses into the camera lens and onto the camera's CCD chip. It was important that the particles reflected enough light to be detectable in the short exposure window of a single image acquisition. It was also important that the particles could be trusted to accurately follow the fluid flow.

Particles denser than the surrounding air incur an inertial lag, resulting in a delayed response to any fluid acceleration. This led to a compromise in the size of the particles: large, heavy particles reflected a lot of light, but their increased inertia meant that they did not follow the flow with sufficient rapidity. It was inevitable that some density difference would exist between the fluid in this study, which was air, and any seedant. It was important to quantify and minimise the effect.

The effect of inertial lag has been quantified for the case of spherical particles suspended in an acoustic flow by Vignola *et al*[Vignola *et al.*, 1992] and Melling[Melling, 1997]. At an acoustic frequency f_{ac} the relationship between the acoustic velocity amplitude of the suspended particle, u_p, and the surrounding fluid, u_{ac}, may be described by the equation

$$u_{ac} = u_p \sqrt{1 + \frac{2\pi f_{ac} d_p^2 \rho_p}{18\mu}} \tag{5.1}$$

where d_p is the diameter of the suspended particle, ρ_p is the density of the suspended particle and μ is the dynamic viscosity of the fluid.

The phase lag between the seeding particles and the surrounding fluid may be described by the equation

$$\begin{aligned} \Delta\angle u_{ac-p} &= \angle u_{ac} - \angle u_p \\ &= \tan^{-1}\left(\frac{2\pi f_{ac} d_p^2 \rho_p}{18\mu}\right). \end{aligned} \tag{5.2}$$

The seeding particles were supplied by a Dantec SAFEX 2004 fog generator. This device turned a liquid solution, in this case SAFEX Normal fog fluid, into a fine mist. The particles were made from a mixture of water together with a small quantity of alcohol. The density ρ_p was thus assumed to be that of water, 1000kgm^{-3}. The manufacturer-quoted particle size was approximately 1μm[Dantec, 1998]. The typical valve oscillation frequencies were of the order of 100Hz, suggesting a primary acoustical propagation frequency of 100Hz. These quantities revealed a difference in the velocity magnitudes of approximately 0.10%, and a velocity phase difference of 0.11°. These errors were considerably smaller than, for example, the measurement error derived from calculation of the pixel-to-metre conversion factor, and were ignored in the analysis. It was thus assumed that the seeding particles followed the fluid flow very closely.

Light scattering properties, density and distribution of the seeding particles

Previous PIV experiments have used the seeding particles described above[Skulina, 2005], and they have proved to be a good compromise between providing enough surface area to reflect the laser light, and being small enough to follow the flow. Other seeding solutions were available, mostly providing larger particles to reflect more light. However, the extremely high power delivery of the copper vapour laser, together with the relatively fast fluid flow speeds, meant that the solution described provided an excellent source of seedant.

The addition of any impurities to a fluid flow changes the overall density and buoyancy. It was thus of crucial importance that a sufficiently small quantity of seedant was added to the air stream through the *in vitro* model to minimise this effect. This was also important because a excessively high seeding density reduces the ability of the cross-correlation algorithm to detect the motion of individual particles. The application of PIV to such a model presented a particular challenge in this regard because a continual process of seedant addition and loss took place during the course of a measurement. As seedant was added to the flow upstream of the valve, it was lost at the flow's exit from the downstream end of the valve. This was in contrast to the application of PIV to purely acoustical systems, such as in the work of Rockliff[Rockliff, 2002] and Skulina[Skulina *et al.*, 2003; Skulina, 2005], or to water waves, such as in Schlicke[Schlicke, 2001]. In these examples the seedant density could be carefully adjusted before the commencement of an experiment.

In any application of PIV it is important that there is an even distribution of seeding

particles. This is to ensure that an even signal-to-noise ratio can be obtained over the whole field of measurement. Once again this presented a particular challenge for the application to *in vitro* musical valves. The separation of the jet from the valve walls greatly reduced the concentration of seeding particles in the regions outside the jet core and shear layers, as the bulk of the seeding was entrained with the emerging jet. Details of the practical implementation of the seeding delivery are described in detail in section 6.4.3.

5.3.3 Image capture and system synchronisation

Most modern implementations of PIV make use of specialised double-exposure digital cameras. Such cameras are capable of capturing two separate images with an extremely low inter-frame time. By synchronising the camera exposure windows with pulsed flashes of the laser it is possible to obtain image pairs ready for immediate cross-correlation processing. This is in contrast to the earliest PIV methods that used double exposures made onto a single film negative. The exposed negatives first required appropriate chemical development, followed by an autocorrelation analysis[Grant, 1997].

The camera used in this study was a PCO Sensicam Double Shutter model. This camera had an image resolution of 1280×1024 pixels. It had two image capture modes relevant for use with PIV, long mode and short mode, which determined the inter-frame capture delay Δt_{cam} when the camera CCD was switched off. For the long mode function Δt_{cam} was 1μs, while for the short mode Δt_{cam} was 20ns. As the minimum inter-pulse time, Δt_{IP} was just 20μs, the long mode function was used. The short mode was only useful in combination with a double-pulsed laser where the inter-pulse time could be set below 1μs.

The minimum possible inter-image-pair acquisition time, Δt_{AQ}, was an uncontrollable variable which was determined by the read-out time of the camera. This was the time required for the current image pair, stored temporarily in the camera's internal memory buffer, to be downloaded to the controlling computer. The read-out time was determined by a number of factors, including the quantity and speed of the computer's memory, and varied between approximately 200ms and 350ms. As will be demonstrated in chapter 6, it was important to fix the inter-image-pair time for the purposes of the experimental setup. This was done using the external triggering system that controlled the overall PIV acquisition system. The camera and laser were forced to acquire image pairs at intervals of 0.5s. Thus to acquire a typical set of 20 image pairs required little more than 10s. Once an experimental run was completed the raw image files were converted to 8-bit bitmap files, readable by a wide range of cross-correlation software applications.

A more detailed description of the image capture and system synchronisation

process is presented in section 6.5.

5.4 Image analysis and the cross-correlation algorithm

The full-field advantage of PIV arises because each image pair is discretised into a large number of individual regions known as interrogation areas. Each interrogation area is typically 32×32 pixels, which for a typical image size of 1280×1024 pixels means that the fluid velocity is sampled at more than 1000 locations within the flow field. A velocity vector is obtained for each interrogation area by the application of a cross-correlation analysis between the two constituent images in an image pair.

5.4.1 Cross-correlation analysis

The cross-correlation function

Cross-correlation provides a means for measuring the similarity of two functions. In the analysis of PIV image pairs, it is used to calculate the optimum spatial displacement of the second image, such that there is a maximal overlap of common pixels with the first image. The underlying process is statistical pattern matching. The analysis is performed separately for each interrogation area, which leads to a full-field set of fluid displacements. Division of each displacement by the inter-frame delay time Δt_{IP} provides a velocity representation of the flow.

Consider an interrogation area measuring $M \times N$ pixels. Each pixel in the interrogation area may be described by a coordinate (m, n), where m and n run from $[1 : M]$ and $[1 : N]$ respectively. The pixel intensities from the first image can be defined by $I_1(m, n)$, and those from the second image by $I_2(m, n)$. The cross-correlation may thus be written as[Keane and Adrian, 1992; Sveen, 2004]

$$R_{I_1 \cdot I_2}(i, j) = \sum_{m=1}^{m=M} \sum_{n=1}^{n=N} I_1(m, n) \cdot I_2(m + i, n + j) \tag{5.3}$$

where i and j represent pixel shifts between the two interrogation areas.

$R_{I_1 \cdot I_2}(i, j)$ is obtained by shifting the second interrogation area by i pixels along the M axis, and j pixels along the N axis, and calculating the shared pixels. This is performed for all values of i and j such that there is at least one overlapping pixel between the two interrogation areas. i and j thus run from $-(M - 1)$ to $(M - 1)$, and $-(N - 1)$ to $(N - 1)$ respectively. The two interrogation areas completely overlap when $i = 0$ and $j = 0$. $R_{I_1 \cdot I_2}(i, j)$ has a large value when there are many shared pixels. The optimum shift of the second interrogation area, such that there are a maximum number of shared pixels, produces a pronounced peak in the correlation function. The correlation function may be represented graphically as a three-dimensional correlation plane. An example of the cross-correlation between two interrogation areas, and the

resulting correlation plane, is shown in figure 5.3. The main peak in the correlation plane may be trivially located at (-1,3), which provides a first order estimate for the optimum displacement vector. An estimate of the mean fluid velocity between the interrogation areas is thus $(\frac{1}{\Delta t_{IP}}, \frac{-3}{\Delta t_{IP}})$. It is possible to calculate this velocity to sub-pixel accuracy using more sophisticated peak finding algorithms, described below. However, no further enhancements can overcome the intrinsic assumption that the fluid velocity within the interrogation area is uniform.

Equation 5.3 describes a convolution in the spatial domain. The convolution theorem states that such a convolution can be evaluated in the Fourier domain using a multiplication of the Fourier transforms of I_1 and I_2. In PIV this relationship is known as the Wiener-Kinchin theorem[Raffel *et al.*, 1998], and may be written mathematically as

$$\tilde{R} = \tilde{I_1} \times \tilde{I_2} \Longrightarrow R = \mathcal{F}^{-1}\{\tilde{R}\} \tag{5.4}$$

where $\tilde{I_1}$ is the Fourier transform of I_1, $\times$ indicates a multiplication and $\mathcal{F}$ indicates a Fourier transform.

It is common practice to calculate the cross-correlation using the Fourier domain representation. The use of fast Fourier transforms allows for a significant computational advantage over a direct convolution-based evaluation.

Peak detection

The preceding commentary, together with the example of a cross-correlation evaluation in figure 5.3, provide an *ad hoc* interpretation of the displacement estimation. In most implementations of PIV, including that in this work, the displacement vector is calculated by fitting a Gaussian curve to the largest correlation peak. The curve takes into account the two nearest neighbours along both the M and N axes. This allows an estimate of the optimum displacement to be made to an accuracy of 0.1 pixels[Raffel *et al.*, 1998]. This process also allows a calculation to be made of the vector's signal-to-noise ratio, which can be used to assist in the filtration of spurious data (see section 5.4.4).

Windowing

It is possible to increase the number of vectors in the velocity field by oversampling the data, a process called windowing. Rather than dividing the image frame into adjacent blocks of 32×32 pixels, the $p^{th} + 1$ interrogation area is chosen to overlap the p^{th} by a fixed amount, typically 50% of the interrogation window width. The windowing can be performed both for adjacent interrogation windows along a horizontal line, working along the image from left to right for example, and for consecutive lines of interrogation

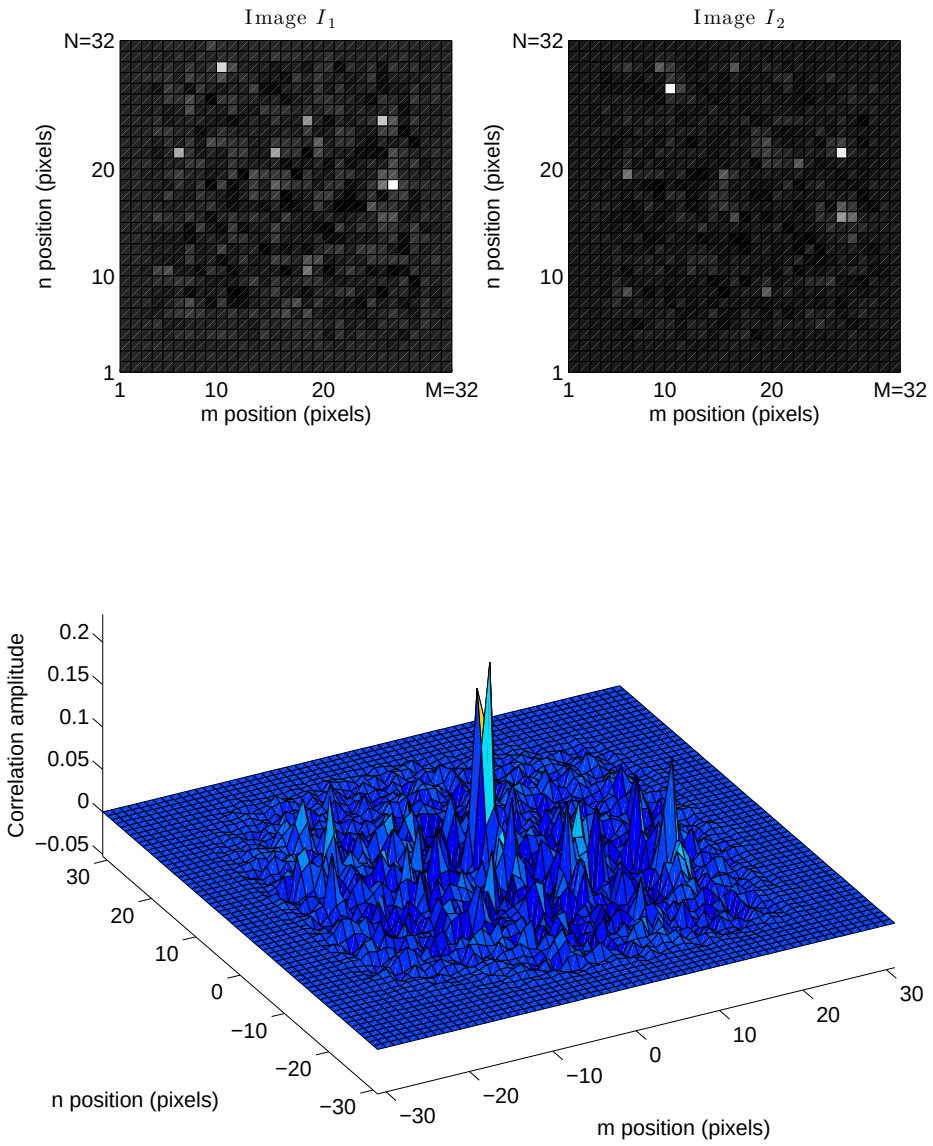

Figure 5.3: An example of a cross-correlation calculation for a single interrogation area. At top are the two raw interrogation areas, with the lighter coloured pixels marking the position of seeding particles. At bottom is the correlation plane representation of the cross-correlation function between the two interrogation areas.

windows, working from top to bottom. Windowing is a standard procedure, widespread in many implementations of PIV[Various, 2004]. In the work presented here the overlap was set to 75%.

The software application used in this work

The cross-correlation analysis in this work was performed in Matlab using the open source software package MatPIV[Sveen, 2004]. This package was developed at Oxford University by J. Sveen[Sveen and Cowen, 2004], and is the most widely used and accredited open source PIV analysis program available. It allowed a wide range of user customisable control, such as the interrogation window size, the window overlap and data filtering, as well as a choice of cross-correlation algorithms. The standard algorithm used in the program is the one presented above.

A short program was written to batch process the multiple image pairs acquired for each PIV measurement run. This program loaded each image pair from the measurement run in order, calling the standard MatPIV program files to do the actual cross-correlation processing.

5.4.2 Measurable velocity range and the Nyquist theorem

Cross-correlation analysis is able to deduce a mean velocity vector for an interrogation area because there is a movement of the seeding particles between the two image acquisitions. It is important, however, that a sufficient percentage of the seeding particles, present in the interrogation area when the first image is acquired, remain within the same interrogation window during the second exposure. If too many seeding particles move out of the interrogation area between image acquisitions the signal-to-noise ratio of the correlation plane will be degraded[Keane and Adrian, 1992; Raffel *et al.*, 1998].

The Nyquist sampling theorem limits the the maximum spatial displacement of a seeding particle to 50% of the interrogation window width. To ensure that the minimum inter-frame acquisition time Δt_{IP} was sufficiently small to satisfy the Nyquist condition, a consideration must be made of how the seeding particle came to be imaged by the camera.

During an image acquisition the seeding particles are briefly illuminated by the laser light sheet. This causes light to be scattered from the particles, some of which is focussed by the camera lens onto the camera's CCD chip. The CCD chip is made up of an array of small light gathering sites known as pixels. The PCO camera used in this work used a CCD chip with an array of 1280×1024 pixels. As a result of the imaging process, each seeding particle scatters light onto a small number of pixels, causing a bright spot in the image.

Interrogation window width (pixels)	**Maximum velocity** v_{max} (ms^{-2})	**Optimum velocity** v_{opt} (ms^{-2})
16×16	8	5
32×32	16	10
64×64	31	21

Table 5.1: A table of theoretical maximum measurable velocities, calculated as a function of the interrogation window width. The optimum fluid velocity has also been calculated

A larger object, such as one of the ventricular bands, may also scatter light. If the length of such an object is L_{obj} in the real world, the corresponding length, measured in pixels, is N_{pix}. The ratio of L_{obj} to N_{pix}, together with the physical dimensions of the CCD, provides a measure of the magnification of the imaging system. For simplicity, L_{obj} may be taken as the width of the field of view, and N_{pix} as the number of pixels along the horizontal CCD length. The field of view for the PIV measurements in this work was typically 2×2cm, imaged along 1280 pixels on the CCD. The width of each interrogation area may be termed I_{pix}, measured in pixels, with typical values of between 16 and 64 pixels. The physical width of the interrogation area, measured in metres, may thus be calculated as

$$W_{int} = \frac{L_{obj} I_{pix}}{N_{pix}}. \tag{5.5}$$

The maximum allowable particle displacement between image acquisitions, Δs_{max}, is thus $\frac{W_{int}}{2}$. It has been pointed out by Keane and Adrian[Keane and Adrian, 1992] that in real-world applications a maximum displacement of approximately 30% of the interrogation window width is a more realistic figure, which ensures a good signal-to-noise ratio ($\Delta s_{max} \approx \frac{W_{int}}{3}$).

Under the maximum theoretical Nyquist limit, and for a field of view of approximately 2.5×2cm, the maximum measurable particle velocity v_{max} may be calculated as a function of the interrogation window size as follows

$$v_{max} = \frac{W_{int}}{2\Delta t_{IP}}. \tag{5.6}$$

Table 5.1 presents several calculations of v_{max}. The minimum inter-frame acquisition time Δt_{IP} was set to 20μs, which was the minimum time possible between light pulses at a pulse repetition rate of 50kHz.

Choice of the minimum inter-frame delay time

It should be noted that the preceding calculation of v_{max} was tailored to the upper limit of measurable fluid velocities, as the minimum possible inter-frame acquisition

time was used. Such an approach means that the best signal-to-noise ratio from a velocity field would be obtained from interrogation areas where the mean fluid velocity was approximately two-thirds of the calculated values of v_{max}[Keane and Adrian, 1992]. Values of the optimum velocity v_{opt} have been included in table 5.1.

The best possible signal-to-noise ratio for a PIV measurement may be expected to occur for fluid velocities close to v_{opt}. A largely uniform fluid flow field, such potential flow, moving at close to v_{opt} may thus be measured with excellent accuracy. Flows that involve strong velocity gradients present more of a challenge. It is not possible to tailor the inter-frame acquisition time to optimally record an excessively large range of fluid velocities. If it is chosen to maximise the SNR of the upper range of velocities, then it is possible that the lower range of velocities may disappear into the noise floor. On the other hand, if it is chosen to maximise the SNR of the lower range of velocities, it is likely that the higher velocities will cause aliasing problems associated with the Nyquist limit outlined above.

Ultimately, the maximum measurable fluid velocity must be determined from a compromise between the size of the interrogation windows and the size of the field of view. A large field of view, for a given size of interrogation window, provides a high upper velocity limit, but with a low spatial resolution. Similarly, a small field of view, for the same size of interrogation window, provides a much lower velocity limit, with an increased spatial resolution of the flow. Some of these quantities, such as the field of view, are fixed by the experimental requirements. This leaves the interrogation window size and the inter-frame acquisition time as the key control parameters.

In the present application a wide range of fluid velocities were to be expected, given the nature of the pulsatile jet flow expected to form at the exit from the valve. The choice of the inter-frame acquisition time was thus of crucial importance to the potential quality of the PIV measurements. Details of this may be found in section 7.2.3.

5.4.3 Evaluation of the vorticity field

Vorticity provides a measure of the rotationality of a flow. A purely potential flow field has a vorticity field that is everywhere zero. A turbulent flow has a vorticity field with a large amount of vorticity. In the standard fluid theories applied to the vocal fold and lip-reed the flow is generally assumed to be describable by a boundary layer approximation for much of the oscillation cycle. Under this assumption the bulk of the flow is assumed to be frictionless. The effects of viscosity are confined to thin regions near the boundary walls known as boundary layers. Within the boundary layers there exists a large velocity gradient between the fluid directly adjacent to the main flow, which moves at approximately the main flow velocity, and the fluid adjacent to the all, which is static. Such a gradient of velocity leads to a non-zero vorticity within the boundary layers.

The process of flow separation causes this vorticity to be injected into the main flow, which leads to a significant rotational component and an eventual break down of the flow through turbulent dissipation. In the case of the separated glottal jet it may thus be hypothesised that regions of vorticity exists throughout the flow. The application of PIV to a flow results in a velocity field, from which it is possible to estimate the vorticity. Mathematically this is defined as

$$\omega(x,y) = \frac{\partial v(x,y)}{\partial x} - \frac{\partial u(x,y)}{\partial y} \tag{5.7}$$

where the velocity u is associated with the x component of the velocity field, and the v velocity with the y component.

A program was included in the distribution of MatPIV that allowed the vorticity field to be estimated with one of several methods. The methods differed in the details of the computational implementation of equation 5.7. The 'centred' option was used in the present work. Full details may be found in [Sveen, 2004].

5.4.4 Signal filtering and sources of error

Assuming that a sufficient number of the seeding particles present in the first interrogation area are also present in the second, the correlation function generally includes peaks related to two types of correlation. These contributions are the peaks associated with true matches of shared seeding particles, and the peaks that occur due to random correlations. If the fluid motion is uniform, and there are sufficient numbers of shared seeding particles, shifts related to the former will produce a correlation peak much higher than peaks resulting from random correlations.

If there is significant non-uniform motion of the seeding particles within the interrogation area, it is likely that there will be multiple correlation peaks. Such peaks would arise from the various shifts required to overlap the smaller groups of particles within the interrogation area that do exhibit uniform motion. The only solution to such non-uniform motion is to use small interrogation areas that more closely encompass the scale of the fluid motion. Such a solution is dependent on sufficiently low flow speeds, to ensure that transport of seeding particles between adjacent interrogation areas is kept to a minimum.

If the raw image quality is poor, or if there is excessive transport of seeding particles out of the interrogation area, it is likely that no clear peak will be formed in the correlation function. Estimation of the mean seeding particle displacement will thus tend to produce a velocity vector with a low signal-to-noise ratio, which may well exhibit a velocity significantly different from that of adjacent interrogation areas. Such a vector is known as an *outlier*.

Outliers are an unfortunate fact of life in almost all PIV experiments. Untreated, they can lead to obviously spurious results, both for the visual representation of a

PIV vector map, and for any calculations based on the vector maps. The process of identifying and filtering outliers from PIV datasets is thus of crucial importance. Two primary methods were used in this work to identify outliers: *signal-to-noise ratio filtering* and *local median filtering*. Both are widely used techniques for cleaning up experimental vector maps.

Signal-to-noise ratio filtering

Evaluation of the cross-correlation function provides an estimate of the local fluid velocity, together with the signal-to-noise ratio (SNR) of the largest correlation peak. It is common practice in PIV to filter the vector field by setting a threshold signal-to-noise ratio. Any vector arising from a correlation peak with a SNR lower than the threshold is classified as an outlier, and replaced with a velocity vector interpolated from the eight nearest neighbours.

The vector maps in this work were SNR filtered as standard, using a value of 1.3, which has been recommended by Keane and Adrian[Keane and Adrian, 1992].

Local median filtering

Local median filtering works by comparing each vector with its eight nearest neighbours. A median vector is calculated for the set of nine vectors, and if the vector of concern differs from this value by more than a critical threshold, it is flagged as an outlier. Any identified outliers are replaced by interpolating the vector from the nearest eight neighbours.

The choice of the median threshold is dependent on the nature of the flow and the quality of the raw images. Typical values are between 2.5 and 3.0[Sveen and Cowen, 2004].

5.5 Summary

An overview of PIV has been presented in this chapter. The important principles of flow seeding, image acquisition, cross-correlation and data filtering have been outlined. Chapter 6 presents a more detailed description of the implementation of PIV for the study of an *in vitro* self-oscillating musical valve. This includes details of the methods for system triggering, timing and synchronisation.

Chapter 6

PIV Setup, Apparatus and Method

"*Something to think about: if you fish the wrong fly long and hard enough, it will sooner or later become the right fly.*" - John Gierach

6.1 Introduction

This chapter presents a detailed description of the apparatus and experimental methods used to apply PIV to the study of *in vitro* self-oscillating musical valves. An overview of the technical considerations is first presented in section 6.2. A description of the *in vitro* model is then presented in section 6.3, followed by an outline of the experimental apparatus in section 6.4. The general system setup and method required to run a PIV experiment is finally outlined in section 6.5.

6.2 Application of PIV to *in vitro* vocal fold and lip-reed models

Oscillation of a musical valve produces a jet of air. In the case of the vocal folds the jet emerges from the glottis and into the lower reaches of the vocal tract. In the case of the lip-reed the jet emerges from between the lips and into the mouthpiece of the instrument. In either case, the cross-sectional areas of the regions immediately upstream and downstream of the valve are typically an order of magnitude larger than the cross-sectional area of the valve where the jet is formed. It has been shown in section 2.5 that the emergent jet may thus be expected to rapidly disintegrate as it transitions from the near-laminar flow regime upstream of the valve, to the region of turbulent mixing downstream.

The flow downstream of the valve is inherently unsteady, as the mechanical

oscillation of the valve causes an oscillation of the fluid flow at its exit. In the case of both the vocal folds and the lip-reed this periodic, pulsatile flow acts as an acoustic volume flow which leads to acoustical standing waves in the downstream cavities. The acoustical traveling waves that make up such standing waves may further be expected to periodically act back on the valve walls. Thus an extremely complicated flow situation may be expected in the region downstream of a musical valve, made up of steady jet-like components, and oscillatory acoustical components.

The work of Krane *et al*[Krane and Wei, 2006] and Erath and Plesnaik[Erath and Plesnaik, 2006a; Erath and Plesnaik, 2006b] has used PIV to investigate the air jet produced by unsteady flow through a rigid model of the vocal folds. Triep *et al*[Triep *et al.*, 2004] have used PIV to study the flow through a driven model of the vocal folds. Neubauer *et al*[Neubauer *et al.*, 2007] have recently used PIV to study the flow produced by a self-oscillating vocal fold replica.

Bamberger[Bamberger, 2005] has used PIV to study the air jet produced at the labium of a flute. His work has successfully showed the oscillation of the air jet across the labium, and the periodic generation and shedding of vortices.

Application of PIV to this situation presented several particular challenges. A setup was required whereby optical access could be gained into the most interesting regions of the flow, namely the areas between the valve walls and immediately downstream. A seeding mechanism was also required that allowed the flow through the valve to contain a suitably dispersed mixture of seedant and air, in order to maximise the quality of the raw images (see section 5.3.2). The standard issues of suitable light sheet intensity, timing and camera alignment were of their usual importance.

6.3 The *in vitro* model

The development of replica B, outlined in section 3.2.3, addressed several of the practical challenges outlined above. However, due to constraints on the availability of experimental equipment, and on the development schedule of the model, the PIV experiments described in this thesis were based on an earlier design of the model, referred to here as replica C. This model was developed by the speech research team at the Institute de la Communication Parlée (GIPSA lab) in Grenoble, France, and is shown in figure 6.1.

Replics C was used in this thesis as part of a collaboration between the Acoustics and Fluid Dynamics group in Edinburgh, and the GIPSA lab. The objective of the collaboration was to investigate the aerodynamic interaction between the human vocal folds and the ventricular bands, also known as the false vocal folds. The ventricular bands are a secondary constriction at the back of the throat, around 15mm downstream of the vocal folds. A detailed description of the mechanical configuration has already been presented in section 2.8.1. In section 7.2 a detailed overview of the motivation for

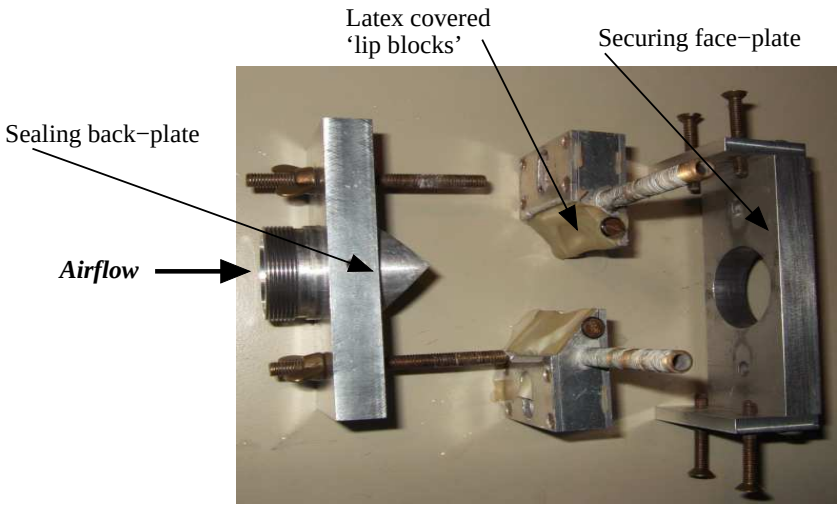

Figure 6.1: A photograph of replica C in a dismantled state. To assemble the replica, the front and back plates were pushed together, sealing the latex against the lip-blocks and creating an air-tight system. The front and back plates prevent direct transverse optical access to the lip opening, as shown in figure 6.3. See figure 3.2 for an illustration of replica B.

the experiment is presented, along with details of how the collaboration was organised.

The combined vocal folds - ventricular folds system presented an overall situation with some interesting similarities to the lip-reed - mouthpiece system that has been studied in chapter 4 of this thesis. The undertaking of a collaborative effort allowed a symbiosis of the expertise of the Grenoble team in the development and study of *in vitro* models, with the long history of PIV experimental experience in Edinburgh.

6.3.1 Replica C - an *in vitro* vocal fold model designed for mechanical stability

The application of PIV to an *in vitro* musical valve called for a model with long-term mechanical stability. It was important that the model could be assembled and used over a period of several days, whilst maintaining sufficient mechanical consistency. This was because the objective of the study was to investigate the fluid flow, and so the mechanical condition of the model presented an important control parameter.

Replica C was created in Grenoble with the criteria of mechanical stability at the heart of its design. As a precursor to replica B it differed in a number of practical ways, but the essential mechanics of the water-filled latex 'lip-blocks' were almost identical. The key difference between the two models lay in the manner of mounting the lip-blocks within the greater structure of the setup. Whilst replica B used glue to provide a reliable seal of the latex to the lip-blocks, and so create the water-filled 'lip', replica C relied on mechanical pressure applied from either side of the face-plate to seal the latex

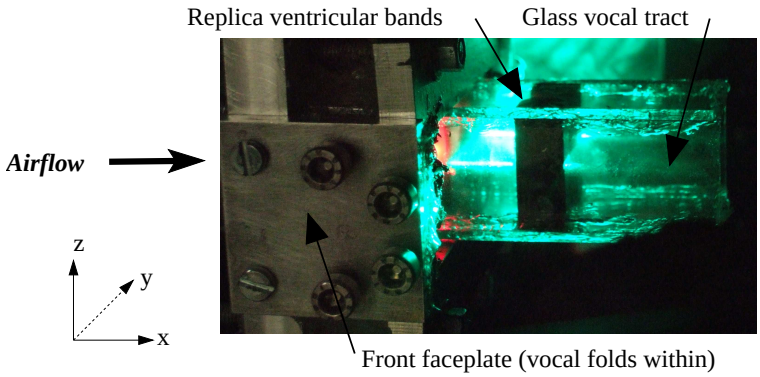

Figure 6.2: A photograph of replica C, complete with an artificial vocal tract made of glass. The replica ventricular bands are labeled.

against each vocal fold (again, see figure 6.1). This necessitated a considerably larger number of components in the vicinity of the face-plate, which meant that direct optical access to the valve opening was not possible. Figure 6.1 illustrates the consequences of these differences in terms of the optical access to the region directly between the latex vocal folds.

The second key difference between the two replicas was the upstream condition. In the mechanical studies presented in chapter 4, replica B, which was primarily designed to simulate the lip-reed, was mounted on a relatively small volume to represent the lung of the player. This volume was in turn connected to the compressed air supply that provided the blowing pressure. Replica C, however, required a large volume upstream of the model. This was to ensure that the upstream pressure P_0 remained as steady as possible, unaffected by the pressure drop across the valve. This allowed any static pressure measurement made upstream of the valve to be directly transfered to a computational simulation of the system.

The upstream volume was in the form of a large artificial lung, damped with acoustical foam to reduce any standing waves. The main construction of replica C, as shown in figure 6.1, was connected to the lung via an artificial trachea. This was a length of cylindrical tubing formed from cast aluminium. Its length could be varied by the addition or removal of extra screw-in sections, according to the requirements of the particular experiment. In the experiments presented here, it was kept at a constant length of 25.4cm.

6.3.2 Configurations of the *in vitro* model

Replica C was designed to allow a number of different configurations of the conditions downstream from the replica vocal folds. An artificial vocal tract was included in the design. This was constructed from four clear glass panels, arranged to form a hollow

Configuration	P_{thresh}	P_0	L_{VT}	L_{VB}	h_{VB}
Free jet (no vocal tract)	410Pa	380Pa	0cm	N/A	N/A
Physically realistic ventricular band config ($VB-A$)	280Pa (decreased)	270Pa	5.8cm	1.6cm	0.3cm
Impeding ventricular band config ($VB-C$)	690Pa (increased)	677Pa	5.8cm	2.4cm	0.1cm

Table 6.1: A table summarising the ventricular band configurations studied in the PIV experiments (see figure 2.16 to identify quantities). Note has been made of the effect of the ventricular bands on the oscillation threshold pressure P_{thresh} in absence of the bands. The upstream pressures P_0 used during the PIV measurements have been noted. Chapter 7 contains a more detailed explanation of the various configurations.

oblong with a square cross-sectional area of 2×2cm. A number of vocal tracts were constructed, some of which included a replica of the ventricular bands. The replica bands were constructed from aluminium blocks, shaped to form a pair of approximately semi-circular oblongs. A photograph of an artificial vocal tract, together with a pair of replica ventricular bands, is shown attached to the front faceplate of replica C in figure 6.2.

Each vocal tract - ventricular band configuration was classified by three parameters; the total length of the vocal tract L_{VT}, the distance between the vocal folds and the ventricular bands L_{VB}, and the minimum height between the ventricular bands h_{VB}. These quantities are shown in part (b) of figure 2.16. In an attempt to quantify the nature of the aerodynamic interaction between the vocal folds and the downstream conditions, a small number of unique configurations were investigated in this study. A summary of each of these configurations is presented in table 6.1. Chapter 7 contains a more detailed explanation of the various configurations together with a detailed account of the precise mechanism of the collaboration.

The choice of the ventricular band configurations were based on the experimental and theoretical work of Lucie Bailly[Bailly *et al.*, 2006], the second key collaborator on the project. It has been demonstrated that certain combinations of the three ventricular band parameters, as presented in table 6.1, may either help, hinder or have no effect on the threshold oscillation pressure of the vocal folds[Bailly *et al.*, 2008].

A realistic configuration ($VB-A$) was used to provide the most physically close interpretation of the ventricular band layout and position. A semi-realistic configuration ($VB-B$) was also used in order to investigate the range of fluid behaviours possible for a perturbation of the realistic configuration. This perturbed configuration was also called the 'impeding configuration'. The impeding configuration used replica ventricular bands of the same shape as the realistic configuration, but

they were positioned further downstream (24mm vs. 16mm), and employed a smaller minimum separation (1mm vs. 3mm).

Figure 6.4 shows a schematic diagram of replica C as used for the PIV experiments. A Brüel & Kjær type 4192 microphone was inserted approximately 2cm upstream of the self-oscillating vocal folds to record the upstream acoustic signal. No probe attachment was necessary as the replica incorporated an appropriate microphone seating. Due to the heavy damping of the upstream pressure reservoir (the 'lung') and the low static overpressure used to drive the replica ($\sim$ 300Pa), the resulting signal was generally quite weak. A Brüel & Kjær type 2691 conditioning amplifier was thus used to boost the signal strength before it was sampled. The signal was almost devoid of harmonic content beyond the fundamental oscillation frequency, which made it an excellent choice to be the global system synchronisation signal. The synchronisation of the PIV apparatus is outlined in more detail in section 6.5.2.

6.4 Experimental apparatus

PIV experiments involve a number of separate components, which must work together in syncronisation in order to acquire pairs of images that are correctly illuminated and seeded, and captured at the desired time. Practical details of these components are presented in the following sections.

6.4.1 The experimental enclosure

The entire PIV measurement system, with the exception of the copper vapour laser, was housed within a purpose built enclosure. During the preparation for a measurement, when the light sheet optics had to be aligned to the replica, access was possible through a number of large removable side windows. The laser output was greatly lowered, to about 5% of its maximum output. This allowed the alignment to be performed using a suitable pair of protective goggles. However, during a measurement run the enclosure was sealed up to prevent any of the laser light from escaping into the wider laboratory. The class IV nature of the copper vapour laser meant that when running at full power it presented a significant safety hazard, to both the eyes and the skin.

6.4.2 PIV illumination

The source of illumination for the PIV experiments was an Oxford Lasers LS20-50 copper vapour laser. Copper vapour lasers are pulsed in nature, and in the absence of any external triggering the natural pulse repetition frequency was approximately 10kHz. The laser used in this study had been previously customised to allow 'forcing' of the pulse clock up to 50kHz with the use of an external triggering system. This allowed for a minimum inter-image acquisition time of 20μs, which made the laser highly suited

to PIV applications. The laser had been previously used for PIV measurements on acoustic fields[Rockliff, 2002; Skulina, 2005], and had allowed for reliable measurements of fluid velocities up to approximately 20ms^{-1}. This velocity limitation is a result of the Nyquist theorem, details of which have been outlined in section 5.4.2. The limit is discussed further in section 7.2.3.

The light sheet

The flow illumination was controlled using an Oxford Lasers Fibresheet light sheet generator. The basic operation of this device has been outlined in section 5.3.1. It took a fibre optic input from the copper vapour laser and generated a thin, quasi-two-dimensional sheet of light that could be positioned in various orientations to light the flow as it emerged from the oscillating vocal folds.

The use of replica C meant that the application of PIV to the study of the emergent valve jet was limited to the region labeled *R*2 in part (b) of figure 6.3. This was the region immediately downstream of the valve, but did not include the region directly between the valve walls (the area *R1* in figure 6.3). This limitation was unfortunate, given the obviously interesting region between the oscillating valve walls. However, it did allow for sufficient illumination of the region between the vocal folds and the ventricular bands. This was the area of principle interest in the study, as it contained the separated pulsatile jet. It was possible, therefore, to study the various properties and behaviours of the jet, with the objective of determining the aerodynamic interaction between the ventricular bands and the vocal folds.

Figures 6.4 and 6.5 illustrate the various possible configurations of the light sheet. The light sheet position labeled *LS1* was the standard orientation. In this configuration the light sheet illuminated the region between the vocal folds and the ventricular bands. The lightsheet was directed at the replica from a position perpendicular to the main system axis, as shown in figure 6.5. This orientation worked consistently well, with the exception of some difficulties with excessive glare from highly reflective metalic components of the replica.

Glare is often a problem is PIV experiments, and usually occurs when reflective surfaces within the PIV image field receive direct illumination from the light sheet. This result is that such areas 'burn out' during the camera exposures, as the relevant CCD pixels are unable to cope with the extremely intense light. Under certain circumstances it is also possible for burnt out pixels to cause a runaway effect whereby adjacent pixels, not directly illuminated by the reflective components, are blown out by the sudden burst of current resulting from the burn out of the illuminated pixels. This effect manifests itself as large streaks of bright light across the image, which mask the underlying flow. It is thus important to try to avoid any regions of excessive glare within the images.

Glare is usually dealt with in two ways. Firstly, the orientation and intensity of

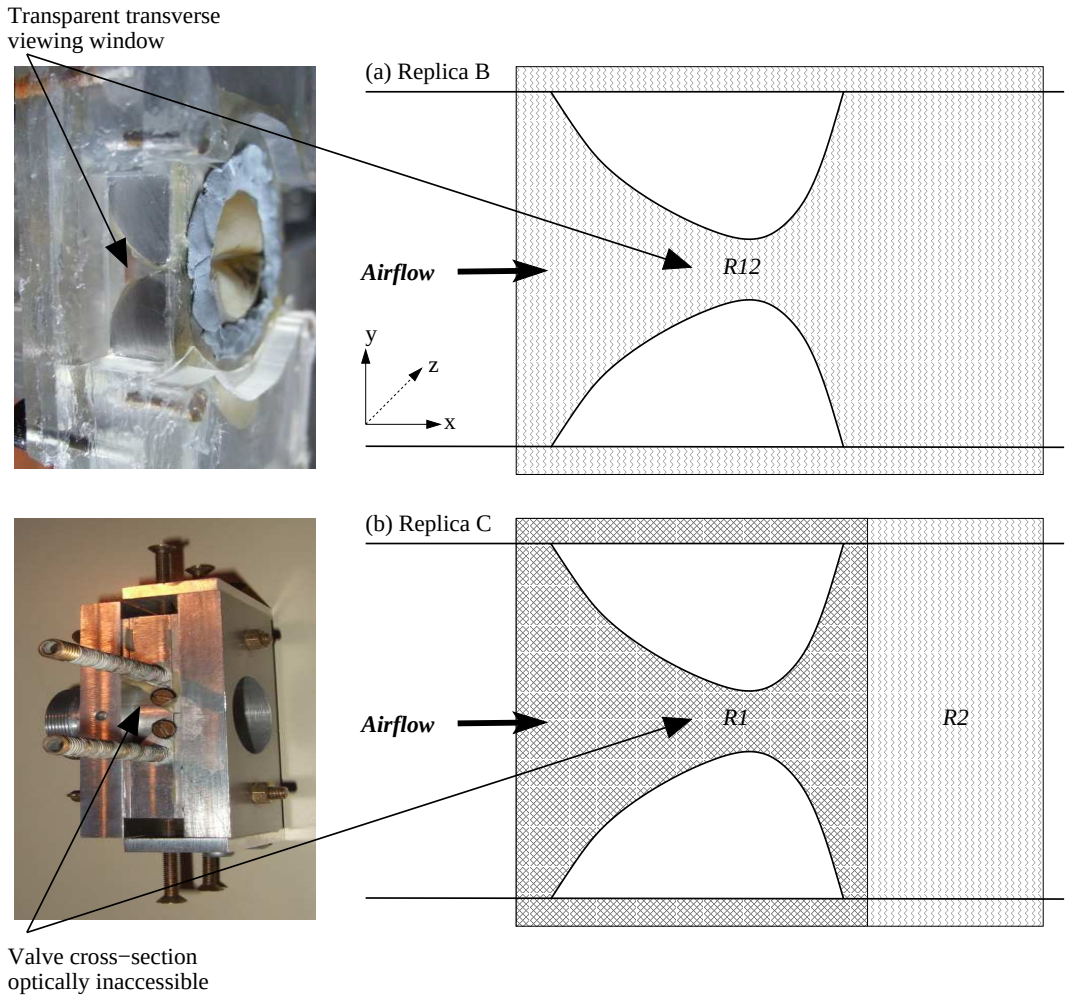

Figure 6.3: A schematic diagram showing a transverse cross-section through replicas B and C, around the vocal fold region. (a) Replica B included a glass viewing window that provided access to the valve opening (see section 4.6 on the transverse mechanical motion). The viewable area is labeled as *R12*. (b) Replica C required extensive metalwork around the lip blocks (see figure 6.1). The viewable area is labeled as *R2*, with the hashed area (*R1*) representative of the region where optical access was obstructed.

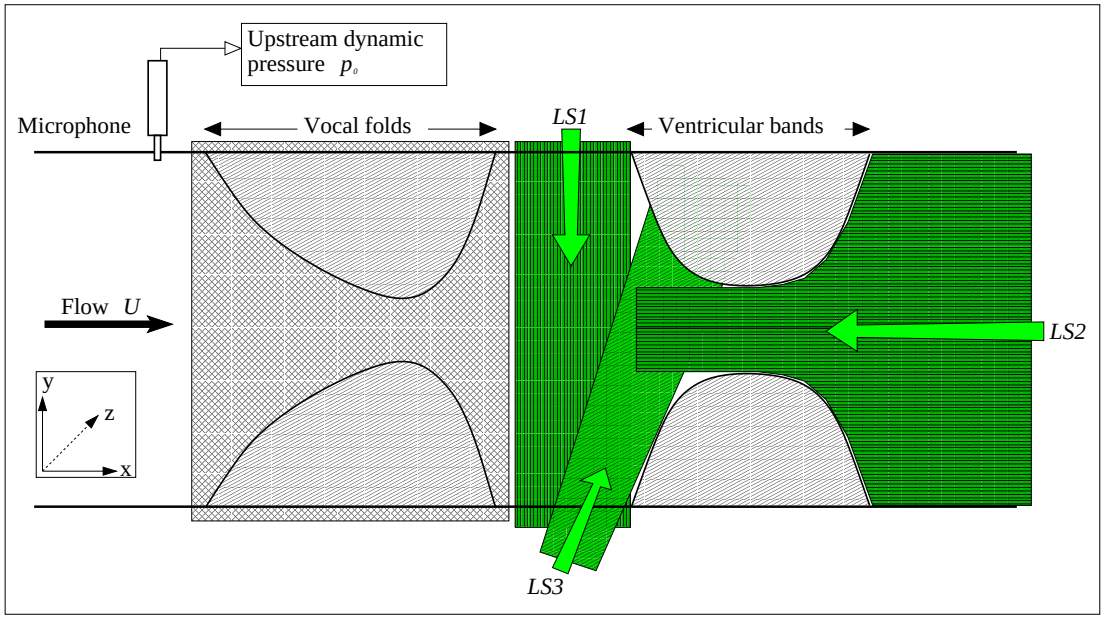

Figure 6.4: A schematic diagram showing the layout of the *in vitro* model used in the PIV experiments. The three possible light sheet orientations for flow illumination downstream of the vocal folds, in and around the replica ventricular bands, are shown as the coloured regions *LS1*, *LS2* and *LS3*.

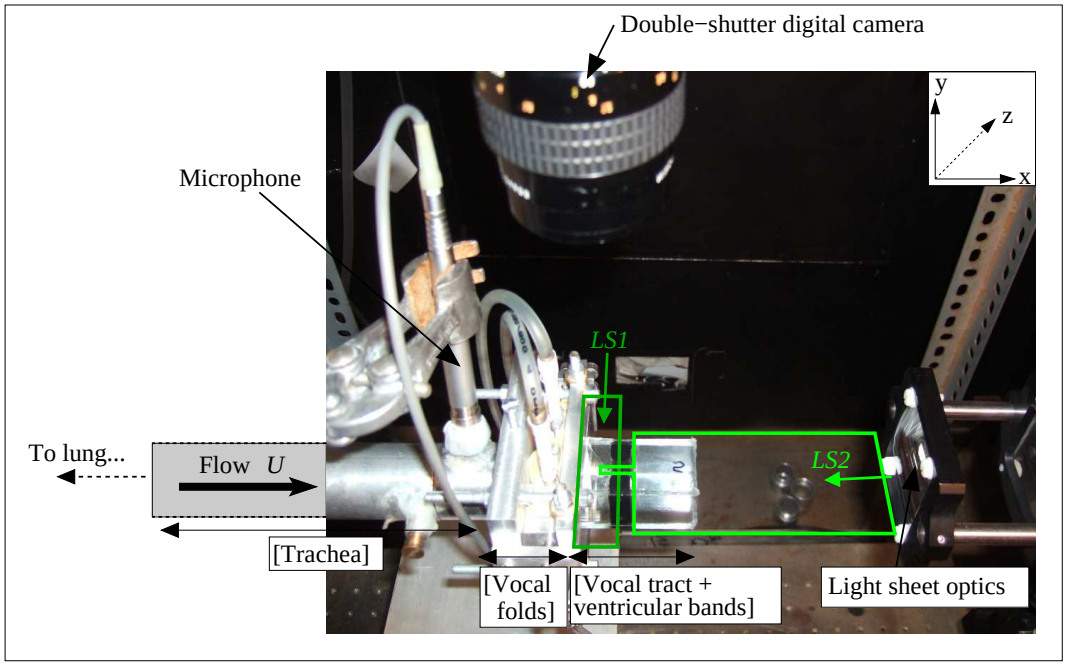

Figure 6.5: A photograph of the PIV setup, including the *in vitro* model. The light sheet orientations $LS1$ and $LS2$ are shown as in the schematic figure at top. For ease of viewing $LS3$ is not shown.

the light sheet can be adjusted so as to minimise the direct illumination of reflective surfaces. It is sometimes useful to incorporate physical masking of parts of the light sheet using thick black card. Secondly, if it is impossible to avoid direct illumination of a reflective surface, the surface may be painted with a heavy matt black paint. This technique was used extensively in the experiments in this thesis, as the entire replica was constructed from aluminium and was highly prone to causing glare.

The light sheet position labeled *LS2* in figures 6.4 and 6.5 was a useful orientation for study of the region downstream of the replica ventricular bands. The entire vocal tract cross-section downstream of the bands was visible, together with the region directly between the bands and a thin portion of the region upstream, towards the replica vocal folds. For this configuration the lightsheet was positioned at the downstream end of the replica, and directed directly upstream past the ventricular bands and towards the vocal folds.

The light sheet position labeled *LS3* was oriented to strike the upstream faces of the ventricular bands, in an attempt to observe the nature of the pulsatile jet as it impinged on them. This configuration was the most difficult of the three in practice, because it presented the largest difficulty for aligning the light sheet.

It is common practice in many PIV experiments to use mirrors to bounce the light sheet around the experimental area of interest, in order to gain maximum illumination of the subject. An attempt was made to use two mirrors to allow a simultaneous measurement to be made of the flow in all three light sheet positions. However, the cramped conditions of the PIV experimental enclosure, together with the slightly cluttered layout of the replica, made this very challenging. It was decided that the time available was better spent obtaining the best quality PIV data possible from the simpler light sheet orientations.

6.4.3 Seeding delivery system

Any PIV measurement requires that the flow field of interest be seeded with small tracer particles to reflect the light provided by the light sheet. In some applications of PIV, such as the study of viscous liquids[Raffel *et al.*, 1998], the fluid field already contains a suitable source of tracer particles. However, in most examples of PIV it is necessary to introduce supplementary seeding particles. For flows in liquids such as water, small neutrally-buoyant glass beads have been used[Schlicke, 2001]. The use of seeding in air flows presents quite more of a challenge due to the inherent density difference between the gaseous phase of nitrogen/oxygen, and the solid or liquid phase of typical seeding particles (see section 5.3.2 for an estimation of this effect).

A Dantec SAFEX 2004 fog generator, together with SAFEX Normal fog fluid[Skulina, 2005], was used as the seeding source in the PIV experiments in this thesis. The fog generator converted the fogging fluid into a fine mist, which could then be transferred

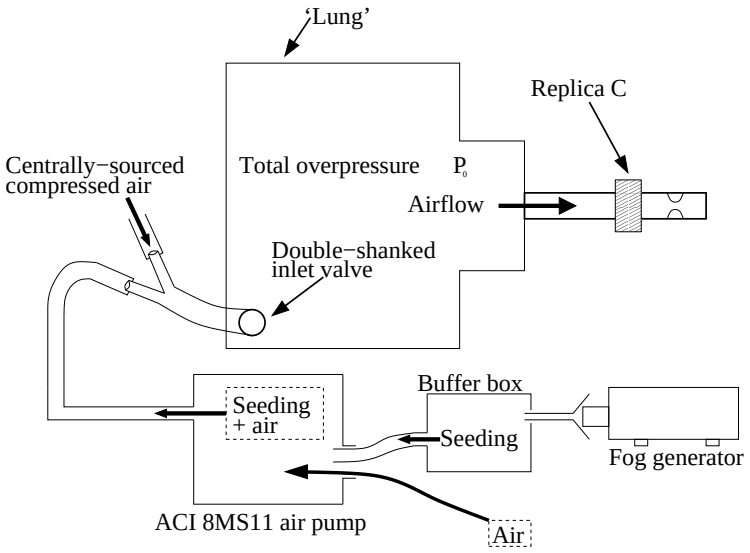

Figure 6.6: A schematic diagram showing the system used to supply the flow through the *in vitro* model with seeding particles during the PIV experiments.

into the flow of interest. In a purely acoustic field the seeding particles could simply be introduced into the confined enclosure to a suitable density[Skulina, 2005]. They would then remain in and around the acoustic field for the duration of a measurement. However, for application to an *in vitro* replica, with a strong net flow, it was necessary to introduce a continuous supply of seeding particles into the flow. This had to be performed well upstream of the replica vocal folds, in order to allow a suitably long period of time for the seeding to become evenly distributed within the flow. A similar solution has been adopted by Bamberger[Bamberger, 2005] for study of the jet flow around a flute labium. Bamberger also used a small box around the head of the flute in order to confine some of the seeding particles around the flute labium, and loading the air entrained by the jet. Such a setup was not adopted in the present work so as to minimise any possible acoustical coupling.

In the present setup the seeding was introduced from the fog generator into the large artificial lung cavity, which was as far upstream as was physically possible. Figure 6.6 shows a schematic diagram of the setup. The lung was supplied with air from two sources. This first of these was a centrally sourced supply of compressed air, and the second was a locally sourced supply of air from a small air compressor (Air Control Industries Ltd. 8MS11 0.25kW air pump). These supplies were separately connected to a double-shanked inlet valve located close to a corner of the lung. The centrally sourced supply provided the bulk of the overpressure required to induce self-sustained oscillations of the valve. The small air compressor, which was insufficient to power the oscillations on its own, was used as a way to introduce seeding particles into the lung. The seeding produced by the fog generator was fed into the air-input port on

the compressor, which then pumped the air-seedant mixture into the lung cavity. It was a trivial task to control the quantity of seedant introduced to the flow by simply adjusting the amount of seeding allowed to be sucked into the air compressor.

The large volume of the lung meant that at the start of an experimental run approximately 30s were required for a suitable mixture of air and seeding particles to build up. The optimum mixture was obtained by careful observation of 'mini-runs', whereby a small number of individual images of the illuminated flow field were captured and downloaded from the camera. Adjustments to the seeding input could then be made, with repeated use of mini-runs if necessary, until the mixture was deemed optimum.

Fogging

One of the most consistent and seemingly unavoidable problems encountered in many PIV experiments is that of fogging. Fogging occurs when seeding particles become stuck to the surface of transparent parts of the setup, through which optical access is required. As an increasing quantity of seedant sticks to a surface, regions of the image that lie behind the surface appear increasingly blurred, until it becomes impossible to distinguish the illuminated seeding particles within the actual fluid flow.

Fogging was a particular problem in the current setup, as the flow regions where optical access was required all lay within the artificial glass vocal tracts. It was essentially impossible to prevent some build up of seedant on the glass surfaces, and so regular inspection and cleaning were crucial steps of the experimental procedure. It was commonly the case that the image quality for a particular experimental run would appear suddenly diminished. A brief investigation of the glass surfaces frequently revealed fogging as the source of the problem, which was easily remedied by swabbing with a solution of 70% methanol.

6.4.4 Fluid pressure measurement

At the start of each the experimental run a measurement of the threshold onset pressure was made. This was so that a particular configuration could be tested for consistency if repeated measurements were required. A pressure manometer was used, which was placed in the side of the replica trachea, just upstream of the vocal folds.

Definition of the threshold onset pressure

The threshold pressure was defined as the upstream overpressure required to just sustain oscillations of the vocal folds. This was obtained by slowly increasing the applied overpressure, controlled from the centrally sourced supply of compressed air, until the vocal folds continually oscillated, as indicated by the presence of an acoustical signal from the upstream microphone. The pressure was then reduced until oscillations ceased.

The pressure was finally increased very slightly until oscillations began again. This was then the threshold oscillation pressure.

Measurement of the acoustic pressure

During PIV measurements that involved full self-sustained oscillations a Brüel & Kjær type 4192 condenser microphone was used to monitor the acoustic signal just upstream from the vocal folds. The microphone was connected to a Brüel & Kjær type 2691 conditioning amplifier, which was in turn connected by a BNC cable to an analogue-to-digital (ADC) interface. The interface was connected to a PC and controlled by the Labview signal acquisition and processing software (version 7.1).

The conditioning amplifier allowed a range of amplifications to be made to the signal. These were provided in units of Pascals/Volt ($\frac{Pa}{V}$), so that multiplication of any recorded signal from the Labview sampling (sampled as a voltage) by the amplification scaling yielded the signal in units of pressure. The Labview software and ADC/DAC interface provided the cornerstone of the PIV system control.

6.5 Experimental method

Application of PIV to a self-oscillating valve presented a particular set of experimental challenges. Once the desired configuration was obtained (internal lip water pressure, downstream conditions), the model was left to oscillate freely during the experiments. This meant that the pulsatilse jet flow was produced completely separately from any of the PIV control apparatus and syncronisation system. The jet depended on the oscillation frequency of the replica vocal folds, a quantity that was not strictly stable. It was found, by application of a continuous spectrogram to the upstream pressure signal, that during a typical experimental time frame of 10s the oscillation frequency could vary by up to 0.5Hz. It was of the utmost importance, therefore, that a method was devised that allowed the acquired image pairs to be accurately syncronised with the oscillation cycle of the replica.

The objective of the PIV measurements was to acquire a series of vector maps throughout the oscillation cycle of the replica. The key problem facing the present implementation was that is was not possible, *a priori*, to determine the precise point in the phase of the vocal fold oscillation at which an image pair were acquired. This was in contrast to the recent implementations of PIV in purely acoustical fields whereby the timing of the laser flashes and camera exposures were phase-locked to the acoustical signal by use of a controlled loudspeaker excitation[Rockliff, 2002; Skulina, 2005]. In recent applications of PIV to the jet flow at a flute labium[Bamberger, 2005] a supplementary acoustic field, generated by a loudspeaker, was used to phase-lock the jet oscillations to the PIV systems. This allowed the jet flow to be studied at

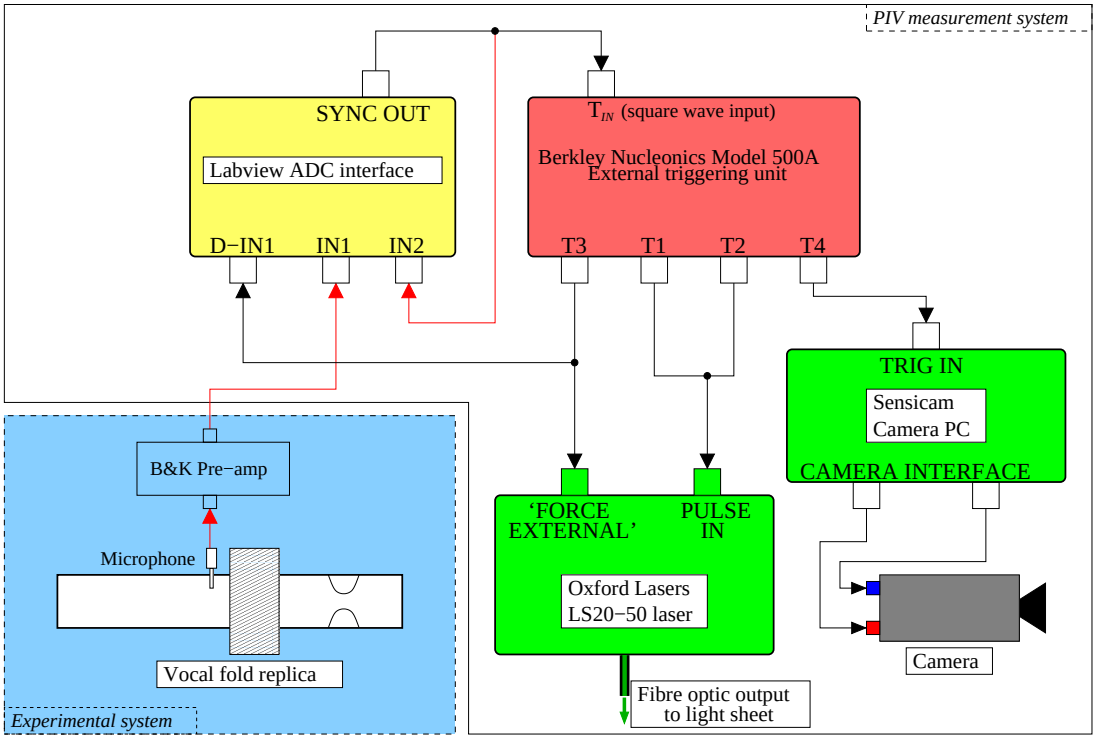

Figure 6.7: A schematic diagram of the global PIV system. The red arrows indicate signals that are sampled by the Labview software for analyis and post-synchronisation. The black arrows indicate the PIV timing signals.

pre-define phase angles throughout the cycle of oscillation.

In the present application the use of a supplementary acoustic field was not a suitable solution. This was because the objective of the study was to investigate the, quite possibly very subtle, effects of the ventricular bands on the nature of the jet flow as it separated and disintegrated downstream of the replica vocal folds. As will be demonstrated in chapter 7, the presence of the ventricular bands can also have a measurable effect on the oscillation frequency of the vocal folds, and one of the mechanisms involved in this process may be acoustical coupling[Bailly *et al.*, 2006; Bailly *et al.*, 2008]. The presence of a strong supplementary acoustic field may well have seriously disrupted the fluid flow and the behaviour of the replica.

The free, uncontrolled oscillations of the vocal folds meant that a large number of PIV acquisitions had to be obtained from quasi-random points throughout the phase of oscillation. The term 'quasi' is used for this description because there was a low level of control over the process, but not the full phase-locked control described above for purely acoustic fields. A detailed explanation of this may be found below.

6.5.1 Basic method for acquisition of an image pair

The basic objective for a PIV experimental run was to acquire a series of approximately 20 image pairs using an automated laser/camera triggering system. A schematic layout of the global PIV acquisition system is shown in figure 6.7. The system had three major components, the Labview software platform running on a PC together with an analogue to digital interface card, the external triggering system and the laser/camera system. Figure 6.8 shows a timing diagram of the various triggering signals relevant to a PIV image pair acquisition. Table 6.2 summarises the timing quantities described in figure 6.8 and in section 6.5.1.

Global PIV system layout

The Labview platform had two functions. The first function was to synthesise a 3V, 2Hz square wave S_{SQ} and to output it to the external trigger input channel, T_{IN}, of the triggering device. This square wave acted as the global system synchronisation signal, with an image pair acquisition occurring at every instance of a positive-going square wave edge. The second function was to sample the acoustic signal p_0 from the upstream microphone (see figure 6.4) on one input channel (IN1), together with the synchronising square wave on a second input channel (IN2). All synthesis and sampling operations were performed at a sample rate of 1MHz.

The laser and camera triggering signals were programmed and sent from a Berkley Nucleonics Model 500A delay generator, set to function as an external triggering unit. The unit had four output trigger channels, T1-T4, which were triggered upon the receipt of a positive-going voltage edge on the external trigger input channel T_{IN}, which was provided by the square wave signal S_{SQ} sent from the Labview system. Each of these output channels could be programmed to send out a voltage pulse with a precise delay and width. A series of four timing pulses were thus sent from the triggering unit at every positive-going square wave edge, causing the laser to fire and the camera to exposure in perfect synchronisation. The 2Hz square wave sent from Labview meant that this occurred every 0.5s.

Triggering the laser

For a suitable image pair to be obtained the laser had to be externally triggered to produce two pulses of light. The first pulse had to lie within the exposure window of the first camera image acquisition, and the second pulse had to lie within the second exposure window. In order to do this the laser's internal pulse clock had to be temporarily overridden with an external triggering signal (see also section 6.4.2). This was accomplished by sending a 4V negative-going voltage step to the 'FORCE EXTERNAL' input on the laser, from channel T3 on the external triggering unit. This

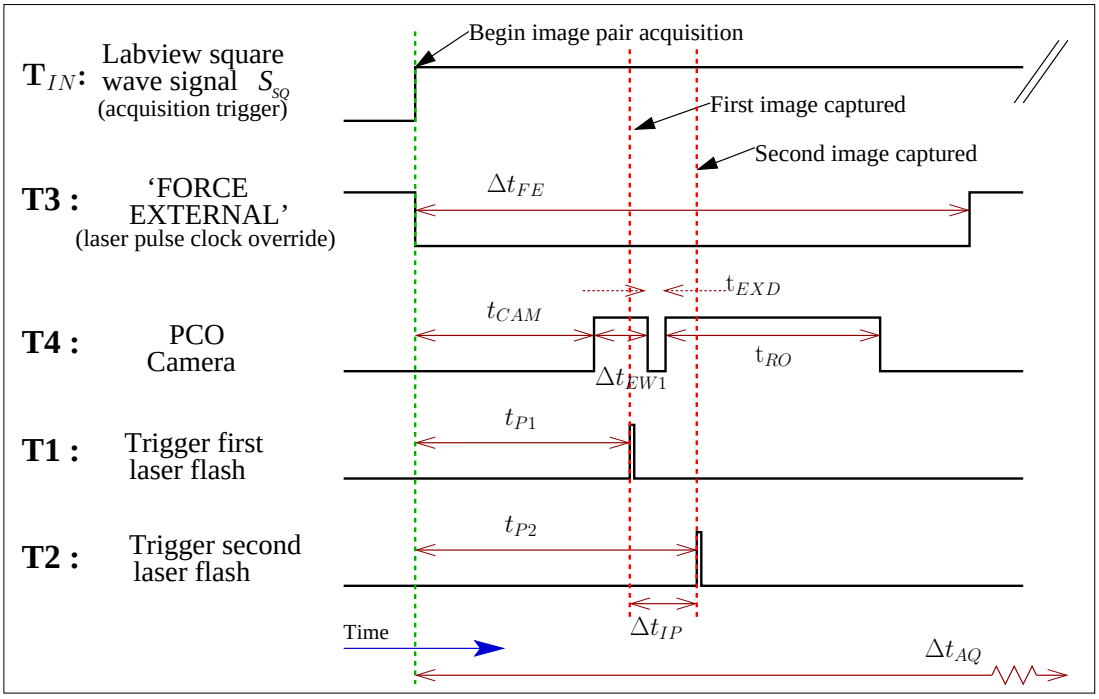

Figure 6.8: A timing diagram showing the various triggering signals required to perform a single image pair acquisition. Channels T1-T4 are triggered upon receipt of the positive-going square wave on input channel T_{IN}, once every 0.5s. A summary of the various values is given below in table 6.2.

occurred as soon as the positive-going square wave edge was detected by the triggering unit on its input channel T_{IN}. There followed a short period of time before the first laser flash. This was to allow enough time for the camera to be triggered to begin exposure of the first image.

When the laser detected the negative-going edge from channel T3, the internal pulse clock was bypassed and remained so for the duration of the 'FORCE EXTERNAL' pulse width, Δt_{FE}. It was important to ensure that Δt_{FE} was set to be longer than the maximum possible readout time of the camera (t_{RO}), plus the first exposure window width. This was to ensure that the laser did not begin to fire according to its internal pulse clock within the camera exposure windows, which would have rendered the images useless. Whilst the laser was being forced in this manner it could be externally triggered to fire individual light pulses. This was accomplished by sending short, positive-going voltage pulses to its 'PULSE IN' input.

Triggering the camera

The camera was triggered to begin exposure of the first image by a positive-going 4V voltage pulse sent from channel T4 on the triggering unit. This pulse was sent to the TRIG IN trigger input on the PCI interface card connected to the camera PC. Upon

Quantity	**Timing**	**Value**
Δt_{FE}	Force external duration (T3 pulse width)	350ms
t_{CAM}	Time to start of first image window (T4 pulse delay)	T_{P1} - 0.09ms
Δt_{EW1}	First exposure window duration (T4 pulse width)	0.1ms
t_{RO}	Camera readout time	250-300ms
t_{P1}	Time to first laser flash (T1 pulse delay)	1/(Rounded f_0)
t_{P2}	Time to second laser flash (T2 pulse delay)	$t_{P1} + \Delta t_{IP}$
Δt_{IP}	Time between laser flashes	20μs
t_{EXD}	Inter-frame time	1μs
Δt_{AQ}	Time between image pair acquisitions (square wave S_{SQ} time period, on channel T_{IN})	0.5s

Table 6.2: A table of the various timing values required to run a PIV experiment (see the timing diagram in figure 6.8).

receipt of the trigger pulse the camera computer instantly triggered the camera to begin an image acquisition. The pulse was outputted a time t_{CAM} following the arrival of the positive-going square wave edge on the input channel T_{IN} of the triggering unit. The T4 pulse was timed to arrive at the camera so that the first image exposure window would begin in advance of the first laser flash. This was to ensure that the laser flash fell within the first exposure window. The length of the exposure window Δt_{EW1} was determined by the width of the voltage pulse sent from channel T4. This time was set to be 0.1ms. The first laser flash was timed to arrive towards the end of this exposure window.

After the first exposure window had elapsed, the camera CCD was temporarily shut off for a short period of time, the inter-frame exposure delay t_{EXD}. This time was determined by the 'mode' in which the camera was selected to run. The *short mode* was used, which meant that t_{EXD} was 1μs. Note that this time was considerably shorter than the minimum possible time between laser pulses Δt_{IP}, which meant that it was not a limiting factor in determining the time between the two image acquisitions.

The second exposure window began a time $t_{CAM} + \Delta t_{EW1} + t_{EXD}$ following the initial acquisition trigger (see the timing diagram,shown in figure 6.8). The length of this exposure window was determined by the camera's readout time t_{RO}, which was not directly controllable (see also section 5.3.3). During this time the camera continued to expose the second image frame. For the setup used in this work the readout time varied between 200-350ms.

The second laser pulse was triggered 20μs after the first, at a time t_{P2} after the initial

global acquisition trigger from the positive-going square wave edge. This meant that it fell towards the start of the second exposure window. This left a substantial period of time during which the PIV system had to wait for the images to be transferred from the camera to the Sensicam PC. As has been mentioned, it was important to ensure that the laser remained in an externally triggered state throughout this time, so that no extra pulses of light were allowed to ruin the second image.

6.5.2 Synchronisation of the PIV system

The preceding sections have described the basic process for the acquisition of a single image pair. In previous applications of PIV to acoustic flows the general procedure has been to acquire multiple sets of image pairs at specific phase points throughout the acoustic cycle[Skulina, 2005]. This technique may be called the *acoustical phase locking (APL)* method. Following cross-correlation analysis the multiple vector maps at each phase point may then be averaged together to produce a single vector map. The final result is a set of 10 or 20 vector maps that describe the acoustic field over a cycle. This approach is attractive because the averaging process allows an estimation to be made of the standard deviation of the velocities at each phase point. Knowledge of the standard deviation may be used to assess the general unsteadiness of the flow, as well as to quantify the quality of the data.

The APL method works because the acoustical signal is generated by the PIV system apparatus, which could be the Labview system in the present context. It is thus possible to exactly synchronise the positive-going zero-crossing of the acoustical signal with the rising edge of the square wave. If the frequency of the acoustical signal is an even integer, such as 100Hz, an even number of cycles elapse during the 0.5s between image pair acquisitions, which in this example would be 50 complete cycles. This means that at every occurrence of a positive-going square wave edge throughout the experiment, the corresponding phase of the acoustical signal is the positive-going zero-crossing. This allows a set of 20 image pairs to be acquired, over a period of 10s and 1000 acoustical cycles, each of which corresponds to precisely the same phase point. Incremental phase shifts may then be applied to the acoustical signal, so that different phase points may be measured throughout a cycle.

In the present application it was not possible to pre-specify precise phase points in the cycle of the vocal fold oscillation at which to acquire multiple sets of image pairs. This was because the vocal folds were left free to oscillate at their own natural frequency, unperturbed by any supplementary acoustic fields. Even in the case of an acoustical frequency very close to an even integer, it would not have been a reliable solution to use the APL method as the vocal fold oscillation frequency was rarely perfectly constant. This meant that it would have been a significant assumption to make that a set of 20 image pairs corresponded to precisely the same phase location.

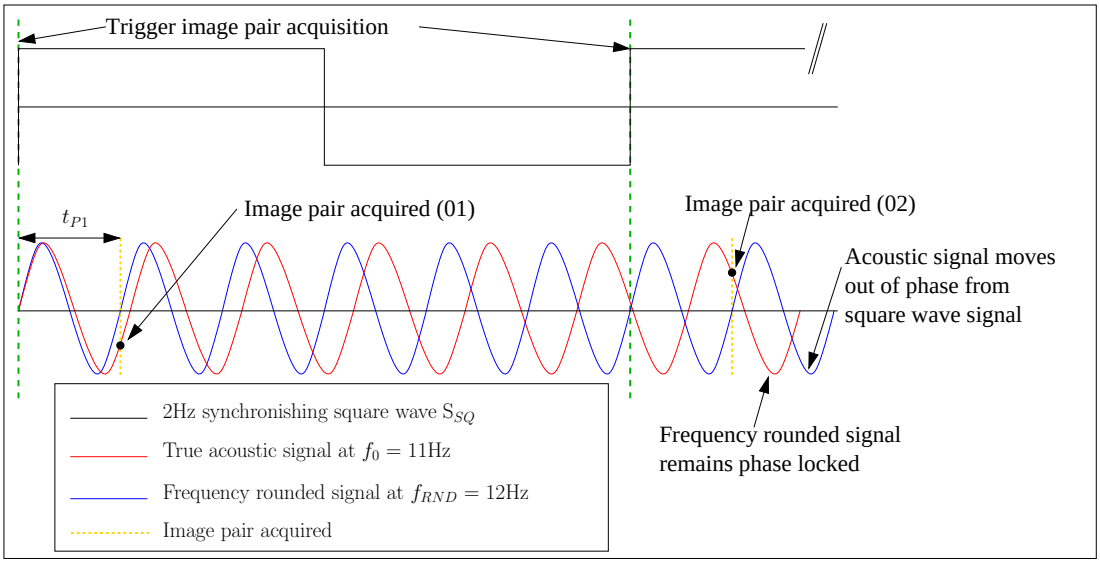

Figure 6.9: A simplified plot of the square wave and upstream acoustical signals, as sampled by the Labview system during a PIV measurement run, together with an equivalent plot of the frequency rounded signal. The frequencies are small for display purposes (in general $f_0 \approx 100Hz$).

It was thus of crucial importance that a method was determined to objectively acquire image pairs throughout the cycle of oscillation, and to maintain exact knowledge of the phase points where measurements occurred.

The approach adopted in the present application was to time the image pair acquisitions to the nearest even integer of the fundamental vocal fold oscillation frequency f_0. This meant that the delay from the positive-going square wave edge to the first laser flash was determined by the rounded frequency value f_{RND}, and it also meant that an integer number of cycles of f_{RND} occurred over the time period of the square wave.

Both the upstream acoustical pressure and the global synchronising square wave were simultaneously sampled by the Labview system. Following the acquisition of 20 image pairs it was possible to plot the two signals together. The precise phase points in the acoustical cycle at which the image pairs had been acquired could then be determined by first identifying the positive-going edges of the square wave, and then identifying the point in the acoustical cycle that corresponded to the time period of one cycle of the rounded frequency signal.

Figure 6.9 provides a simplified signal diagram of the synchronisation process. The rounded frequency was generally within 1Hz of the true acoustic frequency. This meant that between each image pair acquisition, during which 0.5s elapsed, there was a small relative phase shift between the rounded frequency and the acoustic frequency. In the figure the true acoustic frequency was 11Hz, which meant that the rounded frequency

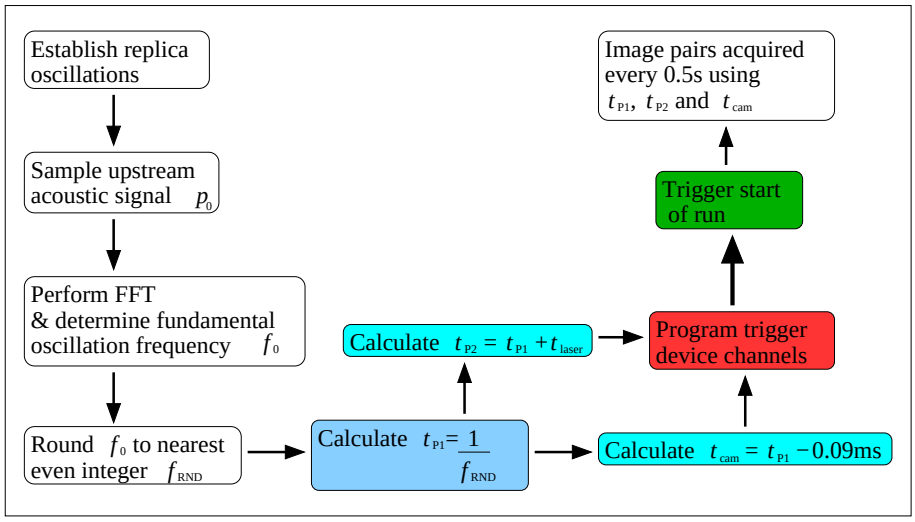

Figure 6.10: A signal flow diagram describing the basic process required to perform a single PIV image acquisition run of (approximately) 20 image pairs. Calculation of t_{P1} and t_{P2}, the laser pulse delay times, and t_{cam}, the camera delay time, form a crucial step of each run.

was 12Hz. In the time period of one square wave oscillation, exactly six full cycles of the frequency rounded signal occured. The true acoustic frequency, however, only completed five and a half cycles. Thus the phase point in the acoustic cycle at which the image pairs were acquired shifted with every new image pair acquisition. With the sampled signals, as presented in figure 6.9, it was possible to precisely identify these phase points (labeled at '01' and '02'). The cumulative result was that a 'strobing' effect occurred over the experimental run, whereby the 20 image pairs were acquired at approximately 20 evenly spaced phase points throughout the oscillation cycle. This was consistently possible because f_{RND} was chosen to be close to, but not exactly the same as, the true oscillation frequency. Ten or more repetitions of the experimental run were carried out, which lead to a total of at least 200 image pair acquisitions distributed almost evenly throughout the cycle.

For a particular configuration of the *in vitro* replica there was a particular natural oscillation frequency, f_0, of the vocal folds. It was thus important to sample a short period of the upstream acoustic signal to determine the fundamental oscillation frequency before each measurement run. The most suitable trigger timings could then be calculated based on the measured frequency. A signal flow diagram of the calculation process is presented in figure 6.10. The timing offset for the start of the first camera exposure window, 0.09ms, was chosen along with the width of the exposure window (0.1ms) to ensure that the first laser flash occurred within the first exposure window.

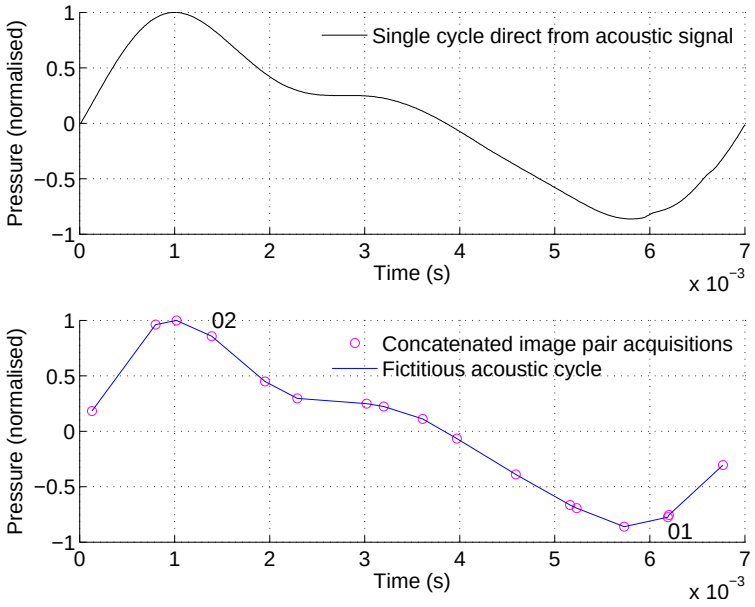

Figure 6.11: An example of the synchronisation of the sampled acoustic pressure signal with the square wave. The upper curve is a single cycle of the true acoustic signal. The lower curve shows the result of extracting the image pair acquisitions from multiple points in the acoustic signal, leading to a 'fictitious' acoustic cycle. The two acquisition points shown in figure 6.9 have been labeled.

Synchronisation stage 1 - image pairs to acoustic signal

At the end of a measurement run there were two sets of data, the timing signals comprised of the upstream acoustical signal and the synchronising square wave, and the raw image pairs. A synchronisation process was required to determine the precise points throughout the acoustic cycle at which each image pair had been acquired. A program was written in Matlab to perform this operation.

The Matlab program first read in the two timing signals. It then indexed all the times at which a positive-going square wave edge occurred. The exact acquisition points in the acoustic cycle were determined by extracting the values of the acoustical pressure at times t_{P1} following each positive-going square wave edge. Each point was then temporally indexed by measuring the time between the extracted point and the nearest positive-going zero-crossing in the acoustic signal.

The final result was a two dimensional data set. The first column comprised the acoustic pressure amplitudes at each image pair acquisition, and the second column described the time delay of each acquisition point from the nearest positive-going zero-crossing of the acoustic signal. When these data points were plotted together, they described a series of points throughout a 'fictitious' acoustic cycle. Figure 6.11 shows an example of a true acoustic cycle, extracted directly from the acoustic signal sampled

by Labview, together with the 'fictitious' acoustic cycle resulting from concatenation of multiple acquisition points. The two acquisition points shown in figure 6.9 have been labeled in the figure. As more and more measurement runs were completed, the number of sample points throughout the fictitious acoustic cycle increased.

Synchronisation stage 2 - image pairs to the vocal fold motion

The synchronisation of the image pair acquisitions with the upstream acoustic signal formed the first stage of the overall synchronisation procedure. The second stage was to synchronise the image pair acquisitions with the physical motion of the replica vocal folds. It was important to have knowledge of the relationship between the flow and the physical motion of the valve. The relationship between the upstream acoustic pressure and the flow was less important in and of itself, as the phasing between the two datasets depended on the position of the microphone along the tracheal wall. It was the motion of the valve itself that had a much stronger bearing on the behaviour of the pulsatile jet, as has been outlined in section 2.5.

The oscillation of the minimum open area between the vocal folds provided the most useful description of the valve motion. The minimum open area corresponded to that discussed for the lip-reed in section 4.3. In the earliest two-mass models of the vocal folds[Ishizaka and Flanagan, 1972] it was assumed that the flow always separated from the valve walls at the minimum constriction. This assumption has been extensively discussed, particularly in the case where the vocal folds form a slowly diverging channel[Deverge *et al.*, 2003; Pelorson *et al.*, 1994; Scherer *et al.*, 2001a].

In the present application it was not possible to sample the open area between the vocal folds during a PIV measurement run. An attempt was made to record the motion using a laser doppler vibrometer directed at a point on the surface of one of the vocal fold. However, it was found that this method produced a signal which was very sensitive to the angle from which the laser was directed, and to the choice of the point targeted on the vocal fold surface. This was probably due to the extensive two-dimensional motion of the *in vitro* replicas, already highlighted in section 4.6. An additional problem was that the strong laser beam required for this technique introduced an extra source of illumination in the region downstream of the vocal folds. This was a particular problem when the main copper vapour laser was being bypassed, as the vibrometer's laser light spoiled the instantaneous nature of the normal image acquisitions.

Synchronisation to the open area was achieved by filming the vocal folds with a high-speed digital camera (Vision Research Phantom version 4.1) whilst simultaneously sampling the upstream acoustic pressure from the same location in the trachea as used in the PIV measurements. This step was performed after the PIV measurement runs had been completed for each vocal volds - ventricular bands configuration. Practical details of the camera, together with a full explanation of its usage, may be found in

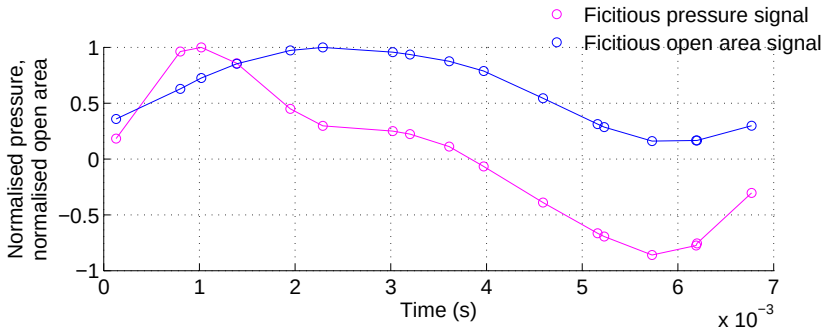

Figure 6.12: An example of the final synchronisation of the image pairs to both the upstream acoustical signal and the open area signal, for a single measurement run. The circles indicate times where an image pair was acquired.

section 3.3.3. Single oscillation cycles for the acoustical pressure and the open area were extracted and saved as 'calibration' data sets for each configuration.

The synchronisation was performed by comparing the acoustical signal from the PIV measurement run with the one obtained during the high-speed filming of the open area. The measurement time for each image pair acquisition was indexed in the calibration data set, and the corresponding open area extracted. Concatenation of the multiple acquisition points for each measurement run lead to a 'fictitious' open area signal, to go along with the fictitious upstream acoustical pressure. Summing together all the measurement runs yielded a fictitious open area curve with at least 200 sample points for each configuration.

After the second synchronisation stage there were thus three key data sets for each configuration, the raw image pairs (later converted to vector maps), the upstream acoustical signal and the open area signal. The two stage synchronisation procedure meant that both the upstream acoustical pressure and the open area between the vocal folds were known for each and every image pair in a configuration. Figure 6.12 shows an example of the two fictitious signals plotted together. The open area signal described an almost sinusoidal motion, while the acoustical signal included at least two harmonic components.

A simple analogy to describe the PIV syncronisation

The preceding method used to acquire image pairs for PIV analysis was rather like the high-speed photography used to establish the winner of an Olympic sprint. As the runners near the finishing line many photos are taken in quick succession, with a known time between the frames. It is not possible, of course, to pre-determine the positions of each runner within the frame as their behaviour is independent of the camera system. However, post-analysis of the photographs, together with a syncronised timing clock,

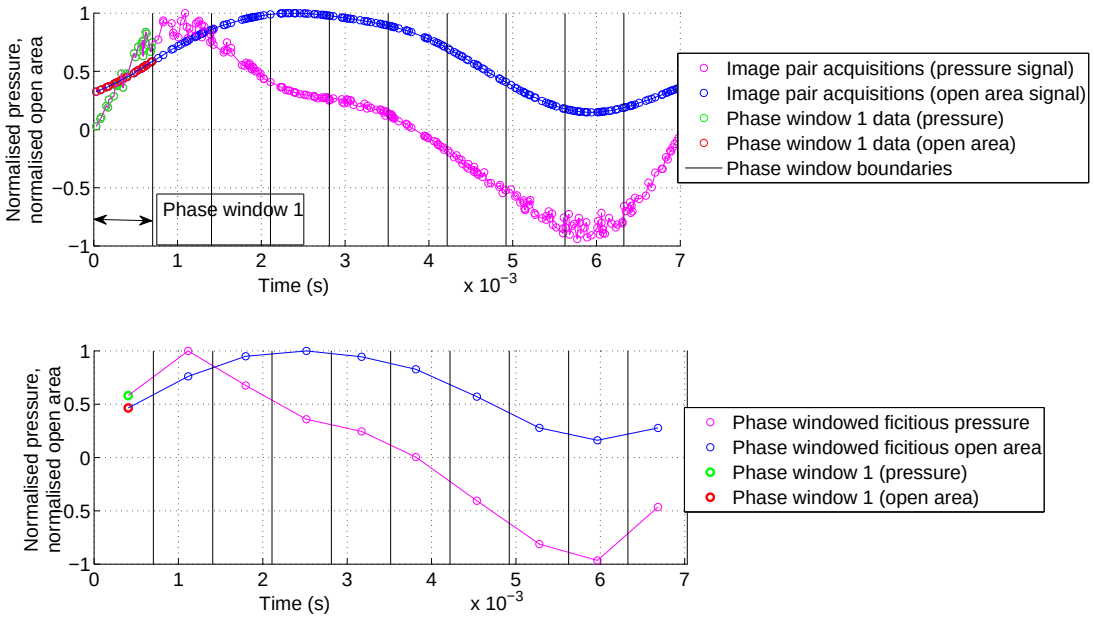

Figure 6.13: An example of the phase windowing process used to average the ≈ 200 vector maps acquired for a single configuration into a small number of discrete phase windows.

allows a precise determination to be made of the exact time at which each runner crossed the line. In a similar fashion it was not possible to pre-determine the precise moment throughout the oscillation cycle of the vocal folds at which an image pair would be acquired. However, with a suitable post-analysis of the recorded upstream acoustic signal and the PIV triggering signals, it was possible to determine the exact point in the acoustic signal at which the acquisition was made.

6.5.3 Phase windowing

The basic experimental approach used in this work was to perform multiple experimental runs for each vocal fold - ventricular band configuration. Each experimental run produced a set of approximately twenty image pairs, distributed almost evenly throughout a single cycle of vocal fold oscillation. By grouping together the data produced from each of the individual experimental runs, a large number of vector maps, typically around 200, were obtained throughout the cycle.

Each vector map represented an instantaneous snapshot of the fluid flow field. Consecutive vector maps were not strictly obtained from consecutive moments within a single cycle of the vocal fold oscillation. Rather, the vector maps were obtained at instants separated by many oscillation cycles of the replica. The maps were ordered together into a quasi-temporal order by the synchronisation procedure outlined in section 6.5.2. The term 'fictitious' has been used to describe the cycle of oscillation

resulting from the synchronisation process.

The large number of vector maps, each obtained from a temporally disparate moment in time, posed an important question in terms of the suitable analysis procedures. This issue almost always occurs in the case of acoustical fields. The general approach has been to perform multiple phase-locked image pair acquisitions at a discrete number of phase points throughout the acoustic cycle. The resulting vector maps may then be averaged together at each phase point to produce a sequence of ten or twenty *phase steps* that describe the acoustic cycle.

In the present application the image pairs were acquired over an almost continuous distribution of phase points throughout the oscillation cycle. To reduce this data set to a more manageable size, and to average out some of the signal noise, a process of *phase windowing* was applied to the maps. All the synchronised vector maps for a particular vocal fold - ventricular band configuration were first grouped together from their individual experimental runs to produce a single super-group for the configuration. This cycle was then broken up into ten or twenty equally spaced windows of time, or *phase windows*. The vector maps within each phase window were averaged together to produce a single vector map, representative of the average flow condition over the course of the phase window.

The use of phase windowing tended to smear out the subtle flow features present in individual vector maps, such as small vortices. The unsteady nature of the pulsatile flow meant that two vector maps, both obtained within phase window one, possessed quite different small scale features. The objective of the phase windowing was to average out the data in order to measure the constant behaviour, at the sacrifice of the smaller details.

Standard deviation of the phase windows

The averaging process used to calculate the phase windowed vector maps meant that a statistical analysis could be performed in order to assess the similarity of the constituent maps within each window. The standard deviation of the velocity fields was a useful calculation that allowed for such an analysis. The standard deviation of each phase window was calculated for each of the horizontal and vertical components of the velocity map using the equation

$$u_{std}(x,y) = \sqrt{\frac{1}{n}\sum_{i=1}^{n}\left[u_i(x,y) - \bar{u}(x,y)\right]^2} \tag{6.1}$$

where there were n maps in the phase window (typically 25 or 30), $u(x,y)$ were the individual vector maps and $\bar{u}(x,y)$ was the average of the individual vector maps (the same as the phase windowed vector field).

The standard deviation was in units of metres per second. Where there was a large

discrepancy between the individual maps and the overall phase windowed map, the standard deviation was large, indicated by high velocity values.

6.5.4 PIV measurement procedures

Once a suitable configuration of the *in vitro* model had been established, the light sheet appropriately aligned and the seeding distributed, the PIV setup was triggered to begin acquiring multiple sets of image pairs. The preceding commentary has outlined the various control systems and synchronisation procedures required to to achieve this process. A brief summary is presented here of the key stages in the overall procedure.

Image pair acquisition (see section 6.5.1)

1. Set up the *in vitro* replica with the appropriate downstream conditions (ventricular bands, vocal tract)
2. Set laser output to 5%
3. Align the lightsheet with the desired observation area
4. Insert and seal upstream microphone into trachea
5. Measure the threshold oscillation pressure
6. Set the vocal folds into oscillation at the desired overpressure
7. Introduce seeding into the flow
8. Sample the upstream acoustical signal, and measure the frequency of the fundamental component (f_0)
9. Calculate the rounded frequency (f_{RND}) and the trigger timings (t_{CAM}, t_{P1}, t_{P2})
10. Program trigger timings into external triggering unit, and check that the all pulse delays and pulse widths are correct
11. Check the seeding density with a 'mini-run', and adjust as necessary
12. Set laser output to 100%
13. Trigger the commencement of a measurement run of 20 image pairs
14. Export image pairs as uncompressed bitmap files
15. Save the square wave and upstream acoustical signals from Labview as a single column-separated text file

PIV processing of measurement runs (see section 5.4.1)

1. Complete image pair acquisition (see above)

2. Measure the pixel-to-metres calibration factor C_{MPIX} by taking a single image of an object of known dimensions, placed in the image field

3. Place image pairs from a run together in a single directory

4. Set up the cross-correlation program (MatPIV[Sveen, 2004], see section 5.4.1) with the appropriate parameters (three passes of cross-correlation, once with $[64 \times 64]$ pixel interrogation area, twice with $[32 \times 32]$)

5. Run cross-correlation analysis, and convert velocities to real world values using C_{MPIX}

6. Filter vector maps as required, typically using a SNR filter and a local median filter (see section 5.4.4)

7. Index and save velocity maps for each measurement run into their own Matlab data file

System synchronisation (see section 6.5.2)

1. For each run in turn, synchronise the image pair acquisitions with the upstream acoustical pressure signal

2. For each run in turn, synchronise the image pair acquisitions and the upstream acoustical signal with the vocal fold opening area

3. Group multiple experimental runs (each of ≈ 20 image pairs) into single batches of data for each vocal fold - ventricular band configuration (each of ≈ 200 image pairs)

4. Perform a full synchronisation of all maps so that they lie in time order relative to the positive-going zero-crossing of the upstream acoustical pressure (in practice this is completed as part of the previous step)

5. Phase window the vector maps into ten or twenty phase windows which describe the average fluid behaviour over a cycle (see section 6.5.3)

6. Perform calculations on the phase windowed data (see section 7.4)

6.6 Conclusions

This chapter has presented the experimental procedures and analysis processes required to perform PIV measurement on a self-oscillating *in vitro* vocal fold replica. The important process of synchronising the image pair acquisitions to the upstream acoustical signal, and then to the open area between the vocal folds, has been extensively discussed. The technique of phase windowing has also been presented as a method to yield a small number of averaged vector maps that describe the fluid behaviour throughout a cycle of vocal fold oscillation.

Chapter 7

Application of Particle Image Velocimetry I: Background Theory and Analysis Methods for Study of an *in vitro* Vocal Fold replica

"*I fish... not because I regard fishing as being so terribly important, but because I suspect that so many of the other concerns of men are equally unimportant - and not nearly so much fun.*" - Robert Traver

7.1 Introduction

Self-sustained oscillations of musical valves, such as the lip-reed and the vocal folds, occur as a result of a coupling between the mechanical structure of the valve and the surrounding fluid. The flow of fluid in and around the mechanical structure causes it to destablise, with a periodic oscillation regime forming one of the possible outcomes.

In the every day world of human phonation and brass playing, the fluid of concern is atmospheric air. In the vicinity of a musical valve the surrounding fluid must interact with the mechanical structure so as to transfer energy to the mechanical motion of the valve. Some of the conditions under which this may occur have been outlined in sections 2.5 and 2.7.

The importance of the valve's mechanical structure and behaviour have been studied in chapters 3 and 4. The degrees of mechanical freedom have been shown to be of particular relevance, together with basic macro-scale properties such as the valve's mechanical damping. Such a study, however, can only hope to shed light on half the

story of musical valve operation at most. The behaviour of the fluid field, and the nature of its interaction with the mechanical structure of the valve, is of central importance to a more complete understanding of the physics involved in the overall process.

The fluid mechanics involved in phonation and lip-reed function is an under-researched area. Although there are many examples of *in vitro* studies performed under steady flow conditions, there have been very few studies conducted under the condition of full self-sustained oscillation. This is most intriguing in light of the rapid development, in the last thirty years, of increasingly sophisticated computational models of the valve mechanics. The most common of these models are the multiple-mass lumped element models[Ishizaka and Flanagan, 1972; Story and Titze, 1995; Lous *et al.*, 1998; Kob, 2002; Kob, 2004b], but the use of distributed models[de Vries *et al.*, 2003] is becomming increasingly popular.

One of the main issues preventing experimental research into the fluid mechanics is that of gaining access for scientific instrumentation. The vocal folds lie deep within the structure of the throat, while the lips of a brass player lie concealed behind an obtrusive mouthpiece. It would be incorrect to suggest that the topic of fluid mechanics has not been discussed, as it has been the subject of increasingly intense debate[Hirschberg, 1992]. It is the body of experimental evidence that merits attention.

7.1.1 Flow studies of *in vitro* musical valve replicas

In vivo measurements of fluid behaviour around musical valves represents a significant challenge, both for the vocal folds and for the lip-reed. In the field of vocal fold physics, the most 'natural' studies have been those made on excised canine larynxes[Slavit *et al.*, 1990; Alipour *et al.*, 1995]. Amongst relatively few others, Elliot and Bowsher[Elliot and Bowsher, 1982] have measured the fluid velocity in the mouthpiece of a trombone under *in vivo* conditions. However, the issue of repeatability highlighted by the *in vivo* work of chapter 4, together with concerns for safety, make fluid studies with humans subjects extremely difficult. For this reason, the most concentrated efforts have been made with *in vitro* replicas (see section 2.3).

Cullen[Cullen, 2000] made one of the few efforts to study the fluid behaviour encountered in the specific case of the lip-reed. The use of laser-doppler vibrometry proved to be very challenging in the noisy, turbulent region of the mouthpiece. Measurements were made of the lip impedance, as well as of the oscillating fluid velocity in the mouthpiece.

Research into the fluid mechanics of speech has undoubtedly seen more attention than research into the fluid mechanics of the lip-reed. There are a number of studies, both theoretically and experimentally grounded, which stretch back over the past sixty years. Van Den Berg *et al*[van den Berg *et al.*, 1957] discussed the relevance of the Bernoulli effect in phonation as far back as 1957, though the idea of a fluid mechanical

origin for speech production can be traced back even further.

Ongoing theoretical discussion of the subject by Ishikaza and Matsudaira[Ishizaka and Matsudaira, 1972] and others in the speech community was of great importance to the early two-mass model of the vocal folds developed by Ishikaza and Flanigan[Ishizaka and Flanagan, 1972]. Teager and Teager[Teager and Teager, 1983] and McGowan[McGowan, 1988] both discussed the role of unsteadiness in phonation, with McGowan[McGowan, 1993] going on to further question the suitability of the increasingly popular quasi-stationary models. In the early 1990's Hirschberg[Hirschberg, 1992] provided an excellent summary of much of the preceding commentary. Most recently, Krane and Wei[Krane and Wei, 2006] performed a theoretical assessment of unsteady aerodynamic effects in phonation.

Experimentally, the aforementioned work on canine larynxes[Alipour *et al.*, 1995] provides an early example of an attempt to quantify the fluid behaviour around a self-oscillating musical valve. The total volume flow through the valve system was measured with a rotameter, while smaller sections of the flow were measured with a hot-wire anemometer in an attempt to improve the spatial resolution.

There have been a number of flow studies performed on so-called 'rigid' *in vitro* replicas of the vocal folds. In most cases research has been based on upscaled, static replicas of the vocal folds, subjected to an imposed constant volume flow. These studies have implicitly relied upon the quasi-steady assumption whereby the continuous flow through the valve may be approximated as a series of discrete steady flow 'snapshots'. By examining the flow behaviour around a number of differently-shaped rigid replicas representative of important points throughout a glottal oscillation cycle, attempt has been made to investigate the temporal evolution of the flow. Scherer *et al*[Scherer *et al.*, 1983; Scherer *et al.*, 2001b; Scherer *et al.*, 2001a; Scherer *et al.*, 2002], in particular, has contributed several papers with this approach.

Quantified investigations of rigid *in vitro* replicas have generally been conducted by studding the surface of the replicas with pressure transducers that allow a picture of the flow to be built up from pressure measurements. The work of Pelorson *et al*[Pelorson *et al.*, 1994; Pelorson *et al.*, 1995] is noteworthy in this regard. A number of studies have also directly examined the flow through the use of flow visualisation techniques[Erath and Plesnaik, 2006b; Kucinschi *et al.*, 2006; Tao *et al.*, 2007].

Of most interest to the present work are examples in the literature that have investigated unsteady flow effects. There are examples of at least three different approaches to tackle the issue. Early work by Pelorson *et al*[Pelorson *et al.*, 1994; Pelorson *et al.*, 1995] investigated unsteadiness by subjecting static vocal fold replicas to short bursts of flow. Pressure transducers in the walls of the vocal folds together with flow visualisations using the schlieren method[Davis, 1971] enabled significant insight into the roles of unsteadiness and viscosity in the glottal flow.

Deverge *et al*[Deverge *et al.*, 2003] have examined the flow conditions encountered

when the vocal folds approach collision. Vilain[Vilain *et al.*, 2004] and Ruty[Ruty *et al.*, 2007] have further examined the validity of the quasi-steady assumption through a combination of computational modeling and pressure measurements using *in vitro* vocal fold replicas.

In the past decade the idea of mechanically driven vocal fold replicas has been widely adopted. In setups suggested by Barney *et al*[Barney *et al.*, 1999], Kucinschi and Scherer[Kucinschi and Scherer, 2006], Park and Mongeau[Park and Mongeau, 2007] and Kob *et al*[Kob *et al.*, 2005], mechanically driven *in vitro* replicas of vocal folds have been subjected to an imposed flow in an attempt to increase the similarity between replica and reality. By mechanically forcing a temporal evolution in the profile of the vocal folds, a larger continuum of dynamically varied flow conditions have been created. Such an approach is arguably an improvement over investigations involving static replicas. However, the ultimate target has to be investigations using a fully self-oscillating vocal fold replica. Under such conditions the mechanical motion of the vocal folds is driven directly by the fluid field. This represents the most realistic possible picture of the fluid behaviour encountered during phonation.

A recent paper by Neubauer *et al*[Neubauer *et al.*, 2007] demonstrated the first peer-reviewed investigation of vocal fold flow dynamics under conditions of fully self-sustained oscillation. The technique of particle image velocimetry was used to examine the flow through an *in vitro* vocal fold replica, in a setup similar to that presented in chapter 6. A conference paper by the author of this thesis, presented in 2006[Newton and Campbell, 2006], has also demonstrated a working PIV setup to measure the flow through an *in vitro* lip-reed replica (replica A, see section 3.2.2), in advance of Neubauer's publication. The experimental development of this early work went on to significantly inform the flow experiments presented in this thesis (see section 7.2 below).

The flow experiments described in part III of this thesis, comprising chapters 5, 6, 7 and 8, attempt to investigate the behaviour of the fluid field around a fully self-oscillating vocal fold replica. This work was conducted as part of a collaboration between the Fluids and Acoustics group at the University of Edinburgh (undertaken through the author of this thesis), and the GIPSA lab in Grenoble, France (undertaken through Ms. Lucie Bailly). Full details of the mechanisms of the collaboration are presented below in section 7.2.2, together with a description of its relevance to this thesis in section 7.2.1.

A more detailed overview of the physics relevant to phonation is provided in section 7.3. In section 7.4 a number of analysis methods used to examine the PIV data obtained from the experimental investigations are presented. The development of these analysis tools forms a significant portion of the original work of this thesis. Chapter 8 presents the results from the flow experiments, together with analysis and discussion of their implications both for phonation and for the lip-reed.

7.2 Flow study of *in vitro* vocal fold replica C using PIV

7.2.1 Motivation

A summary of the physics relevant to the function of both the lip-reed and the human vocal folds has been outlined in chapter 2. An important conclusion from this discussion is that essentially the same set of equations and formulations can be used to describe both systems.

Despite the fact that the vocal folds function to allow speech, and the lip-reed to allow production of musical notes, the two systems require the same set of flow equations. These equations are based on the idea of inviscid flow, fluid boundary layers and flow separation, processes that are essential in allowing the production of a flow-control valve effect (see section 2.5.2). The mechanical equations to describe the vocal fold and lip-reed valves can also be identical in structure. For example, both systems can be well simulated using a lumped element two-mass model (see section 2.9).

The key difference between the systems lies in the treatment of the acoustical propagation; in the case of the lip-reed there is almost always a strong acoustical coupling between the lips and the standing wave in the instrument bore[Elliot and Bowsher, 1982; Campbell, 1999; Saneyoshi *et al.*, 1987b; Adachi and Sato, 1996], whereas in the case of the vocal folds the 'source-filter' approach has been widely adopted, whereby the vocal folds function independently of any acoustical signal. In the latter case, there is some evidence to suggest that process of acoustical feedback may in fact be important for some aspects of speech[Rothenberg, 1981; Guerin, 1981; Titze and Story, 1997; Titze, 2004], if not as the sole source of an alternating aerodynamic driving force within the larynx.

It is clear from the non-dimensional analysis presented in section 2.5.1 that there is likely to be a significant overlap in the basic fluid behaviour, at least in terms of the pulsatile jet formed at the valve exit, encountered in the vocal fold and lip-reed systems. It is thus reasonable to use the scientific platform of research into the physics of vocal fold fluid mechanics if not as conclusive evidence for the behaviour of the lip-reed flow, then at least as a basis for informed conjecture.

Certain questions regarding the fluid behaviour are clearly shared by both systems. For example, the ubiquitous Liljencrants[Liljencrants, 1989] condition prevalent in many computational models of the vocal folds has also found its way into some models of the lip-reed[Richards *et al.*, 2003; Richards, 2003]. This is an *ad hoc* condition used to determine the spatial location of the flow separation point from the vocal folds. It states that when the glottis forms a diverging profile the flow is assumed to separate from the vocal fold walls when the vocal fold separation reaches 1.2 times that of the minimum glottal aperture[Lous *et al.*, 1998].

The Liljencrants condition is used in computational modelling as tool to simplify

the fluid mechanics. It has no empirical basis, but is widely used. There are a number of other assumptions routinely made in both vocal fold and lip-reed modelling, such as the assumption that viscosity can be neglected in the bulk of the flow, or that the quasi-steady assumption is always valid. Such assumptions demand experimental investigation as a way of verifying their validity.

Given the significant similarity between the *in vitro* lip-reed replicas developed over the past decade in Edinburgh[Cullen, 2000; Richards, 2003; Bromage, 2006], and replicas developed for vocal fold research at institutions such as the GIPSA lab in Grenoble[Vilain *et al.*, 2003; van Hirtum *et al.*, 2007; Ruty *et al.*, 2007], the nominal use of a vocal fold replica in the present work is a reasonable departure.

7.2.2 Outline of the collaborative mechanism

Initiation of the collaboration

In the introduction to the chapter it was stated that the work contained in part III of this thesis was undertaken as part of a collaborative project with a researcher at the GIPSA lab in Grenoble, France. The principle thesis aim of the team in Grenoble was to investigate the fluid mechanics of the larynx. The nature of a proposed aerodynamic interaction between the vocal folds and a secondary constriction within the larynx caused by the ventricular bands, or false vocal folds, was of particular interest. Because of the similarity between the case of the lip-reed and mouthpiece system, and the vocal folds - ventricular bands system (see section 2.8.1), it was proposed that a collaborative effort be undertaken. This was of benefit to the present work because the *in vitro* replica designed by the Grenoble team, known in this work as replica C, was able to oscillate at thresholds as low as 200Pa. Using a simple Bernoulli description of the flow behaviour this meant that peak jet velocities were likely to be well below the upper measurable limit of 20ms^{-1} (see section 7.2.3 below).

To briefly summarise the premise of the collaboration, a small number of distinct *in vitro* 'configurations' involving replica vocal folds and ventricular bands were investigated using PIV. The target was to use PIV to quantify the behaviour of the glottal jet as it traversed the laryngeal cavity between the vocal folds and the ventricular bands. The objective was to investigate whether the presence of the ventricular bands could have a direct influence on the vocal folds through an aerodynamic mechanism. This was relevant to the lip-reed study presented in part II of this thesis because it was hypothesised that if a significant aerodynamic effect was observed, there may be a case for arguing its importance in brass playing.

Practical mechanism of the collaboration

Successful collaborative work relies on good communication pathways and an open exchange of ideas, coupled with clear boundaries to determine how the work is carried out. It is thus important to relate in detail exactly what work was done by whom, to make it clear how the collaboration led to the original work contained in this thesis.

The work contained in part III largely resulted from a single set of experiments, carried out on an *in vitro* vocal fold replica provided by the GIPSA lab in Grenoble. The design of this replica, known as replica C throughout this thesis, was not part of the author's work.

The experiments were conducted in Edinburgh by the author and by Ms. Bailly, in April of 2007. The design and practical implementation of the flow measurement apparatus, as described in chapter 6, was entirely the work of the author. Processing of the data to obtain velocity maps was performed by the author using a custom-adapted version of the MatPIV[Sveen, 2004] software package, as described in chapter 5. The significant challenge presented by the issue of system synchronisation was addressed by the author through the use of a high speed camera setup (see section 6.5.2) and the writing of a number of Matlab programs. This allowed the vector maps to be synchronised with the mechanical motion of the vocal folds.

The Grenoble team brought a number of things to the collaboration. In practical terms the development and use of replica C was obviously of central importance to the project. In theoretical terms the experiments were conducted as a way to verify a number of proposed hypotheses for the behaviour of the glottal jet. The formation of these hypotheses was undertaken by Ms. Bailly. One of the key objectives was thus to compare the predictions of these hypotheses with the results of the PIV measurements of the glottal flow. This objective was shared by both collaborators. It was an important target because the behaviour of the glottal jet, and in particular the nature of its expansion and possible interaction with the ventricular bands, was the feature most in common between the vocal fold - ventricular band and the lip-reed - mouthpiece systems. Actual calculations appearing in this thesis based on the jet expansion hypotheses were undertaken by the author.

Given the theoretical background brought to the collaboration by the Grenoble team, it was the job of the author to develop the analysis tools to extract useful information from the PIV vector maps. Section 7.4 provides details of these techniques. The development of the jet variables described in section 7.4.4 was by the author. The development of the non-dimensional analysis of the jet, described in section 7.4.5, was by the author.

One of the most important developments was that of condensing the large number of PIV vector maps obtained for a particular configuration of the vocal fold - ventricular band system into a small number of phase windows. This approach was developed by

the author, and has already been outlined in section 6.5.3.

All the data analysis presented in this thesis is the result of work by the author. Discussion of the data, including reference to the predictions of the theoretical hypotheses for the jet expansion, represents work by the author. Throughout the analysis there was a continuous exchange of ideas and proposals between Edinburgh and Grenoble. However, the resulting work presented in this thesis is the work of the author (with the exception of the initial development of the jet hypotheses).

In order to inform the results, discussion and analysis described in chapter 8 an overview of the physics relevant to the vocal fold - ventricular bands system is presented in section 7.3 below. The work contained in this section is a combination of background research by the author, as with much of the background theory presented in chapter 2, and novel work by Ms. Bailly. In particular, the three jet expansion hypotheses described in section 7.3.2 are attributed to the Grenoble team. Finally, the proposed dimensions of the two *in vitro* configurations involving ventricular bands was by the Grenoble team.

7.2.3 Consideration of the fluid velocity range

It was important to examine the range of fluid velocities likely to to encountered around the valve, and to compare them with the range of fluid velocities that were accurately measurable with the PIV system. The limits of the PIV measurement system have been outlined in section 5.4.2. The upper limits of the measurable fluid velocity are shown in table 5.1, for a range of interrogation window sizes.

An estimation was made of the maximum fluid velocities likely to be encountered for the various proposed configurations of the replica vocal folds and ventricular bands. The estimation used the stationary Bernoulli equation shown in equation 2.25, neglecting the velocity upstream of the vocal folds, and assuming a total loss of pressure downstream. Such a scenario presented the 'worst possible case', whereby the jet velocity was maximal, and unaltered by the presence of any downstream constrictions.

The calculation estimated the velocity at the flow separation point from the vocal folds, which were located approximately 8mm upstream from the limit of the region measurable in the present work (see section 6.4.2 and figure 6.4). Throughout this distance the process of momentum transfer would be expected to lead to a deceleration of the jet, so that the actual jet speed within the camera image window should be somewhat lower than the worst case calculation. Investigation into the degree of the jet deceleration presents one of the avenues of analysis suggested in section 7.4.

Under the aforementioned assumptions the fluid velocity at flow separation may be estimated as a unique function of the total upstream pressure P_0. This quantity was measured using a manometer at the commencement of each measurement run. Table 7.1 shows a summary of the maximum expected velocities calculated for each

Configuration	P_0	L_{VB}	h_{VB}	u_{VF} (ms^{-1}) (Bernoulli)
Free jet (no vocal tract)	380Pa	N/A	N/A	$27.6\mathrm{ms}^{-1}$
Physically realistic ventricular band config ($VB-A$)	270Pa	16mm	3mm	$23.2\mathrm{ms}^{-1}$
Impeding ventricular band config ($VB-B$)	677Pa	24mm	1mm	$36.8\mathrm{ms}^{-1}$

Table 7.1: Estimations of the maximum fluid velocity for each of the configurations, evaluated using a simplified Bernoulli equation at the flow separation point which assumes a total loss of pressure. The upstream pressure was P_0. The specifications of the ventricular band configurations have been repeated for clarity (L_{VB} and h_{VB}).

configuration using the upstream pressure recorded during the actual experiments.

The upstream overpressure P_0 during each measurement run was chosen to be as low as possible for each of the configurations. The threshold onset pressure was first determined (see section 6.4.4). The replica exhibited a hysteresis effect such that the offset pressure was lower than the onset pressure (see section 6.4.4). The value of P_0 during the measurement runs was thus set slightly below the onset pressure, with the aim of minimising the resulting jet velocity, but maintaining self-sustained oscillations.

There was one configuration without ventricular bands, referred to as the free jet configuration. This configuration had no downstream coupling whatsoever, so that the jet emerged through the vocal folds directly into the laboratory. The upstream pressure was set to 380Pa, which meant that the jet velocity at flow separation was calculated as approximately $27\mathrm{ms}^{-1}$.

The values of P_0 in table 7.1 clearly highlight one of the important effects of the ventricular bands, that of their influence on the overpressure required to sustain oscillations of the vocal folds. Configuration $VB-A$, which corresponded to physically realistic ventricular band dimensions, had the effect of lowering the required blowing pressure. The predicted jet velocity at flow separation was similarly lowered to between 22 and $23\mathrm{ms}^{-1}$, neglecting the influence of the ventricular bands. Section 8.3 presents a detailed analysis of configuration $VB-A$.

Configuration $VB-B$ sited the ventricular bands further downstream than in reality, with a minimum separation between the bands h_{VB} of just 0.1cm. This had the effect of significantly raising the onset destabilisation pressure. The Bernoulli-predicted jet velocity was similarly raised, to a value of approximately $36\mathrm{ms}^{-1}$, in the absence of the ventricular bands. Such a velocity could not have been accurately measured with the present PIV setup, given the field of view of 2.5×2cm and the desired interrogation window size of 64×64 pixels (see section 5.4.2). The use of a

larger interrogation window would have permitted a higher velocity limit, but would have significantly reduced the spatial resolution of the flow field.

In the case of the $VB-B$ configuration it was decided that the location of the field of view, beginning 8mm downstream from the vocal folds, together with the possibility of a flow reattachment and pressure recovery, meant that the actual velocities likely to be encountered would be somewhat lower than the absolute maximum measurable limit of approximately 30ms^{-1}. Thus the initial interrogation window size was set to 64×64 pixels for the cross-correlation analysis. As will be shown in section 8.4, this was a reasonable hypothesis. The true jet velocities for configuration $VB-B$ were considerably lower than the Bernoulli-predicted value, and within the measurement limits of the system.

7.3 Aerodynamics of the ventricular bands

7.3.1 Background

It has been shown in chapter 2 that the phenomena of flow separation is of crucial importance in explaining the oscillation of both the vocal folds and the lip-reed. Separation of the flow, leading to the formation of a jet, is the only way that a pressure difference may be established across the lips in the case of the brass instrument lip-reed. Similarly, flow separation is vital to the principle mechanism that drives the motion of the vocal folds, that of an oscillating Bernoulli force within the larynx (see section 2.5.3). The role of an oscillating Bernoulli force between the lips has also been discussed as an important factor in driving the vibration of the lip-reed[Campbell, 1999; Elliot and Bowsher, 1982; Neal, 2002].

Recently, the work of Bailly *et al*[Bailly *et al.*, 2007; Bailly *et al.*, 2008] has sought to investigate the effects of the ventricular bands on phonation. Section 2.8 has already provided a brief overview of this system. It has been shown that for certain geometrical configurations of the ventricular bands, the threshold onset pressure may be considerably lowered relative to what is measured on a similar setup without ventricular bands. For other configurations the threshold onset pressure may be raised. PIV has been proposed as a technique to investigate any aerodynamic explanation for this effect, most notably in terms of the expansion of the pulsatile jet formed at the exit of the vocal folds. The theoretical work of Bailly *et al* forms the backdrop for the study presented in this thesis.

The acoustical effects of the ventricular bands have been studied by Fuks *et al*[Fuks *et al.*, 1998] and Imagawa *et al*[Imagawa *et al.*, 2003] by including them as an additional pair of masses located downstream from a two-mass simulation of the vocal folds. The constriction formed by the ventricular bands, also referred to as the *supraglottal constriction*, causes the cavity between the vocal folds and the ventricular bands (the

laryngeal ventricle) to act as a strong acoustical resonator, modifying the acoustical spectra of the glottal pressure pulses. Careful tuning of this resonance allows certain harmonics within the voice spectrum to be greatly amplified, leading to the perception of a distinct 'ringing' or 'whistling' tone laid over the broad vocal output.

The phenomenon of period-doubling forms one of the most interesting aspects of the vocal fold - ventricular band system. Under certain conditions the ventricular bands may begin to oscillate themselves, most commonly at a frequency exactly half that of the fundamental vocal fold frequency. Several explanations have been postulated in the literature to explain this phenomenon. The possibility of a traveling mechanical wave propagating through the tissues of the larynx and the surrounding muscles has been discussed by Tsai *et al*[Tsai *et al.*, 2004].

Fuks *et al*[Fuks *et al.*, 1998] have proposed that the period-doubling behaviour may occur as a result of an aerodynamic driving force from the glottal jet. It was suggested that this driving force was due to a negative pressure (a 'Bernoulli pressure') generated by the airstream as it passes through the ventricular bands. Under appropriate conditions such a driving force might be expected to produce ventricular band oscillations at integer steps below the fundamental frequency of the vocal fold oscillations. In such a case where ω_0 is the vocal fold frequency, the ventricular band oscillation frequency could thus occur at $\frac{\omega_0}{2}$ or $\frac{\omega_0}{3}$. Fuks *et al* proposed a lumped element model to simulate this behaviour, where the ventricular bands were included as a second pair of masses, located downstream from a traditional two-mass model of the vocal folds. The oscillation of the ventricular bands would be driven by the glottal jet.

7.3.2 Present work

Most recently Bailly *et al*[Bailly *et al.*, 2008] have succeeded in computationally simulating the period-doubling effect by including a new aerodynamic component in a traditional two-mass model of the vocal folds, coupled to a simple one-mass model of the ventricular bands. The model has sought to explain the origin of the aerodynamic contribution to the driving force on the ventricular bands in more detail, by examining three distinct hypotheses for the behaviour of the glottal jet. The proposed jet models are: a *uniform jet*, a *laminar jet* and a *turbulent jet*. Each model assumes a different behaviour for the expansion of the jet after it has separated from the vocal folds, up to the point where it impinges on the ventricular bands, resulting in an estimation of a pressure drop along the jet ΔP_{jet}. Extensive details regarding the computational implementation of these models may be found in Bailly *et al*[Bailly *et al.*, 2008], but a summary of the main points is presented here.

P_0	Total upstream overpressure
U	Volume flow
L_{VF}	Vocal fold length (along x dimension)
L_{VB}	Distance between minimum vocal fold and minimum ventricular band constrictions
u_{VF}	Jet velocity at flow separation from the vocal folds
u_{core}	Jet velocity in the core of the separated jet (measurable anywhere along the jet)
x_0	Streamwise position of the upstream end of the vocal folds
x_{S1}	Streamwise position of the flow separation point on the vocal folds
x_R	Streamwise position of the start of the ventricular bands
h_0	Height at entrance to valve (i.e. height of trachea)
h_{VF}	Minimum vocal fold separation height
h_{S1}	Jet height at flow separation point
h_R	Jet height at start of ventricular bands
h_{VB}	Minimum separation of the ventricular bands
A_0	Cross-sectional area at entrance to valve (i.e. cross-sectional area of trachea)
A_{VF}	Minimum cross-sectional area between the vocal folds ($= h_{VF} \cdot W_{VF}$)
A_{S1}	Jet cross-sectional area at flow separation ($= h_{S1} \cdot W_{VF}$)
A_R	Jet cross-sectional area at start of ventricular bands ($= h_R \cdot W_R$)
A_{VB}	Minimum cross-sectional area of the ventricular bands ($= h_{VB} \cdot W_{VT}$)
W_{VF}	Vocal fold width (along z dimension)
W_R	Width of jet at start of ventricular bands
W_{VT}	Width of the vocal tract (along z dimension)
θ_{jet}	Half-angle of the turbulent jet expansion
ΔP_{VF}	Pressure drop across the vocal folds
ΔP_{jet}	Pressure drop along the glottal jet
ΔP_{VB}	Pressure drop across the ventricular bands

Table 7.2: A summary of the mechanical and fluid mechanical quantities relevant to the formulation of the three glottal jet hypotheses (see figure 7.1), and discussion of the PIV results.

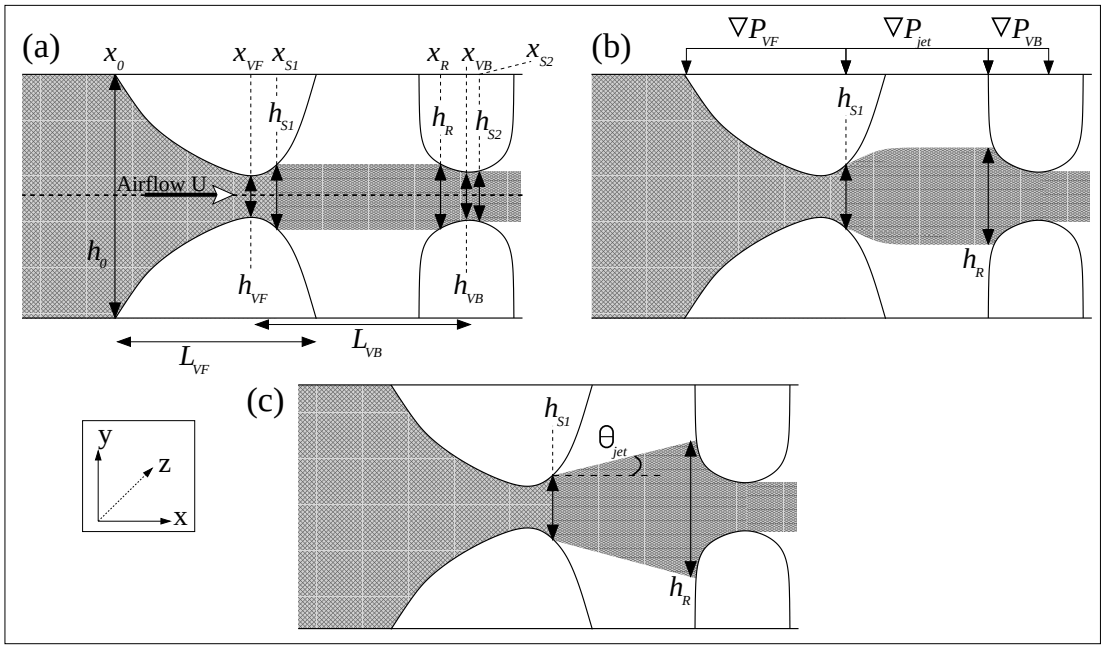

Figure 7.1: Three proposed hypotheses of the jet behaviour following separation from the vocal folds: (a) Uniform jet (b) Laminar jet (c) Turbulent jet (after Bailly *et al*[Bailly *et al.*, 2006]).

Figure 7.1 illustrates the three proposed jet models. The purpose of each model is to predict the degree of jet expansion over the distance between the flow separation point on the vocal folds (located at x_{S1}, with a cross-sectional area A_{S1}), and the flow reattachment on the upstream face of the ventricular bands (located at x_R, with a cross-sectional area A_R). The degree of jet expansion then determines the value of the pressure drop ΔP_{jet} along the jet, as calculated by the quasi-steady Bernoulli equation

$$\Delta P_{jet} = -\frac{\rho U^2}{2A_{S1}^2}\left[2\frac{A_{S1}}{A_R}\left(1-\frac{A_{S1}}{A_R}\right)\right]. \tag{7.1}$$

(a) Uniform jet

The uniform jet hypothesis assumes that the jet does not expand at all as it traverses the laryngeal ventricle. The jet cross-section at the flow reattachment point (x_R) is thus equal to the cross-section at flow separation

$$A_R = A_{S1} = h_{S1} \cdot W_{VF}. \tag{7.2}$$

The cross-sectional area (A_{S1}) is obtained by multiplication of the open height h_{S1} (shown in figure 7.1) with the glottal width W_{VF} (see also figure 2.5). The jet does not expand in the out-of-plane z dimension. The pressure drop along the jet ΔP_{jet}, according to equation 7.1, is thus 0Pa.

(b) Laminar jet

The laminar jet hypothesis considers the glottal jet to be a free shear layer passing through a stationary surrounding fluid. Under this assumption the jet expands non-linearly as it travels towards the ventricular bands, so that at the reattachment point x_R the jet cross section may be calculated as

$$A_R = A_{S1} + 21.8 \cdot W_{VF} \left(\frac{U^2}{A_{S1}} \right)^{-\frac{1}{3}} \cdot \nu^{\frac{2}{3}} \cdot (x_R - x_{S1})^{\frac{2}{3}} \tag{7.3}$$

where U is the volume flow and ν is the kinematic viscosity. As with the uniform jet, expansion is assumed to be confined to the transverse y dimension, with no out-of-plane z-wise expansion. The jet width at the ventricular bands is thus assumed to be equal to the width at flow separation from the vocal folds, W_{VF}.

(c) Turbulent jet

The turbulent jet hypothesis considers the jet to behave like a free turbulent plane jet[Kundu, 1990]. Under this assumption the jet expands linearly at a half angle θ_{jet} of 4°. The jet cross-section at reattachment is calculated as

$$A_R = (h_{s1} + 2 \cdot \tan 4^\circ \cdot (x_R - x_{S1})) \cdot W_{VT}. \tag{7.4}$$

The jet expands in the out-of-plane z dimension as well as the y dimension shown in figure 7.1 part (c). Equation 7.4 implicitly assumes that the expansion leads to the jet stretching precisely across the vocal tract width W_{VT} (along the z axis) as it reaches the start of the ventricular bands at x_R.

The overall vocal fold - ventricular band model

In the computational implementation of the overall vocal fold - ventricular band system the first objective is to predict the cross-sectional area of the jet at various points along its development. Most important is the jet cross-section at separation, A_{S1}; reattachment to the ventricular bands, A_R; and secondary separation from the downstream end of the ventricular bands, A_{S2}.

Knowledge of the jet cross-section, together with the assumption that the flow may be described by the Bernoulli equation, allows the total pressure at each of these crucial locations to also be calculated (P_{S1}, P_R and P_{S2}). As part of the computational implementation, the volume flow through the system U must also be calculated. Definitions of these quantities have been summarised in table 7.2.

A flow separation model is used to estimate the flow separation points x_{S1} and x_{S2}, leading to estimates of the jet cross-sections (A_{S1} and A_{S2}). One of the three jet expansion hypotheses is then used to compute the jet cross-section at reattachment

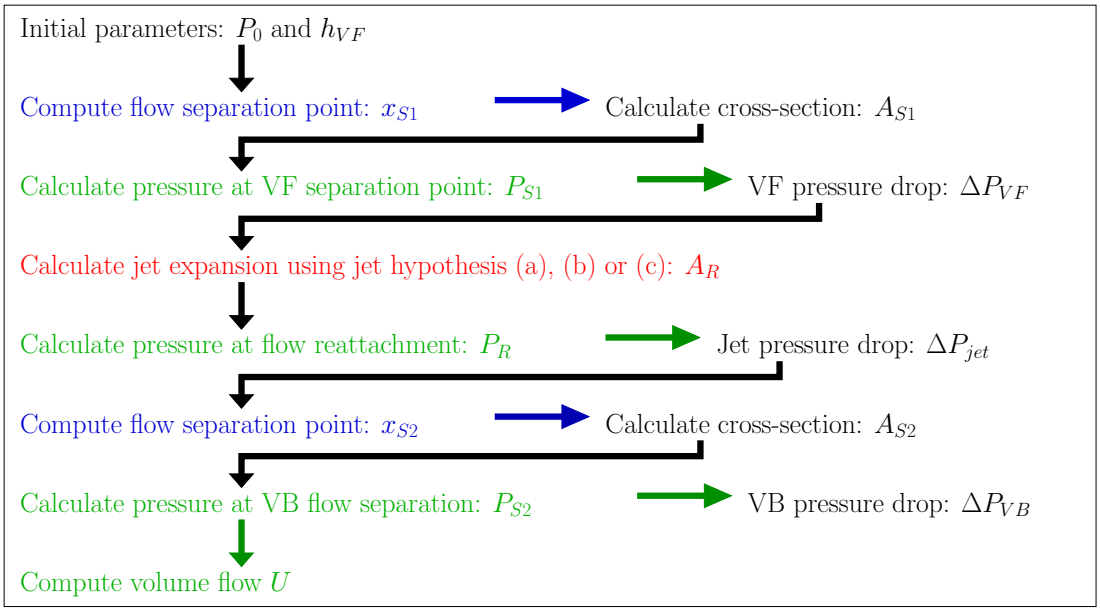

Figure 7.2: A signal flow diagram of the computational implementation of the vocal fold - ventricular band system. Blue text indicates a flow separation calculation, red text indicates a calculation using one of the jet expansion hypotheses, green text indicates a Bernoulli calculation.

(A_R), based on its cross-section at separation from the vocal folds. Formulations of the Bernoulli equation are used to compute the volume flow U and the total pressure at each point along the jet. A signal flow diagram of the overall process is shown in figure 7.2.

The pressure drops across the vocal folds and the ventricular bands are computed using a quasi-stationary Bernoulli formulation, as described in section 2.5.3. The pressure drop across the vocal folds is repeated here for convenience

$$\Delta P_{VF} = P_0 - P_{S1} = \frac{\rho U^2}{2(A_{S1}^2 - A_0^2)}. \tag{7.5}$$

The flow separation point x_{S1}, which leads to a calculation of the cross-sectional area A_{S1}, is determined by a numerical solution to the boundary layer description[Pelorson *et al.*, 1994; Ruty *et al.*, 2007].

The pressure drop across the ventricular bands is described by

$$\Delta P_{VB} = P_R - P_{atm} = \frac{\rho U^2}{2(A_{S2}^2 - A_R^2)}. \tag{7.6}$$

The flow separation point from the ventricular bands may be calculated either by a numerical solution to the boundary layer flow, or by use of the Liljencrants semi-empirical formulation[Liljencrants, 1989]. It is assumed that following the secondary

separation from the ventricular bands the flow disintegrates with a total loss of pressure.

The overall vocal fold - ventricular band system is thus comprised of three discrete pressure drops, ΔP_{VF} (vocal folds), ΔP_{jet} (jet) and ΔP_{VB} (ventricular bands), which combine to produce a total pressure drop across the system of ΔP, such that

$$\Delta P = \Delta P_{VF} + \Delta P_{jet} + \Delta P_{VB} = P_0. \tag{7.7}$$

The three pressure drops are coupled together by computation of the cross-sectional area at flow separation from the vocal folds (A_{S1}), and the cross-sectional area at flow reattachment (A_R). This process is performed iteratively, with the acoustic propagation also taken into account.

Full-scale simulations were not performed as part of the present work. The preceding commentary has been included so as to outline the relevant theoretical jet expansion models, which will be tested by the experiments presented in this work.

7.4 Analysis methods for phase windowed PIV data

7.4.1 Overview of approaches

The overall approach to the processing and analysis of the PIV data was essentially a three step procedure:

1. Obtain approximately 200-300 vector maps distributed evenly throughout the cycle of oscillation.

2. Average the data into ten evenly spaced intervals, known as phase windows (see also section 6.5.3). This provided ten phase averaged vector maps for each configuration that described the entire cycle of oscillation. A synchronisation process allowed the open area and open height of the vocal folds to be deduced for each phase window, so that the fluid behaviour could be observed as a function of the vocal fold motion (see section 6.5.2).

3. Perform analysis on the phase windowed vector maps. A number of techniques were used to study the phase windowed velocity vector maps in detail. These techniques included methods that considered the overall development of the full velocity field, as well as methods that examined small regions of the flow. The former of these approaches was useful for describing the overall behaviour, and for the identification of obvious features in the flow such as vortices. The latter branch of techniques was then useful for examining the behaviour of specific features of the flow, such as the main core of the jet, or its shear layers.

There were two key objectives for the analysis tools presented in part III of this thesis. The first was to characterise the basic flow behaviour of the pulsatile jet

through the vocal folds, as exemplified by the free jet configuration. The second was to investigate the effect of the rigid ventricular bands on the behaviour of the glottal jet. The first objective was important in terms of forming a general understanding of the behaviour of the replica and the surrounding flow field. The second objective sought to find evidence for the aerodynamic influence of the ventricular bands on the jet which has been discussed above in section 7.3.

7.4.2 Comparison between the measured jet velocity field and a simplified Bernoulli calculation

It was important to test the validity of the theoretical description of the vocal fold - ventricular band system presented in section 7.3 in a general way. The theory postulates that the glottal jet encounters a degree of pressure recovery due to a reattachment of the flow on the ventricular bands. This was tested by comparing the velocity field measured by PIV with a theoretical velocity field, resulting from a simplified Bernoulli calculation which assumed a total loss of pressure upstream of the ventricular bands (as in table 7.1).

The objective was to test, in the simplest possible manner, whether the ventricular bands appeared to alter the jet speed relative to the simplified assumption. In section 7.4.5 a non-dimensional term known as the *normalised jet core velocity* is introduced to quantify this effect.

7.4.3 Investigation of the three jet expansion hypotheses

Three possible descriptions of the glottal jet have been outlined in section 7.3, as suggested by Bailly *et al*[Bailly *et al.*, 2008]; the uniform jet, the laminar jet and the turbulent jet. These hypotheses have been designed to be incorporated into a larger computational model of the vocal folds - ventricular bands system.

The computational implementation of the hypotheses functions by taking a small set of input parameters (the minimum glottal height h_{VF} and the upstream pressure P_0) and calculating the flow separation from the vocal folds using a boundary layer flow separation model. The degree of jet expansion between the flow separation point and the flow reattachment to the ventricular bands is then calculated using the geometrical jet expansion descriptions outlined in section 7.3.2. This results in an estimation of the jet cross-section at flow reattachment.

Verification of the jet expansion theories

One of the important benefits of PIV is the full field nature of the velocity measurement. In the present application PIV measurements were made of the laryngeal ventricle, located between the vocal folds and the ventricular bands. It was possible to observe the

glottal jet from approximately 8mm downstream from the vocal folds to the upstream edge of the replica ventricular bands. This allowed an estimation to be made of the jet width just before it impinged onto the ventricular bands, known as h_R. Together with the knowledge of the time-varying glottal open height h_{VF} (see figure 7.1 and table 7.2), a comparison could thus be made between the theoretical jet expansions and the experimentally observed jet expansions.

There were three different configurations of the vocal folds - ventricular bands system; the free jet, realistic ($VB-A$) and impeding ($VB-B$) configurations (see section 6.3.2 for more details). Three different hypotheses were proposed for the behaviour of the jet downstream of the vocal folds. There were thus nine different scenarios to investigate.

Each jet expansion hypothesis was used to compute a theoretical estimate of the jet cross-section at the ventricular bands, based on input parameters measured from the experimental setup such as the total upstream pressure P_0 and the vocal fold open area A_{VF} (obtained by multiplication of the open height h_{VF} with the z-wise width W_{VF}, see figure 2.5). In the case of the uniform and laminar hypotheses the calculation assumed that the jet expansion was confined to the $x-y$ plane. This meant that the width of the jet in the z dimension was assumed to remain constant throughout the expansion. Thus the z-wise jet width at the ventricular bands was assumed to be the same as at the vocal folds, namely W_{VF}.

In the case of the turbulent jet it was assumed that the jet expanded in the z-wise direction as it traversed the laryngeal cavity. The z-wise expansion was assumed to be linear and at such a rate that the jet width at the ventricular bands was precisely equal to the width of the vocal tract, namely W_{VT}.

Figure 7.3 shows a photograph of the *in vitro* setup used in this study. It provides a visual description of the width of the vocal folds W_{VF} and the width of the vocal tract W_{VT} as they relate to the theoretical calculation of the jet expansion.

In the following sections further details regarding the theoretical and experimental estimates of the jet cross-section are outlined. A summary of the various theoretical and experimental calculations of the jet expansion is given in table 7.3.

The uniform jet hypothesis

The uniform jet was the simplest scenario. It assumed that the jet did not expand in any dimension as it travelled through the laryngeal cavity. The cross-sectional area of the jet at the ventricular bands, A_R, was thus assumed to be the same as at flow separation, A_{S1}. The *ad hoc* Liljencrants[Liljencrants, 1989] condition was applied to estimate the cross-section of the jet at flow separation, based on the measured cross-sectional area of the vocal fold opening. This meant that the jet cross-section at the ventricular bands was simulated as

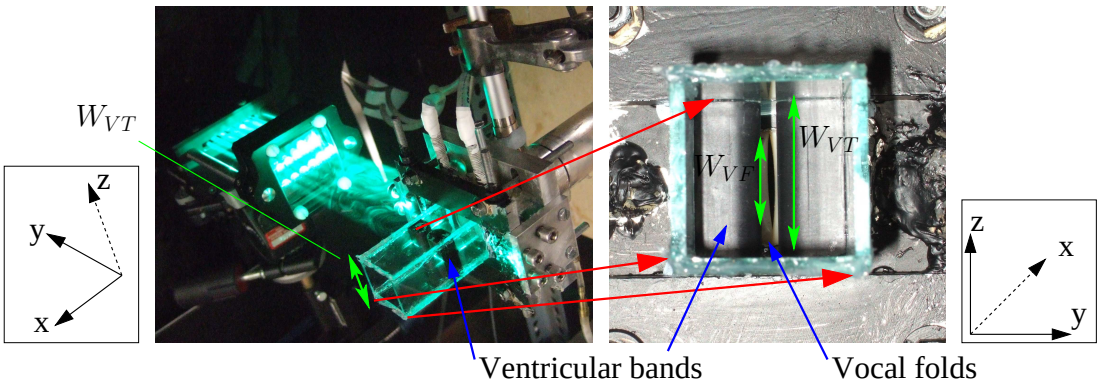

Figure 7.3: Photographs of the *in vitro* vocal folds and ventricular bands of replica C, illustrating the position of the ventricular bands within the vocal tract, and the orientation of the out-of-plane z dimension, into which the turbulent jet was assumed to expand. The jet separated from the vocal folds at a width W_{VF} and expanded to fill W_{VT} when it reached the ventricular bands.

$$\begin{aligned} A_R &= A_{S1} \\ &= 1.2 \cdot h_{VF} \cdot W_{VF}. \end{aligned} \tag{7.8}$$

Where full computational simulations of the vocal folds - ventricular bands system have been performed, A_R would be calculated from the theoretical h_{VF} signal. In the present work no full-scale simulations were performed. The **theoretical estimate** of the uniform jet expansion was thus obtained from experimental measurement of the vocal fold open height h_{VF} and width W_{VF}, as measured during the synchronisation process (see section 6.5.2). In the description of results presented in section 8.5.1, the theoretical prediction of the jet expansion under the uniform jet hypothesis is referred to as **THY-UNI** (theoretical uniform). Note that under the uniform jet condition, and neglecting any viscous losses, no pressure was expected to be lost in the jet ($\Delta P_{jet} = 0$ in figure 7.1).

An **experimental estimate** of the jet expansion was made that could be compared to **THY-UNI**. This was obtained by estimating the height of the jet at the extreme downstream end of the observable region, which was located at the start of the ventricular bands constriction. By multiplying this experimentally measured jet height with the experimentally measured vocal fold width along the z axis, an estimate of the jet cross-section at flow reattachment was achieved. This method implicitly assumed no z-wise expansion of the jet, as with the theoretical uniform jet hypothesis (**THY-UNI**) outlined above.

The experimental estimate of the jet cross-section according to the uniform

Expansion theory	**z-wise jet expansion** (vocal folds→ ventricular bands)	**$x-y$ plane expansion** determined by
	Theoretical predictions	
Uniform jet **THY-UNI**	$W_{VF} \rightarrow W_{VF}$	Equation 7.2
Laminar jet **THY-LAM**	$W_{VF} \rightarrow W_{VF}$	Equation 7.3
Turbulent jet **THY-TURB**	$W_{VF} \rightarrow W_{VT}$	Equation 7.4
	Experimental measurements	
Uniform jet **EXP-UNI/LAM**	$W_{VF} \rightarrow W_{VF}$	h_R, estimated from PIV data
Laminar jet **EXP-UNI/LAM**	$W_{VF} \rightarrow W_{VF}$	h_R, estimated from PIV data
Turbulent jet **EXP-TURB**	$W_{VF} \rightarrow W_{VT}$	h_R, estimated from PIV data

Table 7.3: A table summarising the theoretically and experimentally derived calculations of the jet expansion. Each jet expansion hypothesis can be investigated using either the theoretical predictions (top half of the table), or from the measurements of the experimental PIV data (lower half of the table). See figure 7.1 for an overview of the jet hypotheses and details of the jet dimensions.

expansion hypothesis was obtained in precisely the same manner for the laminar jet hypothesis outlined below, as both hypotheses shared the common assumption of no z-wise expansion of the jet. It is thus referred to as **EXP-UNI/LAM** (experimental uniform/laminar) in the results described in section 8.5.1.

The laminar jet hypothesis

The laminar jet expansion theory was the most sophisticated hypothesis, as it was determined by both the cross-sectional area of the jet at flow separation, and by the volume flow of the jet (see equation 7.3).

A **theoretical estimate** of the jet cross-section at the ventricular bands was achieved by providing the laminar expansion formula (see equation 7.3) with both an experimental measurement of the upstream overpressure P_0, and an experimentally determined estimate of the volume flow U_{VF}. The volume flow was estimated by spatially integrating the flow velocity across the entire flow field, and assuming no z-wise expansion of the jet. The resulting theoretically simulated prediction of the jet expansion is referred to **THY-LAM** (theoretical laminar).

An **experimentally derived** measurement of the jet cross-section according to the laminar jet hypothesis was obtained in the same manner as for the uniform jet hypothesis outlined above. An estimate of the jet height h_R at the ventricular bands

was first made from the experimental data. This jet height was then multiplied by the z-wise width of the jet. As with the uniform expansion theory, it was assumed that no z-wise expansion of the jet occurred. The jet width at the measurement point of the jet height was thus assumed to be W_{VF}. This estimate of the jet cross-section is referred to as **EXP-UNI/LAM** (experimental uniform/laminar).

The turbulent jet hypothesis

The turbulent jet hypothesis predicted the jet expansion by taking the cross-section of the jet at flow separation and adding a linear growth factor (see equation 7.4). Under this hypothesis the jet was assumed to grow linearly in both the in-plane y dimension, and in the out-of-plane z-wise axis.

The jet cross-section at separation from the vocal folds was calculated as for the uniform and laminar hypotheses, by using the Liljencrants condition. The z-wise width was taken to be W_{VF} at the vocal folds (typical values were between 10mm and 20mm, depending on the configuration). The jet was assumed to expand linearly in the z-dimension so as to stretch precisely across the width W_{VT} of the vocal tract at the flow reattachment on the upstream face of the ventricular bands ($W_{VT} = 25$mm in the present case, c.f. figure 2.5). Figure 7.3 shows the relevant vocal fold and vocal tract dimensions.

A **theoretical prediction** of the jet expansion according to the turbulent jet hypothesis was obtained by simulating the turbulent expansion expression described by equation 7.4 in Matlab. This equation called for the height of the jet at flow separation, h_{sep}. This data was not measured directly during the experiments, but was estimated by multiplication of the vocal fold separation with the semi-empirical Liljencrants[Liljencrants, 1989] parameter ($h_{sep} = 1.2 \cdot h_{VF}$). The vocal fold separation signal h_{VF}, also known as the minimum vocal fold open height, was obtained for each phase window throughout the cycle, and for each ventricular band configuration, during the PIV synchronisation process (see section 6.5.2). The jet expansion prediction according to the theoretical hypothesis is referred to as **THY-TURB** (theoretical turbulent) in section 8.5.1.

An **experimental estimate** of the jet expansion according to the turbulent hypothesis was achieved by estimating the jet cross-section from the experimental PIV data at the start of the ventricular band constriction. This was done by estimating the height of the jet h_R, and multiplying it by the hypothesised z-wise width of the jet at the ventricular bands, namely W_{VT}. As with the theoretical prediction outlined above, the jet was assumed to expand linearly in the z-axis between a width of W_{VF} at flow separation to a width of W_{VT} at flow reattachment on the ventricular bands. In the resulted described in section 8.5.1 the experimentally estimated value of the jet cross-section at the ventricular bands is referred to as **EXP-TURB** (experimental

turbulent).

7.4.4 Analysis of the jet core and the surrounding fluid

The core of a free jet is typically seen as a region of high speed flow, located in and around the centre of the separated jet[Schlichting and Gersten, 2000]. It contains low levels of rotation, and thus low levels of vorticity, as it is contained within bounding regions of high vorticity known as shear layers. As long as the jet core forms a cohesive structure it convects fluid downstream at a velocity close to that at flow separation.

The jet core may be expected to persist for a distance of approximately seven times the bounding channel diameter at flow separation[Sinder, 1999; Agarwal, 2004; Schlichting and Gersten, 2000]. In the present work this lead to a jet core persistence range L_{core} of between 3.5mm (at phase window 9, the minimum glottal separation) and 17.5mm from the vocal folds (at phase window 4, the maximum glottal separation). Note that this criteria has been suggested based on empirical results in the noted references, and as such is included to provide only an order of magnitude estimate for the persistence range of the jet core.

The uppermost portion of the velocity data in the figures was located approximately 8mm downstream from the vocal folds. This meant that it was likely that only the tail end of the main jet core was visible in the PIV maps. Based on the criteria outlined above it was estimated that a clear jet core would be visible in the PIV data when the glottal opening was approximately 1.1mm or larger. The estimated jet core persistence range suggested that the jet core would oscillate in and out of the observable region of the PIV maps over the course of the glottal cycle. It was thus anticipated that a large part of the vector maps contained the jet deceleration and turbulent mixing zones.

The work in this section provides an overview of the analysis tools used to investigate the region of high jet velocity visible in many of the PIV maps. This region was located close to the glottal centreline at the upstream end of the measurable field of view. An initial assumption was made that this region formed the tail end of the jet core.

Velocity magnitude and standard deviation contour plots

Figure 7.4 shows four plots of the glottal jet formed during self-sustained oscillations of the vocal folds under the free jet configuration. The upper two plots show the the velocity magnitude and standard deviation of velocity magnitude for phase window 4 (close to maximum vocal fold open height). The lower two plots show the same quantities for phase window 8 (close to minimum vocal fold open height). It is important to explain what these plots display.

The velocity magnitude plots shown on the left half of the figure provide a direct picture of the spatial distribution of fluid velocity within jet and surrounding flow field, averaged from the constituent vector maps within each phase window. Orange and

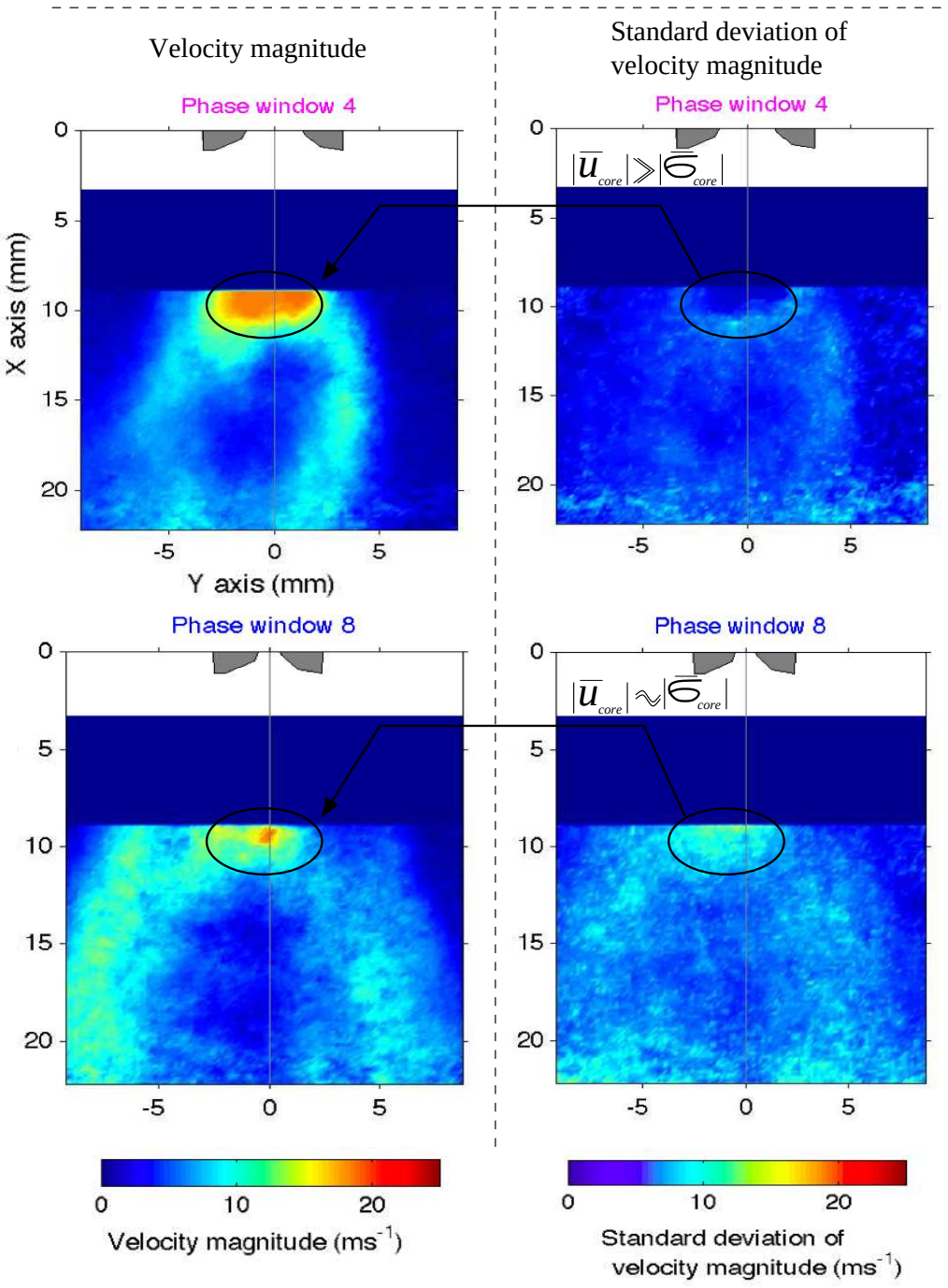

Figure 7.4: Velocity magnitude and standard deviation plots of phase window 4 (close to the maximum vocal fold opening, low jet acceleration) and phase window 8 (just before the minimum vocal fold opening, strong jet deceleration) for the free jet configuration. The jet core region has been circled for each phase window. $\bar{u}_{core}$ represents the average phase windowed jet core velocity, $\bar{\sigma}_{core}$ represents the average standard deviation of the velocity magnitude in the the jet core region.

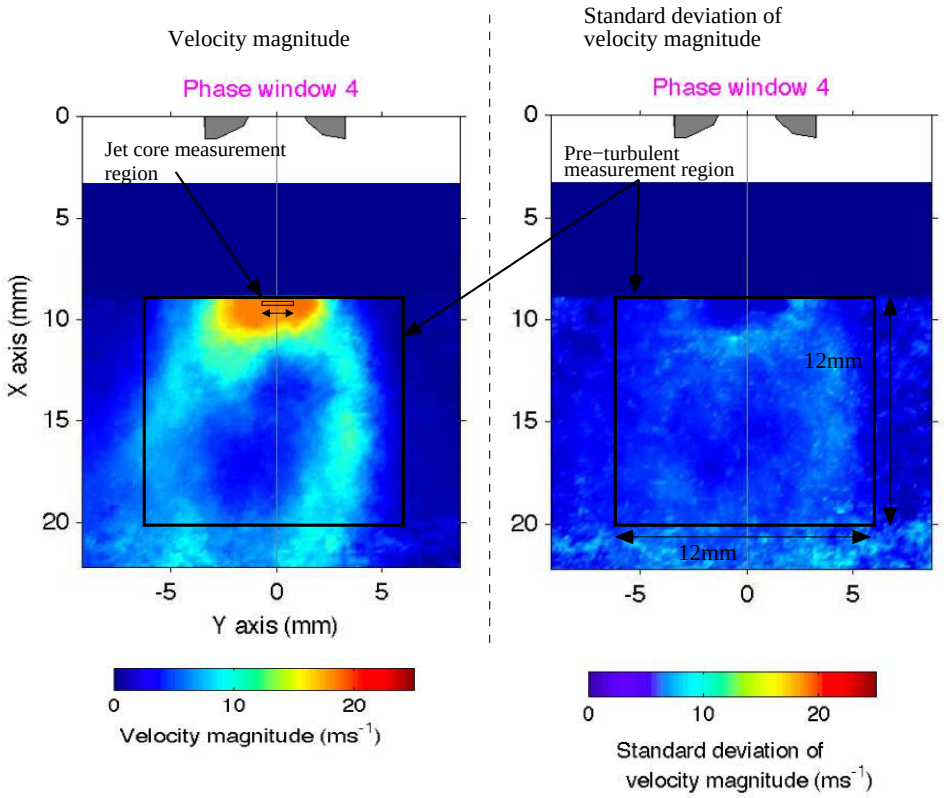

Figure 7.5: Velocity magnitude and standard deviation plots of phase window 4, showing the areas used to compute the average standard deviation velocities for the pre-turbulent and jet core regions at each phase window.

red areas indicate high velocity, up to a maximum measurable limit of approximately 25ms^{-1}. Blue areas indicate low velocity, typically down to a few metres per second.

The right hand half of figure 7.4 shows contour plots of the standard deviation of velocity magnitude. A standard deviation velocity contour plot of a phase windowed vector map provides a measure of the overall similarity of the constituent, individual vector maps, to the averaged sum of all the maps within the phase window (i.e. the phase windowed data itself). This in turn provides a useful tool for assessing the stability and consistency of the flow during each of the phase windows. The mathematical formulation used to calculate the standard deviation of a phase window has been outlined in sectoin 6.5.3 and equation 6.1.

A low standard deviation for a particular vector from a phase windowed vector map indicates that the constituent vectors from the instantaneous vector maps have approximately the same velocity. In the case of a phase windowed PIV velocity map, each constituent vector comes from a different temporal instant, typically spread out over a period of a minute or more. This means that the many measurements of the fluid velocity at the particular spatial location and phase of the glottal cycle closely

Variable	Definition	Range of values
$\bar{u}_{core}$	Average jet core velocity	5 - 22 ms^{-1}
$\bar{\sigma}_{core}$	Standard deviation of the average jet core velocity	2 - 14 ms^{-1}
$\bar{\sigma}_{PT}$	Average standard deviation velocity of the pre-turbulent region	4 - 6 ms^{-1}
$d\bar{u}_{core}$ / dt	Average jet core acceleration	-5 - 5 ms^{-2}
u_{VF}	Predicted jet velocity at flow separation (using Bernoulli equation)	27ms^{-1}

Table 7.4: A summary of the four key variables used to describe the jet core and pre-turbulent region, as calculated from the phase windowed PIV velocity magnitude and standard deviation maps. The range of values correspond to those encountered with the free jet configuration described in the present section.

match each other. The resulting implication is that at such a phase window the jet flow is highly repeatable, and thus rather stable. Plots of the standard deviation of an entire velocity field thus yields information about where the flow is stable, giving a low standard deviation, or rather unstable and even turbulent, giving a high standard deviation.

Figure 7.4 indicates one of the important dynamic behaviours encountered over the course of a glottal cycle, namely that of a clear or unclear jet core. At phase window 4 the core can clearly be see as a region of high velocity magnitude and low standard deviation. This indicates a highly stable phase of the jet flow. At phase window 8 the standard deviation velocity magnitude has risen sharply, so as to become comparable to the mean jet core velocity. This is indicative of an unstable phase of the jet oscillation cycle, where the constituent instantaneous PIV vector maps within a phase window differ significantly from each other.

Variables to describe the time-evolution of the jet core and surrounding flow field

It was important to investigate the validity and behaviour of the apparent 'jet core' located at the top of the optically accessible region visible for all phase windows. This was because the estimate of the jet core persistence range outlined at the start of the present section 7.4.4 suggested that the true jet core would only be observable when the vocal fold opening was greater than about 1.1mm.

Calculation of the standard deviation of velocity magnitude provided the first step in the analysis of the jet core region (see equation 6.1). This initial calculation was performed for the entire field, providing a standard deviation velocity map for each phase window.

Two key areas of the jet were identified as worthy of quantified analysis. The first

of these was the jet core region. A small sliver approximately 2mm wide was taken as being representative of the jet core. This area has been marked in figure 7.5, which shows velocity magnitude and standard deviation of velocity magnitude maps for phase window 4 of the free jet configuration. This central region of the jet was taken to be representative of the typical jet core velocity at each phase window.

The jet core measurement region included approximately six individual velocity vectors. An average jet core velocity $\bar{u}_{core}$ was calculated from these vectors, along with an average standard deviation velocity $\bar{\sigma}_{core}$. The time-derivate of the average jet core velocity $d\bar{u}_{core}$ / dt provided a measure of the jet acceleration. Finally, a theoretical prediction of the jet velocity at flow separation from the vocal folds u_{VF} was calculated, based on the assumption of a total loss of pressure downstream of the vocal folds. This provided a rough measure of the upper limited of the likely jet velocities. Together, these four parameters provided the principle analysis tools used to investigate the behaviour of the jet core.

Figure 7.5 also shows a larger second boxed area, labeled as the 'pre-turbulent' region. This area encompassed a region of 12mm by 12mm, and was drawn so as to include all the major features of the jet at each phase window. The upstream limit was located 8mm downstream from the vocal folds, and the downstream limit was located just before the clearly identifiable region of turbulent mixing. This start of this highly turbulent region can be seen in figure 7.5 commencing from approximately 20mm downstream of the vocal folds. Evaluation of the average standard deviation velocity $\bar{\sigma}PT$ of this pre-turbulent region quantified the general stability of the overall flow field at each phase window.

The five quantities outlined above were termed 'jet variables'. A summary of these jet variables, together with a range of their typical values, is presented in table 7.4. In chapter 8 jet variables are used to analyse and compare the three vocal folds - ventricular bands configurations. The variables are plotted together as a function of time, and in parametric plots as functions of each other.

7.4.5 Non-dimensional analysis of the glottal flow fields

The general theory proposed for the aerodynamic interaction between the vocal folds and the ventricular bands, outlined in section 7.3.2, hypotheses that the separated glottal jet may undergo a reattachment on the upstream walls of the ventricular bands. A reattachment could lead to a recovery of pressure in the jet, in direct opposition to the total pressure loss expected to occur quite quickly in the absence of any downstream constriction[Hirschberg, 1992]. A reattachment of the flow could imply an increase in the overall jet stability, due to the possible 're-laminarisation' of the jet core, which once again lies in contrast to the turbulent disintegration expected of a free glottal jet.

One of the main objectives of the work described in part III of this thesis is to

compare the overall behaviour of the glottal jet for different downstream configurations, in an attempt to quantify the true effect of the ventricular bands.

Jet core analysis using the jet variables described in section 7.4.4 provided the starting point for the development and testing of analysis tools targeted at this objective. Tools such as calculation of the standard deviation of the jet core velocity, and parametric plotting of the four jet variables, are applied to the free jet configuration in section 8.2. This provided a useful overview of the basic behaviour of the glottal jet. These are further applied in sections 8.3 and 8.4 to the two ventricular band configurations, in order to provide an overview of the important differences encountered in the character of the jet due to the presence of the ventricular bands.

In order to allow a more universally acceptable comparison to be made between the various flow conditions encountered throughout the vocal fold oscillation cycle it was necessary to non-dimensionalise the jet variables. This was also crucial to allow deeper comparisons to be made between the different configurations, as it effectively normalised the mechanical and fluid mechanical conditions to each other. Such an approach is standard in most fluid mechanics experiments[Tritton, 1988; Grant, 1997]. In section 8.5.2 a detailed analysis of the three configurations using non-dimensionalised variables is presented. It represtents the most important piece of analysis in the story told by part III of this thesis.

Non-dimensionalised vocal fold open height

The vocal fold open height throughout the glottal cycle was normalised to the maximum vocal fold separation for each configuration, yielding a non-dimensional vocal fold separation parameter h_{norm}. This was calculated as

$$h_{norm} = \frac{h_{VF}}{h_{max}} \tag{7.9}$$

from the terminology shown in figure 7.1 and table 7.2.

The normalised vocal fold separation thus took values between zero and one over the course of the glottal cycle.

Reynolds number of the jet core

The Reynolds number is a useful parameter for assessing the likelihood of encountering turbulence in a flow. Its definition has been outlined in section 2.5.1, but is repeated here for the specific case of the glottal jet core

$$Re_{core} = \frac{h_{VF} \cdot u_{core}}{\mu} \tag{7.10}$$

where $\bar{u}_{core}$ is the experimentally measured average jet core velocity recorded 8mm downstream of the vocal folds, h_{VF} is the minimum glottal channel height (see figure

7.1 and table 7.2) and μ is the fluid viscosity.

The Reynolds number provides a measure of the importance of viscosity in the flow. It is formed from a ratio of the inertial forces in the flow to the viscous forces. Under a moderately high Reynolds number condition (Re $> 10^3$) the flow may be treated as inviscid, such that the viscosity in the bulk of the flow is neglected. In most computational modeling of musical valves this condition is assumed up to the point of flow separation, with the exception of thin boundary layers at the walls where a fully viscous description is needed (see section 2.5.2). It is worth noting that the validity of this assumption during closure of the vocal folds has been extensively questioned[Pelorson *et al.*, 1994; Deverge *et al.*, 2003; McGowan, 1993; Krane and Wei, 2006].

The present PIV measurements allowed a calculation of the Reynolds number at each phase window throughout the glottal cycle. This made possible a direct assessment of the relevance of the inviscid assumption at each phase window. Knowledge of the Reynolds number also permitted the creation of parametric plots involving the other non-dimensional quantities described in this section for each configuration. This greatly aided analysis into the effects of the ventricular bands on the glottal jet.

Normalised jet core velocity

One of the principle hypotheses of the theoretical description of the ventricular bands is that a reattachment of the glottal jet to the upstream surfaces of the ventricular bands may cause a significant pressure recovery in the jet. Under this condition a reduction in the jet velocity and volume flow would be expected, when compared to a simple prediction using the Bernoulli equation and assuming a total loss of pressure.

In order to measure the significance of any alteration to the behaviour of the jet, the average experimentally measured jet core velocity $\bar{u}_{core}$ measured 8mm downstream of the vocal folds (as described in section 7.4.4) was normalised to the jet velocity at flow separation u_{VF}, as predicted by the Bernoulli equation under a quasi-steady assumption with a total loss of pressure. Values of u_{VF} for this calculation have been listed in table 7.1.

The normalised jet core velocity was thus defined as

$$u_{norm} = \frac{\bar{u}_{core}}{u_{VF}} \tag{7.11}$$

where $\bar{u}_{core}$ was the experimentally measured average jet core velocity and u_{VF} was the predicted velocity at flow separation.

It was anticipated that the the measured jet core velocities would be somewhat lower than the predicted velocity at flow separation. Regardless of the influence of the ventricular bands on the flow reattachment, there was a distance of 8mm over which the jet had to travel before impinging upon the secondary constriction.

During this traversal of the laryngeal ventricle the process of momentum transfer was expected to decelerate the jet to some degree. The possibility of a reattachment and a subsequent pressure recovery may then be expected to further retard the jet velocity. The anticipated values of u_{norm} were thus less than one.

Vocal fold flow impedance

The pressure difference across the vocal folds is strictly a function of the volume flow, rather than the jet core velocity. The volume flow, defined in equation 2.18, depends on both the jet velocity and the jet cross-section.

It was possible to estimate the volume flow U_{jet} just upstream of the ventricular bands directly from the PIV measurements. This was achieved by measuring the fluid velocity across the jet as a function of position, and multiplying each velocity vector by the corresponding infinitesimal slice of the jet cross section. Summing together each contribution it was possible to estimate the total volume flow. Estimation of the jet cross-section has been outlined above in section 7.4.3. Together with the upstream static overpressure P_0 an estimate could then be made of the temporal behaviour of the vocal fold flow impedance for each of the configurations

$$Z_{VF} = \frac{P_0}{U_{jet}}. \tag{7.12}$$

The flow impedance provided a quantitative measurement which normalised the volume flow to the upstream driving pressure. It was large when a high driving pressure produced a small volume flow, such as near closure of the vocal folds. Under such a condition the overall system was inefficient at transmitting flow. Similarly, the flow impedance was small when a low driving pressure resulted in a large volume flow. Under such a condition the overall vocal folds - ventricular bands system was efficient at transmitting flow.

The inverse of the impedance, the vocal fold flow admittance, provided an alternative variable, which was large when the driving pressure produced a large flow, and small when the vocal folds admitted a small flow for the given driving pressure. It related essentially the same information as the flow impedance parameter.

Jet core turbulence parameter

The standard deviation of the jet core velocity magnitude provided basic information about the similarity of the constituent vector maps within each phase window. This in turn allowed judgement to be made on the stability of the jet core at each phase window (see section 7.4.4).

For a deeper and more transferable assessment of the flow stability it was necessary to non-dimensionalise the standard deviation velocity $\bar{\sigma}_{core}$ in terms of the average jet

core velocity $\bar{u}_{core}$, and so define a turbulence parameter

$$T_{core} = \frac{\bar{\sigma}_{core}}{\bar{u}_{core}}. \tag{7.13}$$

T_{core} provided a measure of the turbulence in the flow field. It has been shown experimentally that values above about 0.2 are indicative of significant turbulence in the flow[Schlichting and Gersten, 2000].

Evaluation of T_{core} was performed at a distance of approximately 8mm downstream from the vocal folds using velocity vectors located in the centre of the jet core (see figure 7.5), which was the upstream limit of optical access with the PIV setup. The same spatial measurement location was used for all configurations. Analysis of the glottal jet using the turbulence parameter is presented in section 8.5.2.

7.5 Summary

This chapter has provided extensive background details of the flow experiments presented in part III of this thesis. The motivation for working with an *in vitro* vocal fold replica was first outlined in section 7.1.1. Details of the collaboration that was central to the project were then given in section 7.2. An overview of the physics of the vocal folds - ventricular bands system were provided in section 7.3. Experimental tools for analysis of the PIV data have been detailed in section 7.4.

In chapter 8 experimental results are presented that investigate the behaviour of the three configurations. In section 8.6 an analysis of relevance of the results to the case of the lip-reed is presented.

Chapter 8

Application of Particle Image Velocimetry II: Study of the Aerodynamic Interaction between the Vocal Folds and the Ventricular Bands

"*For the truth that can be spoken is not the truth. Yet on the heights of truth one never climbs in vain.*" - W. H. Murray

8.1 Introduction

Part III of this thesis is concerned with experimental investigations into the fluid mechanics of musical valves. In chapter 7 the premise of a flow study into the physics of phonation was presented. The chapter relied extensively on details of the experimental setup provided in chapter 6, and explanation of the principle of particle image velocimetry provided in chapter 5. The relevance of such a study to the case of the lip-reed was outlined, together with extensive details of the experimental analysis procedures.

In this chapter results and analysis from the flow experiments into three *in vitro* vocal folds - ventricular bands configurations are presented. It is important to be conversant with the analysis method of phase windowing described in section 6.5.3, as it is used throughout the analysis contained in this chapter. The bulk of the work is divided into five key sections.

In section 8.2 the free jet configuration is described in detail. Section 8.3 examines the realistic configuration ($VB-A$), paying particular attention to the influence of the

ventricular bands on the glottal jet. Use is made of the jet variables outlined in section 7.4.4. Section 8.4 examines the impeding configuration ($VB - B$) using the same set of analysis tools as for the other two configurations.

A detailed comparative study of the three configurations is presented in section 8.5. This section begins from 8.5.1 with a comparison between the theoretical predictions for the jet expansion (as described in section 7.4.3) and experimentally obtained estimates of the jet expansion. In 8.5.2 the non-dimensional flow parameters developed in section 7.4.5 are used to assess the aerodynamic influence of the ventricular bands on the glottal jet.

Finally, in section 8.6 a discussion about the relevance of the results to the case of the brass playing lip-reed is presented.

8.2 Analysis of the free jet configuration

The free jet configuration presented a useful test case with which to develop analysis methods for use on the other configurations. The lack of any downstream coupling meant that the glottal jet was free to emerge from between the vocal folds, unhindered by any strong downstream acoustic field or aerodynamic interaction with a solid body. The lack of any optically obstructive components also meant that alignment of the light sheet was straightforward, and the risk of fogging (see section 6.4.3) was eliminated. This made the acquisition of high quality raw bitmap images considerably easier than with the other configurations (see section 5.4). For these reasons the free jet configuration was extensively investigated in an attempt to form a basic understanding of the glottal jet dynamics.

8.2.1 Description of the PIV figures

Figures 8.1 and 8.2 show ten phase windowed PIV velocity magnitude plots for the free jet configuration, comprising a full cycle of oscillation. A synchronisation curve is included in each figure, which uses a colour code to show the point in the glottal cycle where each phase window was acquired. The mean jet flow direction is from top to bottom in each plot, along the global x axis (as shown in figure 6.5).

The vocal folds have been marked at the top of each plot as a pair of greyed out regions. The origin of the x axis, at 0mm, has been located at the centreline of the glottis. A grey line extending down the entire y dimension marks this centreline in each plot. The distance between each greyed-out vocal fold has been scaled to exactly describe the minimum glottal open height, as obtained through the post-synchronisation process (see section 6.5.2). The values of the open height are also identified on the vertical axis of the synchronisation curves, with 'PW1' indicative of phase window 1.

8.2.2 Overall behaviour of the free jet

The PIV data shown in figures 8.1 and 8.2 clearly revealed the presence of a strong jet, directed away from the glottis and into the free space of the laboratory. This most basic revelation was expected from the theoretical consideration of vocal fold fluid mechanics described in section 2.5. It was nevertheless a revelation of fundamental significance in terms of the suitability of the present PIV setup to measure the pulsatile glottal jet. The observation of a clearly separated jet with measurable velocity suggested that the approach of using PIV to investigate the fluid behaviour around a self-oscillating valve was a reasonable objective.

Basic elements of the glottal jet

The fundamental make up of the glottal jet was quite consistent for all phase windows. A region of high velocity was observed close to the centreline of the glottis, known as the jet core. Either side of this core the fluid velocity decreased towards the level of the ambient environment. The precise 'fluid boundary condition' of this ambient environment was dependent on the configuration (see also sections 8.3 and 8.4). In the case of the free jet, a region at least 5mm either side of the main jet core was pulled along with the flow, a process known as flow entrainment. In the case of the ventricular band configurations a region of recirculating fluid was frequently observed either side of the main jet (see section 8.5.2). This meant that the exact boundary condition of the ambient fluid was dependent on the coordinate along the x axis.

For some phase windows the jet core became somewhat fragmented and was difficult to visually identify, such as phase window 8 in figure 8.2. For the bulk of the free jet measurements, however, it was a clear feature of the flow.

The process of momentum transfer led to a deceleration and widening of the glottal jet with increasing distance from the vocal folds. This deceleration is clearly visible in the figures as the jet velocity magnitude values progress from around 20ms^{-1} at 8mm from the glottis, to approximately 10ms^{-1} around 13mm from the glottis. Eventually this lead to a total disintegration of the jet structure and a transition to a region of turbulent mixing. This mixing region may be seen throughout the cycle of oscillation as an area of increasingly patchy velocity distribution, commencing at a distance of between 13 and 18mm from the vocal folds.

Figures 8.3 and 8.4 shows the vorticity of the flow for phase windows 1 to 5 and 6-10 respectively, evaluated using the MatPIV software package (see section 5.4.3). Clearly present for all phase windows were two regions of intense vorticity, positioned either side of the main jet core. A positive vorticity value indicates an anti-clockwise rotation, while a negative vorticity indicates a clockwise rotation. These regions of oppositely-sensed rotation were associated with the shear layers of the separated jet. For some phase windows, such as phase windows 4 and 5, there appeared to be a second pair

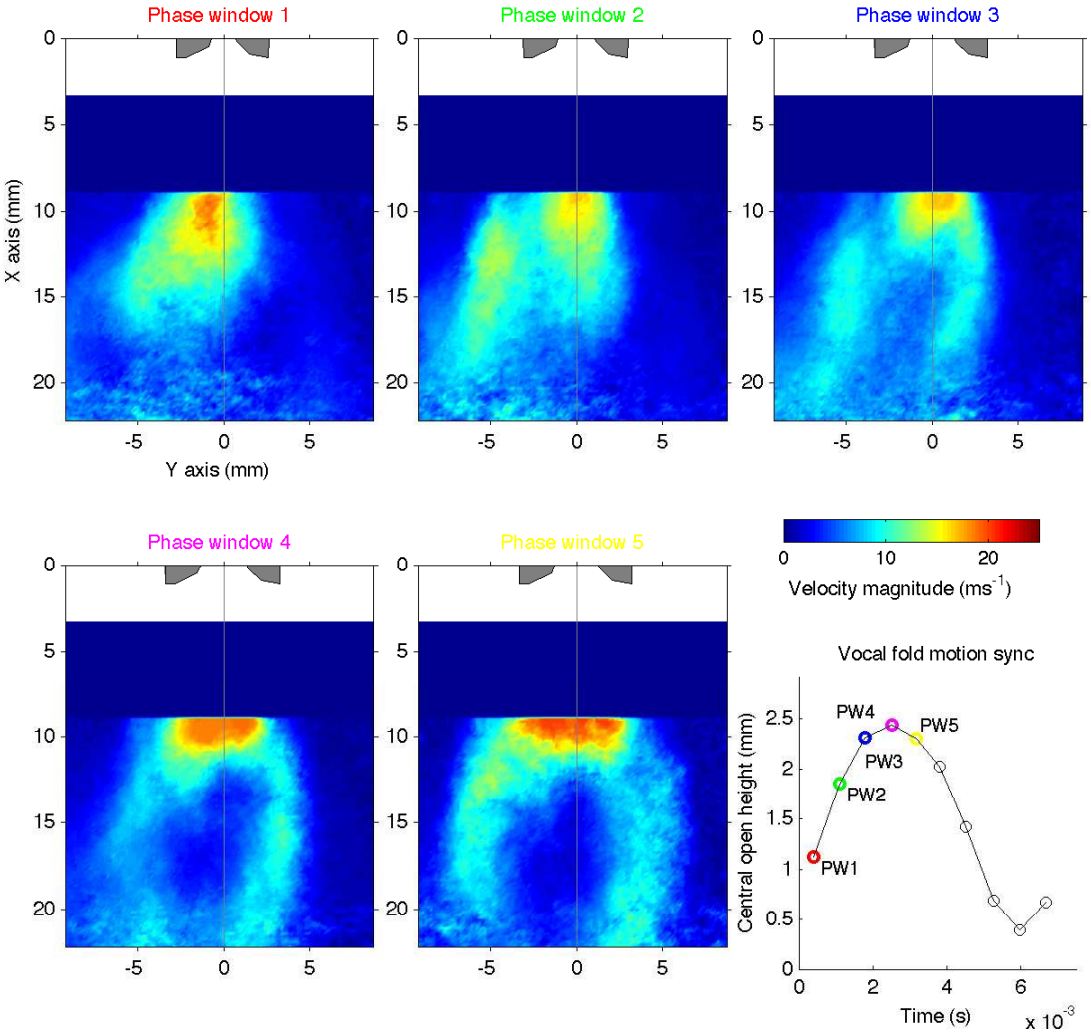

Figure 8.1: Velocity magnitude plots for the free jet configuration for phase windows 1-5.

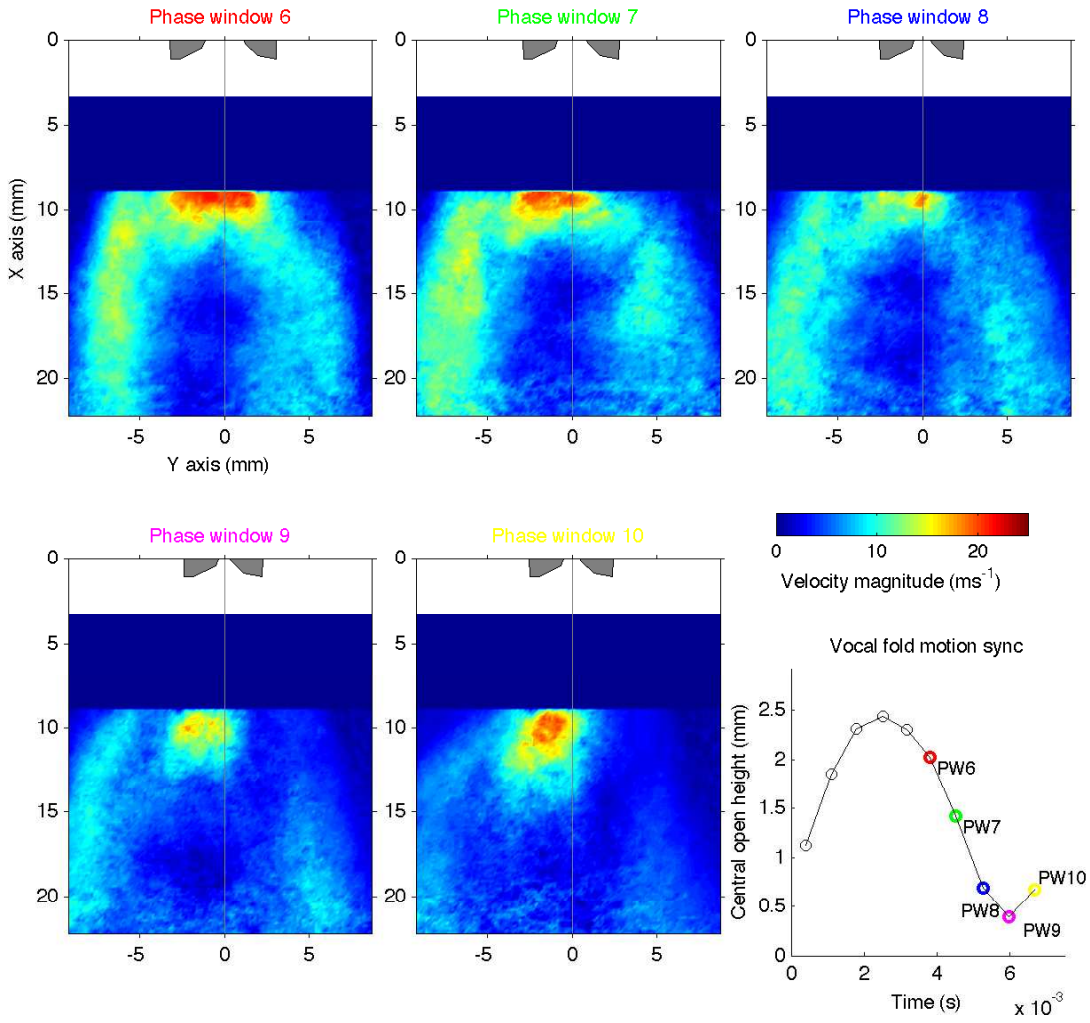

Figure 8.2: Velocity magnitude plots for the free jet configuration for phase windows 6-10.

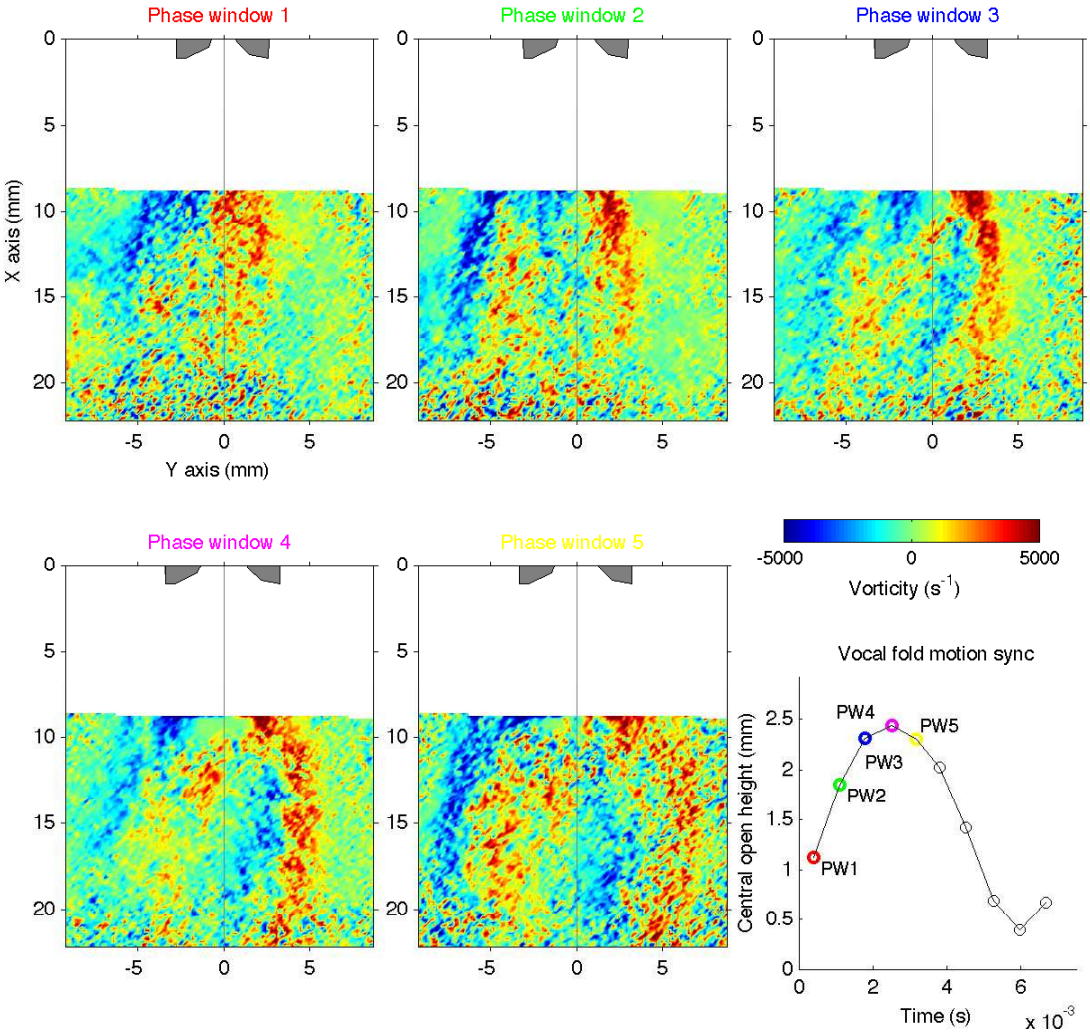

Figure 8.3: Vorticity plots the free jet configuration for phase windows 1-5.

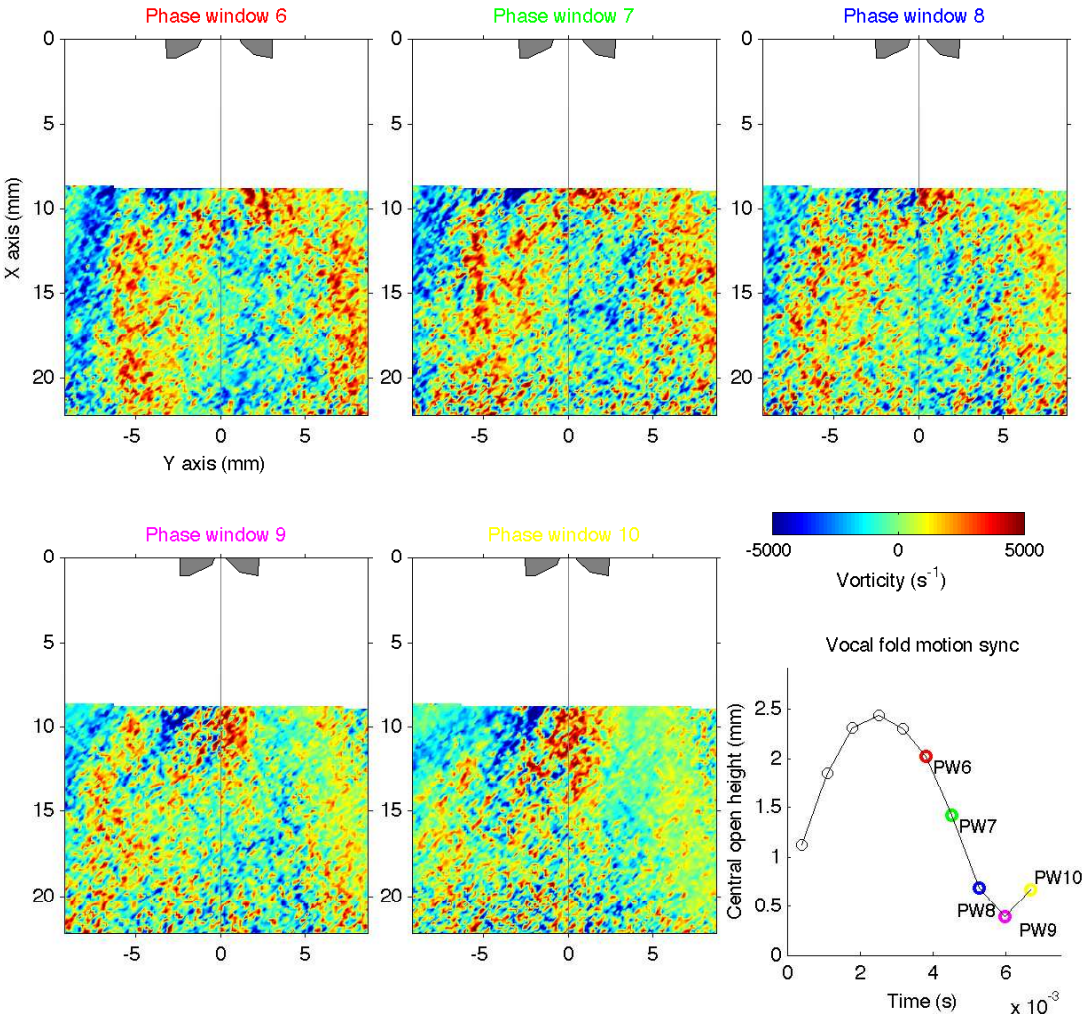

Figure 8.4: Vorticity plots the free jet configuration for phase windows 6-10.

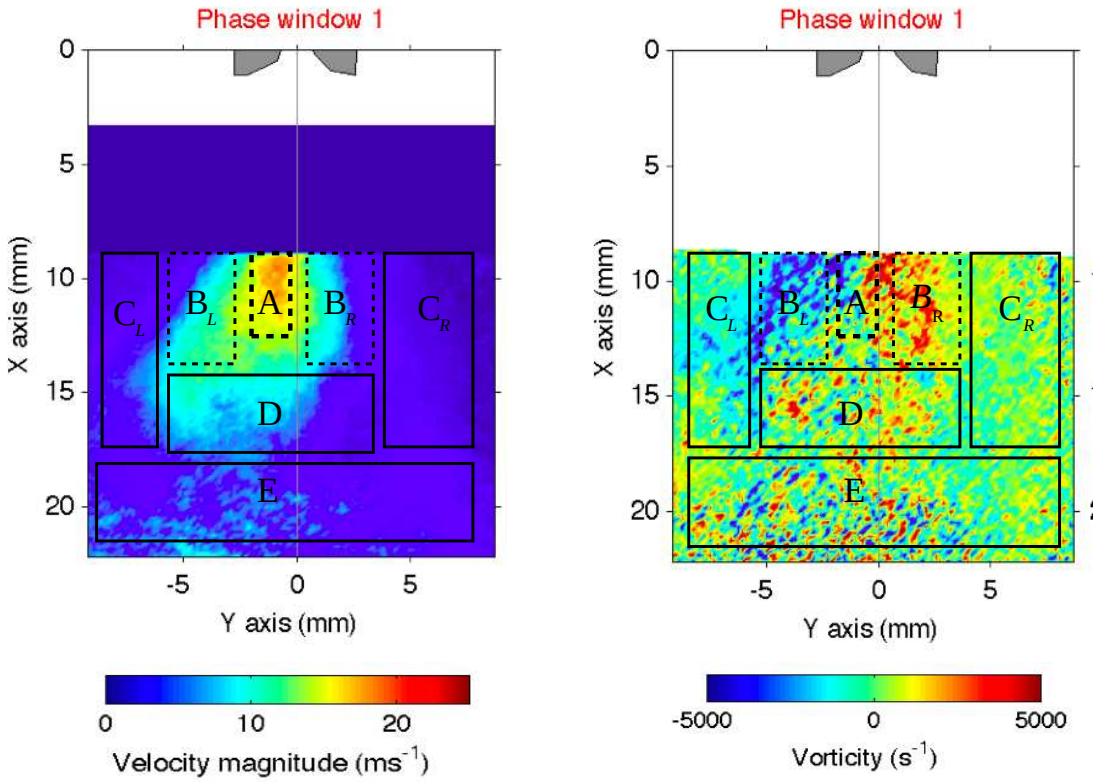

Figure 8.5: An overview of the free jet structure for phase window 1, highlighting the four principle regions: A, jet core; B_L and B_R, shear layers; C_L and C_R, entrainment regions; D, transitional region with strong jet deceleration; E, turbulent mixing.

of oppositely-sensed bands of vorticity located either side of the glottal centreline, but within the larger primary bands of vorticity seen further out from the centreline. These were probably the result of the averaging process used to compute each phase window. This effect is discussed in the following section.

Figure 8.5 shows enlarged versions of the velocity magnitude and vorticity maps of phase window 1 for the free jet configuration. The figure outlines the five main regions of the free jet flow maps that were visible in most phase windows. These are labeled A, B_L and B_R, C_L and C_R, D and E. The jet core is labeled as region A. The left and right jet shear layers are labeled as regions B_L and B_R. The entrainment regions on either side of the jet are similarly labeled C_L and C_R. The transitional region where the jet strongly decelerates is labeled D, and the region of increasingly turbulent mixing is labeled E.

8.2.3 Bi-directionality of the glottal jet

The glottal jet was not steady, but oscillated in speed, width and direction throughout the glottal cycle. For many phase windows a distinct skewing was observed, whereby

the jet was deflected to the right or left of the glottal centreline. Despite the averaging process of the phase windowing technique, a diverse range of unique and dynamically changing jet behaviours were observed over the course of a glottal cycle.

Skewing of the glottal jet in the published literature

Hirschberg[Hirschberg, 1992] pointed out, more than a decade in advance of the present experimental investigations, that the glottal flow separation is probably a rather delicate process, which is strongly influenced by the vocal fold profile and two-dimensional $(x-y)$ trajectory. Separation of the glottal flow, particularly from a diverging glottal profile (see figure 2.10 and section 2.5.3), is also extremely sensitive to the surrounding fluid conditions[Pelorson *et al.*, 1994]. The precise flow separation point, and resulting jet trajectory, may vary over the course of a single cycle as changes to the mechanical boundary condition of the vocal fold walls take place. It may also be expected to differ between the same phase point during consecutive oscillation cycles, depending on the particular instantaneous fluid conditions.

Erath and Plesniak[Erath and Plesnaik, 2006a] have reported that the glottal jet through a scaled model of the human airway had a bimodal behaviour. The model larynx was static, but was driven with a pulsatile flow. Several vocal fold profiles were investigated, each with a different divergence angle. For certain phase angles of the jet cycle the jet was seen to adhere one of the vocal fold walls, resulting in a jet with a trajectory at an angle to the glottal centreline. The jet deflection was a highly unsteady phenomenon, which was explained as a result of the Coanda effect[Coanda, 1936; Tritton, 1988; Pelorson *et al.*, 1994]. This meant that the deflection of the jet varied dynamically over the period of a glottal cycle, and statistically over the course of many glottal cycles.

In Erath and Plesniak[Erath and Plesnaik, 2006a] a statistical analysis was performed for a large number of PIV measurement repetitions at several phase angles throughout the cycle, in order to determine the most common jet deflection behaviour. The jet had a tendency to adhere to the right-hand wall for certain phase angles, whilst for other phase angles it tended to adhere to the left-hand wall. For some phase angles the jet did not show a preference and appeared to randomly fluctuate from wall to wall over consecutive glottal cycles.

The overall picture was one of highly unsteady, and at times unpredictable jet behaviour. Erath and Plesniak[Erath and Plesnaik, 2006a] further pointed out that small asymmetries in the mechanical shape of the replica vocal fold walls significantly altered the stability of the flow. This had the effect of causing the flow to predominantly adhere to one of the vocal folds.

In the present study the dynamical nature of the self oscillating vocal fold replica meant that large asymmetries occurred between the two vocal folds throughout the

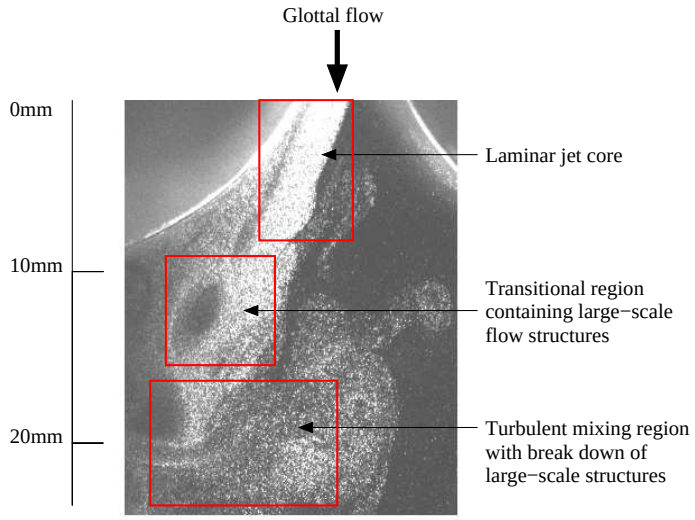

Figure 8.6: Flow visualisation of the jet flow through an earlier *in vitro* vocal fold replica[Newton and Campbell, 2006] similar to replica A (see section 3.2.2). The three principle regions of the flow have been highlighted: laminar core, transitional deceleration and turbulent mixing. The visualisation was obtained by seeding the flow with a high concentration of fog from the SAFEX fog generator (see section 6.4.3).

glottal cycle (see section 4.6 on the two-dimensional motion of the *in vitro* lip-reed). Such asymmetries may be expected to lead to significant skewing of the glottal jet.

Skewing of the glottal jet observed in the present work

An asymmetric jet trajectory has already been observed in flow visualisations performed on an earlier version of the *in vitro* replica used in the present work (replica A, see section 3.2.2), as reported in Newton and Campbell[Newton and Campbell, 2006]. Figure 8.6 shows an example flow visualisation from this earlier work, which was a precursor to the present study.

The flow visualisation was performed during full self-sustained oscillations of the replica, at a phase point close to the maximum vocal fold opening. The upstream pressure was approximately 650Pa, and there was no vocal tract. This resulted in typical jet velocities of more than 30ms^{-1}, which were above the measurement range of the PIV apparatus (see section 7.2.3). Despite this, the flow visualisations did provide a clear graphical example of the three principle streamwise features of the jet flow; the 'laminar core' region, the transitional region and the region of turbulent mixing. They also highlighted the strongly asymmetric jet trajectory which caused the jet to adhere to the left vocal fold throughout much of the glottal cycle.

Figure 8.7 shows a series of instantaneous flow visualisations obtained throughout the oscillation cycle of this older replica, together with corresponding images of the

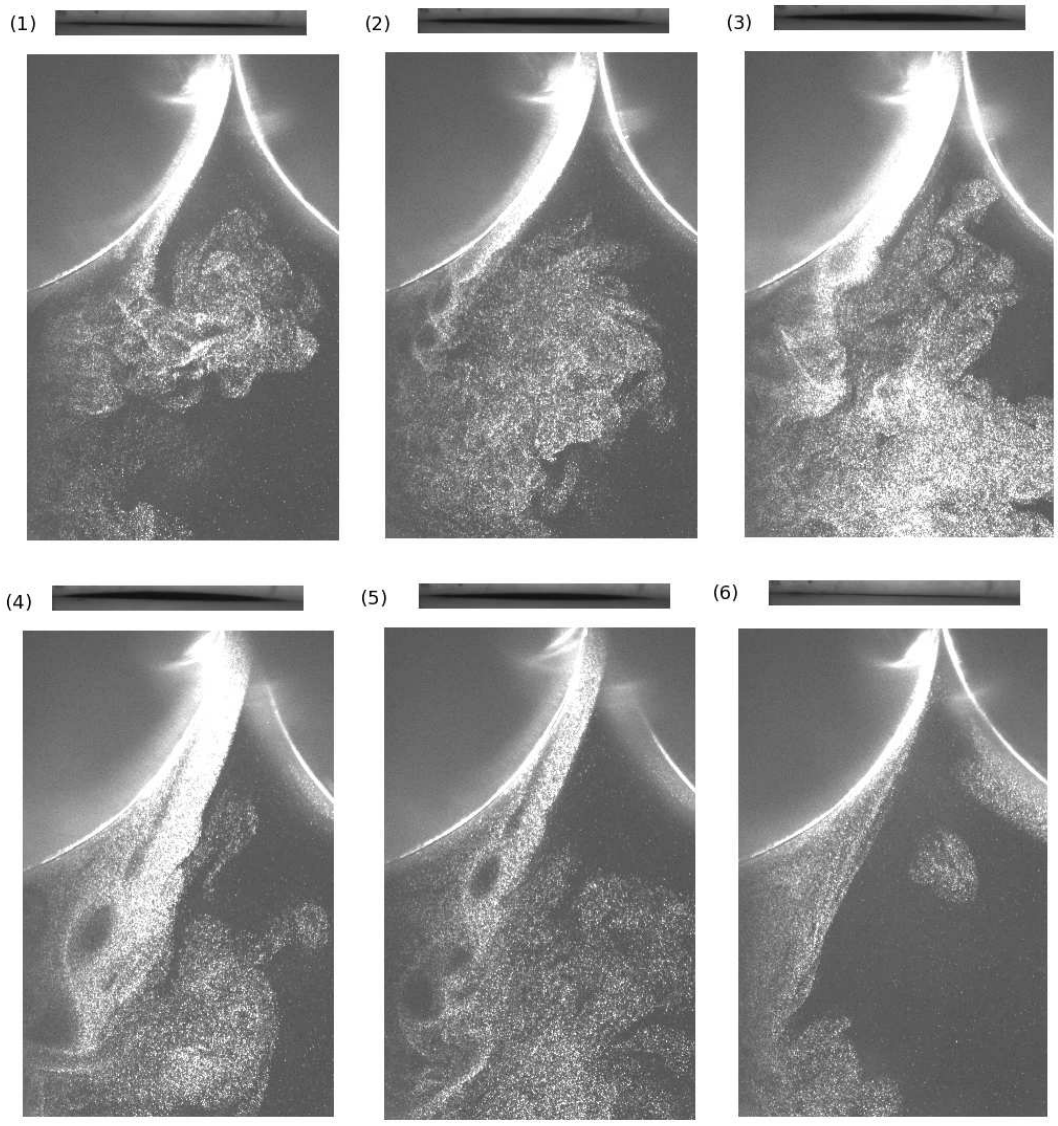

Figure 8.7: A series of instantaneous flow visualisations comprising a full oscillation cycle, performed on an earlier *in vitro* vocal fold replica similar to replica A (see section 3.2.2). Frontal images of the glottal opening are shown below each flow visualisation. The visualisation was obtained in the same manner as figure 8.6.

glottal opening at each visualisation point. Vortices can clearly be seen on either side of the flow. A transverse rotation of the jet trajectory from left to right may be seen between images (1) and (4). The jet appeared to commence the cycle strongly adhered to the left vocal fold, before rotating back towards the glottal centreline. Images (5) and (6) show the jet lowering back down to the vocal fold at the end of the cycle. A large region of back-circulating flow can be seen to the right of the jet, close to the glottal centreline.

Once separated from the vocal folds the jet quickly became transitional as momentum transfer and fluid rotation caused a deceleration of the flow. The most important point to take from the figure is that the separation point of the jet, and the resulting jet deflection angle, varied substantially over the course of a cycle.

The asymmetric flow skewing behaviour reported by Erath and Plesniak[Erath and Plesnaik, 2006a] was explain in terms of the Coanda effect. However, the relevance of the Coanda effect in phonation remains a controversial issue. In particular, it has been questioned whether there is sufficient time within the glottal cycle, during full self-sustained oscillations, for a Coanda effect to be established[McGowan, 1993; Hirschberg, 1992; Pelorson *et al.*, 1994; Pelorson, 2007].

The phenomenon of asymmetric flow separation, resulting in a deflection of the jet from the glottal centreline, also appears to be visible in the free jet PIV measurements performed on replica C, presented in figures 8.1 and 8.2. The main part of the jet core was closely aligned with the glottal centreline during phase window 2, but for all the other phase windows there was a noticeable deflection, the strength of which depended on the particular phase point through the oscillation cycle.

Unfortunately, it was very difficult to reliably extract the precise angle of the jet deflection from the PIV data. This was because the upstream limit for optical access was located approximately 8mm downstream from the flow separation point. The observation window thus appeared to contain only the tail end of the main 'jet core' region, as has been shown in figure 8.5 and outlined in section 8.2.2. Much of the visualisation contained the transitional region where the jet decelerated and began to break down.

The general range of jet deflection angles was measured by considering the most extreme cases. The estimates were obtained by fitting an ellipse to the jet trajectories on either side of the centreline, and taking the angle between the centreline of the glottis and the centreline of the ellipse. The best estimates for the free glottal jet case found the range of skewing angles to be between approximately -30° and +20°, to the left and right respectively in the presented figures.

The difficulty in obtaining reliable estimates of the jet skewing angle over the course of the whole glottal cycle meant that the bulk of the free jet analysis concentrated on the visible jet core region, which was clearly present for all but one of the phase windows (see section 8.2.4). However, the presence of two apparently separate yet simultaneous

'tongues' of flow between phase windows 2 and 8, clearly visible in figures 8.1 and 8.2, also begged further attention. The following section looks at this issue.

In summary, it was not possible to make firm conclusions about the possible relevance of the Coanda effect from the present PIV measurements. However, the strong skewing observed in the PIV data, and the empirical evidence from earlier flow visualisations performed on a similar replica, suggest that an asymmetry in the glottal jet deflection angle could be a common feature of the glottal flow.

Double-tongued jet flow

Phase windowing of the PIV vector maps had the advantage that it was possible to assess the stability of the jet over a relatively long time period. The individual vector maps that comprised a single phase window were obtained from separate repetitions of the glottal cycle, captured from a discrete number of glottal cycles spread out over the period of approximately a minute. The twenty-five or so individual vector maps that were averaged together to produce a single phase windowed vector map were thus snapshots of the glottal jet obtained over a period of time much longer than a single cycle.

One of the most intriguing features of the flow was that of a double-tonguing. Phase windows 2-8, shown in figures 8.1 and 8.2, contain two prominent 'tongues' of medium velocity flow (between 8ms^{-1} and 15ms^{-1}), located either side of the glottal centreline and starting from around 12mm downstream of the vocal folds. A region of low velocity (between 2ms^{-1} and 5ms^{-1}) was located between the tongues.

Figure 8.8 shows an enlarged version of the velocity magnitude and vorticity plots for phase window 3. The left and right tongues of this 'bi-directional' jet flow have been highlighted as J_L and J_R, and the central 'dead' region as J_C. The vorticity plot shows that each of the jet tongues possess regions of negative and positive vorticity, located on the left and right sides of each tongue. These regions have been highlighted with brown (left hand tongue) and black (right hand tongue) ellipses in the vorticity plot. Such coherent structures, correlated with the flow tongues in the velocity magnitude plot, suggest that the two jet tongues were true structures within the flow field, rather than random artifacts of the phase window averaging process.

The instantaneous presence of the two jet tongues was confirmed by examination of individual vector maps within the phase windows. An example of an individual vector map, obtained during phase window 4 (close to the maximum vocal fold opening), is shown in figure 8.9. Plots of the velocity magnitude and the vorticity have been included in the figure. The jet core is visible between 8 and 12mm from the vocal folds. It may be seen in the velocity magnitude plots as a prominent region of high velocity (> 20ms^{-1}). In the vorticity plot the same core region can be identified as an area of low vorticity, surrounded by bands of high vorticity associated with the jet shear layers.

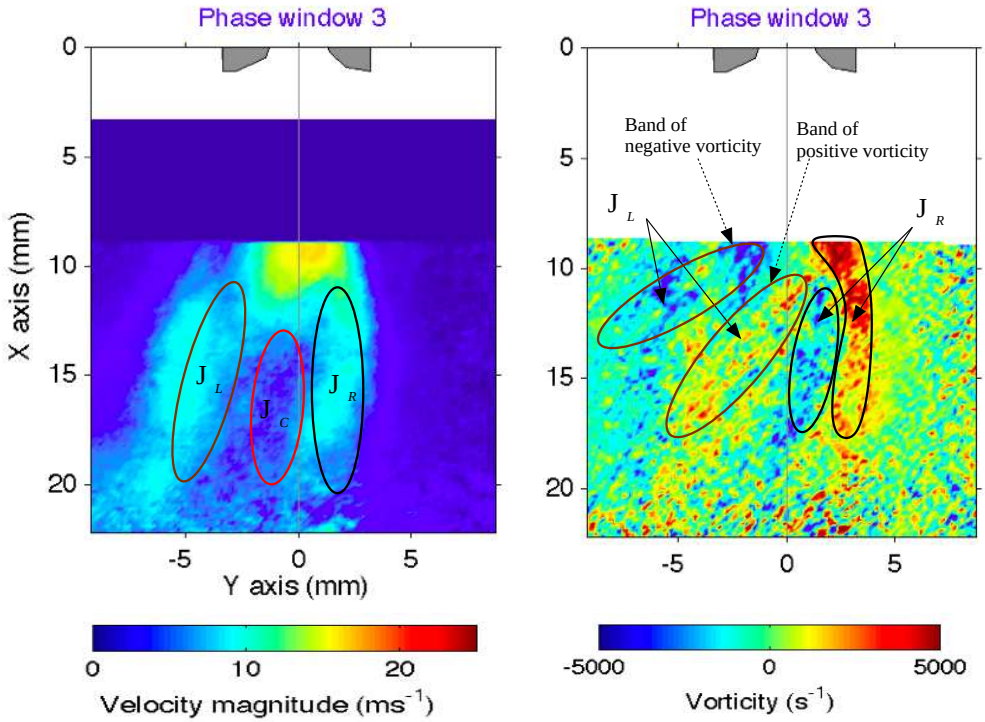

Figure 8.8: Enlarged velocity magnitude and vorticity plots for phase window 3 of the free jet configuration. The two prominent 'tongues' of flow, located either side of the glottal centreline, have been highlighted.

From about 12mm and downstream the jet core appears to diverge into two distinct tongues. This is most clearly seen in the velocity magnitude plot. The fluid velocity in the tongues quickly reduces with increasing distance from the vocal folds, as the tongues become increasingly rotational and transform into a trail of patchy vortices, visible in the vorticity plot.

The individual PIV acquisition, shown in figure 8.9, is remarkably comparable to that of phase window 4, shown in figure 8.1, from where it came. This is because the phase windowed data was derived from multiple individual maps averaged together, each of which was obtained from a different glottal cycle. The windowing process also meant that the individual maps were collected over the period of a tenth of the glottal cycle, and not just at an instantaneous phase point. The similarity suggests that the behaviour of the jet, at least during phase window 4, is well described by the phase windowed data. The compatibility of the individual maps within each phase window is addressed in more detail in section 8.2.4, where the standard deviation of the velocity field is discussed.

The velocity magnitude plots in figures 8.1 and 8.2 show that the two jet tongues formed and decayed over the course of the glottal cycle. In phase window 1 there was no discernible splitting of the jet. The most prominent flow path was directed at an

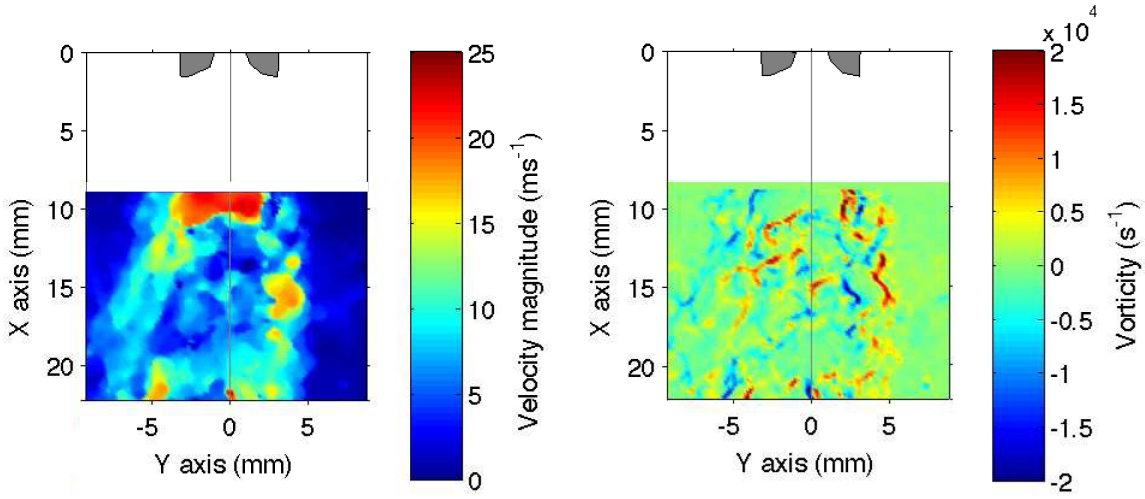

Figure 8.9: A pair of plots showing the velocity magnitude and vorticity of a single PIV acquisition, obtained during phase window 4.

angle of approximately -30° (to the left) from the glottal centreline. The most central core of the jet, indicated by the highest velocities (around 18ms^{-1}) was aligned closely with the glottal centreline. Phase windows 2 and 3 show the initial formation of a double-tongued flow behaviour. A remnant of the left-directed flow path is visible in phase window 2, while the main bulk of the flow swung away to the right, in line with the glottal centreline. The overall effect was of two distinct flow paths.

In phase window 3 the flow further developed into two distinct tongues, with the rightmost of these directed at an angle of approximately 25° (to the right) from the centreline. In phase window 4 the jet core expanded significantly in speed and width, and the two tongues of flow became very clear. In phase window 5 the tongues remained clearly defined. The most probable path of the jet, indicated by the highest tongue velocities, can be seen directed to left of the centreline, seemingly having switched from the main direction during phase window 3. Over the course of phase windows 6 to 8 the most prominent flow tongue remained directed to the left of the glottal centreline. Phase windows 9 and 10 show an apparent degradation of the flow tongues, which are replaced by a single jet directed close to the glottal centreline.

The formation and disintegration of the jet tongues over the course of the glottal cycle is suggestive of a fluid behaviour that was correlated to the periodic movement of the vocal folds. The work of Neubauer *et al*[Neubauer *et al.*, 2007] recently used PIV to investigate the jet flow through a self-oscillating model of the vocal folds under mechanical and fluid conditions comparable to those encountered in the present work. Three principle regions were highlighted: a 'laminar core' region that extended approximately 12mm downstream from the flow separation point (which

included regions of opposite vorticity on either side), a 'transitional' region between 12mm and 20mm downstream, and a region of turbulent mixing that commenced from approximately 20mm downstream of the flow separation.

The overall nature of the flow described by Neubauer *et al* was quite similar to that presented in this work. Of particular interest for the present discussion was the phenomenon of 'jet flapping'. A large scale movement of the jet was seen by Neubauer *et al*, commencing approximately 25mm from the vocal folds, which caused the rapidly expanding jet flow to sway back and forth across the glottal centreline.

The measurement region in the present work commenced approximately 8mm downstream from the vocal folds. As has been outlined in the preceding section this meant that most of the observed flow was in the process of rapid deceleration and expansion. It is possible that the observed jet tongues were the result of a similar jet flapping motion. Such a hypothesis would suggest that the the secondary jet tongue in any particular individual PIV map, such as the right hand tongue in figure 8.9, was a remnant of the jet flow at a phase point some time before the acquisition. It thus represented a secondary jet structure that was being convected away downstream in parallel with the main flow.

It is difficult to draw really firm conclusions about the precise origin of the double jet tongues. However, it is important to draw attention to the possibility that they were related to the three dimensional expansion of the jet. The assumption of a two-dimensional flow field, while justifiable up to the flow separation point (see section 2.5.1), becomes extremely questionable when jet has formed and has begun to decelerate and expand.

Neubauer *et al*[Neubauer *et al.*, 2007] performed a number of flow visualisations at points up and down the out-of-plane z axis of their vocal fold replica (see figure 6.5 for an overview of the relevant vocal fold axes). The flow was shown to be significantly three-dimensional, particularly at distances greater than about 15mm from the vocal fold replica. This was explained as a three dimensional mixing of the jet resulting from the large scale jet flapping behaviour described above. A number of the flow visualisations in Neubauer *et al*[Neubauer *et al.*, 2007] bore remarkable similarity to the bi-directional jet tongues observed in figures 8.1 and 8.2.

The third party evidence of Neubauer *et al*[Neubauer *et al.*, 2007] appears to corroborate the hypothesis that much of the jet in the current free jet analysis was viewed as it underwent a strong deceleration and turbulent mixing, both in the plane of the PIV light sheet, and out of plane up and down the z axis. The persistent presence of the bi-directional flow structure may thus have been a consequence of the particular two-dimensional plane chosen for illumination (the plane was aligned as close to the middle of the glottis as possible).

General behaviour of the free jet flow field

Both steady and unsteady flow experiments through static replicas of the vocal folds have shown a diverse range of fluid behaviour as the flow separates from the vocal fold walls and is convected downstream[Hofmans *et al.*, 2003; Triep *et al.*, 2004; Brücker *et al.*, 2004; Kucinschi *et al.*, 2005; Erath and Plesnaik, 2006b; Neubauer *et al.*, 2007]. Mcgowan[McGowan, 1988] and Hirschberg[Hirschberg, 1992] have suggested that the three-dimensional structure of the separated glottal jet could be of importance in determining both the driving forces on the vocal folds, and the nature of the resulting acoustical generation.

The precise flow structure at flow separation and in the region immediately downstream, including any vortices and three-dimensional expansion, may have a strong bearing on the overall flow profile 'seen' by the vocal tract. The flow profile strongly dictates the nature of the periodic acoustical signal[Zhang *et al.*, 2002], while the presence of vortices may also influence the generation of noise in the voice signal[Kob *et al.*, 2005]. Vortices may also be expected to alter the aerodynamics around the valve, and the resulting pressure field downstream of the vocal folds[McGowan, 1988].

In the present work the self-sustained nature of the vocal fold oscillations meant that the channel profile was an autonomous dynamic variable that could not be controlled during the course of the experiments. The flow through the valve was thus subjected not only to dynamically varying flow conditions, as in previous static vocal fold experiments[Kucinschi *et al.*, 2006; Erath and Plesnaik, 2006a], but also dynamically varying mechanical boundaries. The resulting flow appears to have been highly unstable, exhibiting unpredictable behaviour such as skewing from the glottal centreline, possibly caused by adhesion to one of the vocal fold walls. Switching of the jet adhesion from one vocal fold wall to another also also appears to have occurred within the period a single glottal cycle.

During the main part of the glottal open cycle, from phase windows 2-8, the phenomenon of jet flapping provides the most probable explanation for the strong bi-directionality of the jet flow, as described in the previous section. However, the relatively turbulent behaviour of the jet from around 18mm and downstream made a more detailed analysis of this behaviour beyond the scope of the present work. The following sections thus focus on a more detailed analysis of the general behaviour of the overall flow field, as well as an investigation of the jet core stability throughout the glottal cycle (section 8.2.4).

Standard deviation behaviour of the free jet flow field

The phase windowed velocity magnitude maps of the free jet configuration, shown in figures 8.1 and 8.2, revealed the formation, pulsation and break down of the glottal jet over the period of a glottal cycle.

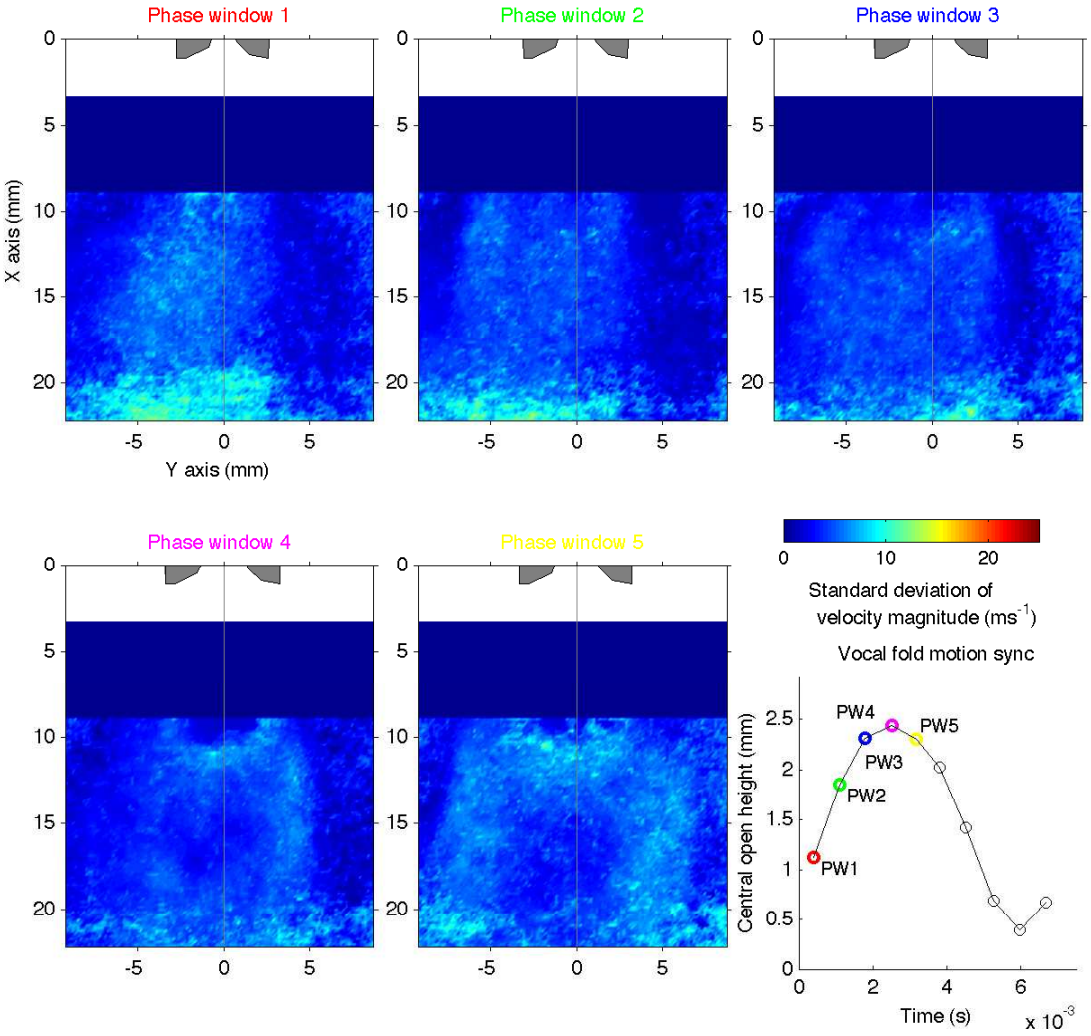

Figure 8.10: Standard deviation of velocity magnitude plots for the free jet configuration, showing phase windows 1-5.

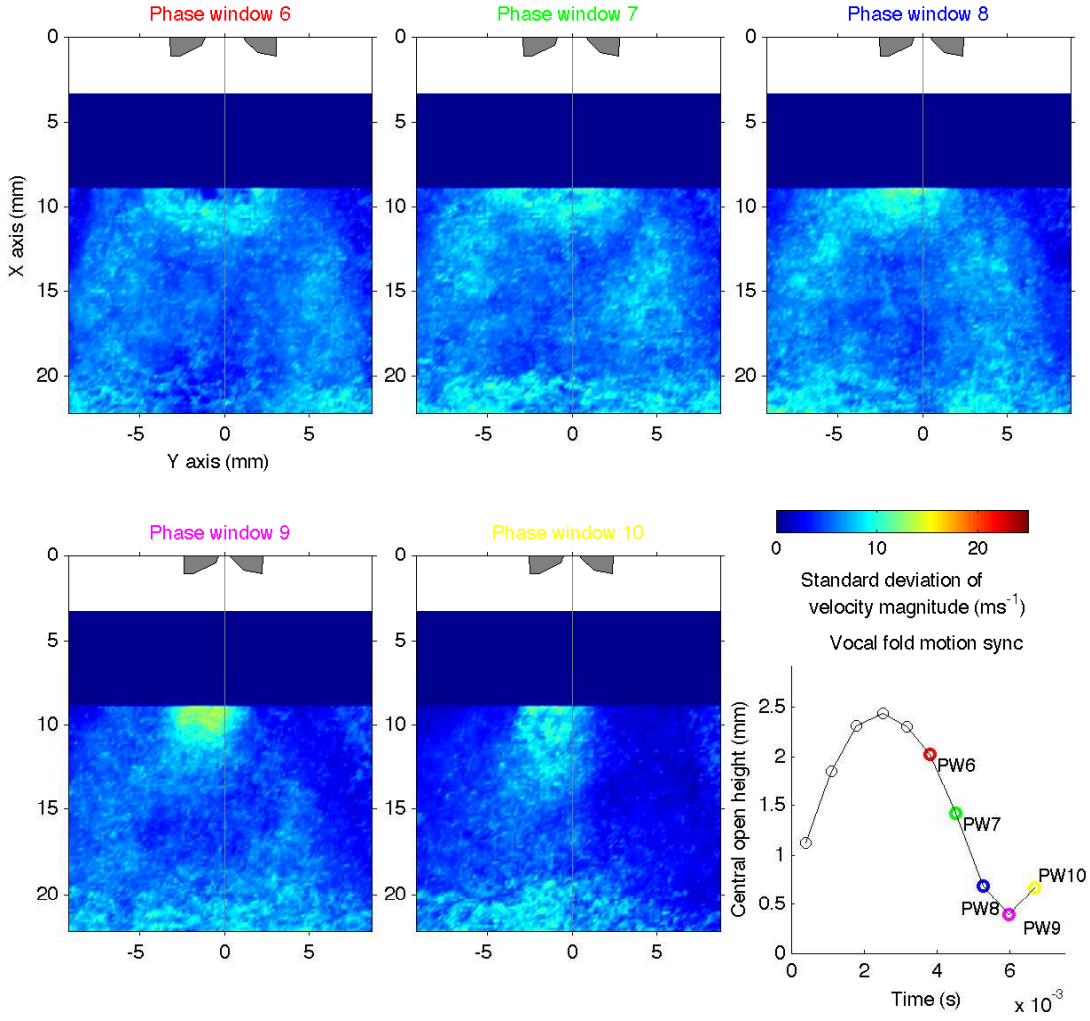

Figure 8.11: Standard deviation of velocity magnitude plots for the free jet configuration, showing phase windows 6-10.

Figures 8.10 and 8.11 show plots of the standard deviation of velocity magnitude for the ten phase windows of the free jet configuration (see also section 7.4.4). The standard deviation velocities showed considerable spatial variation within each phase window map, and between the phase windows over the period of the glottal cycle. Variations were observed in the hypothesised jet core region, as well as in the surrounding flow field.

The phase windowed standard deviation maps can be broadly divided into two groups; the glottal opening phase and the glottal closing phase. Phase windows 1-5 occurred during the main part of the glottal opening phase, as the vocal folds moved apart and reached their maximum separation. The jet accelerated during the opening phase of the glottal cycle. Phase windows 6-9 occurred during the closing phase as the vocal folds moved back together towards their minimum separation. The jet decelerated during the closing phase of the glottal cycle. Phase window 10 occurred at the very start of the opening phase, when the glottal opening was still very narrow. It was thus grouped together with the glottal opening phase maps for the present analysis.

If the general spatial distribution of the standard deviation is considered for all ten phase windows, it can be seen visually from the plots that overall higher values occurred during the glottal closing phase than during the glottal opening phase. This was particular true for the jet core and transitional regions (referred to collectively as the *pre-turbulent* region, see section 7.4.4 and figure 7.5), between 8 and 18mm downstream from the vocal folds. Between phase windows 1 and 5, shown in figure 8.10, much of the pre-turbulent region is coloured deep and light blue, indicating standard deviation velocities up to about 4ms^{-1}. Between phase windows 6 and 10, shown in figure 8.11, the same region is coloured predominantly light blue, yellow and orange, indicating standard deviation velocities up to around 12ms^{-1}.

The average standard deviation of the pre-turbulent region $\bar{\sigma}_{PT}$ was calculated as a function of phase window, in order to observe its behaviour over the course of the glottal cycle. The region measured is shown outlined in figure 7.5. The results of this calculation are presented together with the analysis of the jet core in the following section.

8.2.4 Analysis of the free glottal jet using jet variables

Figure 8.12 shows the behaviour of the four jet variables over the course of the glottal cycle (see section 7.4.4 and table 7.4 for details on the use of jet variables as an analysis technique). A plot of the vocal fold opening h_{VF} has also been included. The left hand plot shows the variables as a function of phase window, which is effectively just time. The right hand plot shows a parametric plot of the average jet core velocity and standard deviation of velocity as a function the vocal fold open height at each phase window.

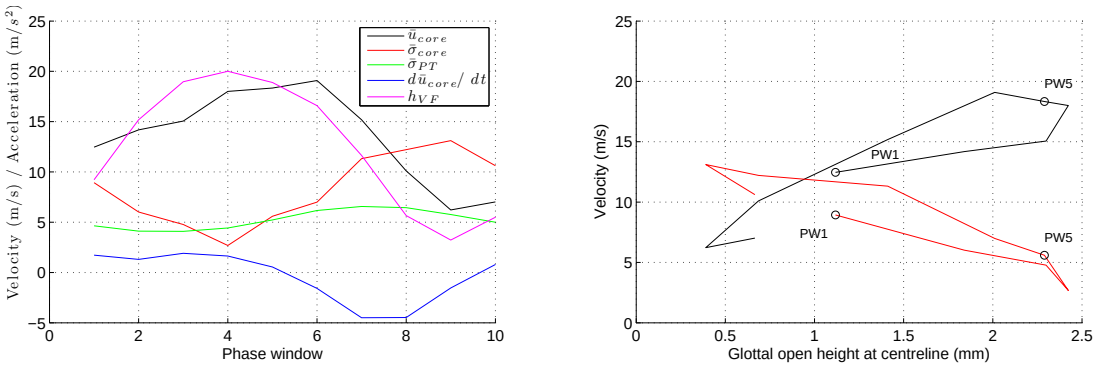

Figure 8.12: Average jet core velocity magnitude ($\bar{u}_{core}$), average jet core standard deviation of velocity magnitude ($\bar{\sigma}_{core}$), average pre-turbulent region standard deviation of velocity magnitude ($\bar{\sigma}_{PT}$) and average jet core acceleration ($d\bar{u}_{core}/dt$) as a function of phase window and glottal opening for the free jet configuration. In the left hand plot the vocal fold open height h_{VF} has been included (normalised to velocity) to illustrate the relative phase behaviour of the variables.

Consider first the left hand plot. All four variables exhibited a cyclical behaviour at a frequency matching that of the fundamental vocal fold oscillation. Taking the vocal fold motion as a reference signal, each of the four jet variables oscillated with some degree of phase offset. Of particular interest was the average jet core velocity, which displayed a hysteresis with respect to the vocal fold opening. This meant that the average velocity was higher during the closing phase of the vocal fold motion, between phase windows 5 and 9, than during the opening phase between phase windows 1 and 4. Phase window 10 corresponded to a vocal fold opening at the start of the opening phase, and is considered along with phase windows 1 to 4. The hysteresis is more clearly seen in the right hand parametric plot of figure 8.12. Equal velocities during opening and closing would produce a straight line in such a plot. However, the experimental curve follows an elliptical path, indicating an asymmetry in the jet core velocity over the glottal cycle.

The standard deviation of the jet core $\bar{\sigma}_{core}$ presented an interesting result. In the left hand time domain plot it can be seen that $\bar{\sigma}_{core}$ remained at a relatively low level ($< 5\text{ms}^{-1}$) during much of the opening phase and into the start of the closing phase. However, with the onset of jet deceleration, commencing from phase window 5, there was a sharp rise in the standard deviation velocity of the jet core. At phase window 9, which corresponded to the minimum vocal fold opening, the standard deviation velocity actually became larger than the average jet core velocity. It can thus be hypothesised that the average flow conditions around this phase step may be, if not indicative of fully turbulent flow, certainly representative of a jet undergoing rapid disintegration.

The standard deviation of the core velocity can be seen plotted parametrically against the vocal fold separation in the right hand plot of figure 8.12. The standard

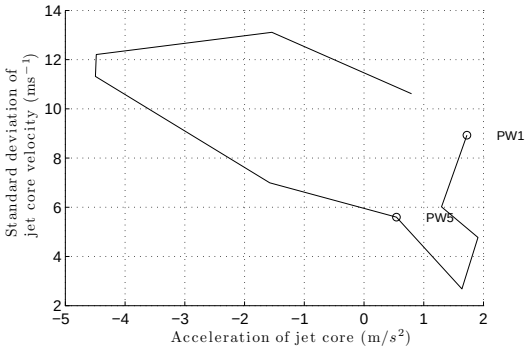

Figure 8.13: Parametric plot of jet core acceleration against the standard deviation of the jet core velocity for the free jet configuration.

deviation also showed a hysteresis with respect to the vocal fold opening. It was higher during the closing phase than during the opening phase. This was most likely due to a number of reasons. The jet decelerated throughout most of the closing phase. The increase in the standard deviation during this period seems to be correlated with this deceleration. Figure 8.13 shows a further parametric plot of the average jet core deceleration verses the standard deviation of the jet core velocity. Apart from phase window 1, which was very close to the minimum vocal fold separation, the standard deviation remained low ($< 5\text{ms}^{-1}$) whenever the jet accelerated. As soon as the jet decelerated there was a significant increase in the standard deviation, indicating a decrease in stability. Apart from the exceptionally high standard deviation of phase window 9, the two highest standard deviations occurred at the highest values of deceleration.

The connection between the deceleration phase of an oscillating pipe flow and the transition to a turbulent regime is well known in the literature [Schlichting and Gersten, 2000; Fishler and Brodkey, 1991]. In the present experiments the free jet described a pulsatile jet, a variety of oscillatory pipe flow. However, it is not possible to draw firm conclusions about the relevance of a turbulent transition using dimensional parameters such as the standard deviation. For a deeper understanding the flow must be considered non-dimensionally, using the techniques described in section 7.4.5. Analysis of all three configurations using non-dimensional flow variables can be found in section 8.5.2.

The standard deviation of the pre-turbulent region of the flow, outlined in figure 7.5, showed a phase behaviour similar to that of the jet core standard deviation. The minimum stability, corresponding to the largest standard deviation velocity, occurred during the closing phase, with the peak at the minimum vocal fold separation.

8.2.5 Acoustical consequences of the pulsating free glottal jet

Mcgowan[McGowan, 1988] and Hirschberg[Hirschberg, 1992] have both discussed the importance of the starting vortices produced by separation of the flow from the vocal folds to the production of noise in the voice signal. Kob *et al*[Kob *et al.*, 2005] has used an *in vitro* vocal fold model to investigate the phenomenon. Zhang *et al*[Zhang *et al.*, 2002] has also investigated the production of sound by pulsating jets using an *in vitro* model of the vocal folds.

The PIV measurements presented in this work show the time-averaged behaviour of the jet, with a large number of instantaneous flow measurements condensed into ten phase windows. It was not possible to extract the acoustical field from the overall behaviour, as the signal to noise ratio of the measurements restricted the resolvability of the acoustical field. This was because the PIV measurements were optimised for the fast moving jet core. The relatively low oscillation threshold used to destabilise the replica vocal folds, however, resulted in a low level of acoustical production that could not be easily resolved from the high speed jet and the surrounding turbulent fluid behaviour.

It may be possible to separate the acoustical field from the main flow by performing many more measurement runs, and averaging over several hundred individual maps at each phase window in order to fully average out the behaviour of the vortices and turbulent jet disintegration. However, this was beyond the scope of the present work.

Despite the inability to resolve the acoustical field, the results presented in this section may still have some implications for the acoustical behaviour of the vocal fold system. It has been suggested that the break down of vortices in the lower vocal tract, particularly where they impinge on a solid boundary, may lead to a secondary acoustical production.

The present work has demonstrated the large decrease in the jet stability associated with the jet's deceleration during the glottal closing phase. It is hypothesised that this decrease in stability may be associated with an increase in the turbulent disintegration of the jet. This turbulent disintegration, which is related to the break down of the jet vortices, may be important in the production of acoustical noise. The fact that this occurs during the closing phase could be a significant contributing factor to the shape of the overall voice signal. In particular, the presence of 'extra' acoustical noise during the closing phase could alter the perceived characteristics of the voice.

The largest jet instability appears to have been associated with the minimum vocal fold separation, when it has been suggested that the effects of viscosity may significantly affect the flow[Pelorson *et al.*, 1994]. The possible acoustical consequences of this behaviour remain an avenue worthy of further investigation.

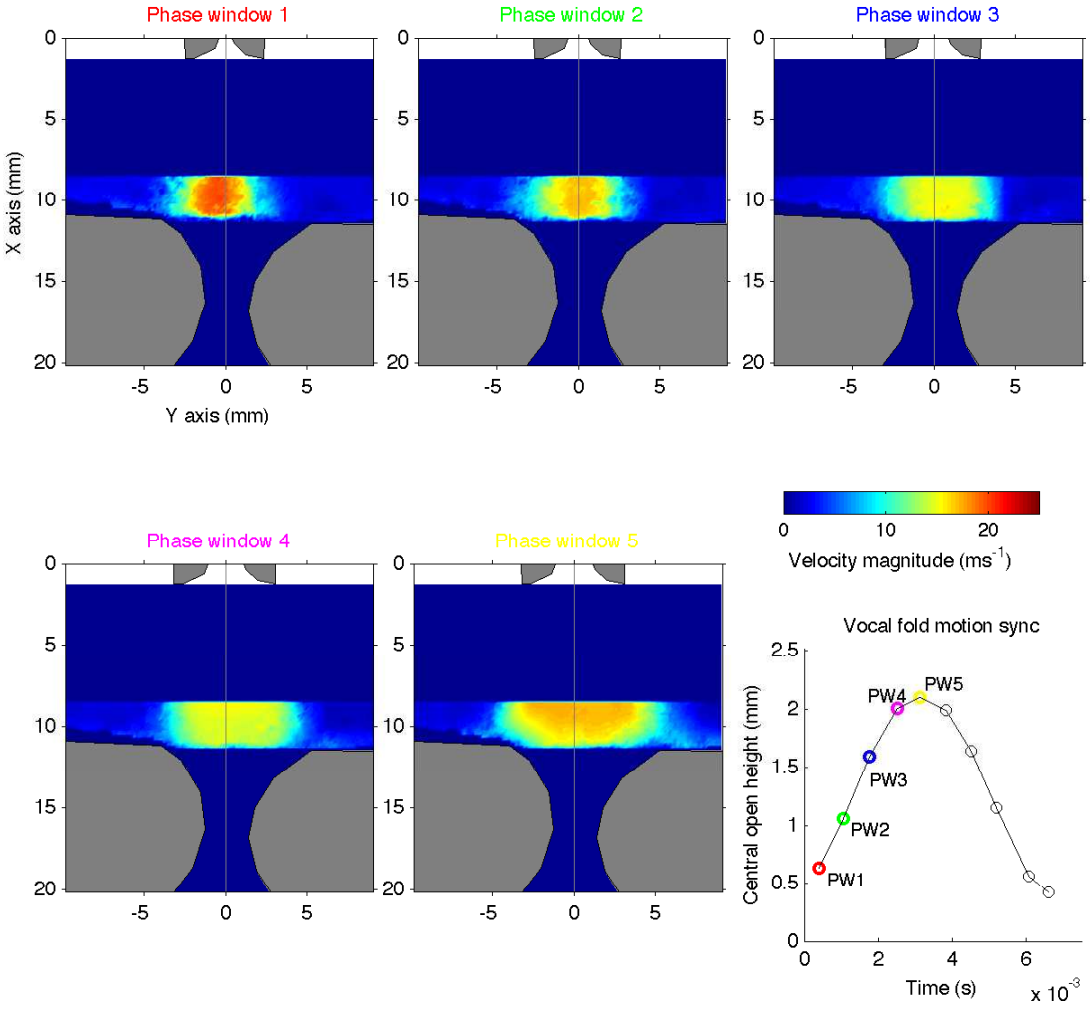

Figure 8.14: Velocity magnitude plots for the physically realistic ventricular band configuration for phase windows 1-5.

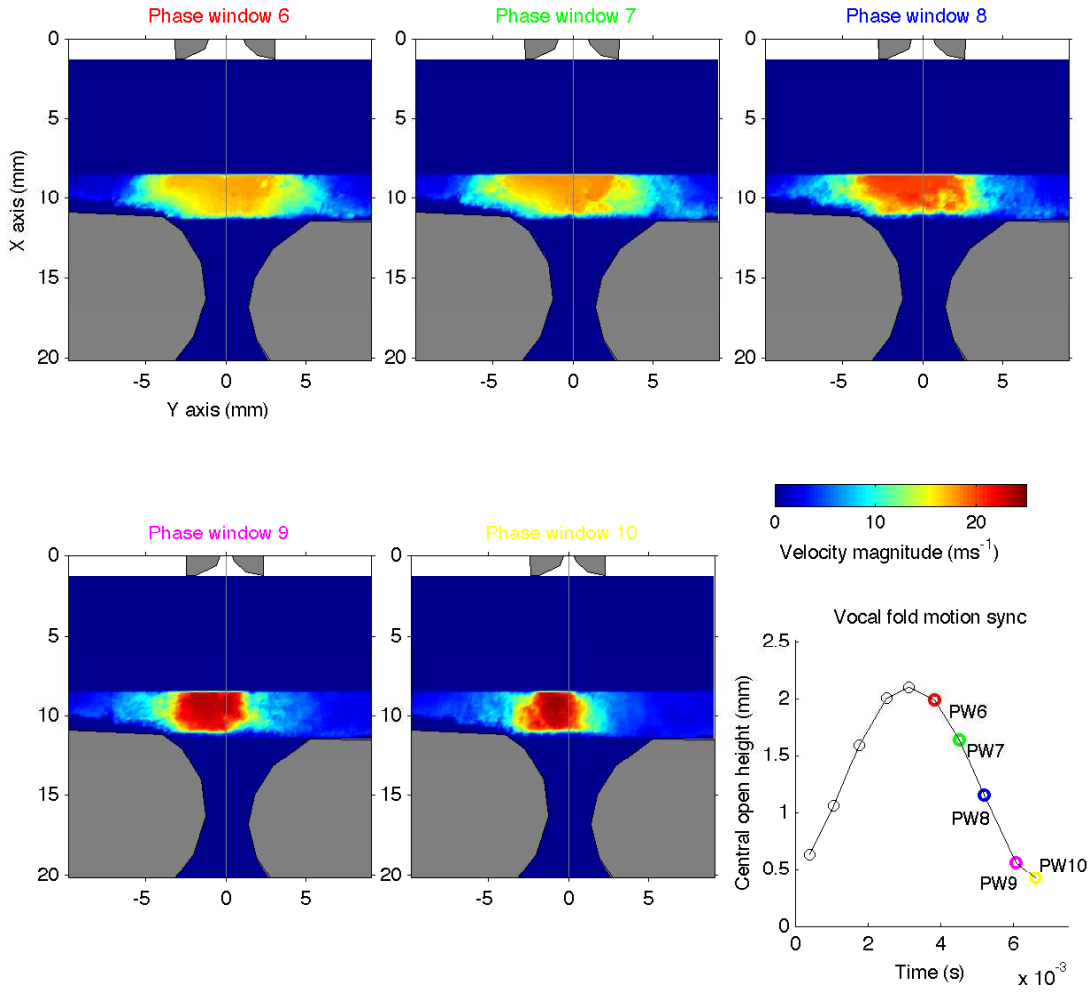

Figure 8.15: Velocity magnitude plots for the physically realistic ventricular band configuration for phase windows 6-10.

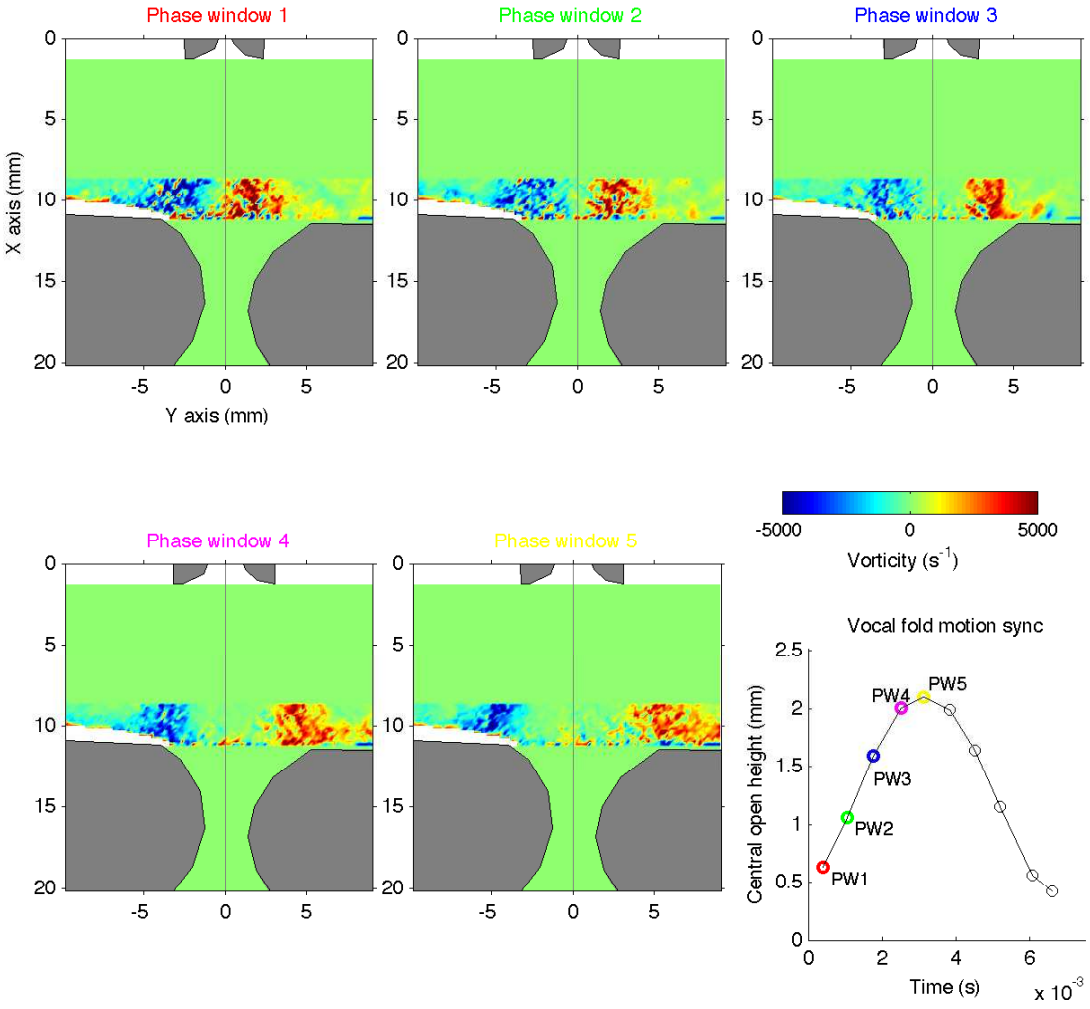

Figure 8.16: Vorticity plots for the physically realistic ventricular band configuration for phase windows 1-5.

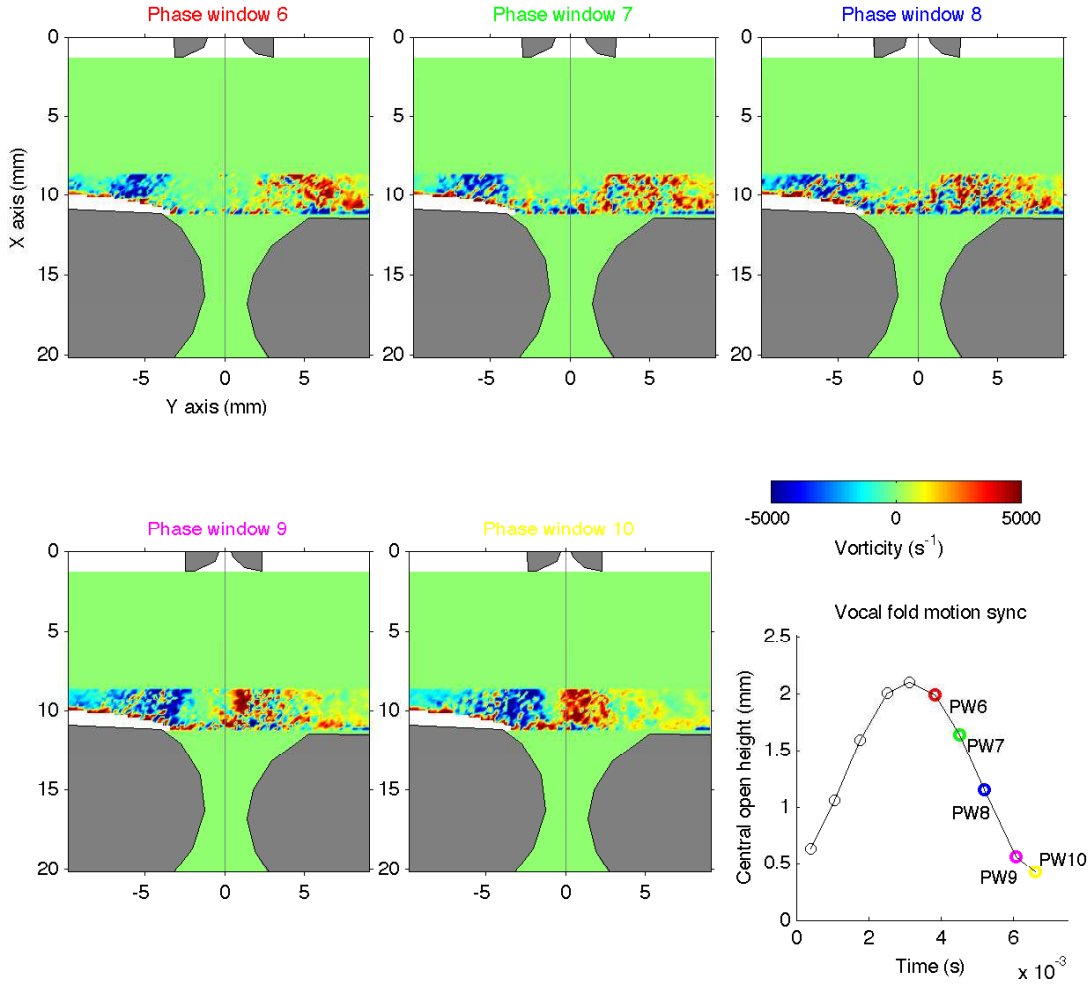

Figure 8.17: Vorticity plots for the physically realistic ventricular band configuration for phase windows 6-10.

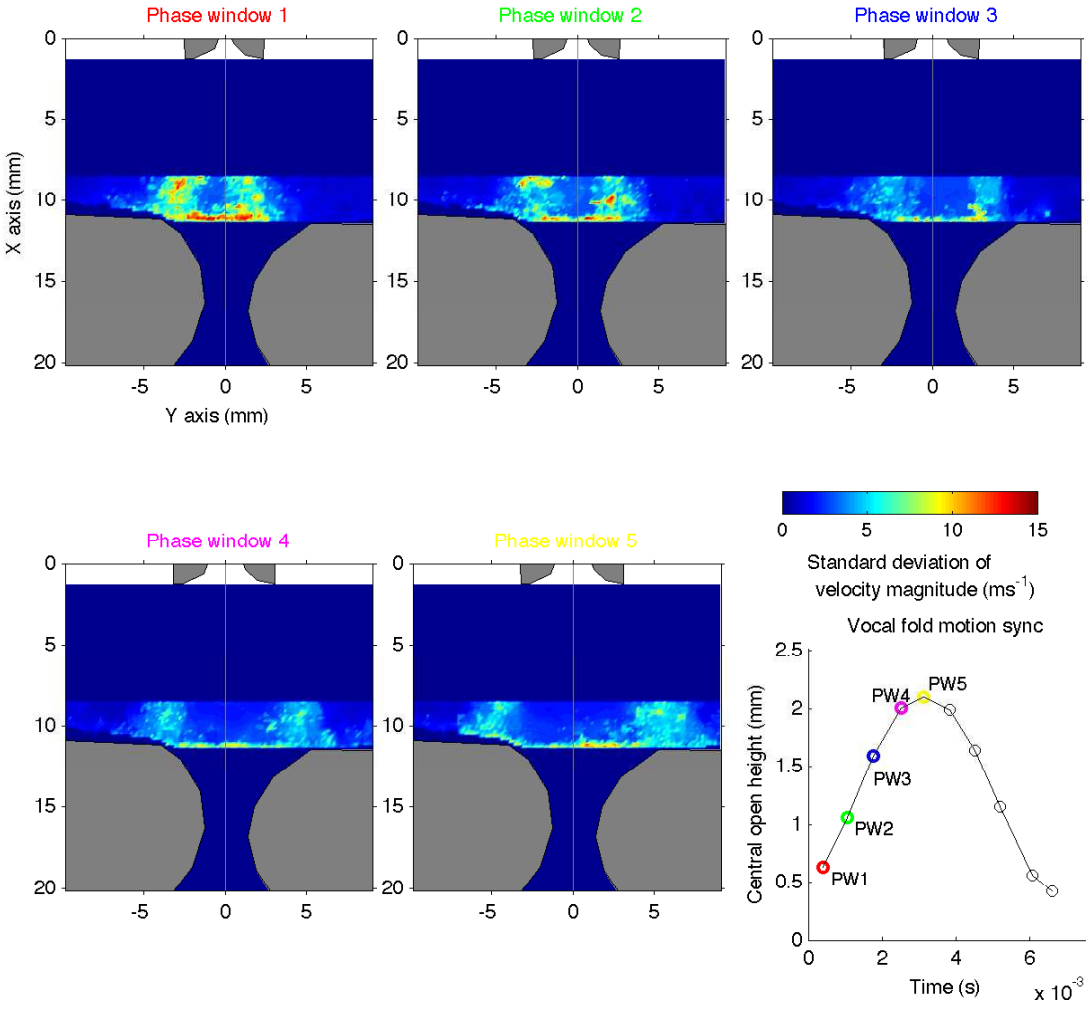

Figure 8.18: Standard deviation of velocity magnitude for the physically realistic ventricular band configuration for phase windows 1-5.

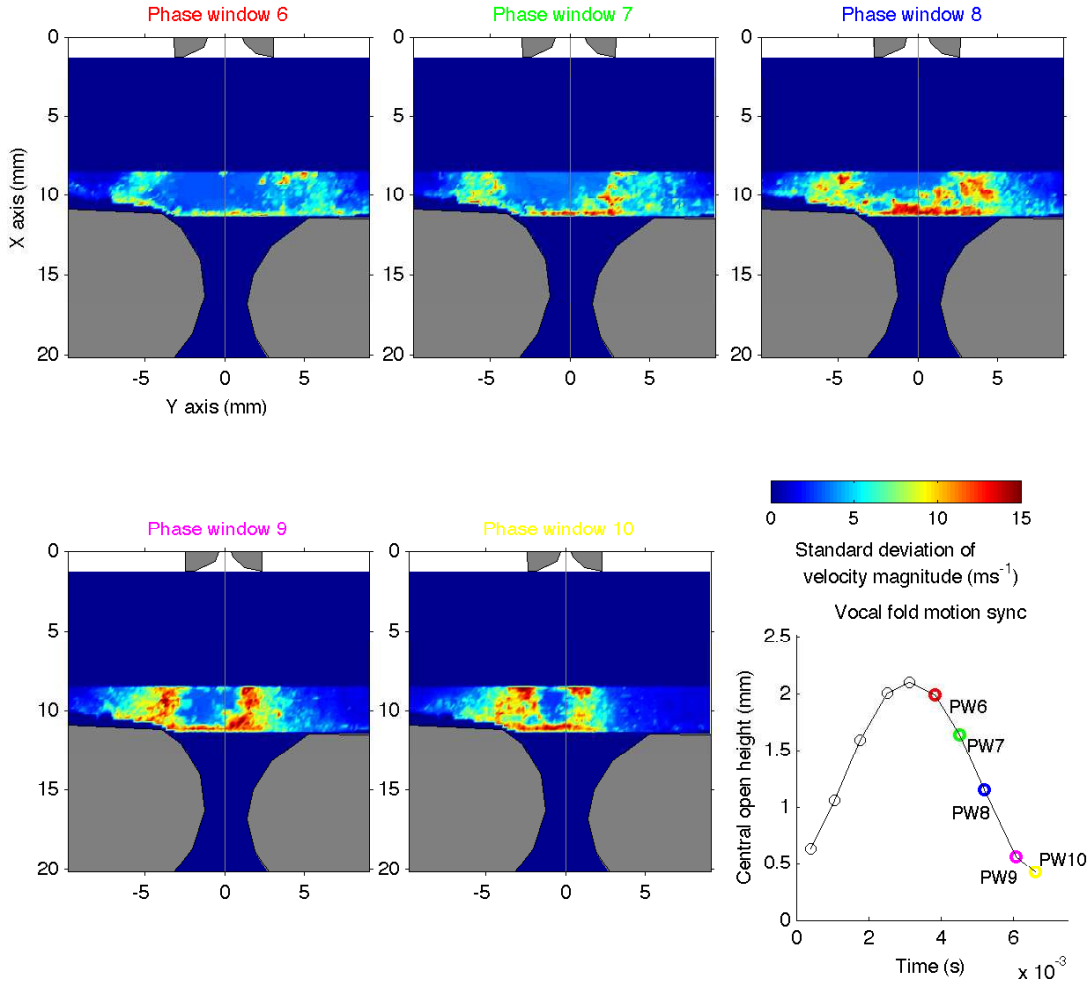

Figure 8.19: Standard deviation of velocity magnitude plots for the physically realistic ventricular band configuration for phase windows 6-10.

8.3 Analysis of the realistic ventricular band configuration ($VB - A$)

Figures 8.14 and 8.15 show velocity magnitude plots throughout the glottal cycle for the realistic ventricular band configuration. The upper limit of the visible region was approximately 8mm downstream from the vocal folds, as with the free jet configuration. The observable portion of the glottal jet was thus confined to a region of approximately 4×20mm ($x - y$ axes), directly upstream from the ventricular bands and within the laryngeal ventricle.

The required lightsheet alignment meant that it was not possible to directly observe the jet behaviour between the ventricular bands (see section 6.4.2). However, the behaviour of the jet within the observable region was clearly measurable, and provided enough data to obtain the four jet variables proposed in section 7.4.4 and described for the free jet in section 8.2.4.

The velocity magnitude PIV plots reveal the production of a jet, directed down from the vocal folds and into the ventricular band opening. The jet was aligned quite closely with the centreline of the glottis throughout the oscillation cycle.

A more detailed understanding of the jet may be gained by consideration of the vorticity plots presented in figures 8.16 and 8.17. These reveal that the central jet core remained almost completely devoid of vorticity, and therefore laminar in character, throughout the whole oscillation cycle. This was in complete contrast to the free jet examples shown in figure 8.3, where the jet core only appeared without significant vorticity around the maximum vocal fold opening.

Figures 8.16 and 8.17 show that either side of the jet core there appear clearly defined regions of negative and positive vorticity, indicative of oppositely rotating fluid. While individual vortices did not appear in the phase windowed data, the averaging process still left trace of the overall vorticity behaviour within these shear layer regions.

Plots of the standard deviation of velocity magnitude are shown in figures 8.18 and 8.19. Much like the vorticity plots, they give the clear impression of a more stabile jet core as compared to the free jet configuration. The standard deviation velocities remain below 4ms^{-1} for much of the oscillation cycle, only rising slightly when the vocal fold separation is at a minimum.

Behaviour of the four jet variables

The principle of describing the behaviour of the glottal jet using a number of jet variables has been outlined in section 7.4.4, and used above in section 8.2.4 for the free jet configuration. The approach is used now to analyse the realistic ventricular band configuration ($VB - A$).

Figure 8.20 shows the behaviour of the four jet variables over the course of the

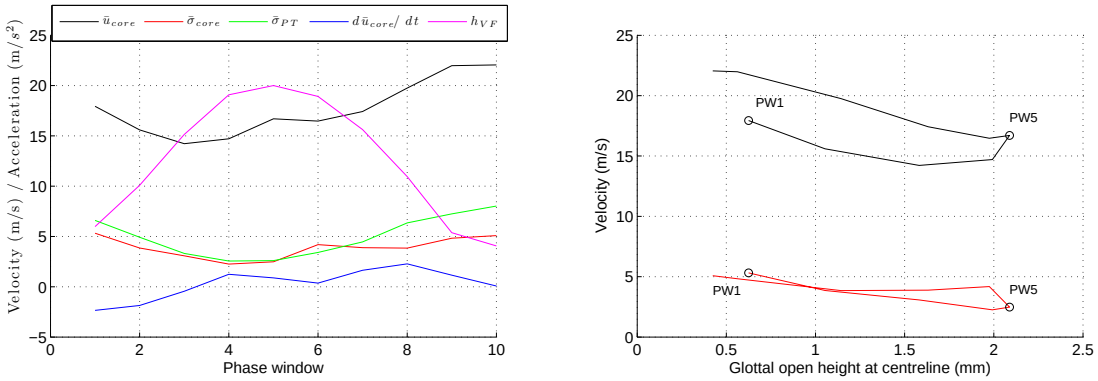

Figure 8.20: The four jet variables as as a function of phase window and glottal opening for the physically realistic ventricular bands ($VB - A$) configuration. In the left hand plot the vocal fold open height h_{VF} has been included (normalised to velocity) to illustrate the relative phase behaviour of the variables.

glottal cycle. At left is a time domain plot where the variables have been plotted as a function of phase window, and at right is a parametric plot of the jet core velocity magnitude and standard deviation as functions of the vocal fold opening. The overall features of the two plots are quite similar to those of the free jet configuration, as shown in figure 8.13, but with some important differences.

The average jet core velocity showed a hysteresis behaviour, whereby the velocities were higher during the closing than during the opening phase. This was similar to the free jet case, and leads to the suggestion that this hysteresis is an important feature of the self-sustained oscillation mechanism. The higher jet velocities during closing imply an asymmetry in the intra-glottal pressure, which may help to drive the vocal folds (see section 2.2.1). This effect is further addressed below, in section 8.5.2, where the average core velocities are compared to a simple Bernoulli prediction.

The right hand parametric plot of figure 8.20 shows that the overall standard deviation velocities were considerably lower than the average jet core velocities throughout the whole cycle. This was in contrast to the free jet example where for vocal fold openings of less than about 1mm the standard deviation velocity became equal to or greater than the core velocity. This implied that the jet was more stable for the realistic ventricular band configuration than for the free jet. Even at the minimum vocal fold separation, when the free jet appeared highly unstable, the standard deviation did not exceed 5ms^{-1}.

The overall behaviour of the standard deviation was also interesting, as it revealed considerably less hysteresis than the free jet example. The jet exhibited similarly low levels of instability during the opening and closing phases. Again, this result seems to suggest that the jet was greatly stabilised by the presence of the ventricular bands, compared to the free jet.

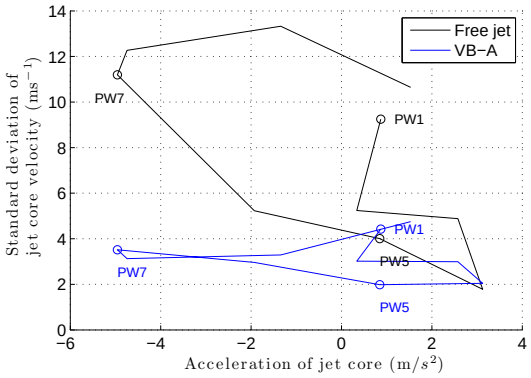

Figure 8.21: Parametric plot of jet core acceleration against the standard deviation of the jet core velocity for the realistic ventricular bands ($VB - A$) and free jet configurations. Phase windows 1, 5 and 7 have been labeled for clarity.

The most likely explanation for the increased stability of the jet in the $VB - A$ configuration was that the flow reattached to the ventricular bands, following an initial separation from the vocal folds. This may have reduced the degradation of the jet because there was simply less time and space for turbulent effects to take over. The average jet core velocity was actually quite high, remaining close to 20ms^{-1} for the entire cycle, compared to the predicted velocity at flow separation, which was around 23ms^{-1}. This implied considerably less deceleration of the jet as it traversed the laryngeal ventricle, compared to the free jet.

The time domain plot revealed some subtly different phase behaviour compared to the free jet configuration. In particular it can be seen that the maximum jet core velocities occurred slightly later on in the phase of the vocal fold motion. The general behaviour of the other jet variables was very similar to the free jet configuration. The highest standard deviations, and thus jet instability, again occurred close to the vocal fold closure.

Figure 8.21 shows a parametric plot of the average jet core standard deviation as a function of the average jet core acceleration. The result for the free jet has been included. The figure highlights one of the important differences between the configurations. During moments of high jet deceleration, the standard deviation velocity of the jet core rose sharply for the free jet case, but not for the realistic configuration. Once again, this evidence seems to point to an overall stabilisation of the jet core in the realistic configuration.

8.4 Analysis of the impeding ventricular band configuration ($VB - B$)

Figures 8.22 and 8.23 show velocity magnitude plots throughout the vocal fold oscillation cycle for the impeding ventricular band configuration. The upper limit of the visible region was again located approximately 8mm downstream from the vocal folds. PIV measurements were performed both upstream and downstream of the ventricular bands. Both regions are visible in the plots. The region directly between the ventricular band constriction at their upstream face was not observed.

Behaviour of the jet within the laryngeal ventricle

The velocity magnitude plots once again reveal the formation, oscillation and break down of the glottal jet. It appears that as the jet traversed the laryngeal ventricle, prior to reattachment to the upstream face of the ventricular bands, it underwent considerably more degradation that with the realistic ventricular bands configuration. This initial observation was confirmed by the standard deviation plots, which are shown in figures 8.24 and 8.25. A clear laminar core was only observed for phase windows 3 to 9. Close to the minimum vocal fold separation the jet became highly unstable. It is important to note that the minimum constriction of the ventricular bands was located 24mm downstream of the vocal folds, rather than 16mm as with the $VB - A$ configuration. This may have helped to decrease the stability of the jet by providing a greater distance for the effects of turbulence in the flow to become important.

Figure 8.26 shows the behaviour of the four jet variables over the course of the glottal cycle. Once again, the variables showed a correlation with the period of the vocal fold oscillation. The standard deviation of the average jet core velocity was low during the bulk of the cycle, and rose sharply when the vocal folds neared their minimum separation. This quantitative result confirmed the general visual observations of the standard deviation velocity figures. It also led to the suggestion that the jet core was stabilised during this phase of the oscillation, in a manner similar to that described in section 8.3 for the physically realistic configuration.

The most interesting feature of the two plots was the behaviour of the average jet core velocity. It showed an initial sharp rise near the start of the cycle. However, upon reaching approximately 17ms^{-1} it was curtailed and dropped back to around 15ms^{-1}. It then remained close to this value for much of the cycle, with the exception of a slight rise at phase window 9, which corresponded to the minimum vocal fold separation. Overall, the core velocity was considerably lower than the simple Bernoulli prediction (assuming a total loss of pressure immediately downstream of the vocal folds) shown in table 7.1, by a factor of around 2:1.

Taken together, the behaviour of the average core velocity and the standard

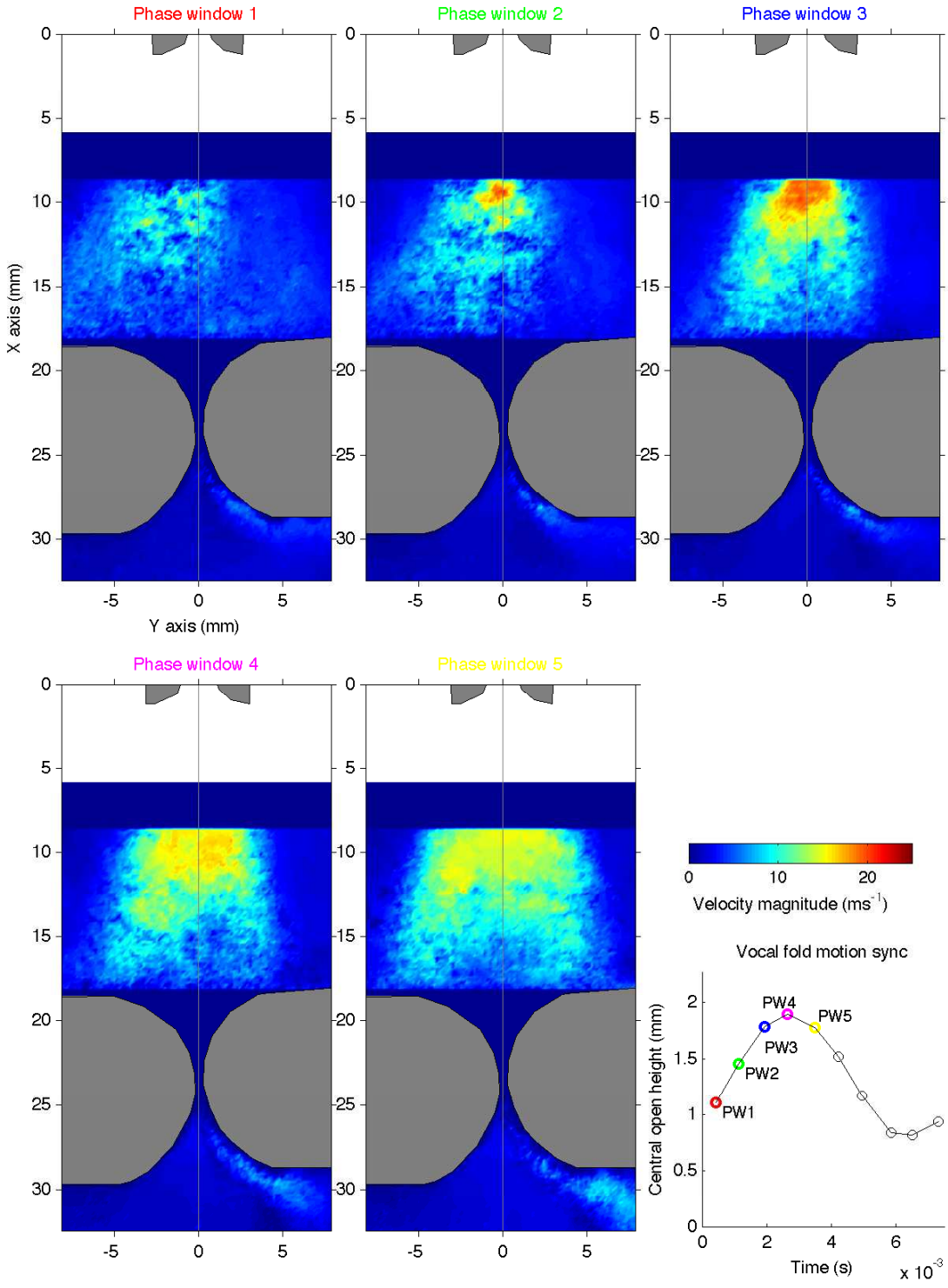

Figure 8.22: Velocity magnitude plots for the impeding ventricular band configuration for phase windows 1-5.

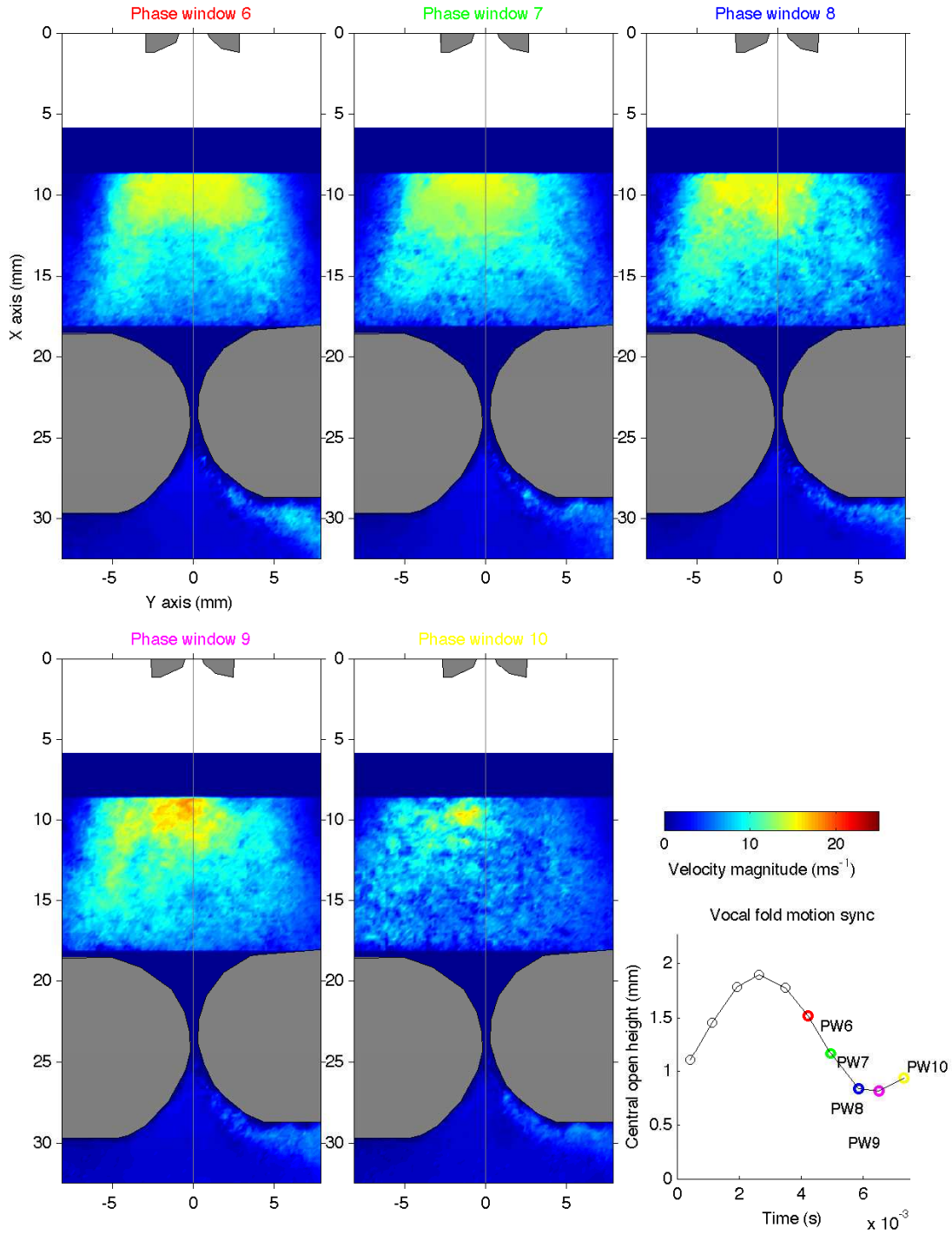

Figure 8.23: Velocity magnitude plots for the impeding ventricular band configuration for phase windows 6-10.

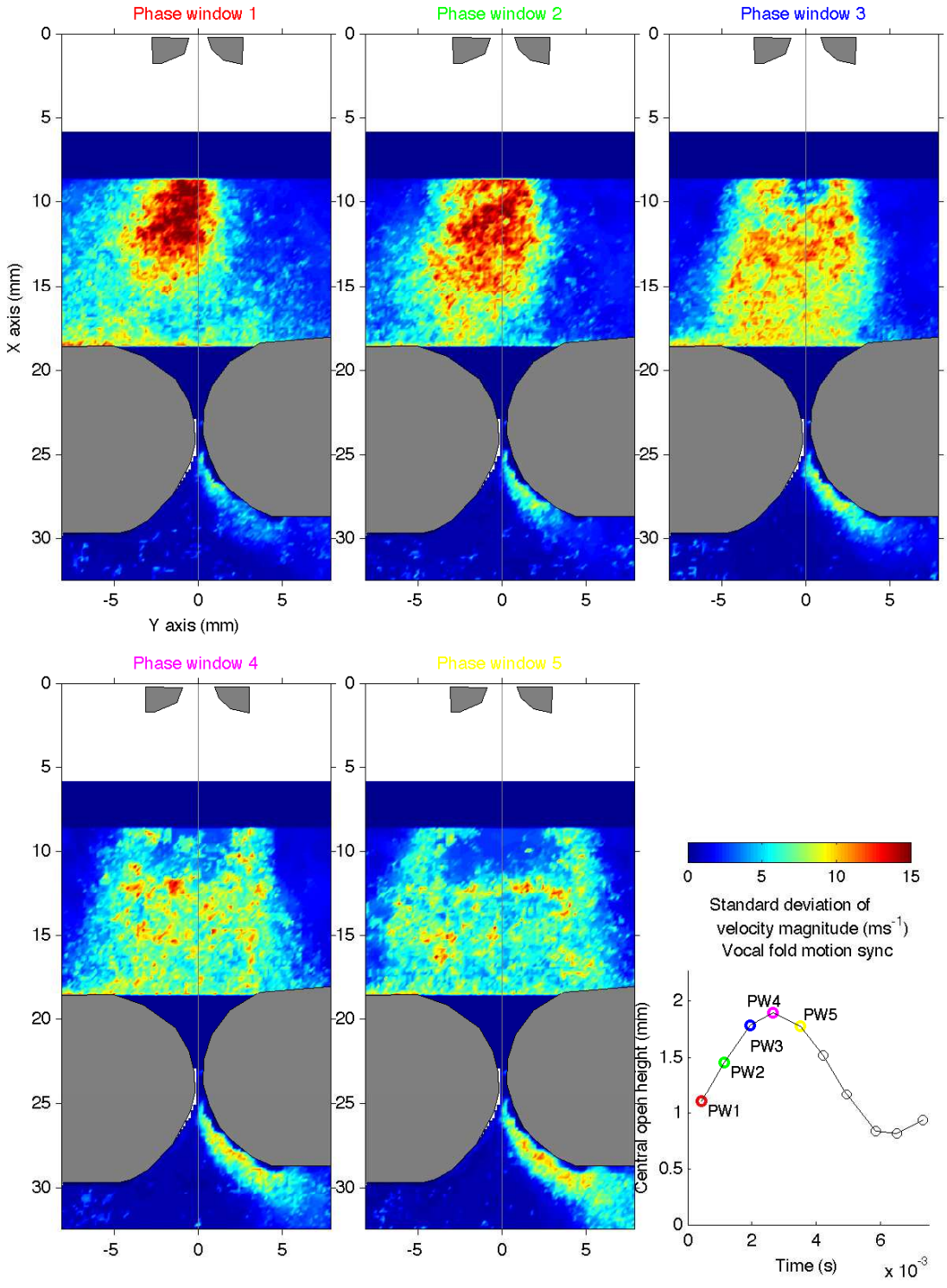

Figure 8.24: Standard deviation of velocity magnitude for the impeding ventricular band configuration for phase windows 1-5.

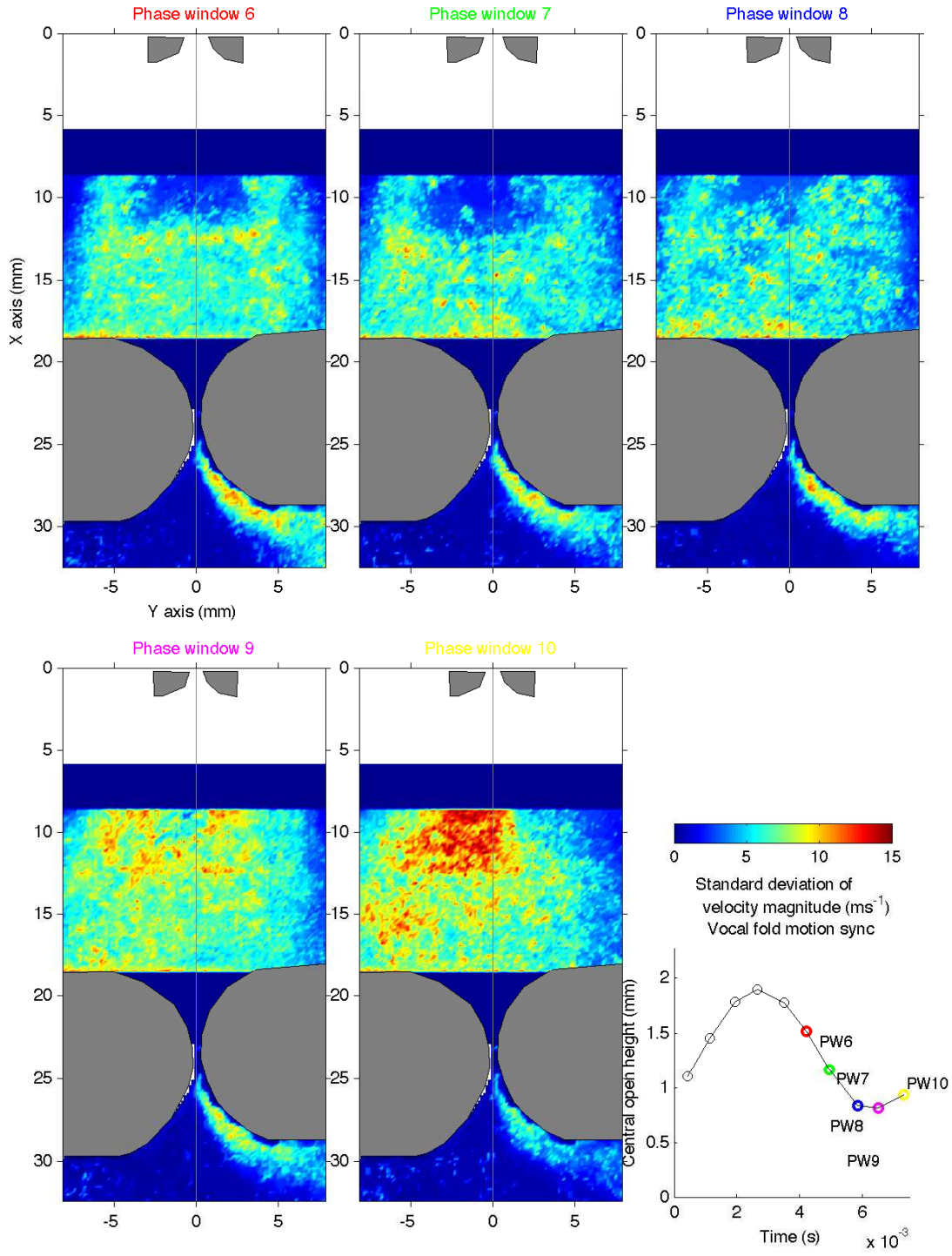

Figure 8.25: Standard deviation of velocity magnitude plots for the impeding ventricular band configuration for phase windows 6-10.

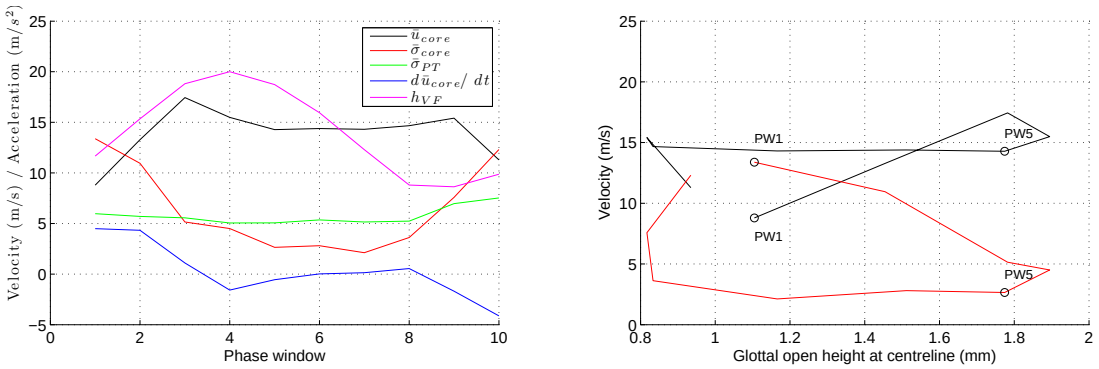

Figure 8.26: The four jet variables as as a function of phase window and glottal opening for the impeding ventricular bands ($VB - B$) configuration. In the left hand plot the vocal fold open height h_{VF} has been included (normalised to velocity) to illustrate the relative phase behaviour of the variables.

deviation of the core velocity allow a hypothesis to be made about the behaviour of the glottal jet, and its influence on the vocal folds oscillations. It is hypothesised that a strong reattachment of the jet occurred on the ventricular bands. The narrow constriction presented to the jet by the impeding configuration resulted in a strong pressure recovery, which curtailed the increase in fluid velocity within the laryngeal ventricle.

This effect is apparent in the trace of average jet core velocity, shown in figure 8.26. The sharp rise in velocity may have resulted from the initial flow separation, with relatively little impact from the ventricular bands. However, upon reaching the bands the jet underwent a reattachment. The very narrow gap between the ventricular bands then curtailed the volume flow of air through the whole system, decreasing the increasing fluid velocity of the jet in the laryngeal ventricle.

The vocal fold amplitude of vibration was considerably less for the impeding configuration than the other configurations. This result can be seen in any of the synchronisation plots within the main data maps, such as in figure 8.22. This behaviour has also been separately observed by Bailly *et al*[Bailly *et al.*, 2008]. The reason may have been the curtailed fluid velocities that occurred throughout much of the glottal cycle. The cause of this curtailing is addressed below in section 8.5.2. As will be shown it may have contributed to a lowering of the volume flow through the vocal folds, which in turn reduced the pressure drop across the vocal folds. This may have then reduced the level of the Bernoulli driving force between the vocal folds, and so increased the relative effect of the vocal fold restoring stiffness and damping, leading to a reduced vibration amplitude.

Behaviour of the jet downstream of the ventricular bands

The velocity magnitude plots of figures 8.22 and 8.23 reveal the formation of a secondary jet within the vocal folds - ventricular bands system. The jet can be seen strongly adhering to the downstream edge of the right hand ventricular band throughout the glottal cycle. This was in interesting contrast to the glottal jet, which appears to be directed slightly to the left of the glottal centreline around the minimum vocal fold separation. The ventricular jet can be seen expanding as it curved around the band, causing a decrease in velocity and an eventual degradation to turbulence. Its maximum width and velocity occurred around the maximum opening of the vocal folds, when the glottal volume flow was at a maximum.

It was probable that the strong asymmetry seen in the case of the secondary jet was caused by the so-called 'Coanda effect'. The presence of a Coanda effect in the case of the glottal jet has been a subject of intense debate over the last half-centuary. Studies on static vocal fold replicas have shown it to be a feature of the glottal flow under steady and unsteady conditions[Erath and Plesnaik, 2006b; Tao *et al.*, 2007]. However, its relevance during full self-sustained oscillations has been questioned[Pelorson *et al.*, 1994; Hirschberg, 1992]. In the case of the static ventricular bands it was perhaps not surprising that it was a feature of the flow. No further analysis was performed on the ventricular jet, and it is left as a possible subject for future investigation.

8.5 Comparative analysis of the three configurations

8.5.1 Investigations into the geometrical expansion of the glottal jet

One of the main objectives of the present work was to use PIV as a tool to quantify the geometrical expansion of the glottal jet downstream of the vocal folds. The nature of the jet expansion is important because it has been hypothesised that the glottal jet may interact with the ventricular bands in such a way as to affect the oscillations of both the vocal folds and the ventricular bands.

Under the assumption that the Bernoulli equation can be applied to the bulk of the separation glottal jet the amount of geometrical expansion is crucial in determining the pressure in the jet when it reaches the ventricular bands. The pressure in the bulk of the jet determines the aerodynamic driving force that can act over the surfaces of the ventricular bands. It is thus a key factor in the ability of the ventricular bands to destabilise and vibrate during certain exotic singing styles (see section 7.3.1).

In section 7.3.2 three theories that describe the geometrical expansion of the jet have been outlined, as postulated by Bailly *et al*[Bailly *et al.*, 2008; Bailly, 2009]. The purpose of the work in this section is to test the validity of the three theories using the experimental measurements obtained as part of this thesis. It is important to recognise that the original postulation of the theories was by Bailly *et al.* The original

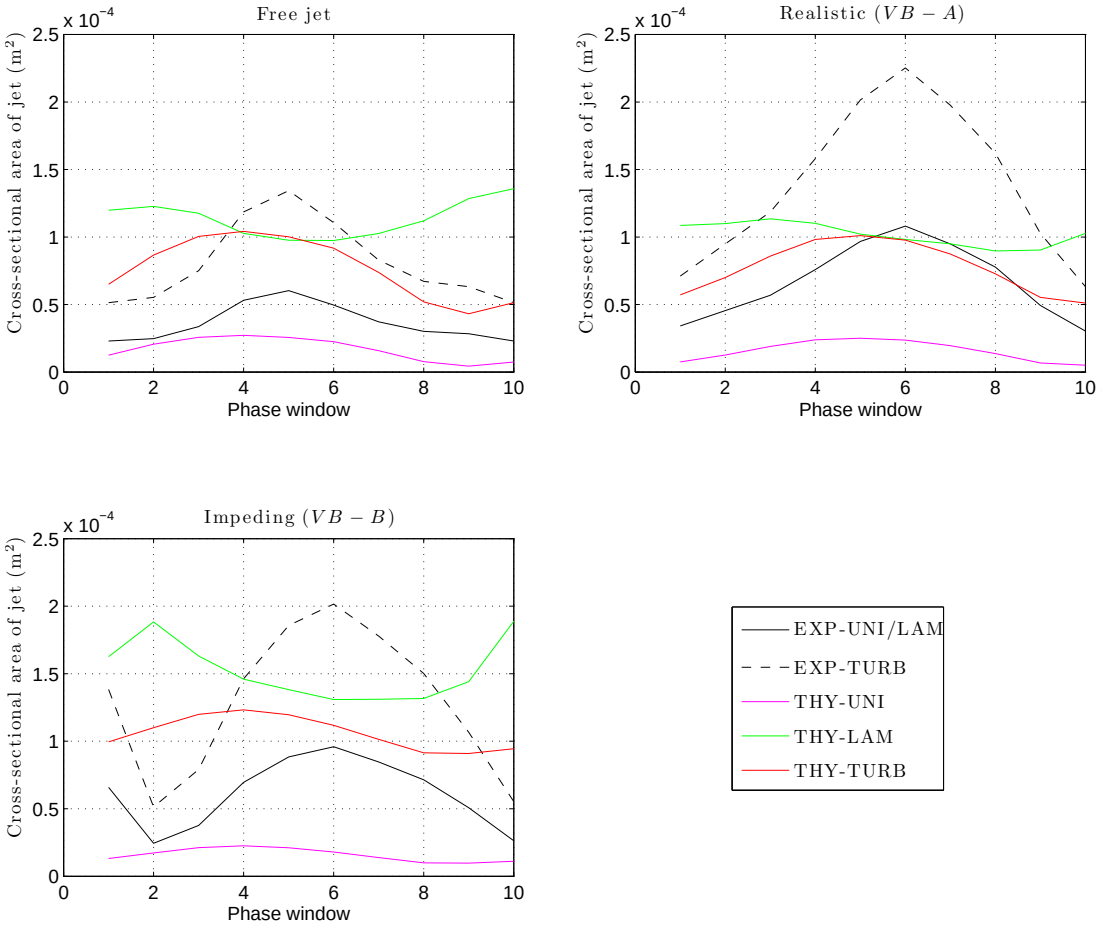

Figure 8.27: Plots of the cross-sectional area of the jet core for each of the three configurations, as estimated from the experimental data (black and dashed black lines), and calculated according to the three jet expansion theories.

contribution of this thesis has been to perform the experimental work, process the experimental data, analyse the experimental data so it can usefully be compared with the theoretical predictions, and draw conclusions about the meaning of the results.

Figure 8.27 shows plots of the theoretical and experimental estimates of the glottal jet expansion for each of the three configurations as functions of phase window (time).

The free jet configuration

Consider first the free jet configuration, shown in the upper left plot. The uniform jet theory (THY-UNI) compares very poorly with either of the experimentally measured jet cross-sections. The turbulent expansion theory appears to be the closest match, showing a particularly close agreement during the closing phase. The laminar jet theory (THY-LAM) poorly matches the experimentally observed behaviour, except close to the maximum opening where it provides a fit similar in quality to that of the turbulent

jet expansion.

It must be pointed out, however, that the assumption of a 25mm z-wise jet expansion for the case EXP-TURB is a rather *ad hoc* one. The value of 25mm has been used in the present case because it features in the turbulent jet expansion theory for the ventricular bands configurations. In these calculations it makes a degree of sense, given the known width of the vocal tract of 25mm, which would indicate the maximum possible z-wise expansion that the jet could undergo.

However, in the case of the free jet there would be no such direct limit on any z-wise expansion of the jet. The seemingly close fit of the turbulent theoretical jet expansion THY-TURB to the experimentally observed data should thus be considered with some caution. Use of a different z-wise expansion in the calculation of the jet cross-section would immediately lead to a uniform raising or lowering of the curve EXP-TURB. It is impossible to know the true z-wise expansion of the free jet case, without further measurements that include an estimate of its three-dimensional behaviour.

The realistic configuration ($VB - A$)

Consider now the realistic configuration, shown in the upper right plot. As with the free jet example above, the theoretical uniform jet expansion is a poor fit to the experimental data. The laminar expansion theory appears to be a poor match to the experimental data. Its overall envelope appears to be follow a curve almost inverse to that of both experimental data sets.

The most interesting results concern the turbulent expansion. At small vocal fold open heights, corresponding to phase windows 1, 2, 9 and 10, the theoretical turbulent expansion (THY-TURB) appears to match quite closely with the experimental data (EXP-TURB). As the oscillation cycle progresses, however, the experimentally observed jet width evaluated with a turbulent z-wise expansion (EXP-TURB) appears to expand considerably more than the theoretical prediction. As would be expected from a purely geometrical calculation of the jet expansion, the basic temporal evolution behaviour of the turbulent expansion theory matches that of the experimental data (as with the free jet configuration). This is because the theoretical and experimental calculations are both directly related to the temporal evolution of the glottal opening.

In the bulk of the cycle, between phase windows 3 and 8, and particularly during the closing phase (windows 5-8), there is then a good agreement between the experimentally observed jet under a laminar expansion assumption (EXP-LAM) where no z-wise expansion is assumed, and the turbulent jet expansion theory (EXP-TURB), where a z-wise expansion of the jet is assumed. Strictly speaking, however, these two data sets would not appear to be comparable, as they are each calculated based on differing assumptions about the z-wise jet expansion.

Variable	Description	Definition
h_{norm}	Normalised glottal height (quantifies the behaviour of the mechanical vocal fold motion)	h_{VF} / h_{max}
Re_{core}	Reynolds number of the jet core (quantifies validity of inviscid assumption, see section 2.5.1)	$h_{VF} \cdot \bar{u}_{core}$ / μ
u_{norm}	Normalised jet core velocity (measures jet velocity relative to simple Bernoulli prediction)	$\bar{u}_{core}$ / u_{VF}
Z_{VF}	Vocal fold flow impedance (measures how efficient a configuration is at transmitting flow)	P_0 / U_{jet}
T_{core}	Jet core turbulence parameter (quantifies levels of turbulence in the core of the jet)	$\bar{\sigma}_{core}$ / $\bar{u}_{core}$

Table 8.1: A summary of the five non-dimensionalised parameters used to describe the behaviour of the vocal fold - ventricular band system (see section 7.4.5 for a more detailed explanation of the quantities).

The impeding configuration ($VB - B$)

Consider finally the impeding configuration, shown in the lower left plot. None of the jet expansion theories provide a good fit to the experimental data. The turbulent expansion theory was the best fit overall. However, it significantly underestimates the jet expansion during the middle part of the cycle, when the vocal fold opening is large. It further overestimates the jet expansion when the vocal fold open height is small. The temporal development of the turbulent expansion theory did match the experimental data, as with the free jet and realistic configurations.

8.5.2 Investigations into the fluid mechanics of the glottal jet using non-dimensional flow variables

Turbulence levels within the jet core

In section 7.4.5 the idea of using non-dimensionalised parameters to describe the evolution of the glottal jet was outlined. Five ket parameters were postulated, each of which used a selection of the experimental quantities to formulate a parameter that described a particular aspect of the vocal fold - ventricular band system. Table 8.1 presents a brief summary of these parameters, including their mathematical definition and a brief explanation of their relevance.

The behaviour of the glottal jet for each of the three ventricular band configurations was explored by parametrically plotting the various non-dimensional flow variables against each other. Figure 8.28 shows four plots which use the non-dimensional parameters.

Consider first the upper left plot, which shows the jet core turbulence parameter T_{core} as a function of phase window (effectively a temporal axis). The free jet

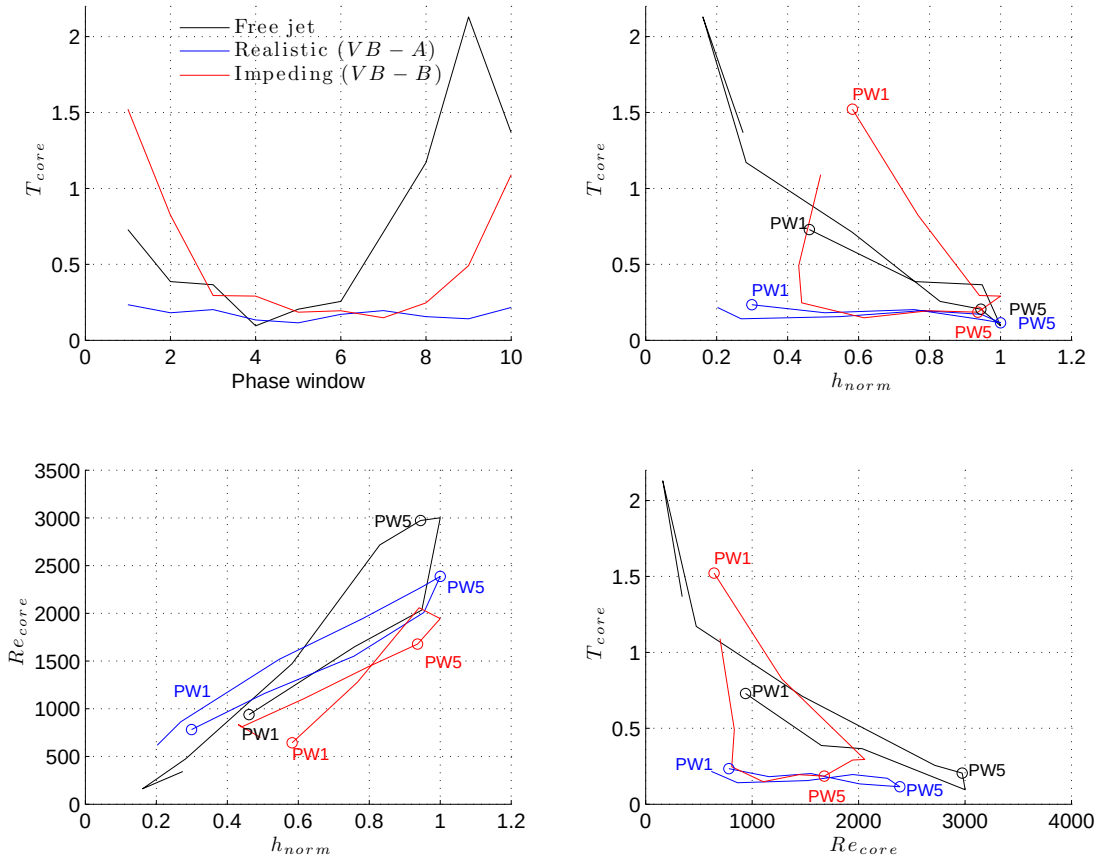

Figure 8.28: Plots of non-dimensionalised flow parameters for the free jet, realistic $(VB - A)$ and impeding $(VB - B)$ ventricular band configurations. Phase windows 1 (PW1) and 5 (PW5) have been marked on the plots.

configuration revealed an extremely unstable jet core, with very high turbulence levels for all phase windows except 4, 5 and 6. The physically realistic configuration revealed low turbulence levels throughout the whole oscillation cycle. The impeding configuration revealed a behaviour somewhere between the free jet and physically realistic configurations. Its overall turbulence levels were lower than the free jet, with the exception of phase windows 2 and 3. It also showed higher stability between windows 6 and 8, during which the free jet turbulence became very large.

The upper right plot shows the turbulence parameter plotted as a function of the vocal fold opening. This plot showed similar behaviour to the upper left plot, with the highest levels of turbulence occurring close to the minimum vocal fold opening (towards the left of the plot). The most interesting feature of the plot was certainly the very low turbulence of the physically realistic configuration. The plot further demonstrated the generally low turbulence levels of the impeding configuration, with the exception of the part of the cycle close to the minimum vocal fold opening. It also clearly illustrated

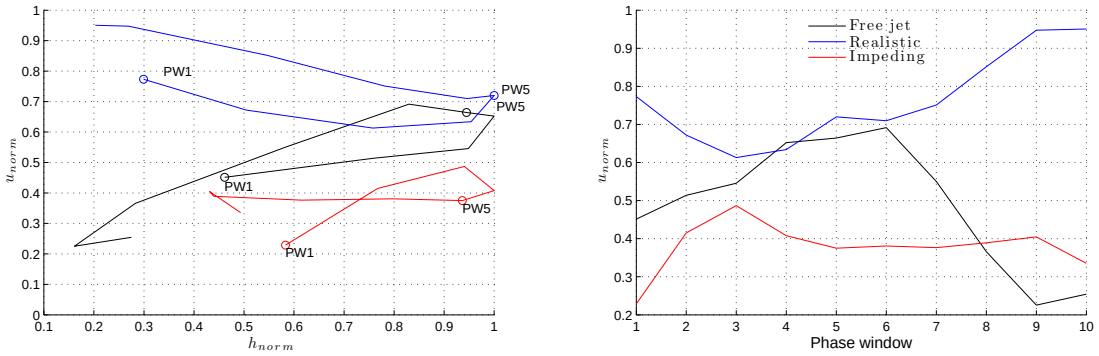

Figure 8.29: Plots of the normalised average jet core velocity against the normalised vocal fold separation (at left), and against phase window(at right) for the free jet, realistic ($VB-A$) and impeding ($VB-B$) ventricular band configurations.

the reduced amplitude of the vocal fold motion for the impeding configuration.

In the case of the free jet and impeding ventricular band configuration, it is possible that the downstream limit of the jet core may have migrated upstream and out of view around the minimum vocal fold opening. The jet core propagation limit of approximately seven times the diameter of the channel at flow separation (see section 7.4.4), did indeed suggest that the true jet core would be expected to move in and out of the field of view throughout the oscillation cycle (it should be visible for glottal openings of greater than about 1.1mm). This would have resulted in the jet core velocity measurements being made on a strongly transitional region of the flow, where turbulent effects became significant. Perhaps the most intriguing point to arise from this is the remarkable stability of the physically realistic configuration. Even at small vocal fold separations, the smallest of which was actually narrower than the corresponding impeding configuration, the flow remained quite stable.

The lower left plot shows the development of the jet core Reynolds number as a function of the vocal fold opening. The plot demonstrated that all configurations operated within approximately the same range of fluid viscosity conditions. Overall, the Reynolds number dropped below 1000 when the vocal fold opening became less than about half of its maximum. In this regime the effects of viscosity are expected to become increasingly important.

The lower right plot shows the relationship between the jet core turbulence parameter and the jet core Reynolds number. The physically realistic configuration maintained a low turbulence throughout the whole range of Reynolds numbers, in contrast to the highly turbulent free jet configuration. Once again the impeding configuration presented an intermediate case, showing an overall stabilised jet behaviour over most of the cycle, with the exception of small vocal fold separations.

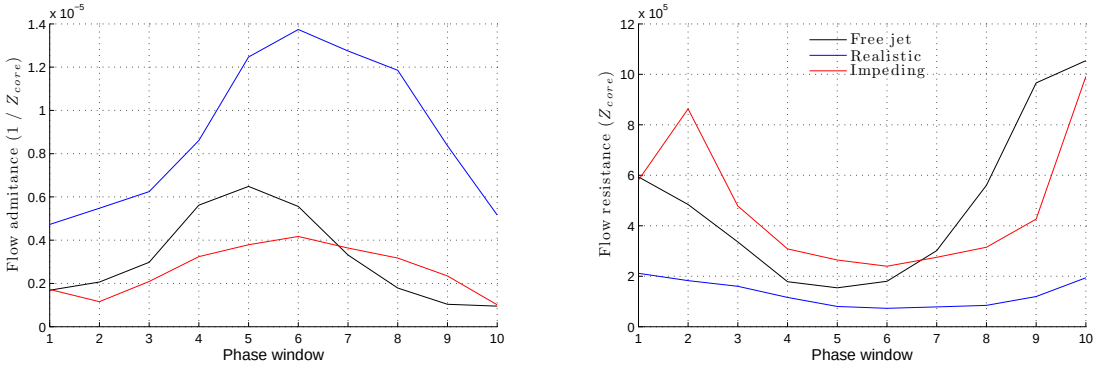

Figure 8.30: The flow admittance (at left) and flow resistance (at right) for all three configurations.

Influence of the ventricular bands on the jet velocity and volume flow

Figure 8.29 shows the normalised jet velocity u_{norm} as a function of the vocal fold opening (left) and as a function of phase window (right) for each of the configurations. The two plots illustrate the influence of the ventricular bands on the jet core velocity throughout the oscillation cycle.

The free jet configuration showed a wide range of normalised jet core velocities, between approximately 0.2 and 0.7. There was a hysteresis in the velocity, such that higher velocities occurred during the closing phase of the vocal fold cycle. The peak value of u_{norm} of 0.69 indicated that even when the measured jet core velocity was highest, considerable deceleration of the jet occurred between flow separation and the measurement point approximately 8mm downstream. This was due to entrainment of the surrounding fluid, which caused drag on the jet

In the case of the realistic ventricular bands configuration, u_{norm} varied between approximately 0.95 and 0.6. This indicated that the jet core velocity remained quite close to the maximum possible velocity predicted by the simple Bernoulli calculation (which assumed a total pressure loss). A hysteresis was clearly evident, whereby the largest jet core velocities occurred during the closing phase of the cycle. The behaviour of the curve implies that the jet did not undergo a strong deceleration following its separation from the vocal folds. It is very likely that this was a direct result of the aerodynamic influence of the rigid ventricular bands.

In the case of the impeding ventricular bands configuration, u_{norm} varied between approximately 0.2 and 0.5. This was an overall reduction in the measured jet core velocity, relative to the Bernoulli-predicted value, over the free jet configuration. It seems unlikely that an increased jet deceleration caused this behaviour. It has already been demonstrated in the preceding section that the impeding configuration resulted in an overall more stable jet compared to the free jet. This implies that a higher jet

deceleration would be unlikely. The most probable cause for the low jet velocity was the narrow constriction presented by the ventricular bands, which acted to strongly retard the volume flow through the valve. This matter is discussed further below.

The most interesting overall feature of the plots in figure 8.29 is thus the vertical offset between the curves. The realistic configuration showed the least jet velocity retardation (relative to the Bernoulli prediction), followed by the free jet and the impeding configuration.

One of the possible mechanisms which resulted in a reduction to the jet velocity retardation in the case of the realistic ventricular bands was the presence of a pair of large 'laryngeal' vortices located on either side of the jet, which remained in position throughout the whole oscillation cycle. These vortices cannot be clearly seen in the vorticity plots shown in figures 8.16 and 8.17, because the high vorticity levels of the jet shear layers resulted in a vorticity scale where the relatively slow rotation of the laryngeal vortices has been masked. In the velocity magnitude plot of figure 8.15 their presence may be inferred by the presence of circular, low velocity regions located either side of the main jet core. Phase window 9 in the figure is perhaps the clearest example of this.

The presence of persistent laryngeal vortices indicates a continuous recycling of the fluid within the laryngeal ventricle. As the glottal jet emerges into the ventricle, it is thus met with a pair of favourably rotating fluid vortices that do not provide as much drag on the jet as with the free jet case. For the free jet configuration the jet is subjected to a nearly continuous supply of almost-stationary fluid as it emerges from the vocal fold opening and entrains the surrounding fluid. The overall result is that the jet in the realistic configuration does not undergo as much momentum transfer as in the free jet case.

The presence of counter-rotating laryngeal vortices was also seen in the impeding configuration. This further adds weight to the aforementioned suggestion that the low jet core velocities did not result from a particularly strong jet deceleration, but were in fact related to the aerodynamic influence of the ventricular bands.

Figure 8.30 shows plots of the experimentally measured vocal fold flow admittance (left) and impedance (right) for each of the three configurations. The plot of admittance is particularly enlightening. It presents a volume flow calculation for each configuration, normalised to the upstream driving pressure. Where the vocal folds are 'efficient' at transmitting flow, the admittance is high. On the contrary, where the flow is subjected to a high impedance, the admittance is low. The plot of impedance thus relates the same information as the plot of admittance.

The realistic configuration acted to transmit flow far more efficiently than the free jet and impeding configurations. This confirms much of the other work in the chapter, which has shown the strong influence of the realistic ventricular bands configuration on the glottal jet.

Configuration	P_0	u_{sep} (ms^{-1}) (Bernoulli)	$\bar{u}_{core}$ (ms^{-1}) (experimental)	u_{norm} ($\frac{u_{core}}{u_{sep}}$)
Free jet (no vocal tract)	380Pa	$27.6\mathrm{ms}^{-1}$	$20\mathrm{ms}^{-1}$	0.69
Physically realistic ventricular band config ($VB-A$)	270Pa (decreased)	$23.2\mathrm{ms}^{-1}$	$21\mathrm{ms}^{-1}$	0.95
Impeding ventricular band config ($VB-B$)	677Pa (increased)	$36.8\mathrm{ms}^{-1}$	$16\mathrm{ms}^{-1}$	0.48

Table 8.2: A table summarising the typical jet core velocity behaviour of the three configurations. Calculation of the maximum jet velocity at flow separation u_{sep}, based on the quasi-steady Bernoulli equation, has been made for each configuration using the noted total upstream pressure P_0 measured during the measurements. The typical peak jet velocity $\bar{u}_{core}$ in the core of the observed jet is also recorded, along with the dimensionless velocity u_{norm} described in section 7.4.5.

The behaviour of the free jet and impeding configurations also suggest a very interesting result. During the opening phase of the glottal cycle, the free jet flow admittance grows quite quickly as the jet separates from the vocal fold walls and accelerates into free space. Conversely, in the impeding configuration the volume flow is immediately retarded due to a high vocal fold flow admittance. This is caused by the very narrow opening between the ventricular bands - just 1mm - which acts to strongly throttle back the airflow through the overall vocal folds - ventricular bands system.

During the closing phase, however, there is a sharp drop in the volume flow admittance of the free jet configuration. In the impeding case, the flow admittance remains low, but there is no evidence of the sudden drop as in the free jet case. It is possible that the sharp drop results from the effect of turbulence in the glottal jet, which, as has been clearly demonstrated in the first part of the present section, is extremely high during the closing phase of the free jet (see figure 8.28 for the evidence of this behaviour). Such a sharp rise in turbulent dissipation in the jet could act to destroy the volume flow through the vocal folds[Bailly, 2008].

8.6 Relevance of the experimental results to the case of the lip-reed

In the background discussion of section 2.8.1 a comparison was made between the physical layout of the vocal folds - ventricular bands system, and the system of the brass instrument lip-reed. It was noted that the overall configurations are remarkably similar. They both consist of a deformable mechanical structure - the vocal fold or the lips - which acts as an oscillating flow control valve, followed by a secondary mechanical

constriction a short distance downstream. The key difference in is that in the case of the vocal folds, the secondary constriction is formed by the ventricular bands, which are soft and deformable. Indeed, they have been shown to undergo periodic oscillations during certain exotic singing styles[Fuks *et al.*, 1998]. In the case of the lip-reeed, the secondary constriction is formed from the mouthpiece throat, which is a rigid structure.

In the present work the aerodynamic interaction between a self-oscillating *in vitro* vocal fold replica and a pair of rigid replica ventricular bands was investigated. This situation presented an overall geometrical layout with even more similarity to that encountered in the case of the lip-reed than the true vocal folds - ventricular bands system in the human larynx.

Consider figure 2.16, which shows a schematic layout of the two systems. The distance between the vocal folds and the ventricular bands L_{VB} used in this study, either 16mm or 24mm, is certainly comparable to the length of the mouthpiece cup L_{MP}, which can be anywhere between 5 and 25mm, depending on the brass instrument to be used with the mouthpiece. The minimum ventricular band separation, between 1 and 3mm in the present study, is also comparable to the throat heights encountered in some mouthpieces, typically between 3 and 8mm. This again depends on the particular instrument. For example, mouthpieces that are used with horns typically have shorter cup distances and narrower throat widths than the typical mouthpieces used with bass trombones.

The most important conclusion from the present work is that a secondary constriction located downstream of a self-oscillating valve has a measurable aerodynamic effect on the behaviour of the air jet formed from the valve. This leads to a direct aerodynamic coupling between the secondary constriction and the valve. Depending on the particular configuration of the secondary constriction, the aerodynamic interaction can either assist or impede the oscillations of the valve by directly influencing the volume flow of air.

The mechanical size and shape of a typical trombone mouthpiece is most comparable to the realistic ventricular bands configuration ($VB-A$). It has been shown in section 8.5.2 that $VB-A$ had a considerable impact on the behaviour of the replica vocal folds and the glottal jet. The volume flow of air was considerably raised, relative to the upstream overpressure, compared to the free jet configuration. It was shown that a reattachment of the glottal jet to the ventricular bands resulted in a much stabilised jet behaviour compared to the free jet. This resulted in the maintenance of a higher overall jet flow throughout the oscillation cycle. It has been hypothesised that this increased flow would result in a higher average pressure drop ΔP_{VF} (according to the quasi-steady Bernoulli equation) across the vocal folds over the course of a cycle. This would lead to a higher overall Bernoulli driving force within the vocal fold channel, relative to the free jet case, which would thus be expected to assist the oscillations and lower the threshold onset pressure.

The distinct geometrical similarity between a typical brass instrument mouthpiece and configuration $VB-A$ leads to the tantalising hypothesis that a similar aerodynamic feedback mechanism could be relevant to the case of the lip-reed. There is strong empirical evidence that, in the absence of a full instrument, the presence of a mouthpiece noticeably aids the ability of a player to 'buzz' their lips[Cullen *et al.*, 2000; Neal, 2002; Richards, 2003]. This behaviour has, up to now, been attributed to the small acoustic compliance provided by the lower end of the main mouthpiece resonance. It has been suggested that this may provide sufficient acoustical feedback to increase the total driving force on the lips and so assist in their oscillation (see figure 3.12 for impedance curves of two brass instrument mouthpieces).

The results of the present work do not discount the possible importance of an acoustical feedback mechanism. However, they do appear to suggest that an aerodynamic effect could also be at work in this phenomenon. It is even possible that the subtle differences between mouthpieces designed for the same instrument, which are frequently noted by players, may be in some way attributable to the effect of a direct aerodynamic interaction between the mouthpiece and the player's lips. However, such a hypothesis is speculative, and the only way to verify or discount such an idea would be to perform a further experiment using the various downstream conditions employed by such mouthpieces. To be truly conclusive, such a study should also employ blind tests of experienced players, asked to give feedback on the characteristics of the mouthpieces. This may allow a correlation to be made between any experimentally observed aerodynamic feedback, and the impressions of the players.

8.7 Conclusions

The work in this chapter has investigated the behaviour of the glottal jet produced downstream of an *in vitro* self-oscillating vocal folds replica. Three different downstream configurations were used; a free jet configuration with no vocal tract, and two different configurations involving rigid replica ventricular bands. Section 7.3 has outlined a number of hypotheses concerning the geometrical expansion of the jet. These hypotheses were initially suggested by Bailly *et al*[Bailly *et al.*, 2006]. They have been investigated by the author of this thesis as part of the collaborative work between the University of Edinburgh and GIPSA in Grenoble. One of the principle objectives of this chapter has been to test the validity of these hypotheses using the *in vitro* vocal fold replica described in section 6.3.

8.7.1 Behaviour of the free jet

The first part of this chapter, described in section 8.2, investigated the free jet configuration. An overview of the jet features and behaviour has been provided in

section 8.2.2. The most important conclusions concerning the free jet are presented below:

- The presence of a distinct air jet was observed throughout the glottal cycle.
- The phase windowed vector maps revealed the presence of counter-rotating shear layers on either side of the jet.
- The jet was observed to oscillate throughout the glottal cycle in velocity, direction and stability.
- The jet core velocity was observed to oscillate between approximately 20 and 70% of the theoretical jet velocity predicted by the Bernoulli equation. This was due to the deceleration of the jet between flow separation and the start of the region with optical access to the flow.
- The maximum jet speeds were encountered at the start of the closing phase. This suggested the presence of an asymmetry in the intra-glottal pressure, which may be evidence for an oscillating Bernoulli force within the larynx. This mechanism has long been suggested as the principle energy transfer mechanism in phonation[Hirschberg, 1992]. Recent work by Thomson *et al*[Thomson *et al.*, 2005] used a finite element simulation of the vocal folds in conjunction with a detailed fluid mechanical simulation of the flow to confirm this.
- The jet showed a distinct asymmetry throughout the oscillation cycle, relative to the centreline of the glottis. At the start of the cycle it was skewed towards the left side, possibly indicative of a Coanda effect. As the cycle progressed it rotated back towards the glottal centreline, before again moving towards the left as the vocal folds approached their minimum separation. It was not possible to provide any firm conclusions about this behaviour as direct optical access to the vocal fold opening was not possible. However, flow visualisation evidence from an earlier experiment using a similar *in vitro* replica has shown that the jet can adhere to one of the vocal fold walls during full self-sustained oscillations.
- The phenomenon of 'jet flapping' appears to have occurred for the free jet configuration. This behaviour has recently been reported by Neubauer *et al*[Neubauer *et al.*, 2007] in a similar self-oscillating *in vitro* vocal fold replica. The jet displayed large scale 'tongues' of flow directed to the left and right of the glottal centreline, as it was dissipated into increasingly turbulent motion by momentum transfer.
- The jet was most stable during the middle part of the oscillation cycle, when the vocal fold height h_{VF} was at its greatest.

- As the vocal fold height became small the standard deviation of the phase windowed average jet velocity became quite large. A turbulence parameter T_{core} was defined to quantify this behaviour. The turbulence was very high at small vocal fold separations ($T_{core} \approx 2$), and much lower at large vocal fold separations ($T_{core} < 0.2$).

- The level of turbulence in the jet appears to be related to both the size of the vocal fold opening, and the level of flow deceleration. During the opening phase, as the jet accelerated towards its peak velocity, the turbulence decreased. As the jet decelerated in the latter part of the closing phase, the turbulence rose sharply. This results seems to be in line with standard findings relating to oscillatory jet flow[Schlichting and Gersten, 2000; Fishler and Brodkey, 1991].

8.7.2 Influence of the ventricular bands

Behaviour of the realistic ventricular bands configuration ($VB - A$)

The realistic ventricular bands configuration appeared to strongly influence the flow behaviour, acting to increase the volume flow through the system and decrease the threshold oscillation pressure. A summary of the important conclusions arising from the initial analysis of $VB - A$ is presented below:

- The jet did not exhibit any measurable skewing from the glottal centreline.

- The jet was observed to oscillate in average jet core velocity and jet core width throughout the glottal cycle.

- The average jet core velocities throughout the oscillation cycle were typically 65 to 95% of the velocity predicted by a simple Bernoulli calculation in the absence of any ventricular bands. This implied considerably less deceleration of the flow, and pointed to a reattachment on the ventricular bands. The possible influence of counter-rotating laryngeal vortices, which act to reduce the effects of fluid entrainment, has also been noted.

- The overall stability of the flow was much higher than the free jet case. The standard deviation of the jet core velocity did not rise above 20% of the averaged velocity for any phase window ($T_{core} < 0.2$). This meant that a clear jet core was recored for all phase windows, again leading to the suggestion that flow reattachment occurred on the ventricular bands, resulting in considerably reduced degradation of the jet structure due to turbulent dissipation.

Behaviour of the impeding ventricular bands configuration ($VB - B$)

The impeding ventricular bands configuration strongly influenced the flow behaviour, in almost exactly the opposite way to the realistic configuration. The overall volume flow through the system was strongly decreased, and the threshold oscillation pressure was increased. A summary of the important conclusions arising from the initial analysis of $VB - B$ is presented below:

- The jet exhibited a skewing towards the left of the glottal centreline throughout the whole glottal cycle. In contrast, the secondary ventricular jet showed a strong Coanda effect which resulted in adherence to the right hand ventricular band.

- The jet was observed to oscillate in average jet core velocity and jet core width throughout the glottal cycle.

- The average jet core velocities throughout the oscillation cycle were typically 20 to 60% of the velocity predicted by a simple Bernoulli calculation in the absence of any ventricular bands. The possible influence of counter-rotating laryngeal vortices, which acted to reduce the effects of fluid entrainment, suggested that this lowering of the jet velocity relative to a simple Bernoulli calculation was due to the direct influence of the ventricular bands, and was not purely a result of increased fluid deceleration.

- The overall stability of the flow was generally higher than the free jet. The standard deviation of the jet core velocity remained close to 20% of the averaged velocity for phase windows 4-8 ($T_{core} < 0.2$), which meant that a clear jet core was recored for these phase windows.

8.7.3 Behaviour of the geometrical jet expansion for all configurations

The experimentally observed jet height at the ventricular bands flow reattachment h_R was used to estimate the cross-sectional area of the glottal jet under uniform, laminar and turbulent hypotheses. In the uniform hypothesis no expansion of the jet was assumed to take place. In the laminar hypothesis the jet was assumed to expand only in the direction transverse to the streamwise axis. In the turbulent hypothesis the jet was assumed to expand both transverse to the flow (the y axis) and in the out-of-plane direction (the z axis).

For each configuration, the experimentally estimated jet expansions were compared to three theoretically calculated jet expansions, described by uniform, laminar and turbulent geometrical jet expansion formulas.

Free jet configuration

In the free jet case the theoretical turbulent expansion was found to closely match the experimentally observed data, particularly during the closing phase. The uniform and laminar jet expansion theories were poor fits of the experimental data.

Realistic configuration

The experimentally observed jet expansion was found to be considerably larger ($\approx$ 100%) than the theoretical turbulent expansion for much of the glottal cycle. Around the minimum vocal fold separation the experimental and theoretical curves became very close.

The uniform jet expansion theory was a poor fit to the experimental data.

Impeding configuration

None of the jet expansion theories were a close fit to the experimental data, although the turbulent expansion theory was the closest. However, it underestimated the jet expansion during the middle part of the oscillation cycle when the vocal folds were near their maximum opening, and overestimated the expansion when the vocal folds were near their minimum opening. The uniform and laminar expansion theories were poor fits to the data.

8.7.4 Behaviour of the non-dimensionalised jet variables for all configurations

The behaviour of the jet core was analysed with the use of non-dimensionalised mechanical and fluid mechanical variables. The most important findings are summarised below:

- The free jet configuration showed the highest overall turbulence levels, which became very large during the closing phase and around the minimum vocal fold opening ($T_{core} \approx 1 - 2$).

- The physically realistic configuration showed the lowest turbulence levels, which remained relatively low throughout the whole oscillation cycle ($T_{core} < 0.2$).

- The impeding configuration showed an improved stability during most of the oscillation cycle ($T_{core} \approx 0.2$), compared to the free jet configuration, with the exception of high turbulence levels in the vicinity of the minimum vocal fold separation ($T_{core} \approx 0.5 - 1.5$).

8.7.5 Behaviour of the volume flow for all configurations

The volume flow through the vocal folds was studied by calculation of the flow admittance and impedance. The realistic ventricular bands configuration was shown to have more than twice the flow admittance than either the free jet or impeding ventricular band configurations. This implied that the ventricular bands used in the realistic configuration strongly assisted the flow of air through the vocal folds. As the pressure difference across the vocal folds was strictly a function of the volume flow, this lead to an increased pressure drop, relative to the free jet case. It is possible that this was the mechanism by which the oscillation threshold pressure was lowered for the realistic configuration. The average volume flow throughout the cycle was so much higher than the free jet case that it resulted in an increased pressure drop across the valve, and thus a decreased oscillation threshold pressure.

In the case of the impeding configuration, the opposite behaviour was seen. The overall flow admittance was lower than that of the free jet for much of the glottal cycle. This was due to the strong influence of the small ventricular band opening, which acted to throttle back the volume flow through the whole system. In turn, this lead to a considerably reduced pressure drop across the vocal folds, for a given upstream overpressure, which meant that the overall threshold oscillation pressure was raised (relative to the free jet configuration). One apparent consequence of this behaviour was the lowering of the overall oscillation amplitude of the vocal fold open height throughout the oscillation cycle, relative to the free jet case.

8.7.6 Suitability of PIV for the present study

The use of PIV to study the glottal jet provided unprecedented qualitative and quantitative information about the general flow features, the stability of the jet and the nature of its interaction with the ventricular bands. It provided direct visual evidence of the size, shape and direction of the glottal jet throughout the oscillation cycle, synchronised with the vocal fold motion. It also allowed a direct calculation of flow variables such as the average jet core velocity, the volume flow and the geometrical expansion of the jet.

The experimental apparatus was superbly suited to the study, with the minor exception of the copper-vapour laser. The single-pulsed nature of the laser placed a limit on the possible inter-frame delay time, which in turn limited the upper range of the measurable fluid velocity. However, careful setup of the *in vitro* model, together with a meticulous experimental technique and choice of upstream overpressure (to minimise the jet velocities), led to universal success in measuring the glottal flow for the three configurations. The use of phase windowing helped to significantly improve the signal-to-noise ratio of the experiments. It also provided a means to quantify the uncertainty - and therefore stability - of the flow at each phase window. This was an important

feature of the study, as significant differences in the jet stability were observed between the configurations.

8.7.7 Summary

The work in this chapter has presented an experimental investigation into the behaviour of the pulsatile jet formed downstream of an *in vitro* vocal fold replica, for a number of downstream conditions. It has been shown that the presence of a pair of ventricular bands, which form a secondary constriction a short distance downstream from the vocal folds, significantly altered the characteristics of the jet. A configuration corresponding to a physically realistic ventricular band configuration stabilised the jet and increased the airflow through the vocal folds. The vocal fold oscillations were thus artificially assisted. A second configuration, which included a much smaller ventricular band separation, lead to a significant pressure recovery and a subsequent reduction in the airflow through the vocal folds. The vocal fold oscillations were thus hindered.

Part IV

Summary and Conclusions

Chapter 9

Summary and Conclusions

"*Wisdom standeth on the top of high places.*" - W. H. Murray

9.1 Introduction

Five primary thesis aims were laid out in chapter 1. These aims have been worked through in chapters 3 to 7. A summary of the important conclusions reached for each objective are presented below.

9.2 Objective One - Develop a new *in vitro* replica of the brass instrument lip-reed

The first objective of the thesis was to develop a new *in vitro* replica of the brass instrument lip-reed. Replica B, described in section 3.2.3, was the result of a successful fulfilment of this objective. The important results of this objective are summarised below:

- The new replica provided a repeatable and stable platform with which to study the mechanical properties of the *in vitro* lip-reed. It also allowed unprecedented optical access to the cross-section of the lip profile.

- The improved optical access to the lip profile allowed for a study of the two-dimensional mechanical response of the lip-reed, described in section 4.5.2. It also permitted an investigation to be made into the two-dimensional motion of the lips during full self-sustained oscillations, described in section 4.6.

9.3 Objective Two - Investigate the mechanical response properties of *in vivo* human lips formed into playable embouchures

The second objective of the thesis was to develop a novel experimental method, capable of measuring the mechanical response of *in vivo* human lips when formed into playable embouchures. The video method, described in sections 3.3.3 and 3.3.4, was the successful result of this objective.

9.3.1 The video method

The most important points concerning the development of the video method are outlined below:

- A mechanical response was obtained for human lips by performing a frequency response calculation between the lip motion, recorded by a high speed digital video camera, and a reference signal provided by a microphone situated in the mouthpiece.

- The novel development of the video method was that it allowed the lip motion to be recorded directly through an appropriate transparent mouthpiece (see below), without the need for the large optical setup required by the previous transmission method technique (described in section 3.3.2). The lip motion signal was the total open area between the lips. As the lips were driven by the loudspeaker they vibrated, causing a modulation to the gap between them. As the lips were acoustically driven, over a range of between 30 and 250Hz for a period of approximately 4s, they were filmed at 2000 frames per second. The open area between the lips was obtained for each image frame by application of a binarisation threshold to separate the dark pixels, constituting the open area, from the lighter pixels indicative of the lip surfaces. Concatenation of the open area from each frame into a single set of data led to a time domain signal describing the modulation of the open area as the lips were acoustically driven.

- A special double-shanked transparent mouthpiece was developed to allow the human subjects to first form a target embouchure while coupled to a trombone. This mouthpiece is described in figure 3.18. After establishing the target embouchure, a control valve was depressed that instantly coupled the player's lips the acoustical driving system. The mechanical response measurement was then performed.

9.3.2 Application of the video method to study the *in vivo* lip-reed

The video method was successfully used to study the mechanical response properties of the lips of a small number of experienced trombone players. The key findings of this investigation are summarised below:

- Most mechanical response measurements of *in vivo* human lips revealed the presence of at least two important resonances.
- The lower resonance consistently lay below the fundamental acoustical bore resonance of the target embouchure. This resonance was almost always the most prominent of the two resonances. The lower resonance was consistently identified as exhibiting an 'outward striking' behaviour, in the terminology of Helmoltz's classical reed descriptions[Helmholtz, 1877].
- The upper resonance consistently lay above the fundamental acoustical bore resonance of the target embouchure. For some embouchures it appeared to disappear below the noise floor of the measurement, due to the very small lip motion imparted by the acoustical driving of the loudspeaker. Where present, the upper resonance consistently displayed 'inward striking behaviour'.
- The presence of a pair of outward-inward striking resonances was a strong indication that the fundamental behaviours of the *in vivo* and *in vitro* lip-reed were compatible. It also provided strong support for the theory of acoustical interaction between the lips and the air column presented by Richards[Richards, 2003]. This theory suggests that a coupling exists between two modes of the lip motion, which allows a seamless transition to be made from oscillation below to above the acoustic resonance. The question of which lip modes were associated with which of the resonances in the mechanical response curve was suggested as a topic worthy of further investigation (see objective three below).
- The Q-values of the lip resonances were obtained by fitting a theoretical one-mass, one degree-of-freedom model, described by equation 4.1, around each resonance. The Q-values of the human lip resonances were typically between 1 and 2.5. This was considerably lower than those seen in the artificial lips, which typically ranged from 10-16. It was noted that a recent study[Gazengel *et al.*, 2007] of the mechanical impedance of a human lip and a glycerine-filled artificial lip had reported a similar range of Q-values. Values of between 1.2 and 1.4 had been reported for the real lip, and values of between 4 and 6 for the artificial lip. This result thus appeared to be in line with the findings of the human lip resonances reported in section 4.4.3.
- The low Q-values found for the human lips have important consequences for the parameter choice in computational lip models. Many lumped-element

simulations of the lip-reed, such as those of Cullen[Cullen *et al.*, 2000; Cullen, 2000] Richards[Richards, 2003], have used Q-value estimations obtained from water-filled artificial lips. While this may be justified when the simulations are directly compared to experimental observations on artificial lips, the present study suggests that it is not justified where the simulations seek to emulate real human lips, and that considerably lower values should be used.

9.4 Objective Three - Investigate the mechanical response properties and three-dimensional motion of replica B, the *in vitro* lip-reed replica developed in objective one

The third objective of the thesis was to investigate the mechanical properties and behaviour of replica B, which was the *in vitro* lip-reed replica developed for objective one. There were two principal approaches to address this objective. The first of the approaches measured the mechanical response of the replica lips. The second approach used the high speed camera to investigate the two dimensional motion of the lip trajectory.

9.4.1 Investigation into the mechanical response properties of replica B using the video method

The mechanical response properties of the lips were first investigated using three different methods. The traditional transmission method, described in section 4.2.2, was used to provide a benchmark measurement. The video method, as developed in objective two for measurements on human lips, was then applied to study the mechanical response of different slices along the lip width in section 4.3.2 (the global z axis in figure 3.14). The video method was finally used to study the lips in cross-section, so that the mechanical response of the lips could could be calculated separately from the horizontal and vertical lip motion. This work is described in section 4.5. The target was to relate the frontal benchmark measurement of the mechanical response to the parametric transverse measurements. The important conclusions from this work were:

- Performing mechanical response measurements of different slices along the lip length showed no significant variation in the resulting magnitude or phase of the mechanical response curves. The reduction of the lips to a two-dimensional approximation, an almost ubiquitous feature of the lumped element computational models, is thus quite a reasonable approach. The remarkable success of even the simplest lumped element models seems testament to this conclusion.

- A comparison between the frontal and transverse mechanical response measurements showed that when driven at the frequency of the lower resonance, the lip executed a large amplitude of motion in the horizontal x dimension. The vertical component of the motion along the y dimension was an order of magnitude lower than this strong 'outward' motion. The frontal mechanical response measurements, which were not directly sensitive to motion along the x axis, revealed a clear resonance at the same frequency as the resonance seen in the transverse x measurement. This implied a strong coupling between the horizontal x motion and the vertical y motion. This was explained as resulting from the elastic restoring force of the lips, which always has a vertical component due to the position of the lip anchor point at the top or bottom of the mouth.
- When driven at the upper resonance frequency the lips executed an almost purely vertical motion along the y axis. The phase angle of this resonance corresponded to the inward striking angle of classical reed physics. The horizontal x component of the transverse measurement did not record any information about the resonance. The behaviour of this resonance was explained as the result of an acoustical excitation of a vertically aligned mechanical resonance.

9.4.2 Investigation of the two dimensional motion of replica B during self-sustained oscillations

The second part of objective three was an investigation into the two-dimensional motion of the new *in vitro* brass instrument lips during full self-sustained oscillations. To achieve this, two black points were marked onto the surface of one of the lips. Each point was then tracked in the x and y dimensions as the lips oscillated, using a high speed digital camera. This work is described in section 4.6, and the important conclusions are presented below:

- Both of the points executed periodic two-dimensional motion along the x and y axes throughout the oscillation cycle. The fundamental oscillation frequency of the motion along both the x and y axes was that of the overall lip oscillation frequency.
- The two points travelled along significantly different trajectories as the lip vibrated. The point furthest upstream executed primarily vertical y motion, perpendicular to the streamwise flow direction. It also displayed a smaller amplitude of motion in the x direction, which resulted in a complex overall figure-of-eight trajectory. The point furthest downstream executed large amplitude motion along both the two axes, resulting in an elliptical trajectory.
- It was concluded that a lumped element model with at least four degrees of freedom would be required in order to accurately simulate the observed

mechanical behaviour. A note of caution was also made about whether such a model would really be required to provide accurate simulations of the overall *acoustic* behaviour of the brass instrument - lip-reed system.

9.5 Objective Four - Development of a new PIV experimental setup

The target of objective four was to adapt the PIV experimental setup developed by Skulina[Skulina, 2005] to allow it to be used to investigate the flow through an *in vitro* vocal fold replica. The basic principles of PIV were first outlined in chapter 5. A detailed description of the new setup was then presented in chapter 6. The most important points concerning the setup are outlined below:

- The new setup was designed to allowed PIV measurements to be made throughout the cycle of oscillation of the vocal fold replica.
- The PIV system could not be phase-locked in to the oscillations of the vocal folds, because they were left to undergo autonomous self-sustained oscillations. This meant that it was impossible, *a priori*, to determine a particular phase point in the vocal fold cycle at which to acquire PIV data. This issue was addressed by synchronising the PIV data acquisitions with a fixed, even-integer frequency that was close to the (non-integer) oscillation frequency of the replica. PIV data was then acquired periodically according to the repetition cycle of the even-integer frequency. The slight difference between the even-integer and non-integer frequencies meant that each consecutive PIV data acquisition occurred at a slightly different phase angle through the true oscillation cycle of the replica. In effect, a PIV 'strobing' technique was implemented. This process is described in detail in the first half of section 6.5.2.
- The PIV data was synchronised to the oscillating open height between the vocal folds using a post-synchronisation method outlined in detail in the second half of section 6.5.2.
- For a particular configuration of the vocal folds, a large number of measurement runs were carried out, each of which resulted in the acquisition of approximately twenty PIV vector maps. The final result was that each configuration was described by approximately 250 vector maps, distributed evenly throughout the oscillation cycle. In order to make the data set more manageable, a process of *phase windowing* was carried out. The oscillation cycle was divided into ten equally spaced intervals. The maps within each window were then averaged together to produce a singe, phase windowed PIV vector map. This meant that

the oscillation cycle was described by ten averaged maps, rather than by a large number of instantaneous maps.

- During the formulation of the phase windows, a calculation of the standard deviation of the constituent maps within each window was performed. This helped to quantify the overall stability of the flow within each phase window. High standard deviation velocities were indicative of significantly different constituent vector maps. Low standard deviation velocities were indicative of a consistent, stable flow.

9.6 Objective Five - Application of PIV to the flow through a self-oscillating *in vitro* vocal fold replica

The final objective of the thesis was to investigate the aerodynamic interaction between the human vocal folds and the ventricular bands. A self-oscillating *in vitro* vocal fold replica was employed to represent the vocal folds, and three different downstream conditions were tested.

The first condition was that of no downstream coupling. The air jet (or 'glottal jet') formed by separation of the flow from the vocal folds was thus free to pass directly into the laboratory, quickly resulting in a total loss of pressure in the flow. Two configurations with replica ventricular bands were then studied. The replica ventricular bands were formed from rigid blocks of aluminium with rounded faces. The configurations were characterised by two key parameters: their position downstream from the vocal folds L_{VB}, and their minimum separation h_{VB}. The 'physically realistic' configuration was based on parameters obtained during *in vivo* measurements on real ventricular bands. The 'impeding' configuration was a slightly perturbed version of the physically realistic configuration, which had previously been demonstrated to impede the vocal fold oscillations[Bailly *et al.*, 2006].

The objective of the study was to first investigate the basic features and behaviour of the air jet in the case of the free jet configuration. A comparative study was then undertaken to analyse the behaviour of the jet in the presence of the two ventricular bands configurations.

9.6.1 The free jet

Study of the free jet configuration provided a useful benchmark case to which the two ventricular band configurations could be compared. The most important features of the flow are summarised below:

- The maximum jet velocity was encountered around the start of the closing phase of the vocal folds. In general, higher velocities were encountered during the closing

phase than during the opening phase. This asymmetry was suggested as being evidence for an asymmetry in the Bernoulli driving force between the vocal folds. This would have allowed the airflow to provide an essential net gain of energy to the vocal folds.

- The jet appeared to oscillate throughout the cycle in its direction relative to the glottal centreline. At the start of the cycle it was skewed strongly to the left. As the cycle progressed it rotated to the right, before moving back to the left during the latter part of the closing phase.
- Large scale jet 'tongues' directed to the left and right of the main flow axis were observed in the transitional region of the jet. These may have resulted from the phenomenon of jet flapping reported by Neubauer *et al*[Neubauer *et al.*, 2007].
- The level of turbulence, both in the 'core' region and the wider flow field, was highest during the deceleration phase of the jet which occurred as the vocal folds closed to their minimum separation. Comment was made about this result in terms of the wider field of oscillatory flow.

9.6.2 Influence of the ventricular bands

The two ventricular band configurations had strong influences on the behaviour of the jet. It appears that these influences could be extensively explained with recourse to the previous experimental work of Bailly *et al*[Bailly *et al.*, 2006; Bailly *et al.*, 2008]. The most important results are presented below.

The realistic configuration ($VB - A$)

The overall turbulence levels of the glottal jet were significantly lowered, throughout the entire glottal cycle, compared to the free jet case. The overall jet core velocities were also considerably higher throughout the cycle than the free jet configuration. These results suggested that the ventricular bands acted to stabilise the glottal jet.

None of the three geometrical jet expansion hypotheses was a close fit to the experimentally observed jet expansion over the course of the whole cycle. The turbulent expansion theory (THY-TURB) did provide a good match for small vocal fold openings. However, during the middle of the glottal cycle the experimentally observed jet expansion was much larger than any of the theoretical predictions. It is possible that this was related to the increased volume flow through the vocal folds for the realistic configuration. The large jet width, coupled with overall high jet core velocities, led to a large volume flow. It was hypothesised that this was the mechanism by which the ventricular bands assisted the vocal fold vibrations. An overall increase in the volume flow provided an overall increase in the pressure drop across the vocal folds, which acted to lower the threshold oscillation pressure.

The impeding configuration ($VB - B$)

The overall turbulence levels of the glottal jet were significantly lowered during the middle of the glottal cycle, when the vocal fold opening was largest. The jet remained quite unstable, however, at small vocal fold open heights, evidenced by the high levels of turbulence around the jet core.

None of the geometrical jet expansion theories provided a close match to the experimentally observed data. The turbulent expansion theory (THY-TURB) was the closest, but it underestimated the expansion during the middle part of the glottal cycle when the vocal fold separation was large, and overestimated it during when the vocal fold separation was small.

The volume flow through the system, quantified with a calculation of the vocal fold flow admittance, was significantly reduced for the impeding configuration compared to the free jet configuration. It was hypothesised that this was the mechanism by which the ventricular bands acted to impede oscillations of the vocal folds. By lowering the volume flow, a reduction in the pressure difference across the vocal folds was achieved. This resulted in an increased threshold oscillation pressure to initiate destabilisation of the vocal folds.

Bibliography

[Adachi and Sato, 1995] S. Adachi and M. Sato. Time-domain simulation of sound production in the brass instrument. *J. Acous. Soc. Am.*, 97:3850–3861, 1995.

[Adachi and Sato, 1996] S. Adachi and M. Sato. Trumpet sound simulation using a two-dimensional lip vibration model. *J. Acous. Soc. Am.*, 99(2):1200–1209, 1996.

[Adachi and Yu, 2005] S. Adachi and J. Yu. Two-dimensional model of vocal fold vibration for sound synthesis of voice and soprano singing. *J. Acous. Soc. Am.*, 117(5):3213–3224, 2005.

[Adrian, 1993] R. J. Adrian, editor. *Selected papers on laser doppler velocimetry.* SPIE, New York, USA, 1993.

[Agarwal, 2004] M. Agarwal. *The false vocal folds and their effect on translaryngeal airflow resistance.* PhD thesis, Graduate College, Bowling Green State University, 2004.

[Agüí and Jiménez, 1987] J. C. Agüí and J. Jiménez. On the performance of particle tracking. *J. Fluid Mech.*, 185:447 – 468, 1987.

[Alipour and Scherer, 2004] F. Alipour and R. C. Scherer. Flow separation in a computational oscillating vocal fold model. *J. Acous. Soc. Am.*, 116(3):1710–1719, 2004.

[Alipour *et al.*, 1995] F. Alipour, R. C. Scherer, and V. C. Patel. An experimental study of pulsatile flow in canine larynges. *Journal of fluids engineering*, 117(4):557 – 581, 1995.

[Backus, 1961] J. Backus. Vibrations of the reed and the air column in the clarinet. *J. Acous. Soc. Am.*, 33:800–809, 1961.

[Bailly *et al.*, 2006] L. Bailly, N. Ruty, A. van Hirtum, J. Cisonni, X. Pelorson, and N. Henrich. Aerodynamic interaction between the vocal folds and the ventricular bands. In *7th International Conference on Advances in Quantitative Laryngology, Voice and Speech Research*, Groningen, Netherlands, 2006.

[Bailly *et al.*, 2007] L. Bailly, N. Henrich, M. Webb, F. Muller, A. K. Licht, and M. Hess. Exploration of vocal-folds and ventricular-bands interaction in singing using high-speed cinematography and electroglottography. In *Proc. 19th ICA, Madrid, Spain*, 2007.

[Bailly *et al.*, 2008] L. Bailly, N. Henrich, X. Pelorson, and J. Gilbert. Influence of a constriction in the near field of the vocal folds: physical modeling and experimental validation. *J. Acous. Soc. Am.*, 124(5):3296–3308, 2008.

[Bailly, 2008] L. Bailly. Private communication, August 2008.

[Bailly, 2009] L. Bailly. *Interaction entre cordes vocales et bandes ventriculaires en phonation: exploration in-vivo, modélisation physique, validation in-vitro.* PhD thesis, GIPSA, Grenoble, 2009.

[Bamberger, 2005] A. Bamberger. Vortex sound in flutes using flow determination with endo-piv. In *Proc. Forum Acusticum*, pages 665–670, 2005.

[Barney *et al.*, 1999] A. Barney, C. Shadle, and P. David. Fluid flow in a dynamic mechanical model of the vocal folds and tract i: Measurements and theory. *J. Acous. Soc. Am.*, 105:444–455, 1999.

[Bromage *et al.*, 2005] S. R. Bromage, J. Gilbert, and D. M. Campbell. Experimental investigation of the open area of the brass player's vibrating lips. In *Proc. Forum Acusticum*, Budapest, Hungary, 2005.

[Bromage, 2006] S. Bromage. *Visualisation of the Lip Motion of Brass Instrument Players, and Investigations of an Artificial Mouth as a Tool for Comparative Studies of Instruments.* PhD thesis, University of Edinburgh, Edinburgh, UK, 2006.

[Brücker *et al.*, 2004] C. Brücker, M. Triep, and M. Kob. Study of the vortex dynamics in a mechanical model of the vocal folds using particle image velocimetry. In *Proceedings of the International Conference on Voice Physiology and Biomechanics*, pages 11–17, Marseille, France, 2004.

[Brun, 1995] H. H. Brun. *Hot-Wire Anemometry.* Oxford University Press, 1995.

[Campbell and Greated, 1987] Murray Campbell and Clive Greated. *The Musician's Guide to Acoustics.* Schimer Books, 1987.

[Campbell, 1999] D. M. Campbell. Nonlinear dynamics of musical reed and brass wind instruments. *Contemporary Physics*, 40(6):415–431, 1999.

[Chen and Weinreich, 1996] F.-C. Chen and G. Weinreich. Nature of the lip reed. *J. Acous. Soc. Am.*, 99(2):1227–1233, 1996.

[Chick *et al.*, 2005] J. Chick, S. Bromage, and M. Campbell. Transient behaviour in the motion of brass player's lips. In *Proc. Forum Acusticum*, pages 753–758, Budapest, Hungary, 2005.

[Coanda, 1936] H. Coanda. Device for deflecting a stream of elastic fluid projected into an elastic fluid. Technical report, U.S. Patent No. 2,052,869, September 1936.

[Copley and Strong, 1996] D. C. Copley and W. J. Strong. A stroboscopic study of lip vibrations in a trombone. *J. Acous. Soc. Am.*, 99(2):1219–1223, 1996.

[Cullen *et al.*, 1999] J. S. Cullen, C. A. Greated, and D. M. Campbell. Lda measurement of sound: amplitude and modulation of laser doppler signals. *Meas. Sci. Technol.*, 10:812 – 823, 1999.

[Cullen *et al.*, 2000] J. S. Cullen, J. Gilbert, and D. M. Campbell. Brass instruments: Linear stability analysis and experiments with an artificial mouth. *Acta Acustica United with Acustica*, 86:704–724, 2000.

[Cullen, 2000] J. S. Cullen. *A study of brass instrument acoustics using an artificial reed mechanism, laser doppler anemometry and other techniques.* PhD thesis, University of Edinburgh, Edinburgh, UK, 2000.

[Dalmont *et al.*, 2003] J.-P. Dalmont, J. Gilbert, and S. Ollivier. Nonlinear characteristics of single-reed instruments: Quasistatic volume flow and reed opening measurements. *J. Acous. Soc. Am.*, 114(4):2253–2262, 2003.

[Dantec, 1998] Dantec. Safex fog generator. Technical report, Dantec Measurement Technology A/S, October 1998.

[Davis, 1971] M. R. Davis. Measurements in a subsonic turbulent jet using a quantitative schlieren technique. *J. Fluid Mech.*, 46(04):631 – 656, 1971.

[de Vries *et al.*, 2002] M. P. de Vries, H. K. Schutte, A. E. P. Veldman, and G. J. Verkerke. Glottal flow through a two-mass model: Comparison of navier-stokes solutions with simplified models. *J. Acous. Soc. Am.*, 111(4):1847–1853, 2002.

[de Vries *et al.*, 2003] M. P. de Vries, M. C. Hamburg, H. K. Schutte, G. J. Verkerke, and A. E. P. Veldman. Numerical simulation of self-sustained oscillation of a voice-producing element based on navier-stokes equations and the finite element method. *J. Acous. Soc. Am.*, 113(4):2077–2083, 2003.

[Decker and Thomson, 2006] G. Z. Decker and S. L. Thomson. Computational simulations of vocal fold vibration: Bernoulli versus navier-stokes. *J. Voice*, 21(3):273–284, 2006.

[Deverge *et al.*, 2003] M. Deverge, X. Pelorson, C. Vilain, P.-Y. Lagróe, F. Chentouf, J. Willems, and A. Hirschberg. Influence of collision on the flow through in-vitro rigid models of the vocal folds. *J. Acous. Soc. Am.*, 114(6):3354–3362, 2003.

[Elliot and Bowsher, 1982] S. J. Elliot and J. M. Bowsher. Regeneration in brass wind instruments. *J. Sound Vib.*, 83(2):181–217, 1982.

[Epps *et al.*, 1997] J. Epps, J. R. Smith, and J. Wolfe. A novel instrument to measure acoustic resonances of the vocal tract during phonation. *Meas. Sci. Technol.*, 8:1112–1121, 1997.

[Erath and Plesnaik, 2006a] B. Erath and M. W. Plesnaik. An investigation of biomodal jet trajectory through scaled models of the human vocal tract. *Experiments in Fluids*, 40:686–696, 2006.

[Erath and Plesnaik, 2006b] B. Erath and M. W. Plesnaik. The occurrence of the coanda effect in pulsatile flow through static models of the human vocal folds. *J. Acous. Soc. Am.*, 120(2):1000–1011, 2006.

[Fishler and Brodkey, 1991] L. S. Fishler and R. S. Brodkey. Transition, turbulence and oscillating flow in a pipe. *Experiments in Fluids*, 11:388 – 398, 1991.

[Fletcher and Rossing, 1991] N. Fletcher and T. Rossing. *The Physics of Musical Instruments*. Springer-Verlag, New York, 1991.

[Fletcher, 1993] N. H. Fletcher. Autonomous vibration of simple pressure-controlled valves. *J. Acous. Soc. Am.*, 93(4):2172–2180, 1993.

[Fletcher, 1999] N. H. Fletcher. The nonlinear physics of musical instruments. *Rep. Prog. Phys.*, 62:723–761, 1999.

[Fuks *et al.*, 1998] L. Fuks, B. Hammarberg, and J. Sundberg. A self-sustained vocal-ventricular phonation mode: acoustical, aerodynamic and glottographic evidences. *KTH TMH-QPSR*, 3:49 – 59, 1998.

[Gazengel *et al.*, 2007] B. Gazengel, T. Guimezanes, J.-P. Dalmont, J. B. Doc, S. Fagart, and Y. Leveille. Experimental investigation of the influence of the mechanical characteristics of the lip on the vibrations of the single reed. In *ISMA 2007*, Barcelona, Spain, 2007.

[Gilbert *et al.*, 1998] J. Gilbert, S. Ponthus, and J.-F. Petiot. Artificial buzzing lips and brass instruments: Experimental results. *J. Acous. Soc. Am.*, 104(3):1627–1632, 1998.

[Gilbert *et al.*, 2005] J. Gilbert, S. R. Bromage, and D. M. Campbell. Influence of the open area of a player's lips on brass instrument behaviour. In *Proc. Forum Acusticum*, Budapest, Hungary, 2005.

[Grant, 1997] I. Grant. Particle image velocimetry: a review. In *Proc. Instn. Mech. Engrs.*, volume 211, pages 55 – 76, 1997.

[Gromada.com, 2003] Gromada.com. Videomach software, 2003.

[Guerin, 1981] B. Guerin. The effect of source-tract interaction using vocal fold models. In I. R. Titze and R. C. Scherer, editors, *Vocal Fold Physiology: Acoustics, Aerodynamics, and Phonatory Control*. The Denver Centre for the Performing Arts, Denver, USA, 1981.

[Helmholtz, 1877] H. J. F. Helmholtz. *On the sensations of tone*. Dover (reprint, 1954), New York, 1877.

[Hirschberg *et al.*, 1996a] A. Hirschberg, J. Gilbert, R. Msallam, and A. P. J. Wijnands. Shock waves in trombones. *J. Acous. Soc. Am.*, 99(3):1754–1758, 1996.

[Hirschberg *et al.*, 1996b] A. Hirschberg, X. Pelorson, and J. Gilbert. Aeroacoustics of musical instruments. *Meccanica*, 31:131–141, 1996.

[Hirschberg *et al.*, 1996c] A. Hirschberg, X. Pelorson, G. Hofmans, R. Hassel, and P. Wijands. Starting transient of the flow through an *in vitro* model of the vocal folds. In P. J. Davis and N. H. Fletcher, editors, *Vocal fold physiology: Controlling complexity and chaos*, pages 31–46. Singular Pub. Group, San Diego, USA, 1996.

[Hirschberg, 1992] A. Hirschberg. Some fluid dynamical aspects of speech. *Bull. Commun. Parlee*, 2:1–30, 1992.

[Hirschberg, 2006] A. Hirschberg. Private communication, November 2006.

[Hofmans *et al.*, 2003] G. C. J. Hofmans, G. Groot, M. Ranucci, G. Graziani, and A. Hirschberg. Unsteady flow through *in-vitro* models of the glottis. *J. Acous. Soc. Am.*, 113(3):1658–1675, 2003.

[Imagawa *et al.*, 2003] H. Imagawa, K. I. Sakakibara, N. Tayama, and S. Niimi. The effect of the hypopharyngeal and supra-glottic shapes on the singing voice. In *Proc. SMAC, Stockholm*, 2003.

[Ishizaka and Flanagan, 1972] K. Ishizaka and L. J. Flanagan. Synthesis of voiced sounds from a two-mass model of the vocal chords. *Bell Sys. Tech. J.*, 50:1233–1268, 1972.

[Ishizaka and Matsudaira, 1972] K. Ishizaka and M. Matsudaira. Fluid mechanical considerations of vocal-cord vibrations. *Speech Commun. Res. Lab. Monograph*, 8, 1972.

[IWK, 2009] IWK. Brass Instrument Analysis System (BIAS), IWK, Vienna, Austria, 2009.

[Joliveau *et al.*, 2004] E. Joliveau, J. Smith, and J. Wolfe. Tuning of vocal tract resonances by sopranos. *Nature*, 427:116, 2004.

[Keane and Adrian, 1992] R. D. Keane and R. J. Adrian. Theory of cross-correlation analysis of piv images. *Applied Scientific Research*, 49:191 – 215, 1992.

[Kob *et al.*, 2005] M. Kob, S. Krämer, A. Prévot, M. Triep, and C. Brücker. Acoustic measurement of periodic noise generation in a hydrodynamical vocal fold model. In *Proc. Forum. Acusticum*, pages 2731–2736, 2005.

[Kob, 2002] M. Kob. *Physical Modelling of the Singing Voice*. PhD thesis, Aachen University, Berlin, 2002.

[Kob, 2004a] M. Kob. Analysis and modelling of overtone singing in the sygyt style. *Applied Acoustics*, 65:1249–1259, 2004.

[Kob, 2004b] M. Kob. Singing voice modelling as we know it today. *Acta Acustica United with Acustica*, 90:649–661, 2004.

[Krane and Wei, 2006] M. H. Krane and T. Wei. Theoretical assessment of unsteady aerodynamic effects in phonation. *J. Acous. Soc. Am.*, 120(3):1578–1588, 2006.

[Krane *et al.*, 2007] M. Krane, M. Barry, and T. Wei. Unsteady behaviour of flow in a scaled-up vocal folds model. *J. Acous. Soc. Am.*, 122(6):3659–3670, 2007.

[Kucinschi and Scherer, 2006] B. Kucinschi and R. C. Scherer. An experimental analysis of the pressures and flows within a driven mechanical model of phonation. *J. Acous. Soc. Am.*, 119(5):3011–3021, 2006.

[Kucinschi *et al.*, 2005] B. R. Kucinschi, R. C. Scherer, K. J. De Witt, and T. T. M. Ng. An experimental analysis of the flow through a driven mechanical model of the vocal folds. *J. Fluid Mech.*, May 2005.

[Kucinschi *et al.*, 2006] B. R. Kucinschi, R. C. Scherer, K. J. De Witt, and T. M. Terry. Flow visualisation and acoustic consequences of the air moving through a static model of the human larynx. *J. Biomech. Eng.*, 128:380–390, 2006.

[Kundu, 1990] P. K. Kundu. *Fluid Mechanics*. Academic, San Diego, USA, 1990.

[Liljencrants, 1989] J. Liljencrants. Numerical simulations of glottal flow. In J. Gauffin and B. Hammerberg, editors, *Vocal Fold Physiology*, pages 99 – 104. Singular Pub. Group, CA, USA, 1989.

[Lous *et al.*, 1998] N. J. C Lous, G. C. J. Hofmans, N. J. Veldhuis, and A. Hirschberg. A symetrical two-mass vocal-fold model coupled to vocal tract and trachea, with application to prosthesis design. *Acustica*, 84:1135–1150, 1998.

[Lucero, 1993] J. Lucero. Dynamics of the two-mass model of the vocal folds: equilibria, bifurcations, and oscillation region. *J. Acous. Soc. Am.*, 94:3104–3111, 1993.

[Martin, 1942] D. W. Martin. Lip vibrations in a cornet mouthpiece. *J. Acous. Soc. Am.*, 13:305–308, 1942.

[McGowan, 1988] R. S. McGowan. An aeroacoustic approach to phonation. *J. Acous. Soc. Am.*, 83(2):696–704, 1988.

[McGowan, 1993] R. S. McGowan. The quasisteady approximation in speech production. *J. Acous. Soc. Am.*, 94(5):3011–3013, 1993.

[Melling, 1997] A. Melling. Tracer particles and seeding for particle image velocimetry. *Meas. Sci. Technol.*, 8:1406 – 1416, 1997.

[Meynart *et al.*, 1987] R. Meynart, P. G. Simpkins, and T. D. Dudderar. Speckle measurements of convection in a liquid cooled from above. *J. Fluid Mech.*, 182(235 - 254), 1987.

[Mulgrew *et al.*, 1999] B. Mulgrew, P. Grant, and J. Thompson. *Digital Signal Processing - Concepts & Applications*. Palgrave, 1999.

[Nasri *et al.*, 1996] S. Nasri, J. Jasleen, B. R. Gerratt, J. A. Sercarz, R. Wenokur, and G. S. Berke. Ventricular dysphonia: a case of the false vocal fold mucosal travelling wave. *American Journal of Otolaryngology*, 17(6):427 – 431, 1996.

[Neal *et al.*, 2002] M. A. Neal, O. Richards, D. M. Campbell, and J. Gilbert. Study of the reed mechanism of brass instruments using an artificial mouth. In *Proc. Institute of Acoustics Spring Conference*, Salford, UK, 2002.

[Neal, 2002] M. Neal. *A Study of the Brass Instrument Lip Reed Mechanism using Artificial Lips and Lattice Boltzmann Flow Simulations.* PhD thesis, University of Edinburgh, Edinburgh, UK, 2002.

[Neubauer *et al.*, 2007] J. Neubauer, Z. Zhang, R. Miraghaie, and D. A. Berry. Coherent structures of the near field flow in a self-oscillating physical model of the vocal folds. *J. Acous. Soc. Am.*, 121(2):1102–1118, 2007.

[Newton and Campbell, 2006] M. J. Newton and D. M. Campbell. An experimental study of the airflow through an *in vitro* model of self-oscillating vocal folds using particle image velocimetry. In *Proceedings of the Institute of Acoustics*, Southampton, UK, 2006.

[Newton *et al.*, 2008] M. J. Newton, D. M. Campbell, and J. Gilbert. Mechanical response measurements of real and artificial brass player's lips. *J. Acous. Soc. Am.*, 123(1):EL14–EL20, 2008.

[Park and Mongeau, 2007] J. B. Park and L. Mongeau. Instantaneous orifice discharge coefficient of a physicsal, driven model of the human larynx. *J. Acous. Soc. Am.*, 121(1):442–455, 2007.

[Pelorson *et al.*, 1994] X. Pelorson, A. Hirschberg, R. R. van Hassel, A. P. J. Wijands, and Y. Auregan. Theoretical and experimental study of quasi-steady flow separation within the glottis during phonation. *J. Acous. Soc. Am.*, 96:3416–3413, 1994.

[Pelorson *et al.*, 1995] X. Pelorson, A. Hirschberg, A. P. J. Wijnands, and H. Bailliet. Description of the flow through in-vitro models of the glottis during phonation. *Acta Acustica*, 3:191–202, 1995.

[Pelorson, 2007] X. Pelorson. Private communication, October 2007.

[Poirson *et al.*, 2005] E. Poirson, J.-F. Petiot, and J. Gilbert. Study of the brightness of trumpet tones. *J. Acous. Soc. Am.*, 118(4):2656–2666, 2005.

[Raffel *et al.*, 1998] M. Raffel, C. Willert, and J. Kompenhan. *Particle Image Velocimetry: A Practical Guide*. Springer-Verlag, Berlin, 1998.

[Richards *et al.*, 2002] O. Richards, D. M. Campbell, J. Gilbert, and M. A. Neal. Use of experimental studies in determining a two-mass lip model. In *Proc. Forum Acusticum*, Sevilla, Spain, 2002.

[Richards *et al.*, 2003] O. Richards, D. M. Campbell, J. Gilbert, and M. A. Neal. Modelling the lip reed - computational and experimental investigations of the two-mode inward/outward striking behaviour. In *Proc. SMAC*, Stockholm, Sweeden, 2003.

[Richards, 2003] O. Richards. *Investigation of the Lip Reed Using Computational Modelling and Experimental Studies with an Artificial Mouth*. PhD thesis, University of Edinburgh, Edinburgh, UK, 2003.

[Rockliff, 2002] D. Rockliff. *Application of particle image velocimetry to the measurement of non-linear effects generated by high-intensity acoustic fields*. PhD thesis, University of Edinburgh, 2002.

[Rothenberg, 1981] M. Rothenberg. Acoustic interaction between the glottal source and the vocal tract. In K. N. Stevens and M. Hirano, editors, *Vocal Fold Physiology*, pages 305–328. University of Tokyo Press, 1981.

[Ruty *et al.*, 2007] N. Ruty, X. Pelorson, A. van Hirtum, I. Lopez-Arteaga, and A. Hirschberg. An in vitro setup to test the relevance and the accuracy of low-order vocal folds models. *J. Acous. Soc. Am.*, 121(121):479–490, 2007.

[Saneyoshi *et al.*, 1987a] J. Saneyoshi, H. Teramura, and S. Yoshikawa. Feedback oscillations in reed woodwind and brass wind instruments. *Acustica*, 62:194–210, 1987.

[Saneyoshi *et al.*, 1987b] J. Saneyoshi, H. Teramura, and S. Yoshikawa. Woodwind and brasswind instruments. *Acustica*, 62:194–210, 1987.

[Scherer *et al.*, 1983] R. Scherer, I. Titze, and J. Curtis. Pressure-flow relationships in two models of the larynx having rectangular glottal shapes. *J. Acous. Soc. Am.*, 73:668–676, 1983.

[Scherer *et al.*, 2001a] R. Scherer, D. Shinwari, K. De Witt, C. Zhang, B. Kucinschi, and A. Afjeh. Intraglottal pressure profiles for a symmetric and oblique glottis with a divergence angle of 10 degrees. *J. Acous. Soc. Am.*, 109:1616–1630, 2001.

[Scherer *et al.*, 2001b] R. C. Scherer, K. J. De Witt, and B. Kucinschi. The effect of exit radii on intraglottal pressure distributions in the convergent glottis (l). *J. Acous. Soc. Am.*, 110(5):2267–2269, 2001.

[Scherer *et al.*, 2002] R. C. Scherer, D. Shinwari, K. J. De Witt, C. Zhang, B. Kucinschi, and A. A. Afjeh. Intraglottal pressure profiles for a symmetric and oblique glottis with a uniform duct (l). *J. Acous. Soc. Am.*, 112(4):1253–1256, 2002.

[Schlichting and Gersten, 2000] H. Schlichting and K. Gersten. *Boundary Layer Theory*. Springer-Verlag, Berlin, 2000.

[Schlicke, 2001] T. Schlicke. *Breaking waves and the dispersion of surface film*. PhD thesis, University of Edinburgh, 2001.

[Shadle *et al.*, 1999] C. Shadle, A. Barney, and P. O. A. L. Davies. Fluid flow in a dynamic mechanical model of the vocal folds and tract. ii: Implications for speech production studies. *J. Acous. Soc. Am.*, 105(1):456–466, 1999.

[Silva *et al.*, 2008] F. Silva, J. Kergomard, C. Vergez, and J. and Gilbert. Interaction of reed and acoustic resonator in clarinetlike systems. *J. Acous. Soc. Am.*, 124(5):3284–3295, 2008.

[Simpkins and Dudderar, 1978] P. G. Simpkins and T. D. Dudderar. Laser speckle measurements of transient bénard convection. *J. Fluid Mech.*, 89(4):665 – 671, 1978.

[Sinder, 1999] D. J. Sinder. *Speech Synthesis Using an Aeroacoustic Fricative Model*. PhD thesis, CAIP, Rutgers University, 1999.

[Skulina *et al.*, 2003] D. J. Skulina, D. M. Campbell, and C. A. Greated. Measurement of the termination impedance of a tube using particle image velocimetry. In *Proc. Stockholm Mus. Ac. Conf.*, Sweeden, 2003.

[Skulina, 2005] D. J. Skulina. *A Study of Non-linear Acoustic Flows at the Open End of a Tube using Particle Image Velocimetry*. PhD thesis, University of Edinburgh, Edinburgh, UK, 2005.

[Slavit *et al.*, 1990] D. H. Slavit, R. J. Lipton, and T. V. McCaffrey. Phonatory vocal fold function in the excised canine larynx. *Otolaryngol. Head Neck Surg.*, 103(6):947 – 956, 1990.

[Story and Titze, 1995] B. Story and I. Titze. Voice simulation with a body-cover model of the vocal folds. *J. Acous. Soc. Am.*, 97(1249-1260), 1995.

[Sundberg, 1987] J. Sundberg. *The Science of the Singing Voice*. Northern Illinois University Press, Dekalb, Illinois, 1987.

[Švec *et al.*, 2000] J. G. Švec, J. Horáček, F. Šram, and J. Veselý. Resonance properties of the vocal folds: in vivo laryngoscopic investigation of the externally excited laryngeal vibrations. *J. Acous. Soc. Am.*, 108(4):1397–1407, 2000.

[Sveen and Cowen, 2004] J. K. Sveen and E. A. Cowen. Quantitative imaging techniques and their application to wavy flows. In J. Grue, P. L.-F. Liu, and G. K. Pederson, editors, *PIV And Water Waves*, chapter 1. World Scientific, 2004.

[Sveen, 2004] J. K. Sveen. An introduction to matpiv v.1.6.1. Eprint no. 2, **ISSN** 0809-4403, Dept. of Mathematics, University of Oslo, 2004.

[Tao *et al.*, 2007] C. Tao, Y. Zhang, D. G. Hottinger, and J. J. Jiang. Asymmetric airflow and vibration induced by the coanda effect in a symmetric model of the vocal folds. *J. Acous. Soc. Am.*, 122(4):2270–2278, 2007.

[Teager and Teager, 1983] H. Teager and S. Teager. Active fluid dynamics voice production, or there is a unicorn in the garden. In I. Titze and R. Scherer, editors, *Vocal Fold Physiology*, pages 387–401. The Denver Center For The Performing Arts, Denver, Colorado, USA, 1983.

[Thomson *et al.*, 2005] S. L. Thomson, L. Mongeau, and H. Frankel. Aerodynamic tranfer of energy to the vocal folds. *J. Acous. Soc. Am.*, 118(3):1689–1700, 2005.

[Titze and Story, 1997] I. Titze and B. Story. Acoustic interactions of the voice source with the lower vocal tract. *J. Acous. Soc. Am.*, 101(4):2234–2243, 1997.

[Titze, 1988] I. Titze. The physics of small-amplitude oscillation of the vocal folds. *J. Acous. Soc. Am.*, 83(4):1536–1552, 1988.

[Titze, 2004] I. Titze. Theory of glottal airflow and source filter interaction in speaking and singing. *Acustica*, 90:641–648, 2004.

[Triep *et al.*, 2004] M. Triep, C. H. Brücker, and W. Schröder. Visualization and high-speed piv measurements of the flow downstream a dynamic mechanical model of the human vocal folds. In *Proc. 12th International Symposium on Applications of Laser Techniques to Fluid Mechanics*, 2004.

[Tritton, 1988] D. J. Tritton. *Physical Fluid Dynamics*. Oxford Science Publications, 1988.

[Tsai *et al.*, 2004] C. Tsai, Y. Shau, and T. Hsiao. False vocal fold surface waves during sygyt singing: a hypothesis. In *Proc. ICVPB*, 2004.

[van den Berg *et al.*, 1957] J. van den Berg, J. T. Zantema, and P. Doornenbal. On the air resistance and the bernoulli effect of the human larynx. *J. Acous. Soc. Am.*, 29:626–631, 1957.

[van Hirtum *et al.*, 2007] A. van Hirtum, J. Cisonni, N. Ruty, X. Pelorson, I. Lopez, and F. van Uittert. Experimental validation of some issues in lip and vocal fold physical models. *Acta Acustica United with Acustica*, 93:314–323, 2007.

[Various, 2004] Various. Special issue: Particle image velocimetry. In *Measurement Science and Technology*, number 6. Institute of Physics, 2004.

[Vergez and Rodet, 1998] C. Vergez and X. Rodet. Experiments with an artificial mouth for trumpet. In *Proceedings of ISMA*, 1998.

[Vergez *et al.*, 2005] C. Vergez, P. de la Cuadra, and B. Fabre. Jet motion in flute-like instruments: experimental investigation through flow visualisation and image processing. In *Proc. Forum Acusticum*, pages 545–549, 2005.

[Vignola *et al.*, 1992] J. F. Vignola, S. Berthelot, S. Jones, and J. Jarzynski. Equation of motion of microparticles in suspension in an isonified medium. *J. Acous. Soc. Am.*, 92(1):332 – 334, 1992.

[Vilain *et al.*, 2003] C. E. Vilain, X. Pelorson, A. Hirschberg, L. Le Marrec, W. Op't Root, and J. Willems. Contribution to the physical modeling of the lips: Influence of the mechanical boundary conditions. *Acta Acustica United with Acustica*, 89(5):882–887, 2003.

[Vilain *et al.*, 2004] C. E. Vilain, X. Pelorson, C. Fraysse, M. Deverge, A. Hirschberg, and J. Willems. Experimental validation of a quasi-steady theory for the flow through the glottis. *J. Sound Vib.*, 276:475–490, 2004.

[Vilain, 2002] C. E. Vilain. *Contribution à la synthèse de parole par modèle physique. Application à l'étude des voix pathologiques.* PhD thesis, Institut National Polytechnique de Grenoble, 2002.

[Wright and Campbell, 1998] H. A. K. Wright and D. M. Campbell. The influence of the mouthpiece on the timbre of cup-mouthpiece wind instruments. In *Proceedings of the International Symposium on Musical Acoustics*, pages 159–164, Leavenworth, WA, USA, 1998.

[Yoshikawa and Muto, 2003] S. Yoshikawa and Y. Muto. Lip-wave generation in horn players and the estimation of lip-tissue elasticity. *Acta Acustica United with Acustica*, 89:145–162, 2003.

[Yoshikawa, 1995] S. Yoshikawa. Acoustical behavior of brass player's lips. *J. Acous. Soc. Am.*, 97(3):1929–1939, 1995.

[Zhang *et al.*, 2002] Z. Zhang, L. Mongeau, and H. Frankel. Experimental verification of the quasi-steady approximation for aerodynamic sound generation by pulsating jets in tubes. *J. Acous. Soc. Am.*, 112(4):1652–1663, 2002.

Publications

M. J. Newton and M. Campbell. An experimental study of the airflow through an *in vitro* model of self-oscillating vocal folds using particle image velocimetry. In *Proceedings of the Institute of Acoustics Meeting 2006*, Southampton, UK, April 2006.

M. J. Newton and R. MacDonald. Application of Particle Image Velocimetry in Musical Acoustics. In *Proceedings of the Scottish Fluid Mechanics Meeting 2007*, St. Andrews, UK, June 2007.

M. J. Newton, J. Gilbert and M. Campbell. Mechanical response measurements of real and artificial lips. In *Proceedings of ISMA 2007*, Barcelona, September 2007.

M. J. Newton, J. Gilbert and M. Campbell. Mechanical response measurements of real and artificial lips. *Journal of the Acoustical Society of America* 123(1), EL14-EL20, 2008.